NOTICE

The quality of this microform is heavily dependent upon the quality of the original thesis submitted for microfilming Every effort has been made to ensure the highest quality of reproduction possible

If pages are missing, contact the university which granted the degree

Some pages may have indistinct print especially if the original pages were typed with a poor typewriter ribbon or if the university sent us an inferior photocopy

Reproduction in full or in part of this microform is governed by the Canadian Copyright Act, R S C 1970, c C-30, and subsequent amendments

AVIS

La qualité de cette microforme dépend grandement de la qualité de la thèse soumise au microfilmage Nous avons tout fait pour assurer une qualité supérieure de reproduction

S'il manque des pages, veuillez communiquer avec l'université qui a conféré le grade

La qualité d'impression de certaines pages peut laisser à désirer, surtout si les pages originales ont été dactylographiées à l'aide d'un ruban usé ou si l'université nous a fait parvenir une photocopie de qualité inférieure

La reproduction, même partielle, de cette microforme est soumise à la Loi canadienne sur le droit d'auteur, SRC 1970, c C-30, et ses amendements subséquents

Canada

ISBN 0-315-56095-9

Canada

Performance of Single Screw Anchors and Group Action in Sand

Ashraf Ghaly

A Thesis
in
The Department
of
Civil Engineering

Presented in Partial Fulfillment of the Requirements
for the Degree of Doctor of Philosophy at
Concordia University

February 1990

ABSTRACT

Performance of Single Screw Anchors and Group Action in Sand

Ashraf Ghaly, Ph.D.
Concordia University, 1990

Experimental and theoretical investigations on the performance of single screw anchors and group action in sand are presented. A testing program included 60 tests on single anchors and 144 tests on anchor groups was conducted. Five models of screw anchors installed in dense, medium, and loose sand were tested. A sand placing technique was developed and utilized over all the testing program in order to assure reproductibility of the predetermined unit weight. The experimental set-up was instrumented to allow the measurement of the total pullout load, the upward displacement, the sand surface deflection, installation torque value, and the stress development in the sand layer during all phases of the testing procedure. The experimental set-up was equipped such that the uplift capacity and the upward displacement of every individual anchor in a group of anchors can be measured. Special tests were conducted on coloured-layered sand to define the rupture surface which was found to be a segment of a logarithmic spiral. The results of these tests, together with the measurements of the deflection of the sand surface have been utilized to establish the failure mechanism.

A theoretical model was developed utilizing the limit equilibrium method of analysis and the observed failure mechanism to predict the uplift capacity of a single screw anchor as well as group of anchors. Shear stresses were calculated on the surface of rupture using Kotter's differential equation. The effect of the overconsolidation ratio (OCR) on the uplift capacity was also studied and presented in a form of a semi empirical relationship. The densification effect on the angle of shearing resistance of the sand was presented in an empirical relationship. The installation procedure of screw anchors was examined and a theoretical model was developed to predict the required installation torque value in terms of the influencing parameters. A correlation between the uplift capacity and the installation torque was proposed. From this correlation the uplift capacity can be predicted from the measured installation torque value. Comparisons between theories developed and the experimental results of the present investigation as well as field results reported in the literature, showed good agreement.

TO THE SOUL OF MY FATHER

AND

TO MY MOTHER AND BROTHER

ACKNOWLEDGEMENTS

I wish to express my gratitude to Professor A. M. Hanna, my supervisor, for his encouragement and his drive for excellence. He has provided valuable guidance which made it possible to complete this research.

Special thanks are due Messrs. Andrew Chociwski, Daniel Roy, and Rocco Lombardo of the Geotechnical Laboratory, Concordia University, for their continuous help during the preparation of the experimental set-up and throughout the course of this research program.

I also wish to acknowledge Mr. Paul Scheiwiller and Mr. Miguel Artola of the Machine Shop, Concordia University, for their interest and patience during the fabrication of many complicated parts used in the present experimental study.

Thanks also to Ms. Gianna Venettacci for typing the entire text of this thesis. The financial support of the National Science and Engineering Research Council of Canada is gratefully acknowledged.

TABLE OF CONTENTS

	Page
LIST OF FIGURES	ix
LIST OF TABLES	xv
LIST OF PLATES	xvi
LIST OF SYMBOLS	xviii
CHAPTER 1	
Introduction	1
CHAPTER 2	
Review of Previous Work and Scope of Research	6
2.1 Review of Previous Work	6
2.2 Discussion and Scope of Present Research	27
CHAPTER 3	
Experimental Investigation and Results on Single Screw Anchors	29
3.1 Concept	29
3.2 Experimental Set-Up	29
3.3 Stress Transducer Units	32
3.4 Data Recording	36
3.5 Sand Properties	40
3.6 Model Screw Anchors	41
3.7 Installation Technique	41
3.8 Test Program	52
3.9 Test Results and Discussion	52
3.10 Shape of Rupture Surface	83
CHAPTER 4	
Group Action of Screw Anchors	87
4.1 Concept	87

Page

4.2 Experimental Set-Up 87
4.3 Model Screw Anchors 88
4.4 Group Configuration 88
4.5 Testing Program 92
4.6 Test Procedure 92
4.7 Test Results and Discussion 94

CHAPTER 5

Theoretical Analysis 118
5.1 Single Anchors 118
5.1.1 Shallow single anchors 118
5.1.2 Deep single anchors 129
5.1.3 Transit single anchors 140
5.2 Group of Anchors 143
5.2.1 Shallow square or rectangular group of anchors 143
5.2.2 Shallow triangular group of anchors 149
5.2.3 Deep square or rectangular group of anchors 152
5.2.4 Deep triangular group of anchors 158
5.2.5 Transit square or rectangular group of anchors 160
5.2.6 Transit triangular group of anchors 162
5.3 Effect of Overconsolidation on Uplift Capacity 162
5.4 Comparison of Experimental and Theoretical Results 164
5.5 Comparison of Theoretical and Field Results 172

CHAPTER 6

Installation Torque of Screw Anchors 177
6.1 General 177
6.2 Test Results and Discussion 178
6.3 Theoretical Model 194
6.3.1 Single pitch screw anchor 195
6.3.2 Multi equal pitch screw anchor 202
6.3.3 Multi variable pitch screw anchor 204
6.4 Comparison of Theoretical and Experimental Results 206
6.5 Comparison of Theoretical and Field Torque Results 212

Page

CHAPTER 7

Conclusions and Scope of Future Research 214

7.1 Conclusions 214

7.2 Scope of Future Research 219

REFERENCES 221

LIST OF FIGURES

Page

CHAPTER 1

Fig. 1.1: The use of screw anchors to support guyed "V" transmission line tower. 2

Fig. 1.2: Field applications of the screw anchors in the civil engineering practice. 3

CHAPTER 2

Fig. 2.1: Proposed failure suface for mushroom foundations; after Balla, (1961). 7

Fig. 2.2: Conical failure surface for underreamed footings; after Turner, (1961). 7

Fig. 2.3: Cylindrical failure surface for shallow footing; after Adams and Hayes, (1967). 10

Fig. 2.4: Proposed failure surfaces for shallow and deep footings; after Meyerhof and Adams, (1968). 10

Fig. 2.5: Selection of anchors for guyed transmission towers; after Robinson and Taylor, (1969). 12

Fig. 2.6: Test apparatus showing layout of vertical and horizontal sand movement gages; after Carr andHanna, (1971). 13

Fig. 2.7: Laboratory apparatus used to create overconsolidated sand; after Hanna and Carr, (1971). 15

Fig. 2.8: Laboratory equipment used by Healy, (1971). 15

Fig. 2.9: Stress cell placement plan for multi helix anchor in deep state, after Clemence and Pepe, (1984). 22

Fig. 2.10: Details of experimental set-up and tested anchor plate, after Hanna et al., (1988). 26

CHAPTER 3

Fig. 3.1: Experimental set-up used in the present investigation 30

Fig. 3.2: Detail of the fulcrum of the simple lever. 34

Fig 3.3: Transducers box unit used to measure lateral and vertical stresses 34

Fig. 3.4: Placement technique of stress transducers box units 37

Page

Fig. 3.5: Grain size distribution. 44
Fig. 3.6a: Single pitch screw anchor, small pitch (Type1). 45
Fig. 3.6b: Single pitch screw anchor, medium pitch (Type2). 46
Fig. 3.6c: Single pitch screw anchor, large pitch (Type3). 47
Fig. 3.6d: Multi pitch screw anchor, equal pitch, unsymmetrical screw (Type4). 48
Fig. 3.6e: Multi pitch screw anchor, variable pitch, parallel blades screw (Type5). 49
Fig. 3.7: Guide frame used to keep the anchor vertical in position during installation. 50
Fig. 3.8: Torque wrench used for producing and measuring torque. 53
Fig. 3.9: Ultimate pullout load versus installation depth for dense, medium, and loose sand; experimental results. 56
Fig. 3.10: Pullout load versus upward displacement in dense, medium and loose sand. 57
Fig. 3.11: Ultimate pullout load versus installation depth for tested types of anchors installed in dense sand; experimental results. 59
Fig. 3.12: Installation depth versus lateral stress after installation of screw anchors in dense sand. 60
Fig. 3.13: Installation depth versus lateral stress at failure of screw anchors in dense sand. 62
Fig. 3.14: Stress development in sand due to anchor installation. Type 1 screw anchor installed in dense sand; experimental results. 64
Fig. 3.15: Stress development in sand due to anchor installation. Type 2 screw anchor installed in dense sand; experimental results. 65
Fig. 3.16: Stress development in sand due to anchor installation. Type 3 screw anchor installed in dense sand; experimental results. 66
Fig. 3.17: Stress development in sand due to anchor installation. Type 4 screw anchor installed in dense sand; experimental results. 67
Fig. 3.18: Stress development in sand due to anchor installation. Type 5 screw anchor installed in dense sand; experimental results. 68
Fig. 3.19: Stress development in sand during pullot load application. Type 1 screw anchor installed in dense sand; experimental results. 70
Fig. 3.20: Stress development in sand during pullot load application. Type 2 screw anchor installed in dense sand; experimental results. 71
Fig. 3.21: Stress development in sand during pullot load application. Type 3 screw anchor installed in dense sand; experimental results. 72
Fig. 3.22: Stress development in sand during pullot load application. Type 4 screw anchor installed in dense sand; experimental results. 73

Fig. 3.23: Stress development in sand during pullout load application. Type 5 screw anchor installed in dense sand; experimental results. 74
Fig. 3.24: Typical stress development in the sand after placing, during anchor installation, and at failure. 76
Fig. 3.25: Relationship between installation depth and lateral earth pressure in dense sand; experimental results. 78
Fig. 3.26: Typical deflection of sand surface at failure. 84

CHAPTER 4

Fig. 4.1: Tested group configurations and anchors identification. 91
Fig. 4.2: Pullout load versus upward displacement for anchor groups installed in dense sand and spaced at S=3B. 96
Fig. 4.3: Pullout load versus upward displacement for anchor groups installed in medium sand and spaced at S=3B. 97
Fig. 4.4: Pullout load versus upward displacement for anchor groups installed in loose sand and spaced at S=3B. 98
Fig. 4.5: Pullout load versus upward displacement for triangular 3 anchors installed in dense, medium, and loose sand. 99
Fig. 4.6: Pullout load versus upward displacement for square 4 anchors installed in dense, medium, and loose sand 100
Fig. 4.7: Pullout load versus upward displacement for rectangular 6 anchors installed in dense, medium, and loose sand. 101
Fig. 4.8: Pullout load versus upward displacement for square 9 anchors installed in dense, medium, and loose sand 102
Fig. 4.9: Relationship between ultimate pullout load and embedment depth for single and groups of anchors installed in dense sand 105
Fig. 4.10. Relationship between ultimate pullout load and embedment depth for single and groups of anchors installed in medium sand 106
Fig. 4.11: Relationship between ultimate pullout load and embedment depth for single and groups of anchors installed in loose sand 109
Fig. 4.12: Load on a group as a percentage of load at failure versus load on anchor as a percentage of the load on the group at failure S=3B, 6 anchors, dense sand 110
Fig. 4.13: Load on a group as a percentage of load at failure versus load on anchor as a percentage of the load on the group at failure S=3B, 6 anchors, medium sand 111

Fig. 4.14: Load on a group as a percentage of load at failure versus load on anchor as a percentage of the load on the group at failure. S=3B, 6 anchors, loose sand. 112
Fig. 4.15: Load on a group as a percentage of load at failure versus load on anchor as a percentage of the load on the group at failure. S=3B, 9 anchors, dense sand. 113
Fig. 4.16: Load on a group as a percentage of load at failure versus load on anchor as a percentage of the load on the group at failure. S=3B, 9 anchors, medium sand. 114
Fig. 4.17: Load on a group as a percentage of load at failure versus load on anchor as a percentage of the load on the group at failure. S=3B, 9 anchors, loose sand. 115
Fig. 4.18: Efficiency of group of anchors versus spacing. 117

CHAPTER 5

Fig. 5.1: Geometrical properties of rupture surface of shallow anchors. 119
Fig. 5.2: Weight factor for shallow single anchors versus angle of shearing resistance. 125
Fig. 5.3: Schematic representation of shearing force acting on rupture surface of shallow anchors. 127
Fig. 5.4: Shear factor for shallow single anchors versus angle of shearing resistance. 130
Fig. 5.5: Geometrical properties of rupture surface of deep anchors. 132
Fig. 5.6: Weight factor for deep single anchors versus angle of shearing resistance. 135
Fig. 5.7: Schematic representation of shearing force acting on rupture surface of deep anchors. 137
Fig. 5.8: Shear factor for deep single anchors versus angle of shearing resistance. 139
Fig. 5.9: Geometrical properties of rupture surface of transit anchors. 142
Fig. 5.10: Geometry of rupture mechanism for shallow square group of anchors. 144
Fig. 5.11: Weight factor for shallow group of anchors versus angle of shearing resistance. 147
Fig. 5.12: Shear factor for shallow group of anchors versus angle of shearing resistance. 150
Fig. 5.13: Geometry of rupture mechanism for shallow triangular group of anchors. 151
Fig. 5.14: Geometry of rupture mechanism for deep square group of anchors. 154
Fig. 5.15: Weight factor for deep group of anchors versus angle of shearing resistance. 155
Fig. 5.16: Shear factor for deep group of anchors versus angle of shearing resistance. 157
Fig. 5.17: Geometry of surface of rupture for deep triangular group of anchors. 159
Fig. 5.18: Geometry of rupture mechanism for transit square group of anchors. 161
Fig. 5.19: Geometry of surface of rupture for transit triangular group of anchors. 163

Fig. 5.20: Relationship between ultimate pullout load and overconsolidation ratio for anchor installed at constant depth of sand; after Hanna et al., (1971). 165
Fig. 5.21: Comparison of experimental and theoretical results for single anchor installed in dense, medium, and loose sand. 166
Fig. 5.22: Comparison of experimental and theoretical results for groups of anchors installed in loose sand. 168
Fig. 5.23: Comparison of experimental and theoretical results for groups of anchors installed in medium sand. 169
Fig. 5.24: Comparison of experimental and theoretical results for groups of anchors installed in dense sand. 170
Fig. 5.25: Values of coefficient of densification for the tested group configurations. 171
Fig. 5.26: Comparison of experimental and theoretical results for groups of anchors spaced at S=3B. 173
Fig. 5.27: Comparison of experimental and theoretical results for groups of anchors spaced at S=4B. 174
Fig. 5.28: Comparison of experimental and theoretical results for groups of anchors spaced at S=5B. 175
Fig. 5.29: Comparison of present theoretical results and field results reported in the literature. 176

CHAPTER 6

Fig. 6.1: Installation torque versus installation depth for tested types of anchors installed in dense, medium, and loose sand. 180
Fig. 6.2: Stress development in sand due to the applied installation torque. Type 1 screw anchor installed in dense sand; experimental results. 183
Fig. 6.3: Stress development in sand due to the applied installation torque. Type 2 screw anchor installed in dense sand; experimental results. 184
Fig. 6.4: Stress development in sand due to the applied installation torque. Type 3 screw anchor installed in dense sand; experimental results. 185
Fig. 6.5: Stress development in sand due to the applied installation torque. Type 4 screw anchor installed in dense sand; experimental results. 186
Fig. 6.6: Stress development in sand due to the applied installation torque. Type 5 screw anchor installed in dense sand; experimental results. 187
Fig. 6.7: Influence of screw anchor installation on sand top surface. 189

Page

Fig. 6.9: Ultimate pullout load versus installation torque for tested types of anchors installed in loose, medium, and dense sand. 193
Fig. 6.10: Forces acting on single pitch screw anchor during installation. 196
Fig. 6.11: Forces acting on multi equal pitch screw anchor during installation. 203
Fig. 6.12: Forces acting on multi variable pitch screw anchor during installation. 205
Fig. 6.13: Comparison of theoretical and experimental torque results for anchors with different pitches. 207
Fig. 6.14: Comparison of theoretical and experimental torque results for anchors installed in loose, medium, and dense sand. 208
Fig. 6.13: Comparison of theoretical and experimental torque results for unsymmetrical and parallel blades screw anchors. 209
Fig. 6.16: Relationship between uplift capacity factor and torque factor. 211
Fig. 6.17: Comparison of theoretical torque results and field results reported in the literature. 213

LIST OF TABLES

Page

CHAPTER 3

Table 3.1: Physical properties of the tested sand. 42

Table 3.2: Geometrical properties of single screw model anchors. 43

Table 3.3: Test program on single screw anchors. 54

Table 3.4: Test results of tested types of single screw anchors. 55

CHAPTER 4

Table 4.1: Test program on group action of screw anchors. 93

Table 4.2: Summary of testing program and results of group action. 95

Table 4.3: Efficiency of anchor groups. 108

CHAPTER 5

Table 5.1: Weight factor FW_{ss} for shallow single anchors. 125

Table 5.2: Shear factor FF_{ss} for shallow single anchors. 130

Table 5.3: Weight factor FW_{ds} for deep single anchors. 135

Table 5.4: Shear factor FF_{ss} for deep single anchors. 139

Table 5.5: Weight factor FW_{sg} for shallow group of anchors. 147

Table 5.6: Shear factor FF_{sg} for shallow group of anchors. 150

Table 5.7: Weight factor FW_{dg} for deep group of anchors. 155

Table 5.8: Weight factor FF_{dg} for deep group of anchors. 157

CHAPTER 6

Table 6.1: Installation torque for tested types of anchors. 179

LIST OF PLATES

Page

CHAPTER 3

Plate 3.1: General view for the experimental set-up. 31
Plate 3.2: Front corner view for the testing tank. 31
Plate 3.3: Back corner view for the testing tank showing the loading system and the gear box device. 33
Plate 3.4: Conical knifed edge supporting the double cantilever beam. 33
Plate 3.5: Details of the supporting seat of the loading frame. 35
Plate 3.6: Pressure gages controlling and measuring the air pressure inside the testing tank. 35
Plate 3.7: Top view showing locations of stress transducers box units. 38
Plate 3.8: Corner view showing the staggared arrangement of stress transducers inside the testing tank. 38
Plate 3.9: Data Acquisition System and computer used for measuring and recording data. 39
Plate 3.10: Displacement transducers (LVDT) used for measuring sand suface deflection. 39
Plate 3.11: Air hammer used to compact the sand. 44
Plate 3.12a: Single pitch screw anchor, small pitch (Type1). 45
Plate 3.12b: Single pitch screw anchor, medium pitch (Type2). 46
Plate 3.12c: Single pitch screw anchor, large pitch (Type3). 47
Plate 3.12d: Multi pitch pitch screw anchor, equal pitch, unsymmetrical screw (Type4). 48
Plate 3.12e: Multi pitch screw anchor, variable pitch, parallel blades screw (Type5). 49
Plate 3.13: Guide frame used to keep the anchor vertical during installation. 51
Plate 3.14: Torque-meter used for measuring the value of installation torque. 51
Plate 3.15: The logarithmic spiral surface of rupture observed experimentally. 86

CHAPTER 4

Plate 4.1: Triangular configuration of anchors group (3 anchors). 89
Plate 4.2: Square configuration of anchors group (4 anchors). 89

Page

Plate 4.3: Rectangular configuration of anchors group (6 anchors). 90
Plate 4.4: Square configuration of anchors group (9 anchors). 90

CHAPTER 6
Plate 6.1: General view of sand strings before placing the sand inside the tube. 191
Plate 6.2: General view of sand strings after placing the sand inside the tube. 191
Plate 6.3: Effect of screw installation on the vertical sandy strings placed on the inner perimeter of the testing tube. 192
Plate 6.4: Effect of screw installation on horizontal coloured layers of sand. 192

LIST OF SYMBOLS

Symbol			Chapter
A_b	=	bottom surface area of the screw blade	6
A_g	=	cross sectional area of a group of anchors	6
A_t	=	top surface area of the screw blade	6
b	=	radius of the screw anchor's blade	5
B	=	diameter of the screw anchor's blade	5
B_0	=	inner diameter of the upper suface of the screw anchor's blade	6
B_1	=	inner diameter of the lower suface of the screw anchor's blade	6
B_{av}	=	average diameter of the screw anchor's blade	6
c_1	=	constant	5
c_2	=	constant	5
c_3	=	constant	5
c_4	=	constant	5
c_d	=	densification factor	5
C_c	=	coefficient of curvature	3
C_u	=	coefficient of uniformity	3
C	=	constant	5
CN	=	central anchor in a group of anchors	4
CR	=	corner anchor in a group of anchors	4
d	=	radius of the anchor's shaft	6
dF	=	shear stress acting on an infinitesimal area	5
dF_{ds}	=	shear stress acting on an infinitesimal area in case of deep single anchor	5
dF_{ss}	=	shear stress acting on an infinitesimal area in case of shallow single anchor	5
dh	=	infinitesimal height	5
dH	=	infinitesimal height	5
$d\theta$	=	infinitesimal angle	5

Symbol		Chapter
$d\tau$	= shear stress acting on an infinitesimal distance	5
$d\omega$	= infinitesimal angle of revolution	5
D	= diameter of the anchor's shaft	6
D_r	= relative density of the sand	3
e	= constant equals 2.718 approximatly	5
E	= efficiency of group of anchors	4
F	= lateral force acting on the screw anchor's blade	6
F_{dg}	= resisting shear force of a deep group of anchors	5
F_{ds}	= resisting shear force of a deep single anchor	5
FF_{dg}	= shear factor for a deep group of anchors	5
FF_{ds}	= shear factor for a deep single anchor	5
F_{sg}	= resisting shear force of a shallow group of anchors	5
F_{ss}	= resisting shear force of a shallow single anchor	5
FF_{sg}	= shear factor for a shallow group of anchors	5
FF_{ss}	= shear factor for a shallow single anchor	5
F_r	= reduction factor	3
F_t	= torque factor	6
F_{tdg}	= resisting shear force of a transit deep group of anchors	5
F_{tds}	= resisting shear force of a transit deep single anchor	5
F_{tsg}	= resisting shear force of a transit shallow group of anchors	5
F_{tss}	= resisting shear force of a transit shallow single anchor	5
FW_{dg}	= weight factor for a deep group of anchors	5
FW_{ds}	= weight factor for a single deep anchor	5
FW_{sg}	= weight factor for a shallow group of anchors	5
FW_{ss}	= weight factor for a single shallow anchor	5
h	= height of failure bulb of deep anchors	5
h - h	= horizontal line	5
H	= installation depth of the screw anchor	3
K1	= constant	5
K2	= constant	5
K3	= constant	5

Symbol		Chapter
K4	= constant	5
K5	= constant	5
K6	= constant	5
K7	= constant	5
K8	= constant	5
K9	= constant	5
K10	= constant	5
K11	= constant	5
K12	= constant	5
K13	= constant	5
K14	= constant	5
K15	= constant	5
K16	= constant	5
K17	= constant	5
K18	= constant	5
K_A	= coefficient of active earth pressure	6
K_f	= coefficient of friction between the anchor's shaft and the sand	6
K_F	= coefficient of earth pressure at failure	3
K_I	= coefficient of earth pressure after anchor's installation	3
K_O	= coefficient of earth pressure at rest	3
$K_{O(NC)}$	= coefficient of earth pressure at rest for normally consolidated sand	3
$K_{O(OC)}$	= coefficient of earth pressure at rest for overconsolidated sand	3
K_P	= coefficient of passive earth pressure	3
K'_P	= modified coefficient of passive earth pressure	6
K_S	= coefficient of earth pressure after placing the sand	3
LN	= length of the anchors group	4
MS	= midside anchor in a group of anchors	4
n - n	= normal line	5
N	= number of anchors in a group of anchors	6
Nq_u	= uplift capacity factor	3
OCR	= overconsolidation ratio	3
p	= pitch of the screw anchor	6

Symbol			Chapter
P_1	=	force acting on the anchor's shaft during installation	6
P_{1x}	=	horizontal component of the force P_1	6
P_{1y}	=	vertical component of the force P_1	6
P_2	=	force acting on the sand column overlying anchor's blade during installation	6
P_{2x}	=	horizontal component of the force P_2	6
P_{2y}	=	vertical component of the force P_2	6
P'_{2y}	=	force	6
P''_{2y}	=	force	6
P'''_{2y}	=	force	6
P_{dg}	=	surcharge pressure acting on a deep group of anchors	5
P_{ds}	=	surcharge pressure acting on a deep single anchor	5
P_f	=	perimeter of the failure surface of a group of anchors	5
P_g	=	perimeteree of a group of anchors	5
P_{tdg}	=	perimeter of a transit deep group of anchors	5
P_{tds}	=	perimeter of a transit deep single anchor	5
Q_u	=	experimental value of ultimate pullout load of a single anchor	3
Q_{ug}	=	experimental value of ultimate pullout load of a group of anchors	4
QU_{dg}	=	theoretical value of ultimate pullout load of a deep group of anchors	5
QU_g	=	theoretical value of ultimate pullout load of a group of anchors	5
QU_s	=	theoretical value of ultimate pullout load of a single anchor	5
QU_{tg}	=	theoretical value of ultimate pullout load of a transit group of anchors	5
QU_{ts}	=	theoretical value of ultimate pullout load of a transit single anchor	5
r_1	=	radius of revolution	5
r_2	=	radius of revolution	5
r_3	=	radius of revolution	5
r_4	=	radius of revolution	5
r_0	=	initial radius of revolution	5
r_ω	=	radius of revolution at an angle ω	5
RR	=	radius of circle of intersection of the rupture surface with the sand surface	5

Symbol			Chapter
RT	=	radius of circle produced from the intersection of a tangent to the rupture surface in the case of deep anchor, with a horizontal plane	5
S	=	center to-center spacing between anchors	4
t	=	thickness of the screw blade	6
t - t	=	tangential line	5
T	=	total value of installation torque	6
T_1	=	torque	6
T_2	=	torque	6
T_3	=	torque	6
T_4	=	torque	6
T_5	=	torque	6
T_6	=	torque	6
T_7	=	torque	6
U	=	upward displacement	3
U_u	=	upward displacement at ultimate pullout load	3
v - v	=	vertical line	5
V	=	volume	5
V	=	vertical pushing down force	6
V_1	=	vertical force	6
V_2	=	vertical force	6
V_3	=	vertical force	6
V_4	=	vertical force	6
V_{ds}	=	volume of sand inside the rupture surface of a deep single anchor	5
V_{ss}	=	volume of sand inside the rupture surface of a shallow single anchor	5
$VSR_{(NC)}$	=	vertical shearing resistance of a normally consolidated sand	5
$VSR_{(OC)}$	=	vertical shearing resistance of an overconsolidated sand	5
W_1	=	weight	5
W_2	=	weight	5
WD	=	width of the anchors group	4
W_{dg}	=	weight acting against uplift in the case of deep group of anchors	3
W_{ds}	=	weight acting against uplift in the case of deep single anchor	3

Symbol			Chapter
W_{sg}	=	weight acting against uplift in the case of shallow group of anchors	3
W_{tdg}	=	weight acting against uplift in the transit phase of a deep group of anchors	3
W_{tds}	=	weight acting against uplift in the transit phase of a deep single anchor	3
W_{tsg}	=	weight acting against uplift in the transit phase of a shallow group of anchors	3
W_{tss}	=	weight acting against uplift in the transit phase of a shallow single anchor	3
W_{sg}	=	weight acting against uplift in the case of shallow group of anchors	3
x'	=	distance	6
x''	=	distance	6
x'''	=	distance	6
X	=	distance	6
X'	=	distance	6
X_ω	=	distance	6
Z_1	=	constant	6
Z_2	=	constant	6
α	=	constant	5
α_1	=	angle of revolution	5
α_2	=	angle of revolution	5
α_3	=	angle of revolution	5
α_4	=	angle of revolution	5
β	=	constant	5
γ	=	unit weight of the sand	2
δ	=	angle	5
δ	=	angle of friction between the anchor's material and the sand	6
δ_s	=	sand surface deflection	3
θ	=	angle	5

Symbol			Chapter
μ	=	Poisson's ratio	3
π	=	constant equals 3.142 approximatly	5
ρ	=	radius of curvature	5
Σ	=	sum	6
σ_A	=	effective lateral stress in the active state	3
σ_F	=	effective lateral stress at failure	3
σ_I	=	effective lateral stress after anchor's installation	3
σ_n	=	normal stress	3
σ_O	=	effective lateral stress at rest	3
σ_P	=	effective lateral stress in the passive state	3
σ_S	=	effective lateral stress after placing the sand	3
τ	=	shear stress	3
ϕ	=	angle of shearing resistance of the sand	2
ϕ'	=	the amount of increase in the angle of shearing resistance of the sand due to densification effect	5
ϕ_{AI}	=	the value of the angle of shearing resistance of the sand after installation	5
ψ	=	helix angle of the helical-shaped screw unit	6
ω	=	angle of revolution	5
$\int$	=	integral	5

CHAPTER 1

Introduction

In many applications in the Civil Engineering practice, the requirement to resist substantial uplifting force or overturning moment arises. A conventional solution for such a problem is to provide the structure by a massive-sized foundation able to withstand the unstabilizing forces. An economical competitive alternative to the massive-sized foundation is a light weight foundation provided by anchors. Anchors are structural elements that can be found in a variety of configurations. They exist as footing, plate, cylinder, sphere, cone, and single or multi pitch helical screw. Anchors can be made of steel or concrete, whereas screw anchors are usually manufactured from steel. Single screw anchors can be made of a prefabricated steel screw helix element and a steel shaft connected together by suitable means, or as a helical-shaped circular steel plate welded to a steel rod. For multi helix screw anchors, the helical-shaped steel plates are welded to the steel rod at a predetermined spacing.

The placement technique for the plate, cylindrical, spherical, and conical anchors, is accomplished by excavating a hole in the ground and placing the anchor unit inside, then the hole is back filled or filled by concrete or grout. This procedure results in an appreciable disturbance to the initial soil properties (unit weight and angle of shearing resistance). Screw anchors are installed into the soil by applying torque to the anchor's shaft where it advances into the virgin soil due to the existence of the self-propelled unit. This minimizes the disturbance of the original soil. Figure 1.1 shows the use of the screw anchors to resist substantial overturning moment produced by a tower of power transmission. Figure 1.2 shows the use of the screw anchors to resist an overturning moment resulting from deep

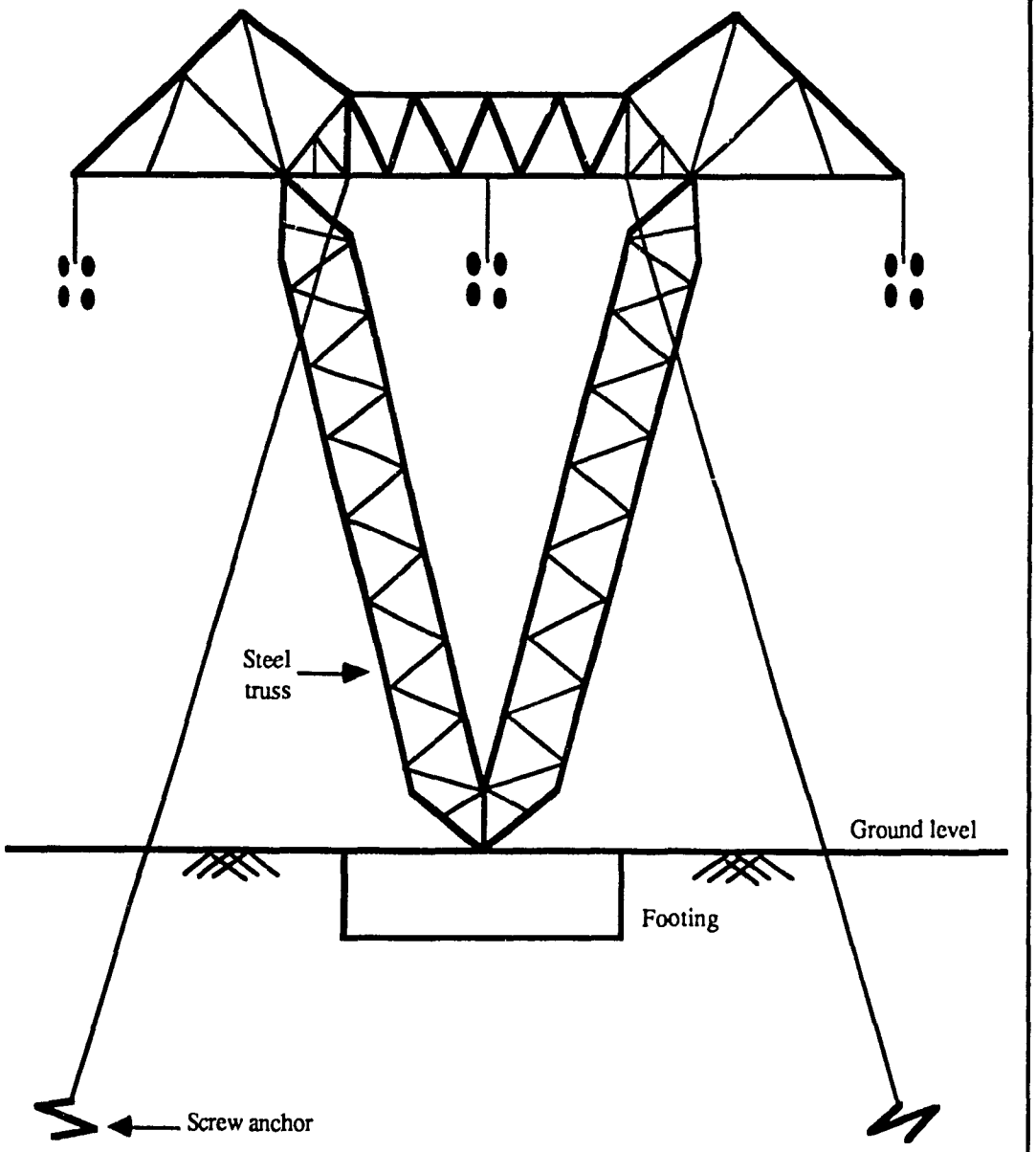

Fig. 1.1: The use of screw anchors to support guyed "V" transmission line tower.

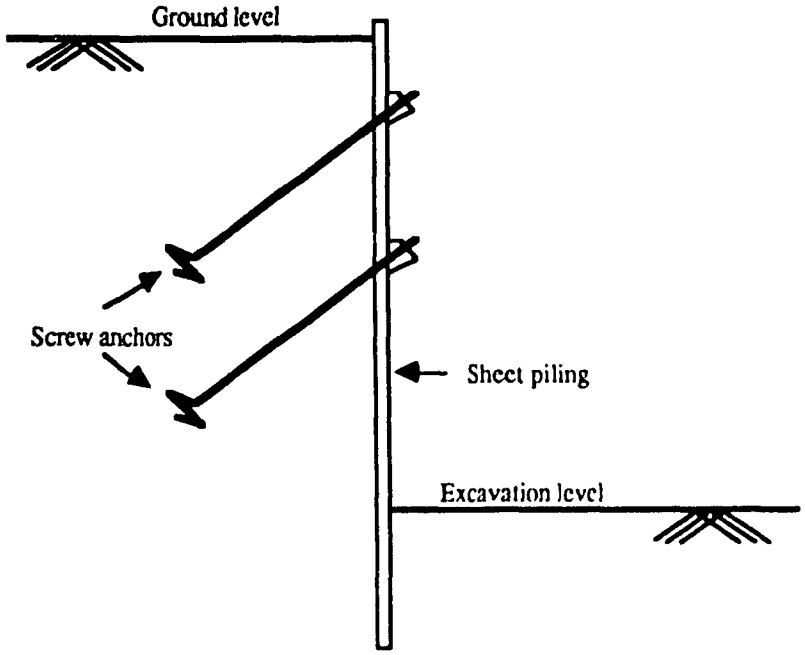

(a) The use of screw anchors with a sheet piling supporting deep excavation.

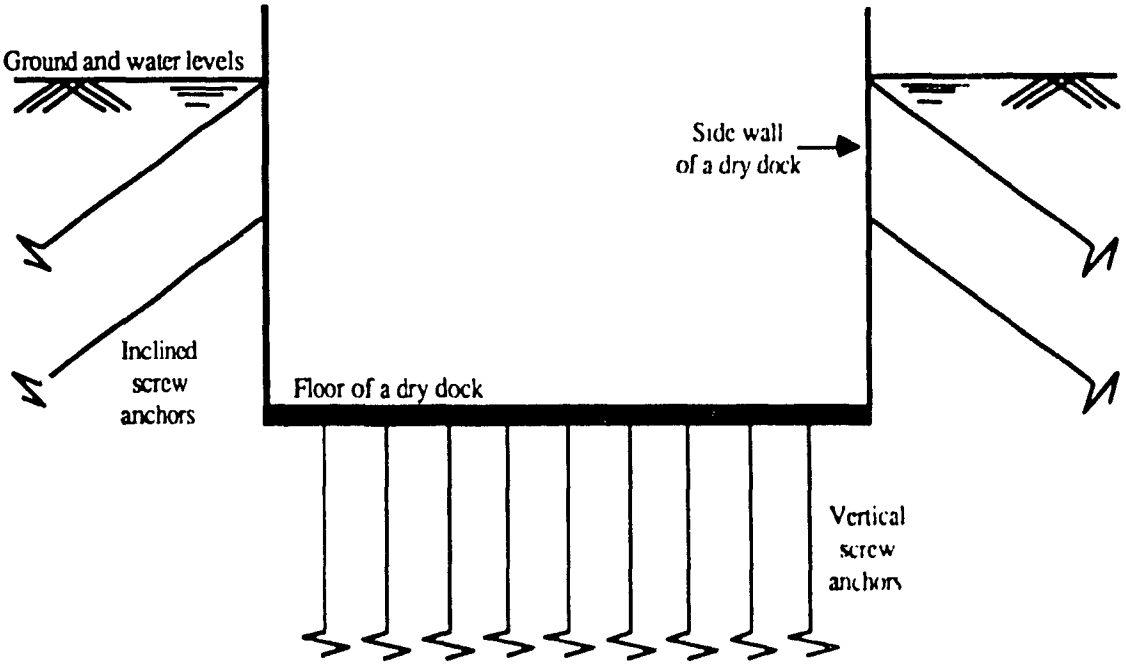

(b) The use of screw anchors in marine structures.

Fig. 1.2: Field applications of the screw anchors in the civil engineering practice

excavation, and uplifting force due to the existence of high water table such as the case of hydraulic and marine structures.

The present research program is directed to present the results of an experimental and theoretical study on the performance of single screw anchors as well as the group action of anchors installed in sand. Five different types of model screw anchors were tested to investigate the influence of the shape of the screw unit on the pullout behaviour and the installation torque. Anchors were installed in sand layers previously prepared according to a developed calibrated placement technique to obtain the required unit weight and angle of shearing resistance. Stress transducers were located inside the sand deposit to measure stress variation due to the adopted sand placing technique, anchor installation, pullout load application, and anchor's failure. Displacement transducers were positioned on top of the sand surface in order to measure the sand surface deflection. These measurements, together with side experiments on coloured-layered sand, were employed to define the shape of the rupture surface which was defined as a segment of a logarithmic spiral. These observations were used to develop a theoretical model to predict the uplift capacity of screw anchors. Stress was calculated on the observed surface of rupture utilizing Kotter's defferential equation. Based on stress measurements, the sand tested in the present investigation was found to be overconsolidated sand due to the utilized placing technique. The value of the overconsolidation ratio (OCR) was determined for all tested depths and sand types. The OCR was found to be increasing with the depth of sand and with the angle of shearing resistance. Based on data reported in the literature, an empirical relation was proposed to relate the uplift capacity of overcondolidated sand to that of normally consolidated one, by using the value of the OCR.

A testing program was conducted to explore the influence of the group configuration, group size, center-to-centre spacing between anchors, order of anchors' installation, and embedment depth ratio on the group performance in uplift. The uplift load distribution amongst the individual anchors of the group was also studied, together with its effect on the differential upward displacement of the individual anchors of the group. Proper modifications

were applied to the proposed theory to make it suitable to predict the uplift capacity of a group of anchors. An empirical formula was proposed to account for the densification effect that a group of anchor causes to the sand during the installation process. Comparison of the experimental and theoretical results showed good agreement.

Based on the results of the experimental investigation, the factors affecting the value of the installation torque were identified. A theoretical model was developed, from which the required installation torque value can be predicted. A torque factor was established, and a correlation between this factor and the uplift capacity factor was proposed utilizing the theoretical torque values, together with the uplift capacity estimated from the proposed theory for uplift capacity determination. From this correlation, the uplift capacity of a screw anchor can be determined from the measured installation torque value.

CHAPTER 2

Review of Previous Work and Scope of Research

2.1 Review of Previous Work

Anchors may be found and used in a variety of configurations. They exist as footing, plate, cylinder, sphere, bulb (cone), concrete block, steel block, injected shaft, single screw or multi screw. Published materials on screw anchors, generally, and single screw anchors, specially, are scarce. This chapter reviews the important contributions of different researchers reported in the literature with special emphasis on screw anchors.

Balla (1961) [6], studied the performance of mushroom foundations, experimentally and theoretically. Based on laboratory model test observations, he indicated that the failure mechanism of this type of foundation is of curved surface. He represented this surface by a circular arc, the tangent of which is vertical at the upper edge of the foundation slab and, at the ground level, the tangent intersects the latter at an angle of $(45° - \phi/2)$ (Fig. 2.1). Theoretically, Balla considered that the problem of breaking out resistance of mushroom foundations is a plane stress one. He concluded that the total resistance against breaking out is the summation of the dead weight of the soil body within the failure surface, the weight of the foundation, and the resultant shear stress acting on the sliding surface. He introduced empirical coefficients to account for the soil characteristics and the geometrical properties of the foundation. Balla reported good agreement between his experimental and theoretical results, however, the comparison was limited to a depth-diameter ratio of 3.3 (maximum tested ratio).

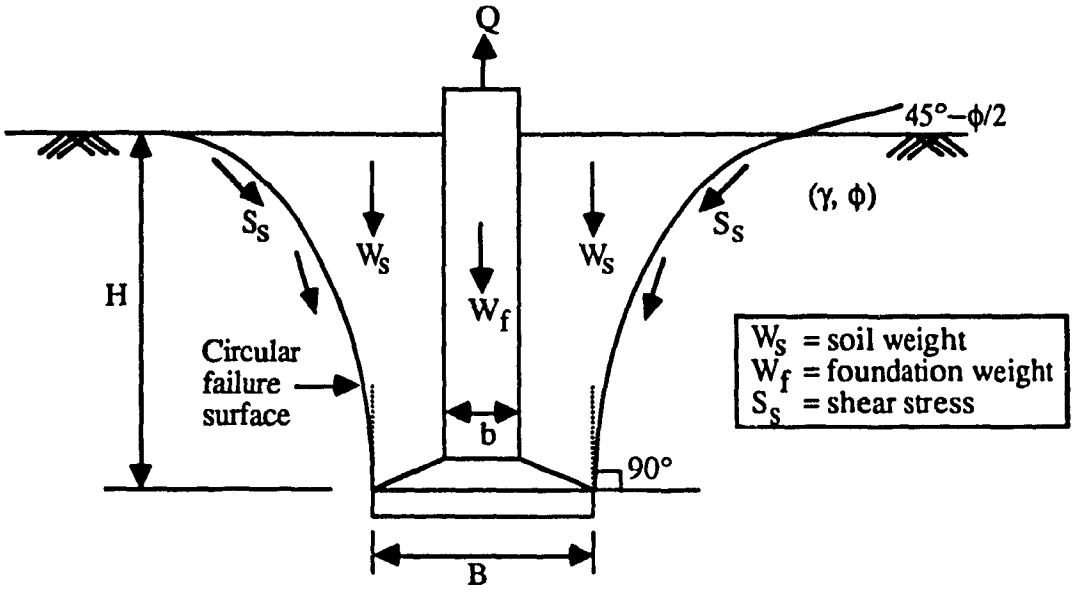

Fig. 2.1: Proposed failure surface for mushroom foundations; after Balla, (1961).

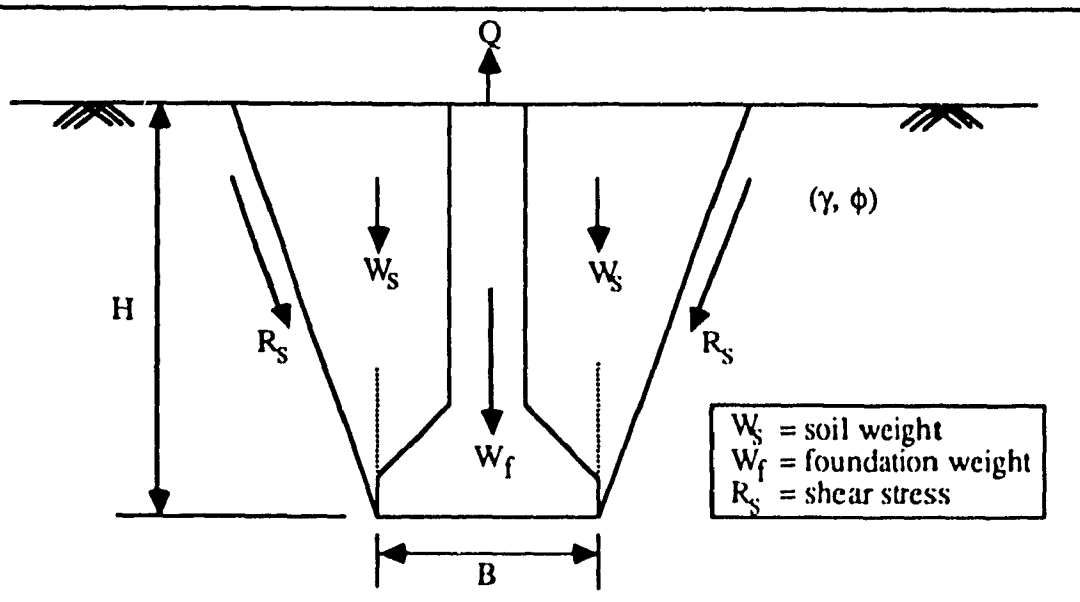

Fig. 2.2: Conical failure surface for underreamed footings; after Turner, (1962).

In 1962, Turner [64] conducted a number of laboratory tests on the uplift resistance of the transmission tower footings. He evaluated some of the existing theories and introduced empirical relationships to correlate the uplift resistance of footings to the geometrical properties of the footing and the soil characteristics. He considered that the uplift resistance of an underream footing is the sum of the shear resistance along the failure surface and the weight of the footing. He adopted the cone concept in his theoretical model for the uplift capacity determination. This concept assumes that the failure surface is of conical shape with side walls inclined at a certain angle to the vertical (Fig. 2.2). Based on the experimental results, Turner defined the limiting value of H/B = 1.5 (H is the footing embedment depth and B its diameter) as a separating value between shallow and deep footings. He stated that beyond this ratio, the uplift resistance is not significantly influenced by depth increase.

Trofimenkov and Mariupolskii (1965) [62], reported the results of field investigation on screw piles used for tower foundations. The experimental program included a large number of tests on single and groups of piles. The screw piles were installed with the aid of a self-propelled unit firmly attached to the pile's body. Based on test results, they have given a method to determine the bearing capacity as well as the uplift resistance of these piles. According to this method, the uplift resistance of screw piles is a function of soil strength parameters (unit weight, γ and angle of shearing resistance, ϕ) and the depth of the pile plate. From their experiments they concluded that a critical depth/diameter ratio of 5 to 6 is the limit of discrimination between shallow and deep piles. Also, they have shown that the action of a group of piles spaced at a distance of 1.5 B (B is pile diameter) is equal to that of the single pile in the same soil conditions and at the same depth.

In 1967, Adams and Hayes [2] presented full detailed field and laboratory tests on the behaviour of shallow foundations subjected to uplifting forces. They utilized the results of these tests, in conjunction with the available theories, to introduce an approximate general solution for predicting the uplift resistance of foundations subjected to uplift. From the

laboratory model tests, they recorded the mode of failure photographically. They concluded that the failure mechanism in sand under uplift loading is of complex nature. Moreover, they stated that the shape of failure in dense sand is distinctly different from that of loose sand, and consequently the degree of shear mobilization is certainly different. To provide a practical design procedure, they assumed that the failure surface is a cylindrical one and the pullout resistance is the friction force mobilized on the surface area of the cylinder, projected on the perimeter of the anchor, together with the weight of the soil enclosed by the cylinder (Fig. 2.3). Based on this method of uplift capacity calculation, they reported reasonable agreement with the results of full-scale uplift tests.

Meyerhof and Adams (1968) [42], studied the uplift capacity of footings by conducting and evaluating the results of model and full-scale tests. They examined the failure mechanism of shallow and deep footings (Fig. 2.4). Using simplifying assumptions, they presented a general theory from which the ultimate pullout resistance of foundations subjected to uplift can be calculated. They concluded that the uplift capacity is a combination of the soil weight and the shear resistance mobilized on the boundary representing the failure surface. Based on test results, they stated that the geometrical properties of rupture surface varies with the foundation's depth/width ratio and on the relative density of the sand. They modified their general theory to take into account the effect of continuity of strip footing. They based their solution to this problem on the assumption that the forces are considered to be acting on a cylindrical surface above the foundation's perimeter. They applied shape factors to account for the three-dimensional effect of an individual square or circular footing. In addition, they introduced simplifying modifications to the general theory in order to calculate the uplift capacity of a group of footings. They reported reasonable agreement with the field results.

Robinson and Taylor (1969) [49], provided the criteria upon which the selection of anchors for guyed transmission towers has been based. They have conducted full scale tests on five types of anchors, namely, buried plate with compacted backfill, buried steel mat or grillage with loose backfill, cast in place concrete with loose backfill, power installed screws,

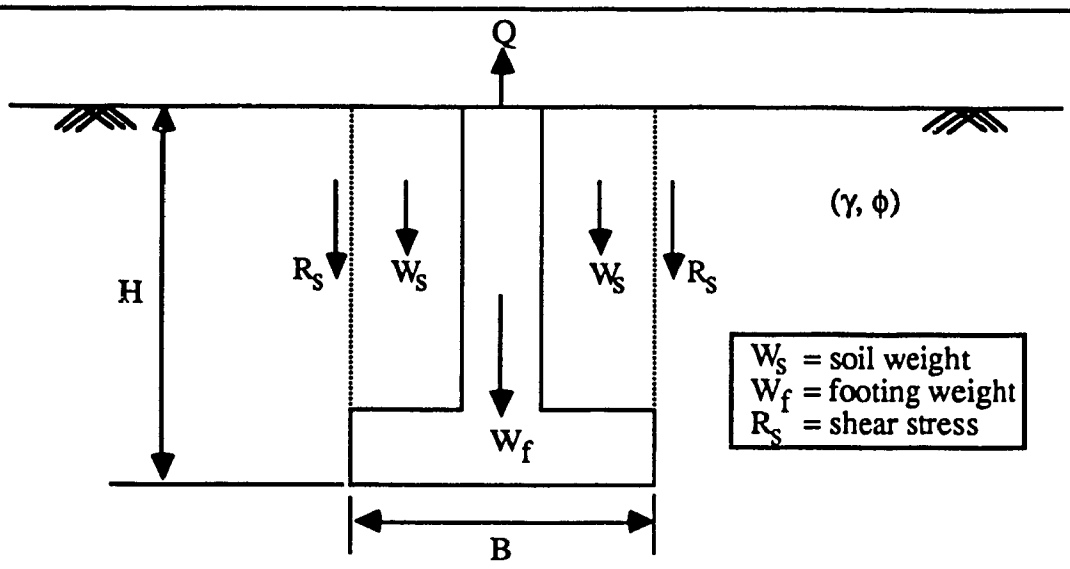

Fig. 2.3: Cylindrical failure surface for shallow footing; after Adams and Hayes, (1967).

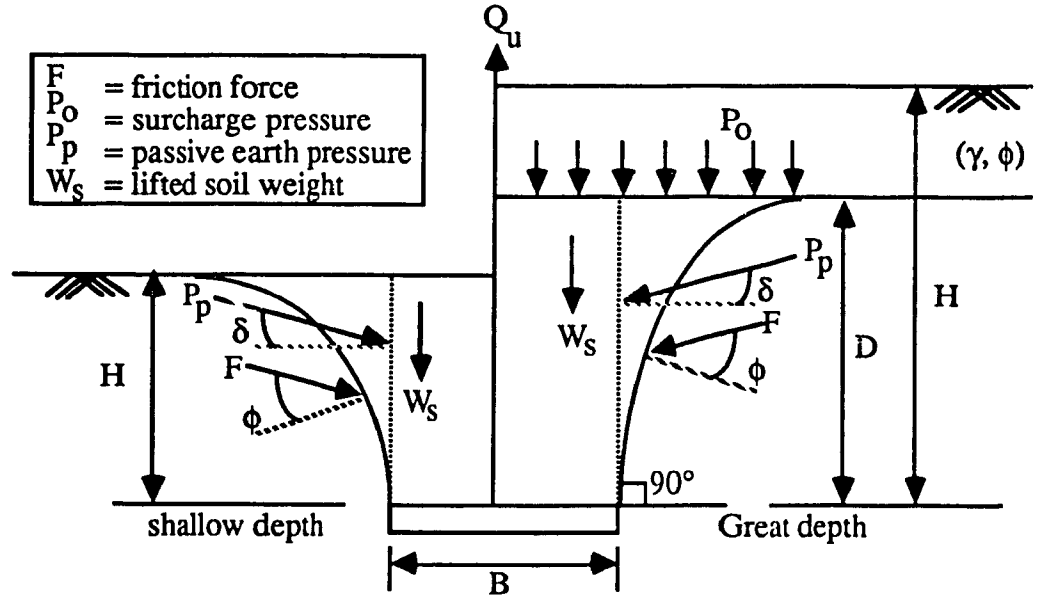

Fig. 2.4: Proposed failure surfaces for shallow and deep footings; after Meyerhof and Adams, (1968).

and grouted rod anchors (Fig. 2.5). They aimed to find the suitable type of anchors to be used in the erection of transmission line towers crossing difficult terrain with a wide range of soil conditions. Based on the field test results, they concluded that the plate and grillage anchors are too expensive because of the compactive effort and control required to ensure satisfactory backfill. They also stated that the cast in place concrete anchors backfilled with loose soil provided suitable solution at a relative low cost. They reported that the screw and grouted rod anchors provide an acceptable alternative for competitive bidding in some soil conditions and they are comparable in cost in case of uniform soil conditions.

Sowa (1970) [55], examined the behaviour of cylindrical straight shaft cast-in-place bored piles. This type of piles has been chosen to provide adequate resistance against upward pulling loads as well as downward bearing loads. From the data provided by the experimental field tests he indicated that the pulling capacity of these piles in sandy soils is considerably difficult to estimate. He reported that it depends on the skin friction developed by the lateral pressure effective on the pile shaft and the weight of the pile. He showed that the lateral pressure varies over a wide range, depending on the procedure of excavating the pile hole and on the subsequent placement of concrete. He indicated that a major disadvantage of this type of pile is that its resistance against uplift is low. Sowa concluded that the calculation of the uplift capacity of cast-in-place bored piles should include the arching effect of the concrete during placement and the influence of the method of boring the hole and placing the concrete on the coefficient of lateral pressure. To increase the effective lateral pressure and the corresponding skin friction, he recommended rapid placement for the concrete and vibrating it thoroughly.

In 1971, Carr and Hanna [7] developed a mechanical method to measure the sand movement in the vicinity of laboratory scale circular anchor plate. They installed gages to measure the horizontal movement during sand bed preparation in predetermined locations. Vertical movement was measured by gages fixed to a rigid plate above the sand surface and pushed through conductor tube to the required position inside the sand deposit (Fig. 2.6). The vertical and horizontal components of the sand movement have been measured at every position

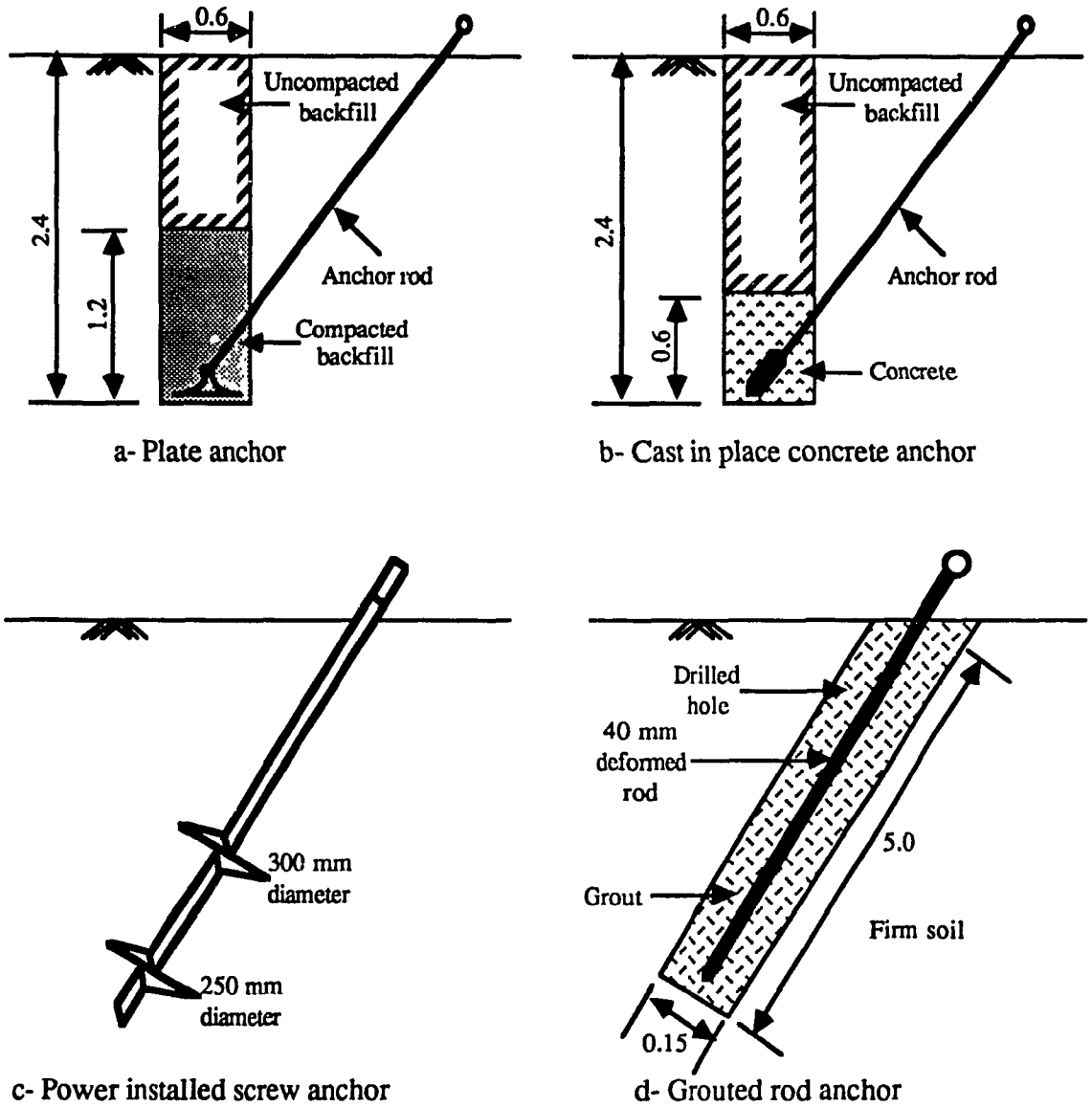

Fig. 2.5: Selection of anchors for guyed transmision towers; after Robinson and Taylor, (1969).

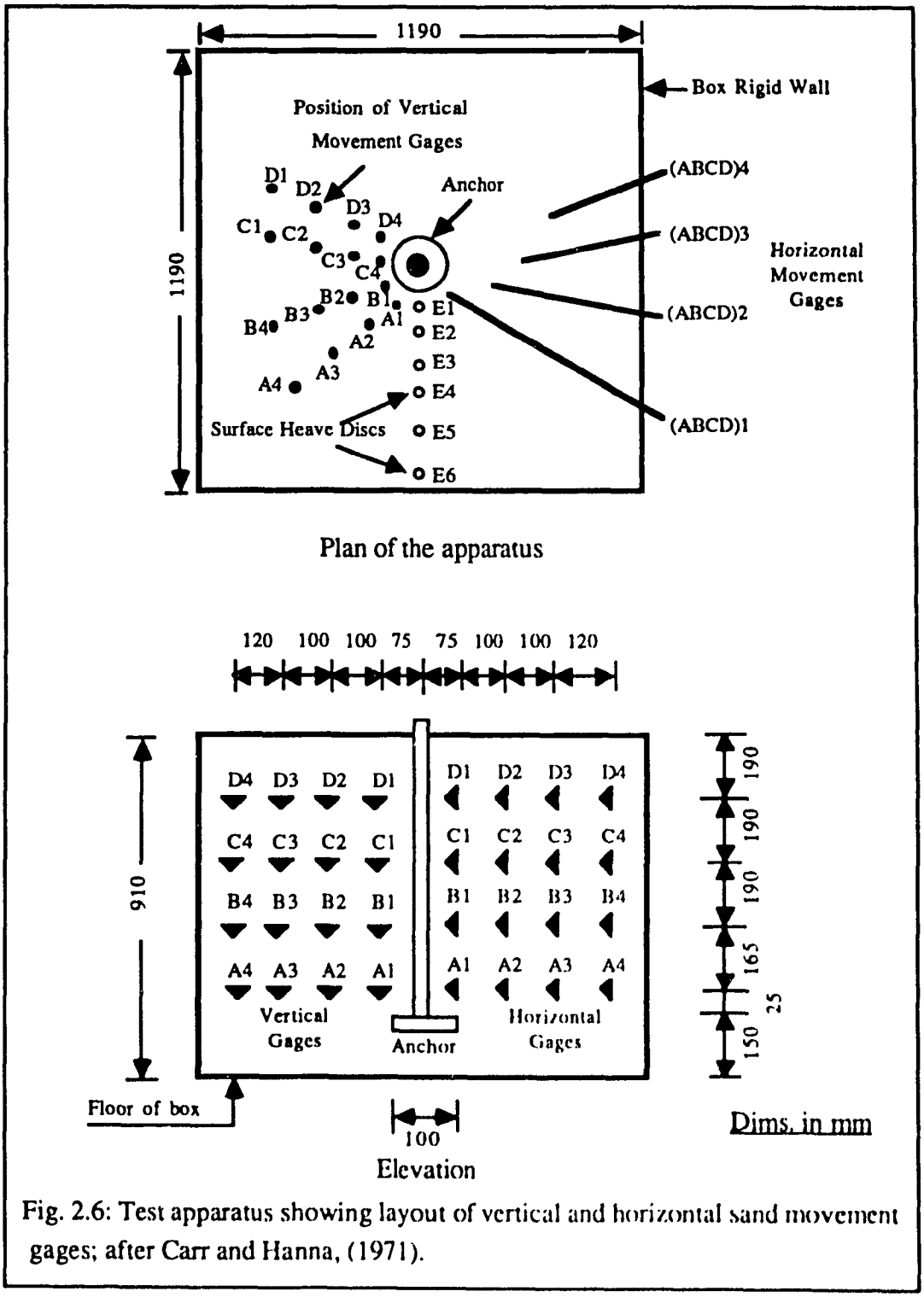

Fig. 2.6: Test apparatus showing layout of vertical and horizontal sand movement gages; after Carr and Hanna, (1971).

of the gages. They showed that the sand movements around an anchor plate are symmetrical. They also reported that the sand movement vector is almost a straight line whose direction is independent of the applied load level. Carr and Hanna noted that the influence of the movement gage instrumentation of the uplift load was not significant at loads less than 50% of the ultimate value, while an increase of about 5% was recorded at failure. They concluded that this system of sand movement measurement is useful, however, reliable data can be obtained by using larger scale of testing.

Hanna and Carr (1971) [20], studied the loading behaviour of plate anchors in normally and overconsolidated sands. They conducted laboratory tests in an apparatus specially developed, such that any desired stress state in the sand mass can be created (Fig. 2.7). They indicated that the pullout capacity of an anchor in sand is not a unique one and it is dependent on the initial stress level existing in the sand mass. They have shown that the peak uplift capacity of an anchor plate in a normally consolidated sand increases in proportion to the depth of burial. For constant depth of embedment, the uplift capacity of anchors in overconsolidated sand increases with the increase in overconsolidation ratio and approached a limiting value at a large overconsolidation ratio. Hanna and Carr compared results of tests performed in normally consolidated sand with tests performed in overconsolidated sand where the preconsolidation pressure is equal to the surcharge pressure of the normally consolidated tests. They concluded that at low overconsolidation ratios, the peak uplift loads were slightly smaller in the overconsolidated sand but a considerable decrease was recorded at higher overconsolidation ratios. They attributed that to the unability of the sand to retain all of the initial stress system setup during the overconsolidation stage.

In 1971, Healy [24] conducted a laboratory and field testing program on the pullout resistance of anchors buried in sand. He directed his study to clarify the relationship between sand density, anchor size, overburden stress, and pullout resistance of anchors buried in sand. The tested anchors were smooth balls made of wood or concrete and the sand was tested in loose and dense states. Healy developed a test set-up allowing the application of an overburden

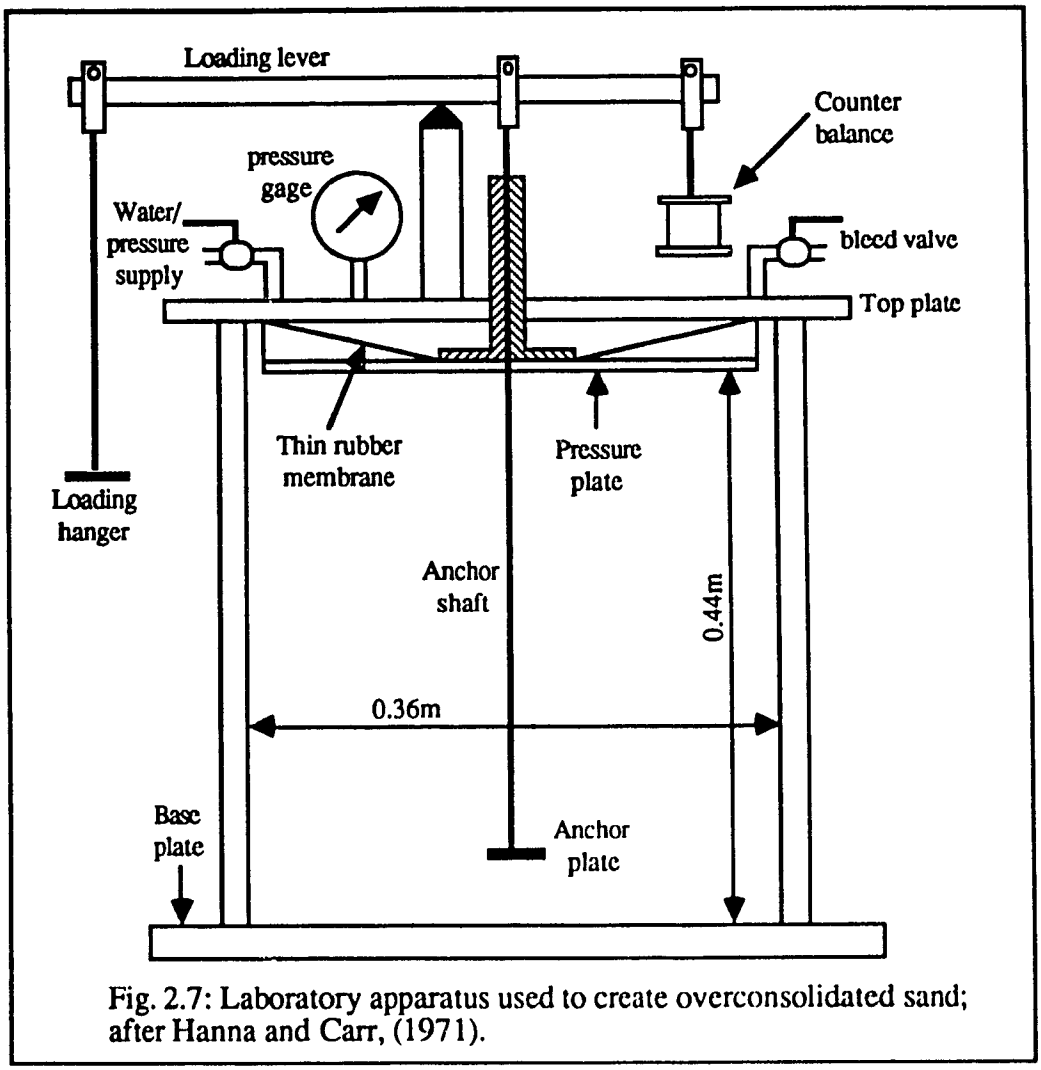

Fig. 2.7: Laboratory apparatus used to create overconsolidated sand; after Hanna and Carr, (1971).

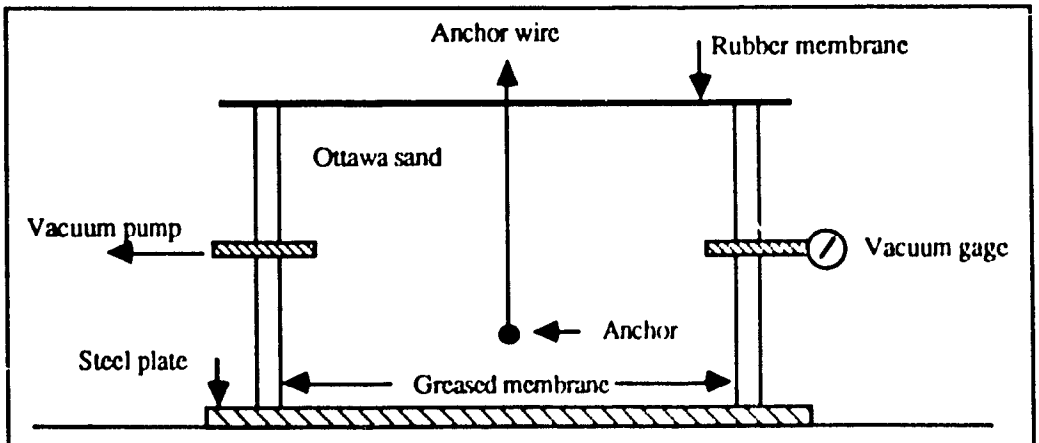

Fig. 2.8: Laboratory equipment used by Healy, (1971).

pressure over the entire depth of the sand by means of flexible rubber membrane (Fig. 2.8). Based on test results, Healy indicated that no peak in the pullout load was recorded versus the anchor's movement, for either the loose or the dense sand. However, a cavity of about one-quarter of the anchor diameter was developed underneath the anchors as they were pulled up. The sand surface rise was less than 0.01 mm when the embedment depth ratio was at least 6. He concluded that, at these depths all the plastic flow was occurring below the sand surface. He also concluded that, when the embedment depth ratio is at least 6, the pullout resistance of anchors in dense sand varies directly with overburden stress and this ratio is 2 for loose sand. Also, the average pullout stress of anchors in dense sand decreases as the anchor size increases while it is independent of anchor size in case of loose sand.

Khadilkar et al., (1971) [32] studied the rupture surface and ultimate pullout resistance of piles with enlarged base (underreamed piles). They conducted laboratory model tests on a one-sided glass plate steel tank to facilitate recording the geometry of rupture surface. They also placed white sand layers within the sand deposit for accurate determination of the rupture surface. They observed that the experimentally developed rupture surface can be closely approximated to a segment of a log-spiral. Moreover, they indicated that the pile is pulled out initially with a cylindrical cavity followed by a log-spiral rupture. Based on test results, they showed that the pullout capacity of underreamed piles is the summation of the dead weight of the foundation and the broken out soil, and the vertical component of shearing resistance mobilized along the rupture surface. They derived mathematical expressions for calculating the uplift capacity utilizing Kotter's equation for the variation of stresses along the rupture surface. They concluded that the shear resistance mobilized along the rupture surface represents the largest portion in the total uplift capacity.

In 1971, Vesic [66] examined the behaviour and the breakout resistance of objects embedded in ocean bottom. He identified the components that making the total value of the breakout force. He adopted a circular failure surface similar to that proposed by Balla (1961), Fig. 2.1. He noted that this assumed failure surface is not applied to very deep anchors as they

do not fail in general shear failure. He indicated that these anchors move vertically a considerable distance during pulling out by producing a failure pattern similar to punching shear in deep foundations. From his experiments, Vesic indicated that the critical relative depth ratio (H/B), separating between shallow and deep anchors, can not be assigned to a single value as this ratio differs from one type of sand to another and it depends on the sand relative density. He developed a theory to predict the uplift capacity of embedded objects, yet poor agreement was achieved when the experimental and theoretical values were compared, although the theory confirms the expected general trend. Vesic reported that the problem of breakout resistance of embedded objects is of a very complex nature and he concluded that there is no solution that can be fully satisfactory for all cases because it remains limited to a particular soil type and a particular set of placement and pullout conditions.

Adams and Klym (1972) [3], conducted field investigations at seven different sites to study the performance of multi-helix and grouted anchors. The multihelix anchor used in this investigation consists of a number of helix plates, varying in size, attached to a rod or pipe extending to the surface. Every grouted anchor was reinforced by a single reinforcing rod They also carried out a few tests to investigate the group action of these anchors in uplift and compression. They made an attempt to analyze the test results with the conventional theories of bearing capacity. They assumed that the helix plates would mobilize approximately the same capacity in uplift as in bearing because of the large ratio of depth to helix diameter They employed the bearing capacity theory for uplift determination and they utilized the field test results to provide numeric values to the uplift capacity factor They concluded that this method of uplift capacity calculation appears to be good indication for giving a preliminary estimate of the uplift capacity of these anchors They also concluded that the multi helix and the grouted anchors can be successfully used in groups to provide foundation for both bearing and uplift loading

Hanna et al (1972) [22], studied the behaviour of [illegible] and groups of plate anchors in normally consolidated and overconsolidated sand They carried out a program of laboratory

scale experiments. They showed that the uplift resistance of a single plate anchor increases rapidly with the increase of overconsolidation ratio up to about 4, then it almost linearly increases with the increase of the overconsolidation ratio. Hanna et al. examined the efficiency of anchor groups, load distribution among the anchors in the group, sand movement around the group, and group size and configuration. Based on test results they indicated that the efficiency of the group was generally less than 100% for H/B $\leq$ 12 and S/B $\leq$ 4 (S = center to center spacing between anchors). They also reported that load distribution among the anchors is almost uniform at low load levels, while the central core of anchors carries the smallest load when approaching the moment of failure. They concluded that the movement of an average anchor in a group is generally greater than that of an isolated anchor loaded at the same load level.

Vesic (1972) [67], presented a theoretical solution for the problem of expansion of cavities in infinite soil mass. He considered, in his derivation, the case of the spherical cavity as well as the cylindrical one. He considered the soil to behave as a rigid plastic, incompressible solid in a plastic region surrounding the cavity, and as a linearly deformable solid beyond that region. He introduced the effect of volume change in the plastic region as a parameter and he evaluated its importance numerically. Vesic concluded that the principal parameters affecting ultimate pressure are the initial effective ground stress, strength and volume change characteristics of the soil, and its rigidity index. He defined the rigidity index of the soil as the ratio of its shear modulus to its initial shear strength. Vesic summarized the general solution of the problem of expansion of cavities in the form of tables and graphs suitable for application in engineering practice. He stated that this method of calculation can be an effective tool for bearing capacity determination of deep foundation, as well as the calculation of breakout resistance of anchors.

Larnach and McMullan (1974) [37], examined the performance of inclined groups of plate anchors embedded in sand. They carried out laboratory model tests on groups of up to 16 anchors. They reported that the load distribution amongst the anchors within a group is

complex and it depends on many factors such as group size, depth, spacing, cap stiffness, testing scale, degree of inclination, and the applied load level. Based on test results, they indicated that efficiency of a group of anchors increases by the increase of spacing. They concluded that two phenomenae of interference between anchors are existing. At very close spacing (S = 4B), the interference is intense and at wider spacings this interlock effect is reduced by the anchors tend to act as individuals. They suggested that some interferences can still occur at spacings of the order of 14B.

Radhakrishna (1976) [48], reported the results of a field investigation on helix anchors in sand. He tested different sizes of single and multi-helix anchors installed to shallow and deep depths. He also investigated the group action of multi-helix anchors spaced at three times the largest diameter of the anchors helixes, where he observed group efficiency of about 60%. Radhakrishna estimated the uplift capacity of single helix anchors by using standard bearing capacity formulae. He applied the same formulae to the case of multi helix anchors but a lower value for the uplift coefficient factor was considered, due to the interference between individual helix plates. Following this method of uplift capacity calculation, Radhakrishna observed good agreement between theoretical and experimental results. Based on test results, he concluded that the uplift capacity of a single helix anchor increases significantly with depth and reaches a maximum value at a certain depth beyond which it remains constant. He also indicated that the triple helix anchor with tapered plate sizes exhibits a much higher uplift capacity than the anchor with uniform plate sizes. He attributed this behaviour to the difference in the degree of soil disturbance caused by each type of anchors during installation process.

In 1979, Udwari et al. [64] suggested a rational approach for the design of high capacity multi-helix screw anchors. They indicated that the design of multi helix screw anchors is usually provided by the manufacturer and it is often based on semi empirical methods of analyses formulated from load tests conducted on prototype anchors. They stated that the reliability of anchor design, based on these semi empirical methods and their associated assumptions, is not known. Also, they mentioned that the available methods of analysis

reported in the literature, appear to be limited in their range of applicability for design purposes. They listed all the factors that influence the uplift capacity of screw anchors and they concluded that a further consideration to these factors will provide reliable and efficient anchors' design. Udwari et al. stated that an effort should be made to standardize the field test procedure so that the interpretation of test results, among the engineering profession, can be more meaningful.

Wang and Wu (1980) [71], conducted an experimental and analytical studies on the yielding load of anchors in sand. They observed that the shape of failure of vertical or inclined anchors, can be approximated to a straight line and a log-spiral. Based on the data obtained from the experimental investigation, they developed a theoretical model to calculate the yeilding load of anchors. They utilized the upper bound limit analysis to carry out the analytical approach. They presented equations to relate the rate of work done by external forces, acting on the rupture surface, to the rate of internal energy dissipation (force representing the yielding load). Also, they developed a computer program to solve this system of equations and to calculate the required values of the proposed factors. Wang and Wu reported that the results of the analysis agreed fairly well with the test results, and also compared satisfactorily with available data reported in the literature.

In 1981, Andreadis et al. [4] performed an experimental investigation on the response of embedded anchors to uplift loading. They concluded that the mode of failure is mainly controlled by the relative depth of embedment, soil relative density, and anchor shape. They indicated that the static breakout factors and relative anchor movements up to failure, increase sharply with relative depth of embedment at shallow depths, tending to an approximate constant at greater depths. Based on the experimenal results, Andreadis et al. stated that a significant horizontal stress developed in the sand mass might extended in a zone in excess of 10 times the anchor's diameter either side of a deeply installed anchor.

Clemence and Pepe (1984) [11], examined the effect of installation and pullout of multi-helix anchors on the lateral stress in the sand layer. Lateral stresses were measured

before and after anchor installation, at anchor failure, and continuously during the application of the uplift load. Lateral stress were measured by stress cells placed in the sand deposit, according to the arrangement shown in Fig. 2.9. The test results indicated that helical anchor installation causes considerable increase in lateral stress around the anchor. This stess increase was significantly larger in dense sand. Also, they reported that the lateral stresses increased as the anchor was loaded to failure. They attributed this behaviour to the effect of arching stresses and soil dilatancy develop in the sand as it was sheared by the anchor. Clemance and Pepe concluded that the magnitude of stress increase in the sand, due to anchor installation and/or pullout, is dependent on the relative density of the sand and embedment depth ratio.

In 1985, Kulhawy [35] presented an overview of the static uplift behaviour of shallow anchors. He discussed the installation technique of helical anchors and its effect on the development of the failure surface. He evaluated the failure modes and examined the effect of installation procedure on the shear strength of the soil mobilized on the observed shape of failure. For a single helix anchor, Kulhawy stated that the shearing resistance, developed on the failure surface, is controlled by the friction angle and state of stress in the disturbed cylinder of soil above the anchor. He approximated the disturbance effect by relating the disturbed properties to the in-situ properties using $\delta/\phi = 0.9$ and $K/K_o = 5/6$ where δ = average angle of mobilized shearing resistance of the failure surface, ϕ = angle of shearing resistance of the soil, K = coefficient of lateral earth pressure of disturbed soil, K_o = coefficient of earth pressure at rest. For multi-helix anchors, Kulhawy indicated that the installation disturbance is minimized due to anchor geometry and he stated that it is appropriate to use $\delta/\phi = 1$ and $K/K_o = 1$ in this case.

Mitsch and Clemence (1985) [43], presented results of field and laboratory investigations of the uplift capacity of multi helix anchors in sand. Based on experimental results, they indicated that a cylindrical soil failure surface develops below the top helical shaped plate during pullout and, above the top plate, the failure surface is dependent on the anchor

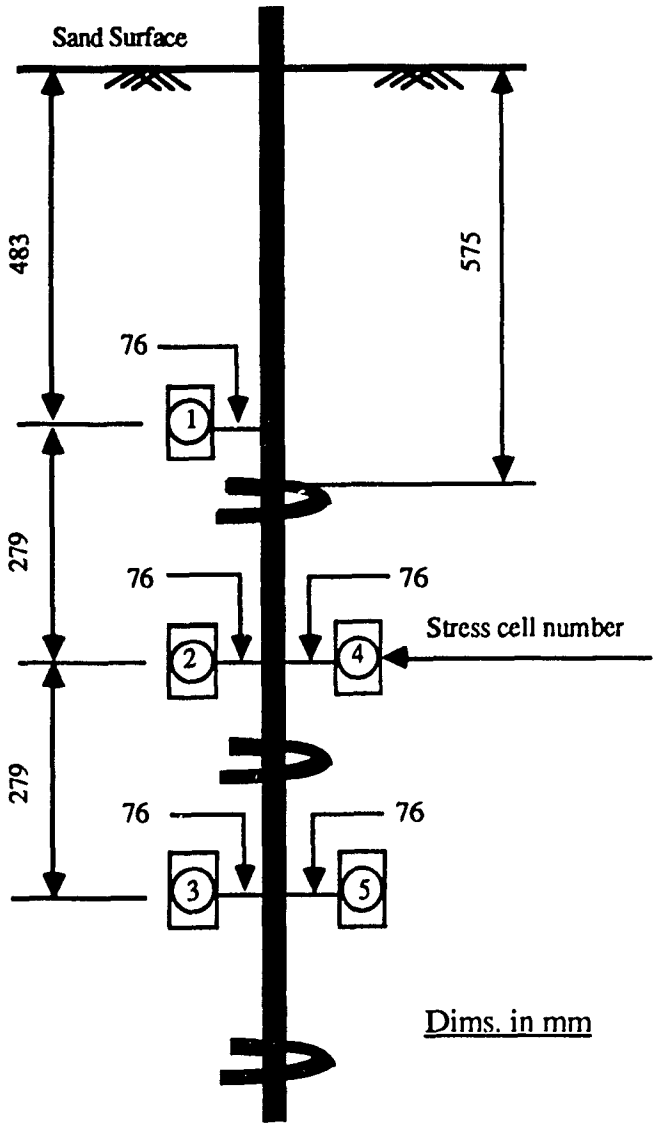

Fig. 2.9: Stress cell placement plan for multi helix anchor in deep state; after Clemence and Pepe, (1984).

embedment depth. They showed that the anchor installation technique, relative density of the sand, and embedment depth ratio influence the development of failure surface. They proposed a semi-emperical method to estimate the uplift capacity of helical anchors. This method is founded on the results of the laboratory study and suggests that the uplift capacity is made of bearing resistance on the upper helical plate, frictional cylinder resistance, and friction on anchor shaft.

Mitsch and Clemence proposed uplift coefficients for theoretical estimation of the uplift capacity of helical anchors. These proposed coefficients are dependent on soil friction angle and embedment depth. Also they have taken into account the effect of soil disturbance due to anchor installation.

In 1986, Ghaly [18] conducted an experimental investigation on five types of single screw model anchors installed in dry, submerged sand, and sand subjected to upward seepage flow. Model anchors were installed into prepared sand deposits in loose, medium and dense state. He utilized the test results to develop an analytical approach to predict the uplift capacity of these anchors. He presented modified values for the coefficient of passive earth pressure due to the difference between the assumed failure surface and the observed one. Also, he examined the effect of submersion of the sand layer on the uplift capacity of the anchors. He introduced a reduction factor to be applied to the analytical equations, to account for the submersion or for the existence of upward seepage flow.

Ghaly presented a theory to calculate the value of installation torque. He considered, in this analysis, the geometrical characteristics of the screw element as well as the properties of the sand deposit. He related the uplift capacity to the magnitude of the installation torque. He concluded that the results of such a study can be of good practical use.

Das and Jin (1987) [13], performed small scale laboratory experiment tests on the uplift behaviour of shallow horizontal circular single and group anchors embedded in sand. They

compared their results with available theories provided by previous researchers [42, 66]. They reported that the experimental value of the breakout factor increases with the embedment ratio and remains practically constant at deep depths. Based on test results of group anchors, they indicated that the uplift efficiency varies with the number of anchors, center-to-center spacing, embedment ratio, and soil friction angle. They concluded that for a given soil type, degree of compaction, and embedment ratio, the uplift efficiency of a given anchor group increases practically in a linear manner with spacing/diameter ratio to reach 100%. According to their tests, they showed that for a rectangular group configuration of 2x1 or 3x1 installed to an embedment depth ratio (H/B) of 4, the efficiency (E) of anchors group reaches 100% at spacing ratio S/B = 5, and for H/B = 6, E = 100% at S/B = 6. However, they reported substantial variation between test results and the theory of Meyerhof and Adams [42].

Murray and Geddes (1987) [45], investigated the uplift behaviour of anchor plates in sand experimentally and theoretically. They utilized the results of laboratory tests, together with limit equilibrium method of analysis to predict the ultimate resistance. They stated that the formulation of a satisfactory theory depends on the reliability of the assumed shape of failure. For shallow anchors that resist vertical uplift loads by developing a passive form of resistance, they showed that the failure surface is a curved one and for practical considerations, it can be considered an inverted conical shape. They considered the angle of inclination of the cone surface to the vertical equal to ($\phi/2$). Also, they adopted an average value of the mobilized angle of shearing resistance of ($3\phi/4$). For theoretical determination of uplift capacity, they assigned the coefficient of lateral earth pressure to a value equal to the lateral earth pressure coefficient at rest (K_o). They concluded that in some cases there is a scatter of plots when theoretical and experimental results are compared. They attributed these discrepancies to the inability to describe mathematically the stress history or degree of overconsolidation of the sand arising from the sand placement techniques.

Rodgers (1987) [50] and Weikart and Clemence (1987) [72], reported several case histories on the behaviour of multi-helix screw anchors which have been designed to provide

combined resistance against uplift and bearing forces. This type of anchor was chosen because of the light equipment required for installation at sites where difficult construction conditions were encountered. The manufacturer recommended that the anchor should be installed to a depth where a predetermined magnitude of installation torque should be reached in order to get the required uplift resistance. The recommended installation depth and installation torque were designed based on soil nature, type of screw anchors, required uplift capacity, permissible displacement, and machinery provided for construction. The authors concluded that the field performance confirmed that sufficient resistance against bearing and uplift was developed by the anchor foundation.

Weikart and Clemence presented an empirical expression to correlate the ultimate pullout capacity of multi-helix screw anchors to the installation torque. This correlation is based on data of field measurement and site experience. This expression was first developed by A B. Chance Company [8] and it reads as follows:

Ultimate Pullout Capacity (kN) = 2.44 [Installation Torque (kN m)]

Using this formula provided a good base to estimate the anticipated ultimate pullout capacity from the measured refusal installation torque.

Hanna et al. (1988) [19] presented experimental and theoretical studies on the behaviour of shallow inclined plate anchors in sand. They developed a technique from which the pressures on predetermined points on the surface of the anchor plate can be measured during testing procedure by using a system of pressure transducers located on the plate's surface, Fig. 2.10. They utilized the data obtained from the experimental investigation to develop a theoretical model to predict the uplift capacity of shallow anchor plates inclined at a given angle. They employed the concept of limit equilibrium to calculate the shearing resistance acting against uplift. They applied simplifying assumptions to the theoretical analysis such as a two-dimensional failure mechanism was considered and a plane failure surface was adopted. However, they provided a semi empirical relationship , based on the experimental results, to account for the effect of the mobilized angle of shearing resistance on the assumed failure

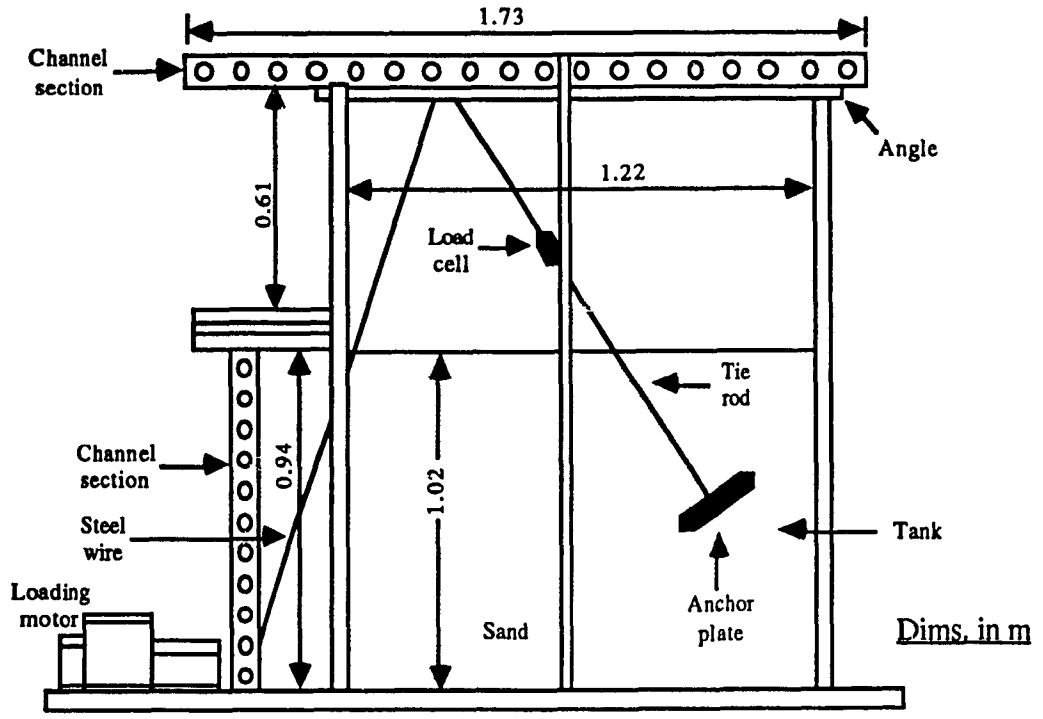

(a) Schematic diagram of the experimental set-up

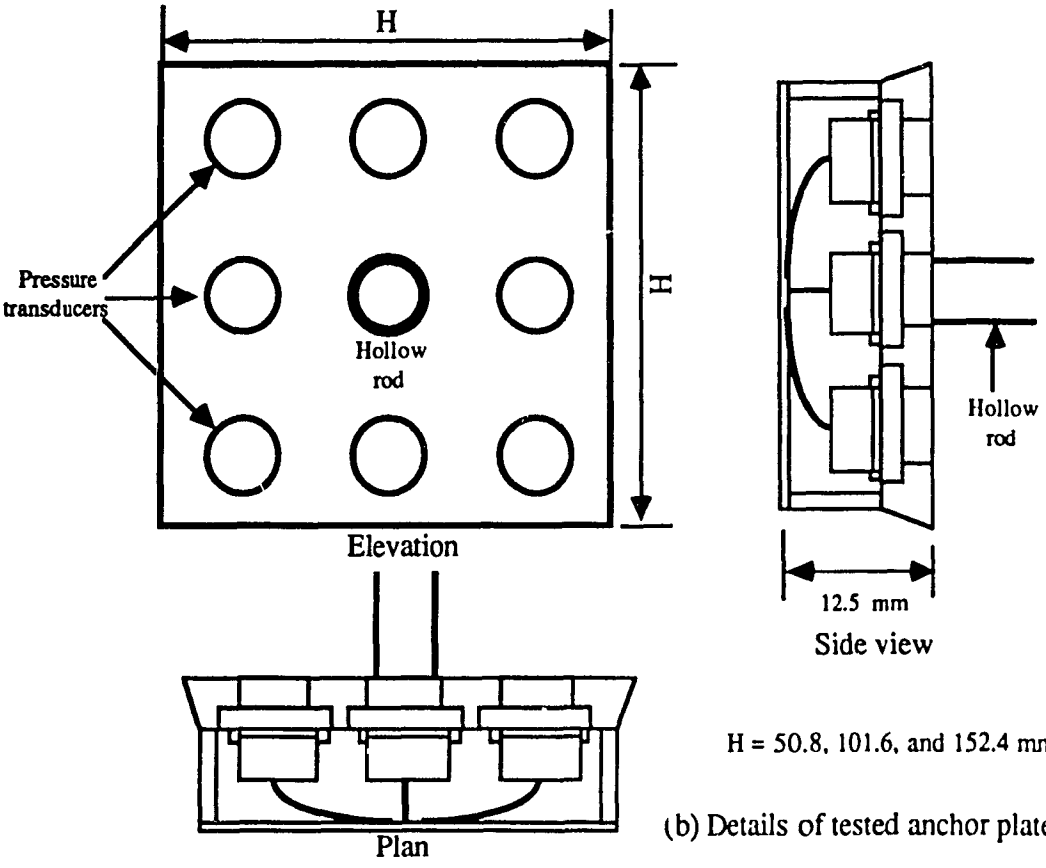

H = 50.8, 101.6, and 152.4 mm

(b) Details of tested anchor plate.

Fig. 2.10: Details of experimental set-up and tested anchor plate; after Hanna et al., (1988).

surface with reference to the actual one. They established an uplift coefficient, for which they have provided design charts, together with the average mobilized angle of shearing resistance and the anchor's angle of inclination. They concluded that these charts can be of good use to the civil engineering practice.

Recently in 1989, Hoyt and Clemence [26] presented correlation from which the total uplift capacity of single or multi-helix screw anchors can be calculated from the recorded value of installtion torque. This correlation is written as $Q_u = K_t \cdot T$, where Q_u = uplift capacity, K_t = empirical factor, and T = average installation torque for the final distance of penetration equal to three times the diameter of the largest helix. They proposed that $K_t = 33\ m^{-1}$ for all square shaft anchors and round shaft anchors less than 89 mm diameter, $K_t = 23\ m^{-1}$ for 89 mm diameter round-shaft anchors, and $K_t = 9.8\ m^{-1}$ for anchors with 219 mm diameter extension shafts. Based on the results of a statistical analysis, they concluded that the calculated uplift capacity, by using installtion torque correlation method, yields more consistent results than the cylindrical shear and individual bearing methods.

2.2 Discussion and Scope of Present Research

It can be noticed that most of the theories related to single or multi screw anchors, and reported in the literature so far, are based on results of experimental investigations or recommendations of the manufacturer. Empirical factors are usually involved in these theories. These empirical factors are, often, back calculated from field or laboratory results, or based on the conventional theory of bearing capacity. Also, most of the available theories are founded on assumed failure surfaces where the degree of shear mobilization is significantly different from that on the actual one. It can also be reported that no theory is available for predicting the uplift capacity of a group of screw anchors. A comprehensive theory is needed to allow better understanding for the performance of screw anchor as an individual or in a group. Also, it would appear that, although the effect of the anchor installation on the soil layer was reported

in several papers, no trial has been made to study the forces acting on the screw anchor during installation, and no theory is available to predict the required installation torque value in terms of the parameters affecting this value, although this prediction serves many purposes in field applications. Moreover, the available correlations reported in the literature, that relating the uplift capacity to the measured torque value, seem to be limited to certain types of anchors with specific geometry. No rational solution exists from which the uplift capacity can be correlated to the measured value of installation torque. Furthermore, in many circumstances, the stress history represented by the overconsolidation ratio, is not accounted for. This yields considerable discrepancy between the uplift capacities of anchors installed in similar types of sand with different stress histories. It is believed that this discrepancy will vanish if the effect of the overconsolidation ratio (OCR) is introduced in the uplift capacity calculations.

The present study is directed to narrow the gap between theory and practice. Attempts are made to develop a rational theory based on the principles of soil mechanics to predict the uplift capacity of single screw anchors as well as group of anchors. Also, forces acting on the screw anchor during installation procedure are examined and a theoretical analysis is performed, in which all the parameters affecting the magnitude of the installation torque are presented. The results of the theory of uplift capacity prediction, together with those of the theory of installation torque determination, are employed to introduce a correlation from which the uplift capacity can be predicted from the measured installation torque. Also, utilizing previously published data, a trial is made to present an empirical relationship from which the uplift capacity of an anchor installed in overconsolidated sand can be determined knowing the value of the OCR. Furthermore, based on the results of the present investigation, an empirical formula is proposed to account for the effect of sand densification that a group of screw anchors causes during the installation procedure.

CHAPTER 3

Experimental Investigation and Results

3.1 Concept

The design of the experimental set-up involved several factors necessary to be considered to achieve the goal of the present study. Vertical and lateral stresses of the sand around and in the near vicinity of screw model anchors were required to be measured during installation and pulling-out procedures. For that purpose, pressure transducers were placed inside the tested sand layer in proper positions. Also, the deflection of the sand surface due to anchor installation or uplift was necessary to be measured in order to determine the extent of the sand wedge involved in failure surface. Linear Variable Displacement Transducers (LVDTs) were positioned in suitable locations on the top of the sand to determine the shape of sand surface deflection. The size of the testing tank was chosen such that the boundary effect is completely eliminated.

The method used to apply the pullout load to the anchor was selected to be a constant strain rate and the load application period was intended to be short term. To achieve this purpose, a gear box device providing different values of constant strain rate was mounted on a loading truss fixed to the floor to provide reaction against the pullout force

3.2 Experimental Set-Up

Figure 3.1 and Plate 3.1 show an overall view of the experimental set up used in the

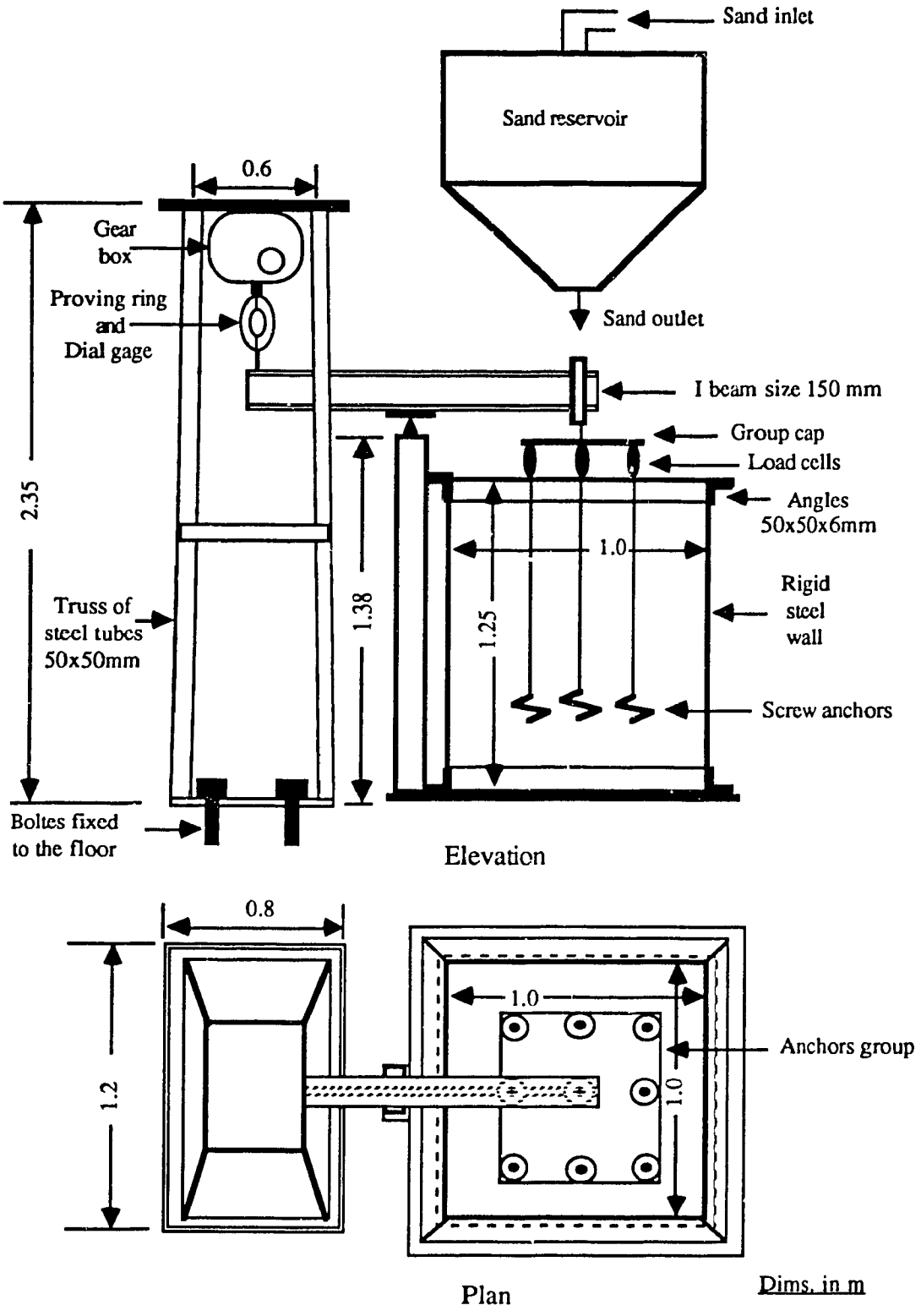

Fig. 3.1: Experimental set-up used in the present investigation.

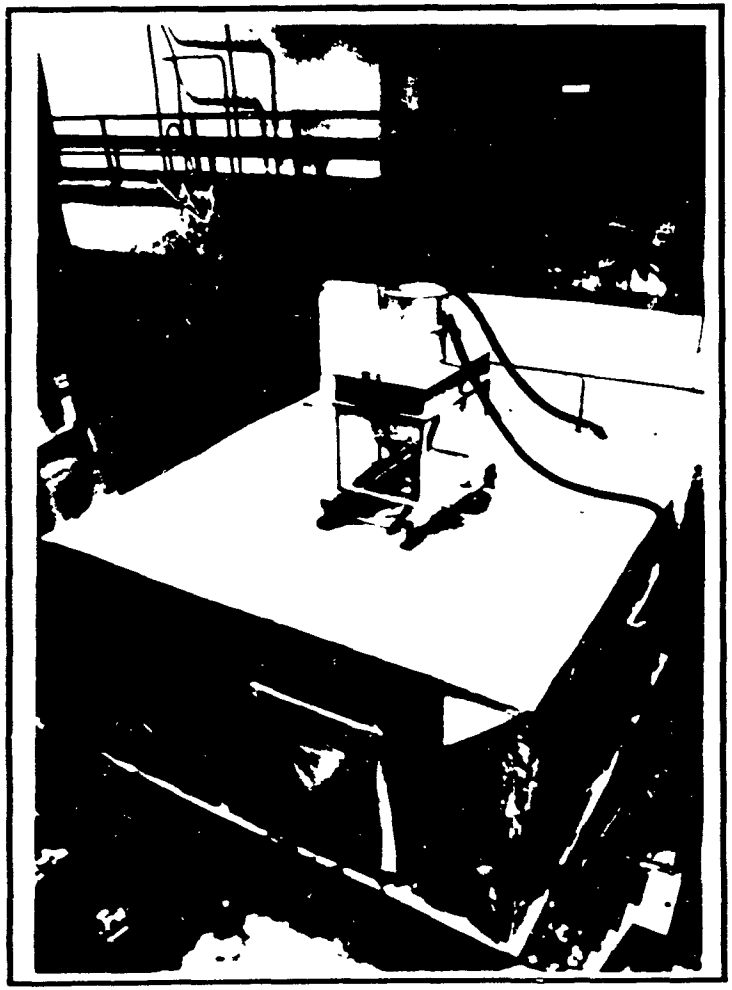

Plate 3.1 General view for the experimental set-up.

Plate 3.2: Front corner view for the testing tank.

present investigation. The testing tank was made of steel plates with dimensions of 1.0 x 1.0 x 1.25 m, length, width, and depth respectively. The thickness of the base and the walls is 6.5 mm. The walls were braced with frames of steel angles to increase their stiffness and to prevent their lateral buckling (Plate 3.2). The loading system consists of a gear box device producing different strain rates, mounted on a steel truss made of steel box sections and braced with steel angles spaced at suitable distances (Plate 3.3). This steel truss was fixed to the floor by means of four anti-tension bolts 50 kN capacity each. The pushing down force produced by the gear box is transmitted to the anchor through simply supported double cantilever beam and transferred to vertical pulling out force (Plate 3.4). The double cantilever beam was provided by a base plate with a conical groove resting on a conical knifed edge to minimize frictional resistance between the lever and the support (Fig. 3.2). The model screw anchor was attached to a tie rod 10 mm in diameter and the latter was attached to a frame of steel sections resting on ball bearing on the top of the simple lever (Plate 3.5).

3.3 Stress Transducer Units

Figure 3.3 shows different views of the unit containing the assembly of the three stress transducers used in measuring vertical and lateral stresses. The design incorporates a metal box 40 x 40 x 80 mm, height, width, and length respectively, with three internal machine cut positions for placing stress transducers inside. Each one of the stress transducers was protected against stress concentration by a surrounding inactive area.

Furthermore, each one of these transducers is functioned to serve the purpose of measuring the stresses acting in the direction perpendicular to its surface. However, two transducers measure the vertical stresses during installation and pulling out of the anchor, while the third one measures the lateral stress. The design also incorporates a hollow bar attached to the metal box, through which the electrical cables of the stress transducers pass to where they are connected to a Data Acquisition System (DAS) for stress registration. The hollow bar is

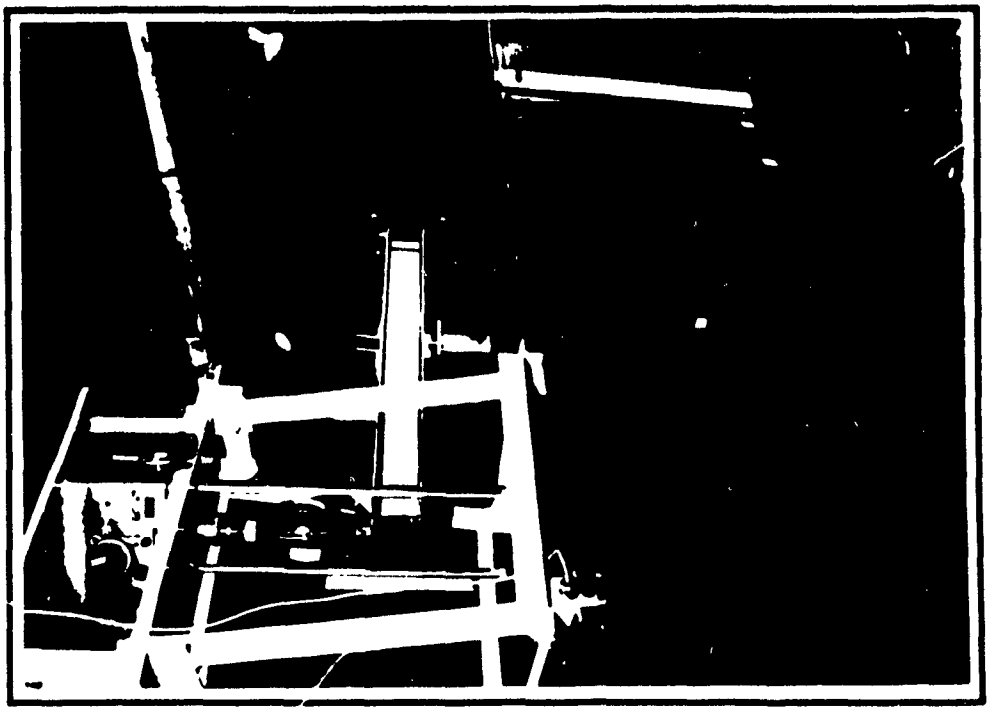

Plate 3.3 Back corner view for the testing tank showing the loading system and the gear box device

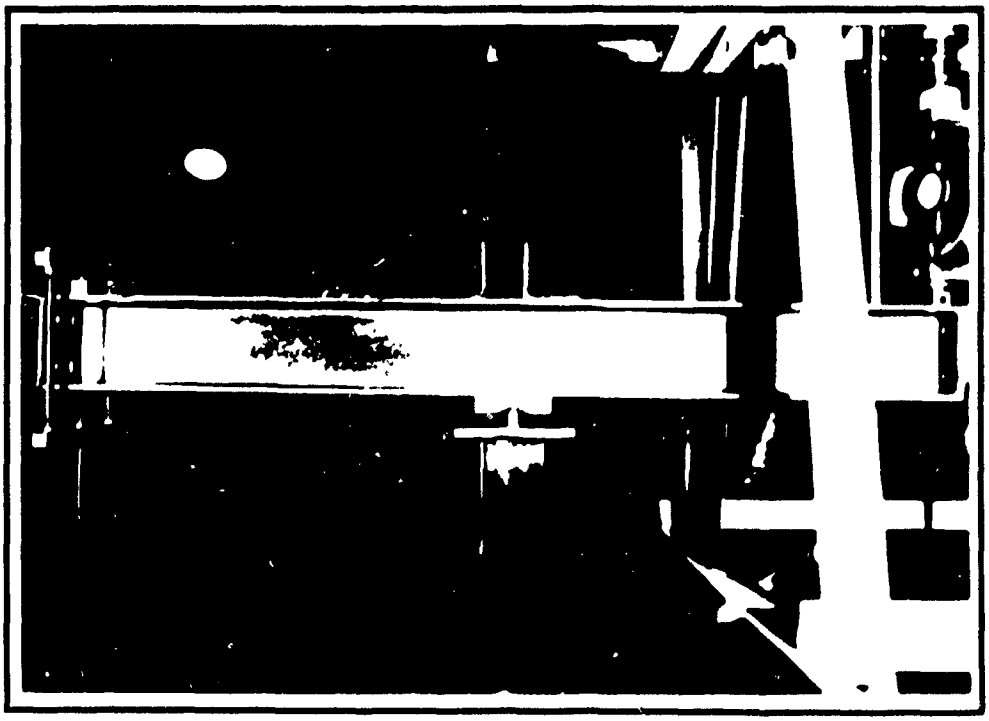

Plate 3.4 Conical knifed edge supporting the double cantilever beam

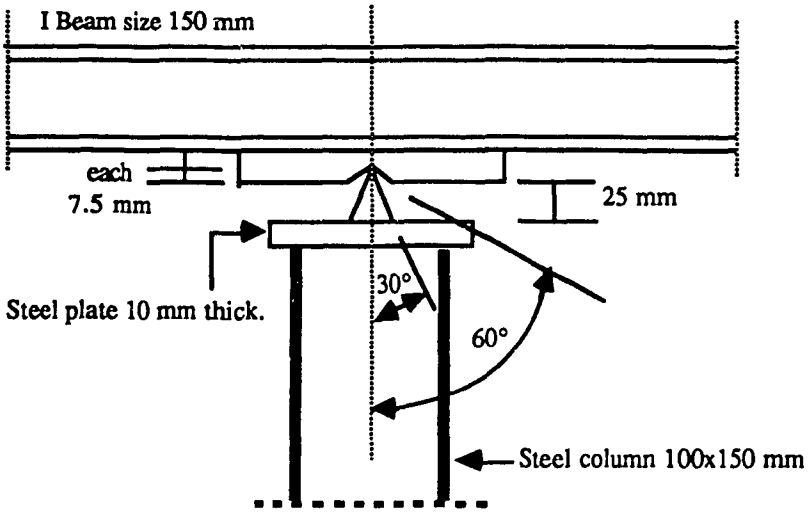

Fig. 3.2: Detail of the fulcrum of the simple lever.

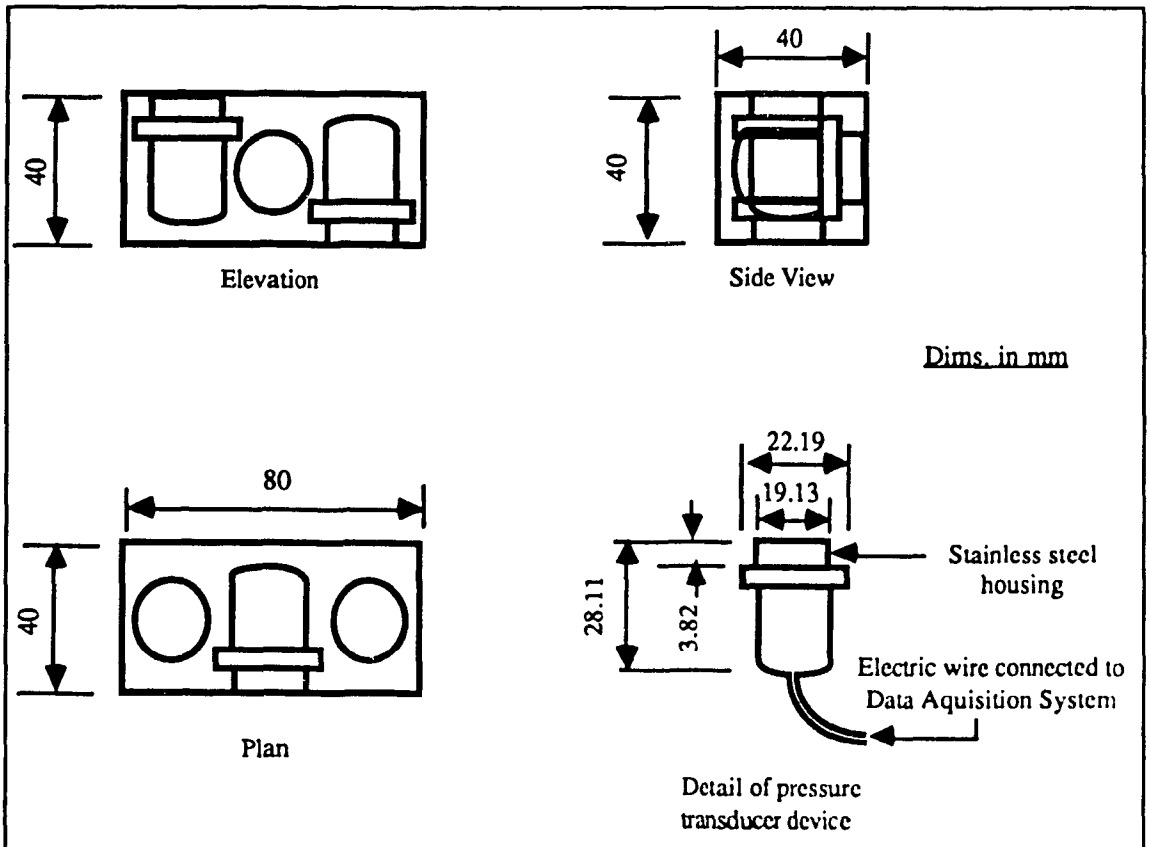

Fig. 3.3: Transducers box unit used to measure lateral and vertical stresses.

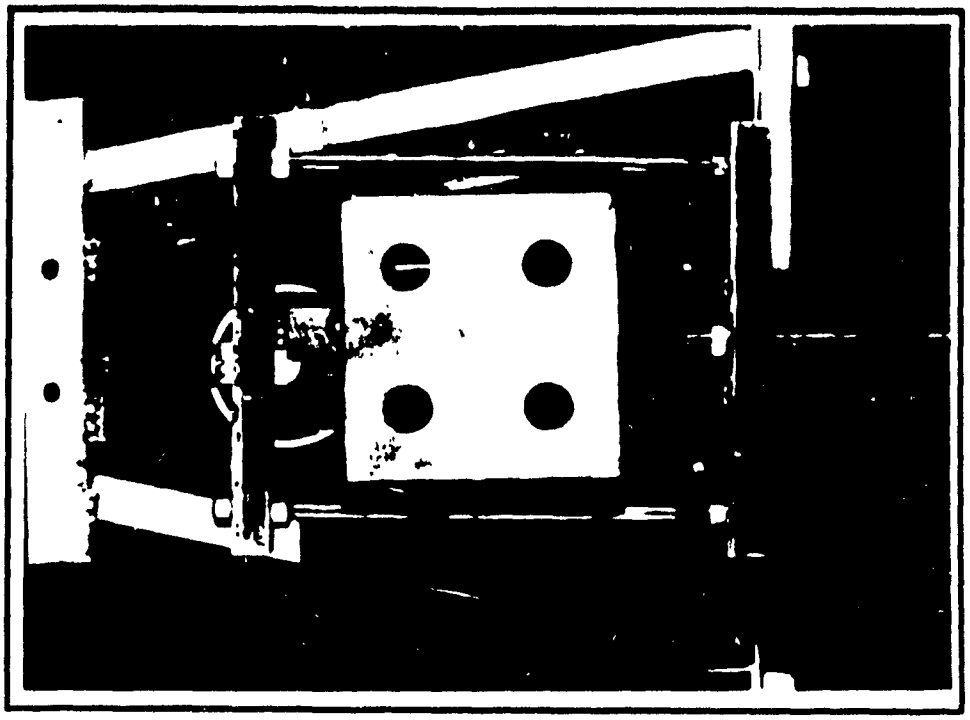

Plate 3.5 Details of supporting seat of the loading frame

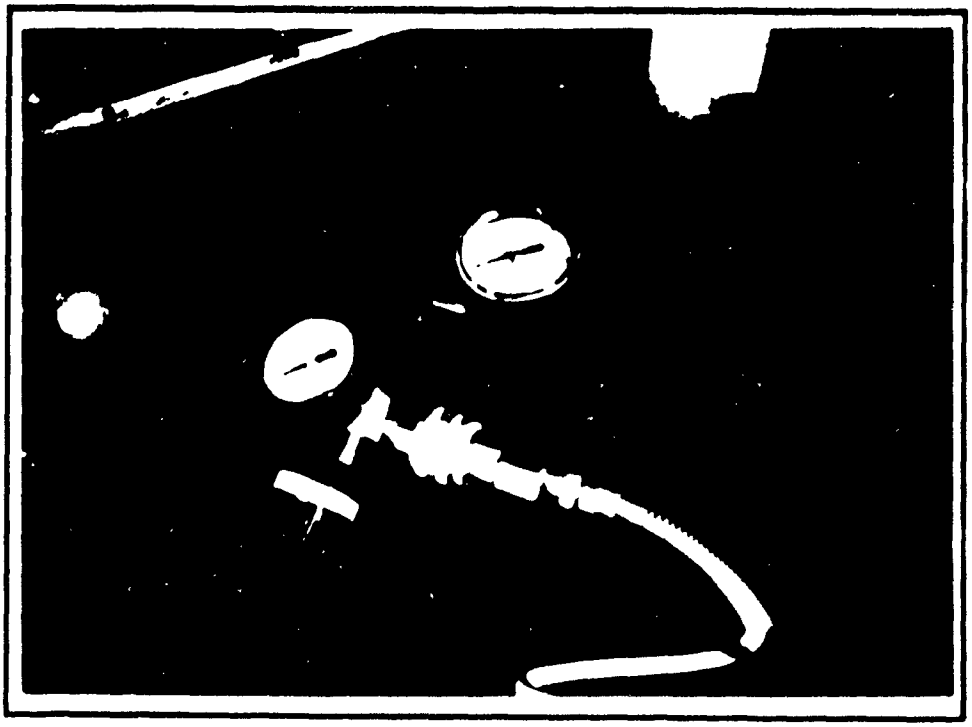

Plate 3.6 Pressure gages controlling and measuring the air pressure inside the testing tank

fixed to the rank wall by suitable means. The stress transducers were calibrated in air by adopting a technique allows the calibration of a number of stress transducers in one shot. This technique was performed by subjecting all the stress transducers to the same amount of air pressure, at the same time. Knowing the value of the applied air pressure on the system and the pressure measured by every individual stress transducer, a calibration factor was calculated for every one. A computer program was developed to calculate the calibration factors utilizing the stresses measured by the Data Acquisition System which was automatically dumped into the computer to determine the calibration factors. The stress transducers were subjected to the same value of air pressure in one shot by placing them in the predetermined locations inside the tank, closing firmly the upper surface of the tank by steel plate provided by a rubber coat on its circumference, and then applying air pressure to the inside of the tank through an assembly of adjustable valves provided by sensitive pressure gages, Plate 3.6. Appropriate size of O-rings were setted between the area of contact of stress transducers and the metal box, to prevent air pressure dissipation through the box.

A typical placement plan of stress transducer units is shown in Fig. 3.4. Top and corner views of these units are shown in Plates 3.7 and 3.8 respectively. The units are located such that the stress transducers that measure the vertical and lateral stresses lay on the perimenter of two imaginary concentric circles of 200 and 400 mm in diameter, the anchor's axis represents their centers. In elevation, the vertical spacing between the units is 200 mm. As shown in elevation and plan, the units are placed in a staggared arrangement so that each unit is functional.

3.4 Data Recording

The data recorded from the experimental investigation was measured by a variety of devices. A Data Acquisition System (Plate 3.9) was used to measure the stresses in the sand deposit for every 50 mm installation depth of the anchor until the final desired depth was reached, then for 1 min. time intervals during the pullout procedure. A computer program was

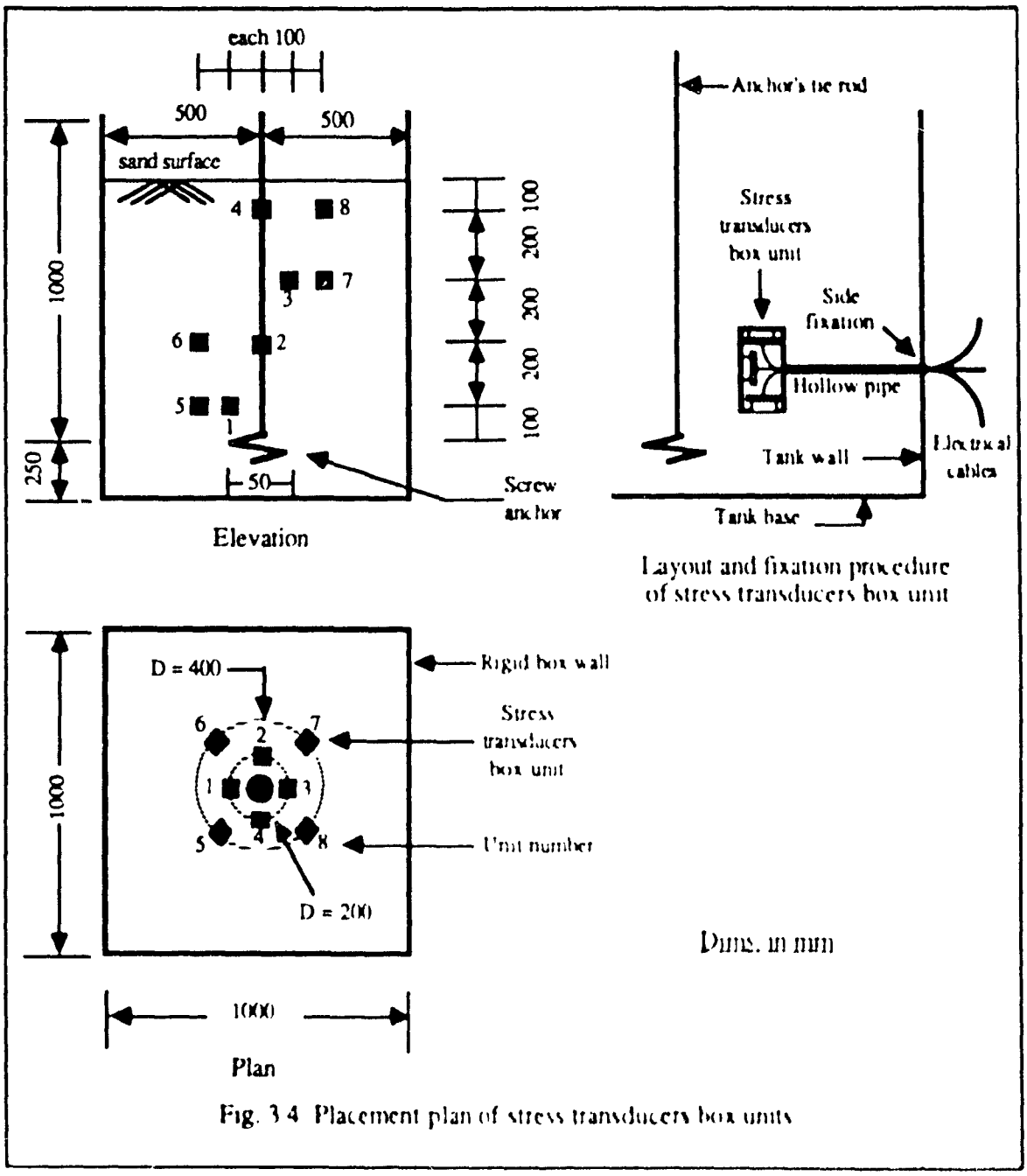

Fig. 3.4 Placement plan of stress transducers box units

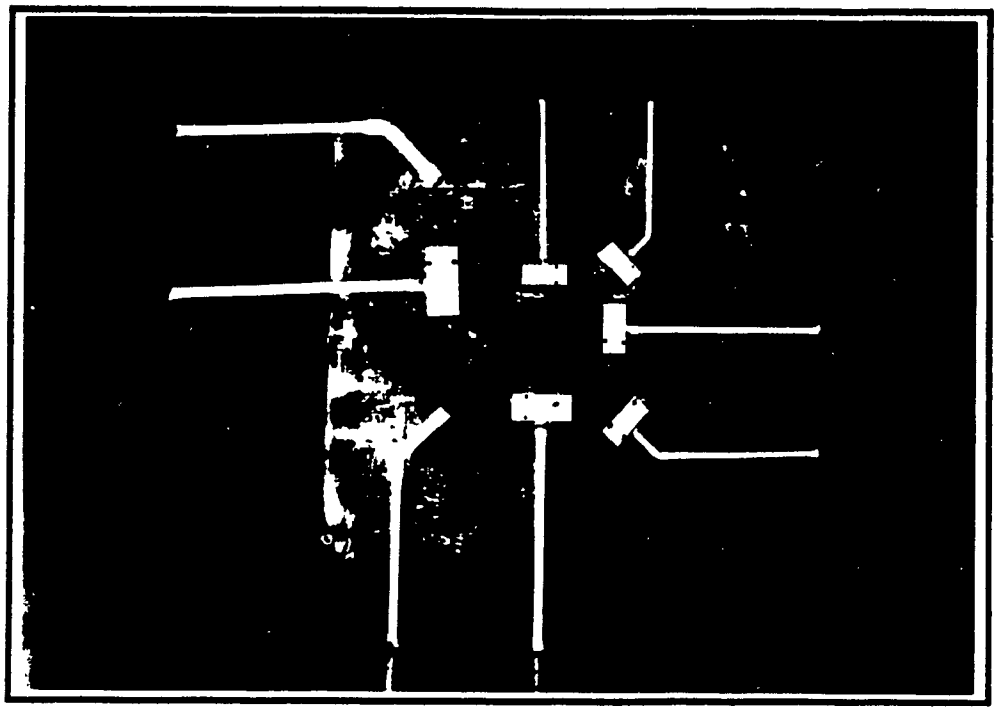

Plate 3.7: Top view showing locations of stress transducers box units.

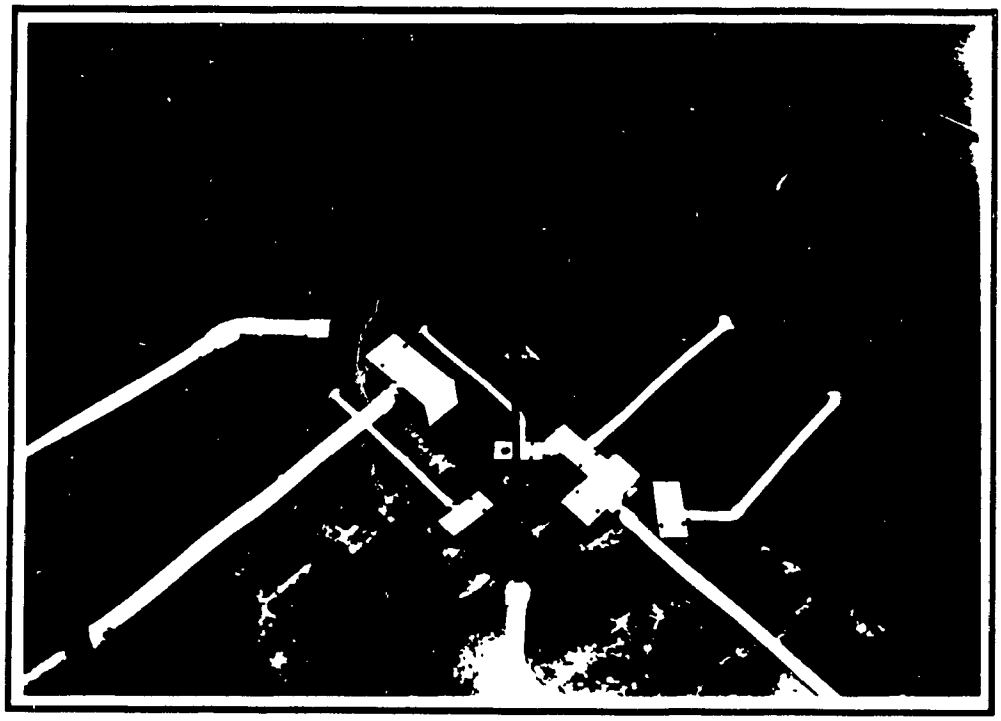

Plate 3.8: Corner view showing the staggared arrangement of stress transducers inside the testing tank.

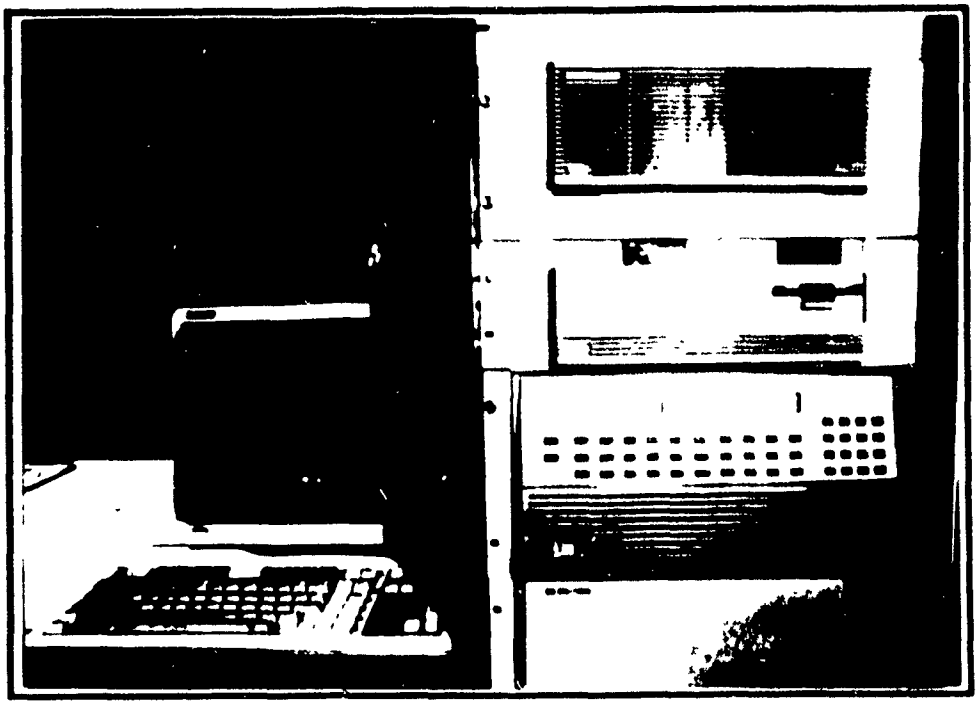

Plate 3.9: Data Acquisition System and computer used for measuring and recording data

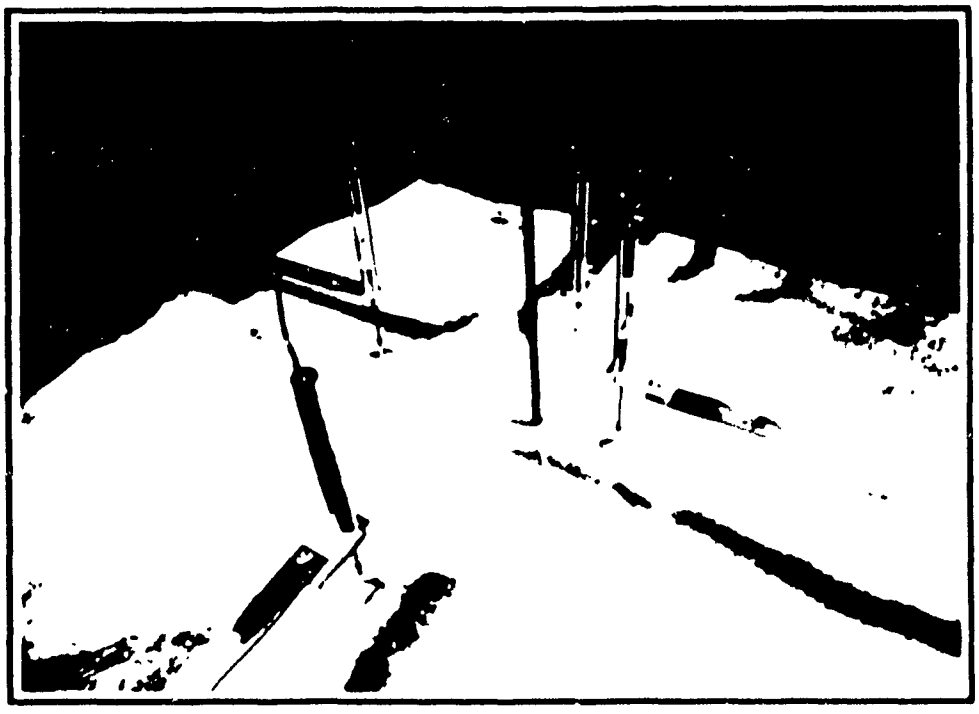

Plate 3.10 Displacement transducers (LVDT) used for measuring surface deflection

developed to record the stresses acting on the stress transducers at the same moment for all. Also, this computer program can be set to manual or automatic mode, i.e., manual mode gives the freedom to measure the stresses at any desired time by hitting a special key, while the automatic mode records the stresses according to predetermined time intervals. Manual mode was used during installation procedure as it was required to measure the stresses in the sand when the anchor reaches predetermined locations, while the automatic one was used during the uplifting process since the pullout load was applied according to a constant strain rate.

Deflections occurring to the top of sand layer during installation and pulling out procedures were measured by Linear Variable Displacement Transducers (Plate 3.10) connected to the Data Acquisition System. Also, the upward displacement accompanied the pulling out of the model anchor was measured by LVDTs connected to DAS. An additional section was included in the developed computer program to measure the variation of voltage of the LVDTs and to transfer these values to displacement in mm by multiplying every single value by the proper calibration factor. The gradual increase in the pullout load was constantly measured according to 1 min. time intervals during pullout process till the moment of failure was reached. Load cells and proving ring were used to measure the uplift load and to verify it on the two sides of the double cantilever beam. The load cells was connected to the DAS and another section was added to the computer program to measure directly the pullout load in weight units. From the measured data, the peak (failure) point was defined as the point at which there was no further increase in the pullout load, while the upward displacement kept increasing. This peak point can be found from the plot of stress-strain relationship (load-displacement curve).

3.5 Sand Properties

The present research program was intended to be on loose, medium and dense sand. It was necessary to have well graded sand in order to obtain the required relative densities by controlling the degree of compaction applied to the tested sand. For this reason, trials were made in the laboratory on eleven different gradation to find out the percentage that should be

used to produce mixture of well graded sand. Three gradation of 99.9% high silica sand imported from the same quarry in the United States, were found to be suitable to produce the required well graded sand. The mixture percentage was, Passing Mesh 16: Passing Mesh 32: Passing Mesh 142 = 3: 2: 1, and Uniformty coefficient C_u = 6.5, and coefficient of curvature C_c = 2.0. Figure 3.5 shows mechanical sieve analysis of grain size distribution of a sample taken from 3 m^3 of the produced mixture.

Table 3.1 summarizes the physical and mechanical characteristics of the sand used in the experimental investigation. A placing technique was developed and calibrated before starting the testing program to ensure the reproduction of the desired unit weight. This technique was adopted after many trials and was achieved by placing the sand in layers of 150 mm each and applying mechanical compaction by means of air hammer (Plate 3.11). Controlling the compactor acceleration by adjusting the air pressure and the compaction duration, makes it possible to produce the required densities.

3.6 Model Screw Anchors

Five types of screw anchors with different geometrical characteristics were designed to study the effect of shape on the installation and uplift behaviour of the model anchor. These anchors were machine made of high quality stainless steel as one unit with no welded, rivited, or bolted joints to eliminate side effects of these joints on the anchor behaviour. Table 3.2 introduces a comparison between the five types of screw model anchors and they are shown in Fig. 3.6 a, b, c, d, e, and Plates 3.12 a, b, c, d, e.

3.7 Installation Technique

After placing the sand in the testing tank, a guide frame of steel angles was mounted on the top of the tank (Plate 3.13 and Fig. 3.7). The anchor was carefully located on the sand surface

Table 3.1: Physical properties of the tested sand.

Property	Value
Dense sand, unit weight	19.03 kN/m^3
angle of shearing resistance*	42^o
relative density	83 %
Medium sand, unit weight	18.74 kN/m^3
angle of shearing resistance*	36^o
relative density	52 %
Loose sand, unit weight	17.75 kN/m^3
angle of shearing resistance*	31^o
relative density	20 %
Specific gravity, G_s	2.70

* As per direct shear box test.

Table 3.2: Geometrical properties of single screw model anchors.

Type	Anchor Definition	No. of Pitches	First blade diameter*		Screw Pitch*	Tie Rod Diameter*	Blades Thickness*	Remarks
			Outer	Inner				
1	One Pitch Screw Small Pitch (Fig. 3.6a)	1	50	16	10	10	2.5	Has conical end.
2	One Pitch Screw Medium Pitch (Fig. 3.6b)	1	50	16	15	10	2.5	Has conical end.
3	One Pitch Screw Large Pitch (Fig. 3.6c)	1	50	16	20	10	2.5	Has conical end.
4	Multi Pitch Screw Equal Pitch (Fig. 3.6d)	3	50	16	15	10	2.5	First blade is not a full circle in plan as the initial radius decreases by 5 mm each half pitch. Pitch is constant.
5	Multi Pitch Screw Variable Pitch (Fig. 3.6e)	3	50	16	Variable	10	2.5	Pitches are not equal as the blades are parallel.

* All dimensions in mm.

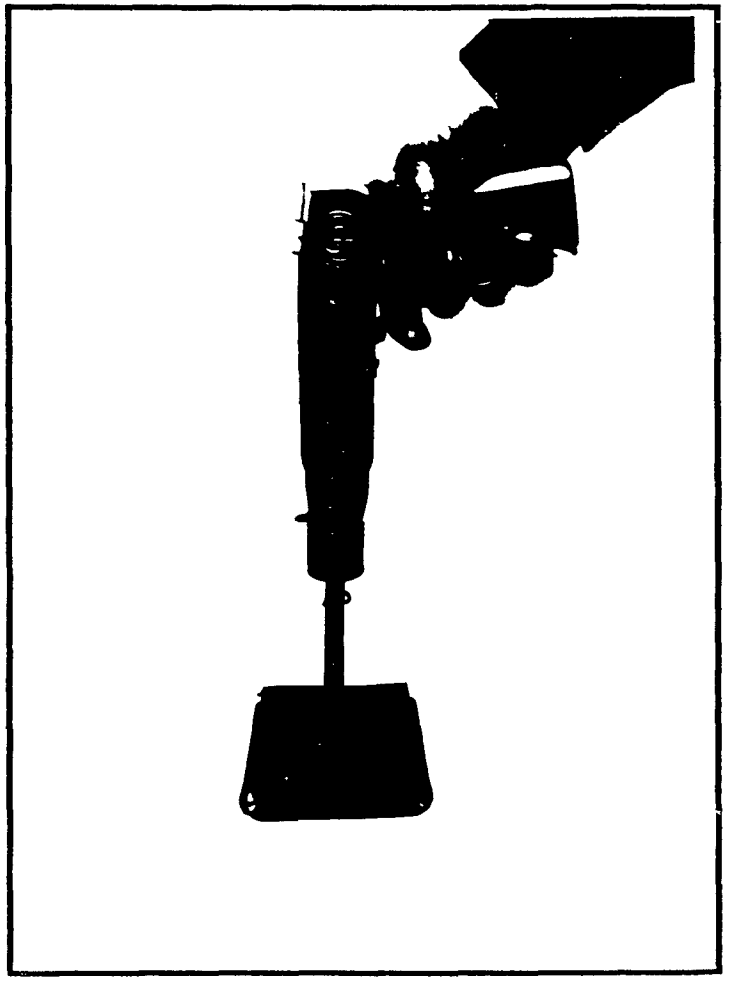

Plate 3.11: Air hammer used to compact the sand.

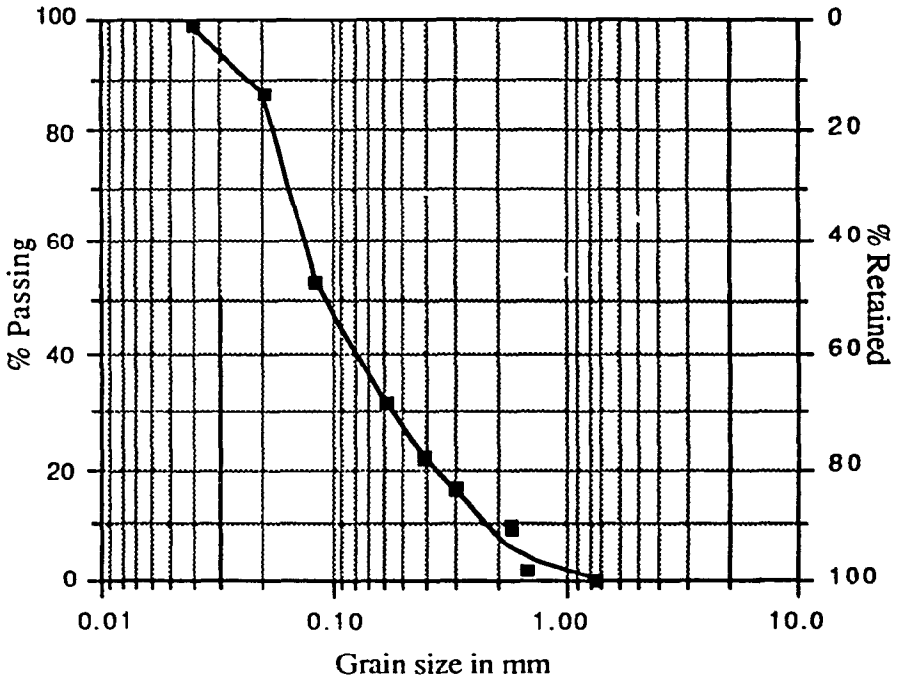

Fig. 3.5: Grain size distribution.

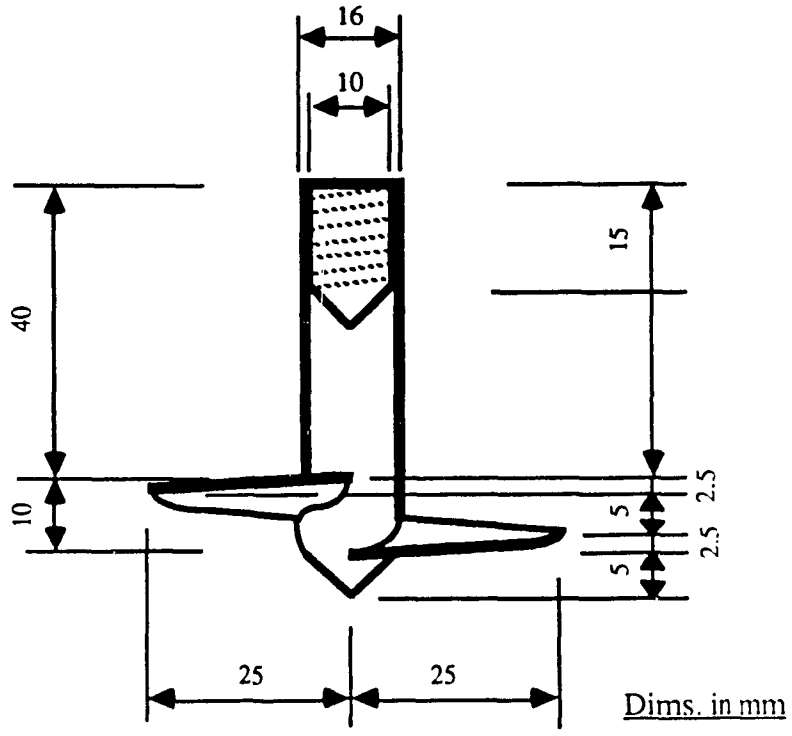

Fig. 3.6a: Single pitch screw anchor, small pitch (Type 1).

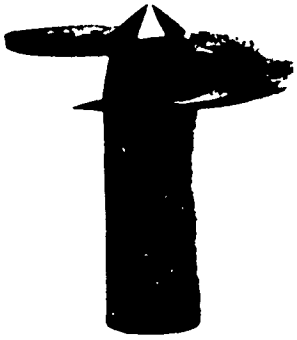

Plate 3.12a: Single pitch screw anchor, small pitch (Type 1).

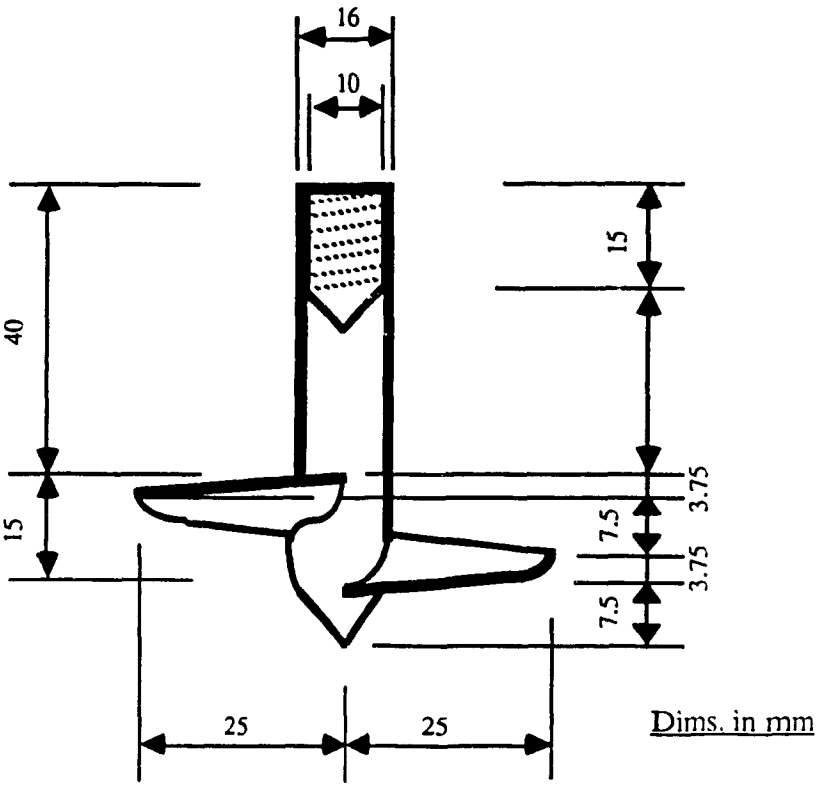

Fig. 3.6b: Single pitch screw anchor, medium pitch (Type 2).

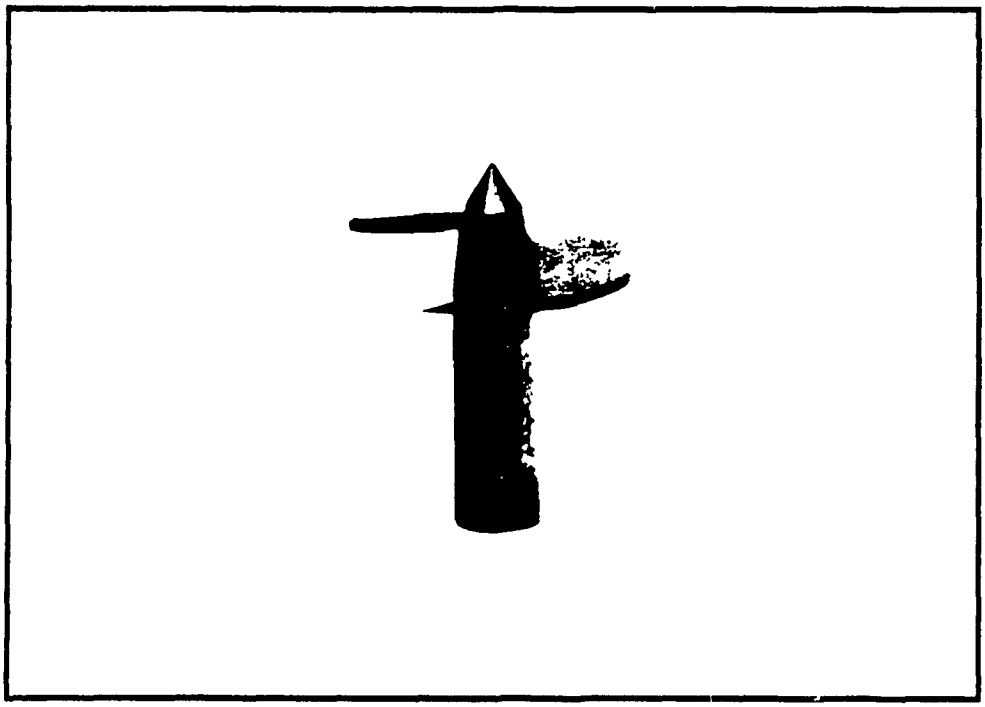

Plate 3.12b: Single pitch screw anchor, medium pitch (Type 2).

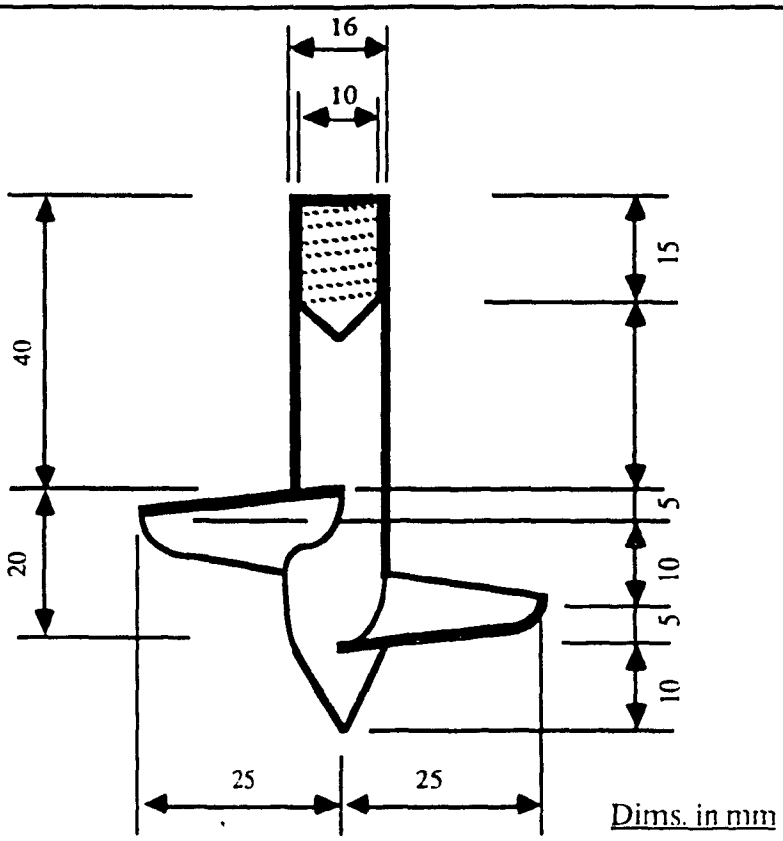

Fig. 3.6c: Single pitch screw anchor, large pitch (Type 3).

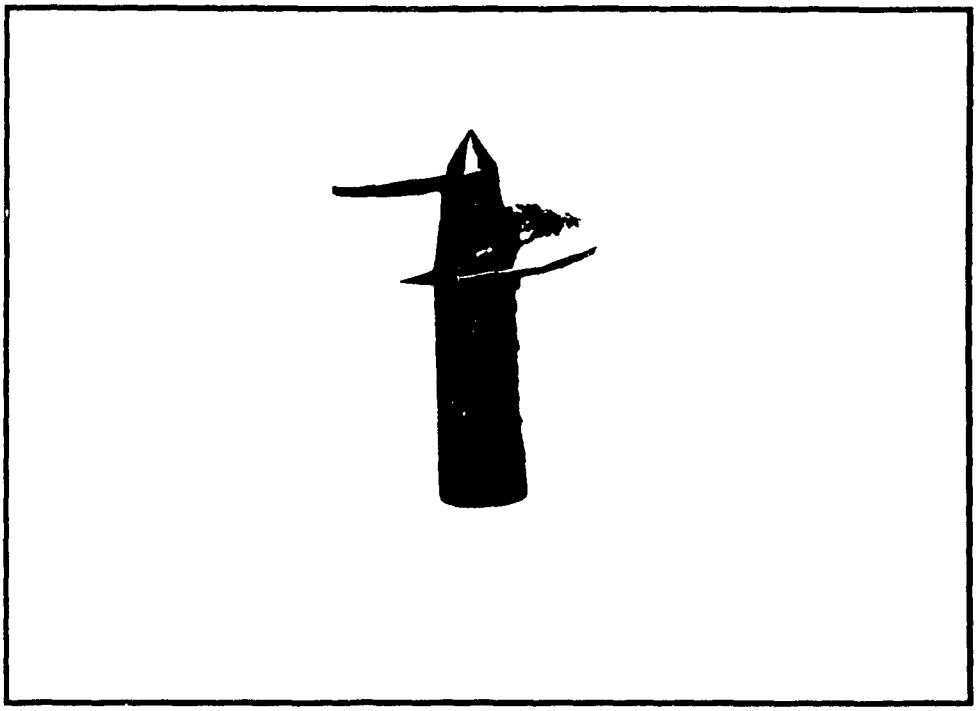

Plate 3.12c: Single pitch screw anchor, large pitch (Type 3).

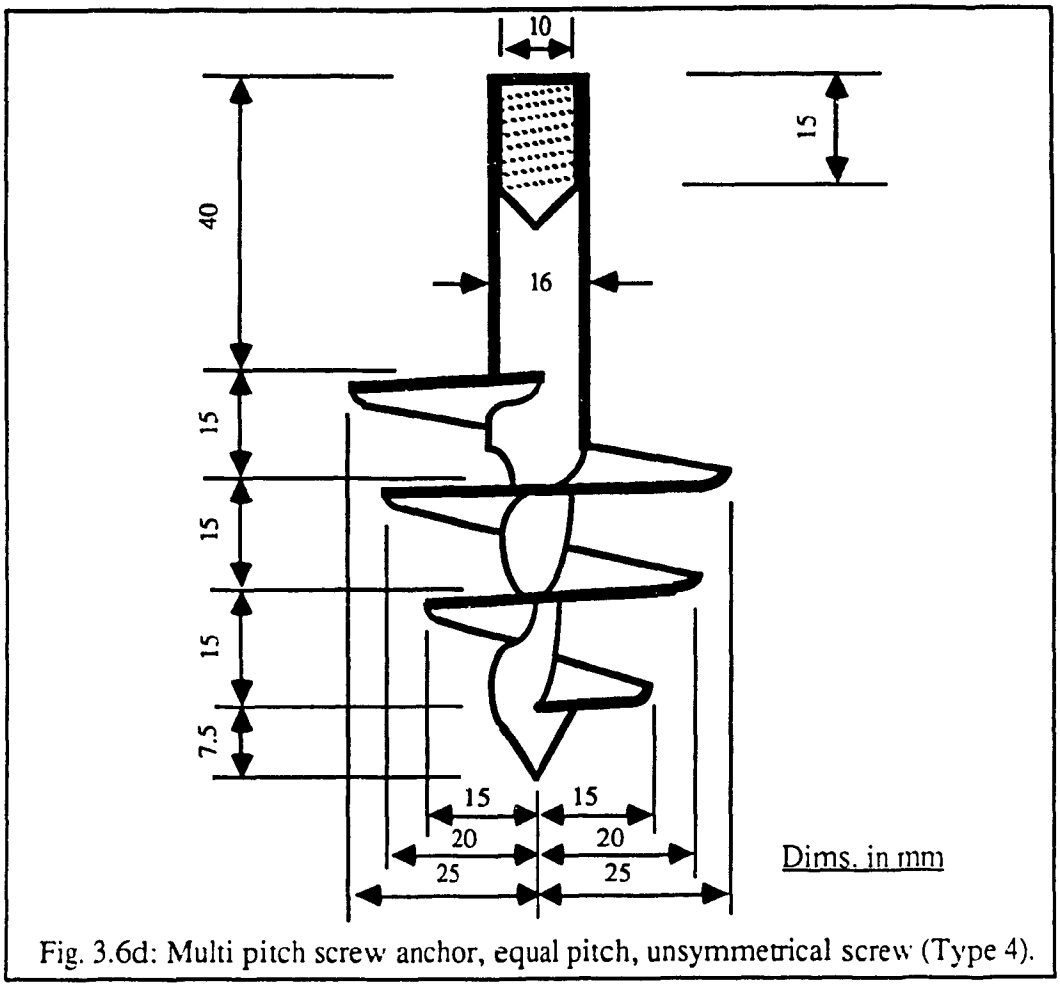

Fig. 3.6d: Multi pitch screw anchor, equal pitch, unsymmetrical screw (Type 4).

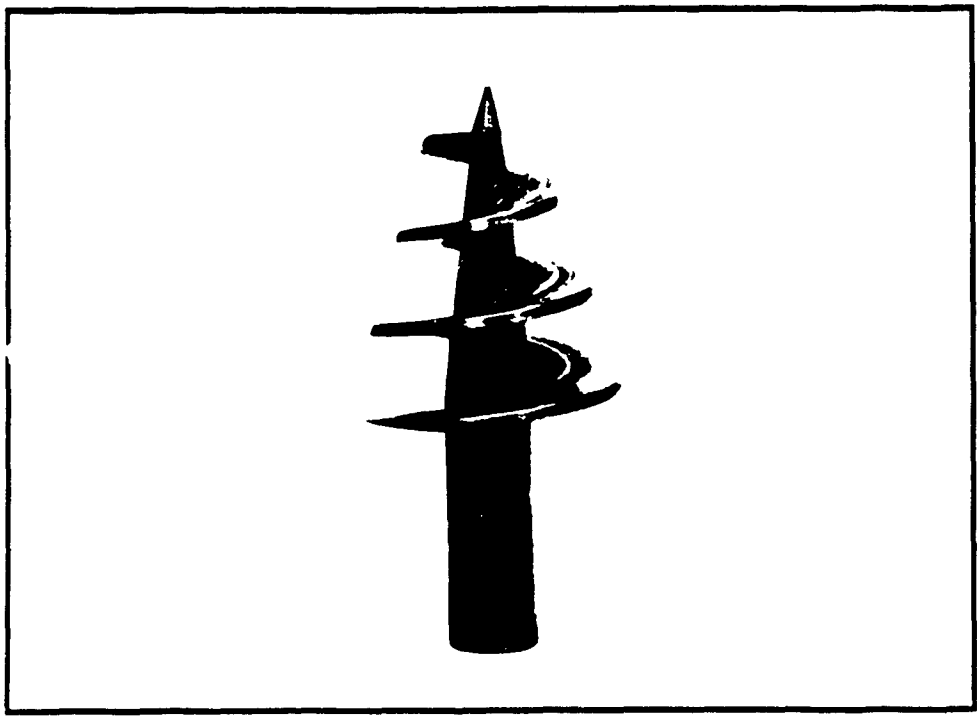

Plate 3.12d: Multi pitch screw anchor, equal pitch, unsymmetrical screw (Type 4).

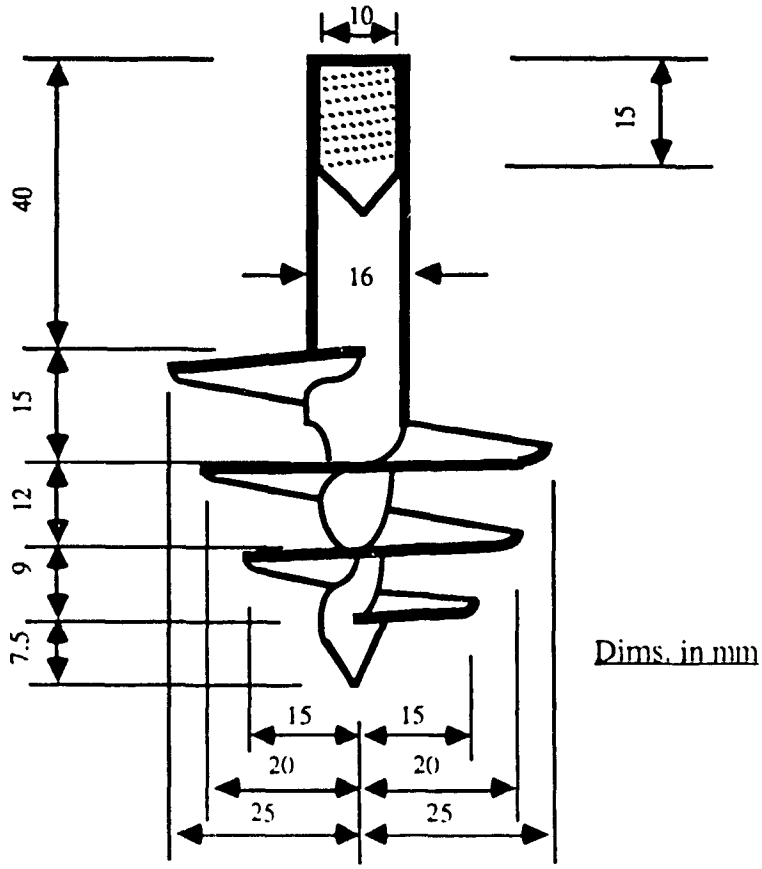

Fig. 3.6e: Multi pitch screw anchor, variable pitch, parallel blades screw (Type 5)

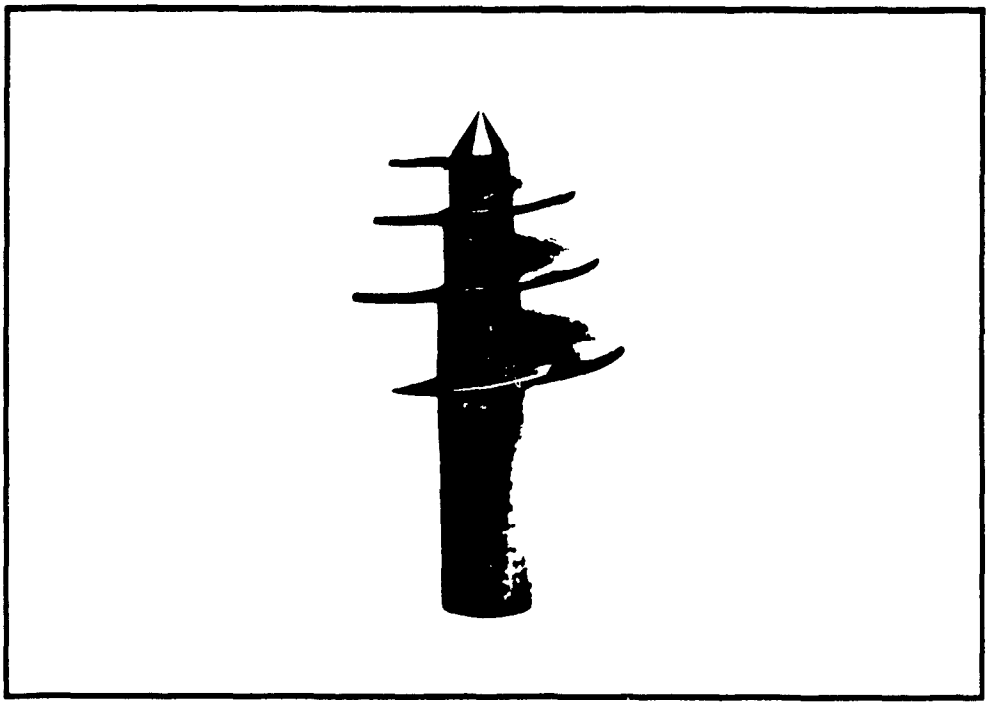

Plate 3.12e. Multi pitch screw anchor, variable pitch, parallel blades screw (Type 5).

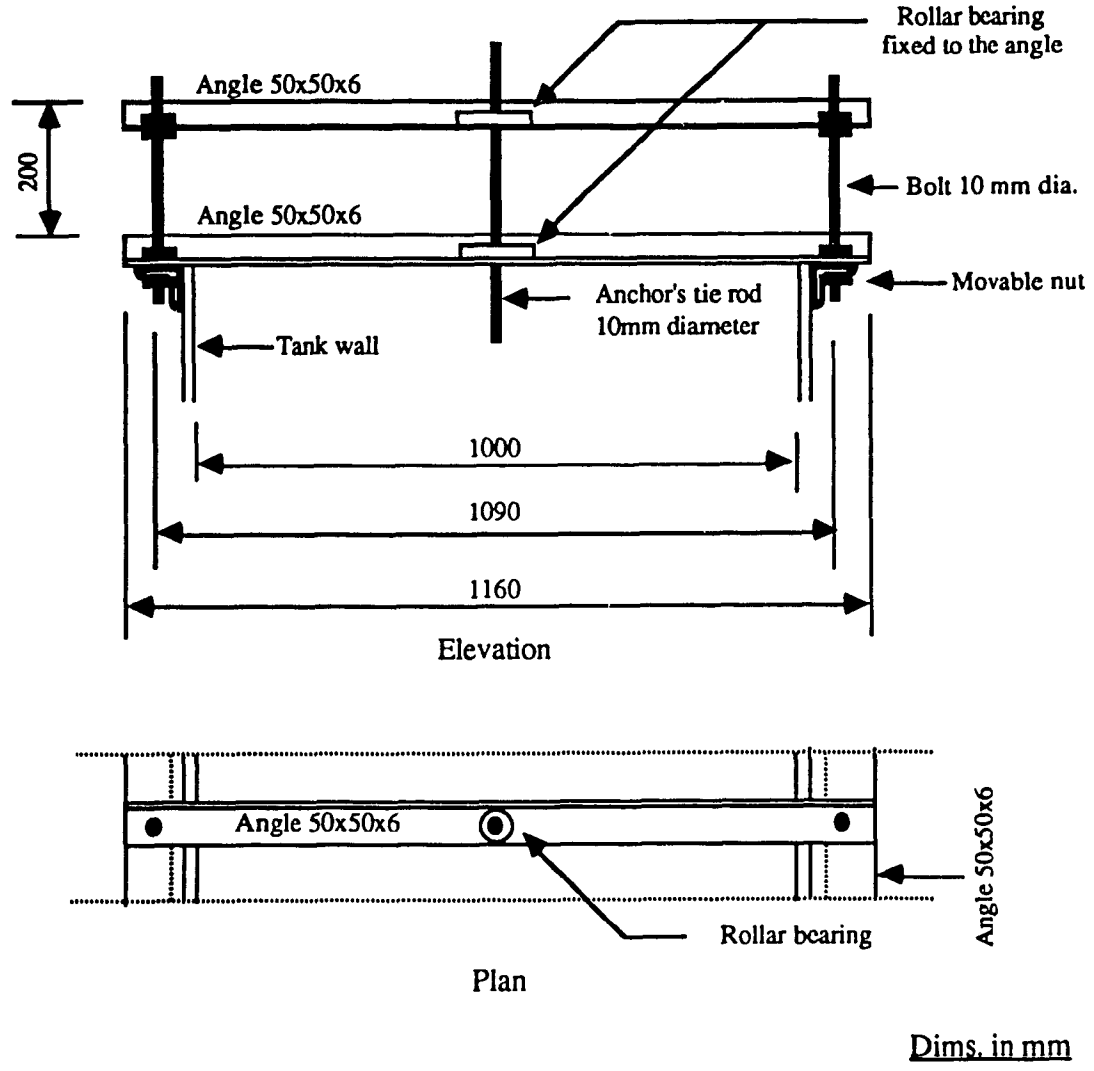

Fig. 3.7: Guide frame used to keep the anchor vertical in position during installation.

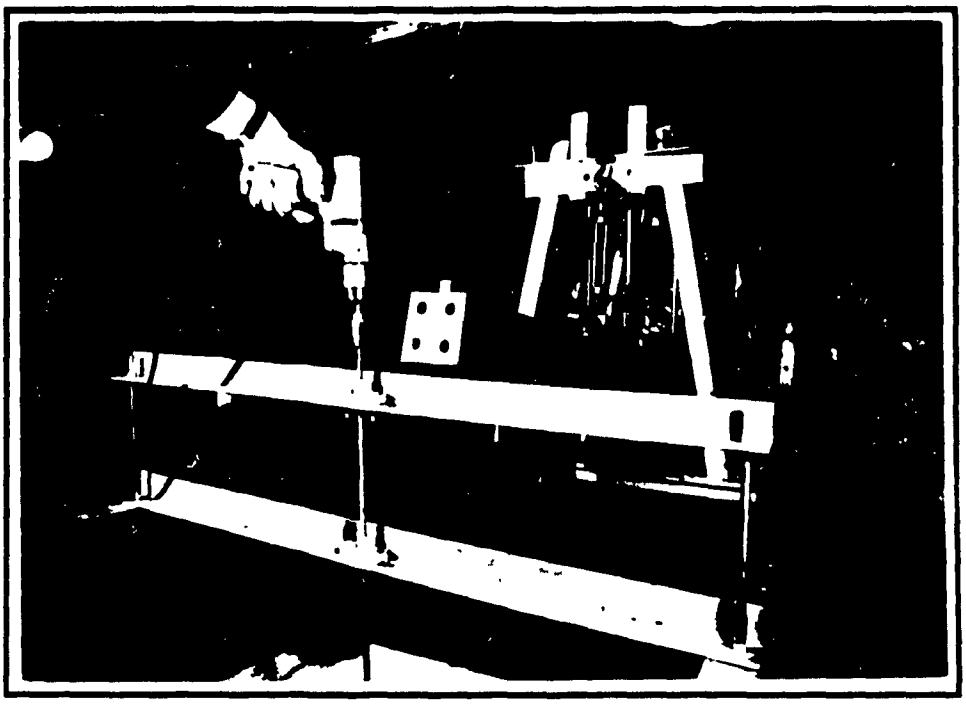

Plate 3.13: Guide frame used to keep the anchor vertical during installation.

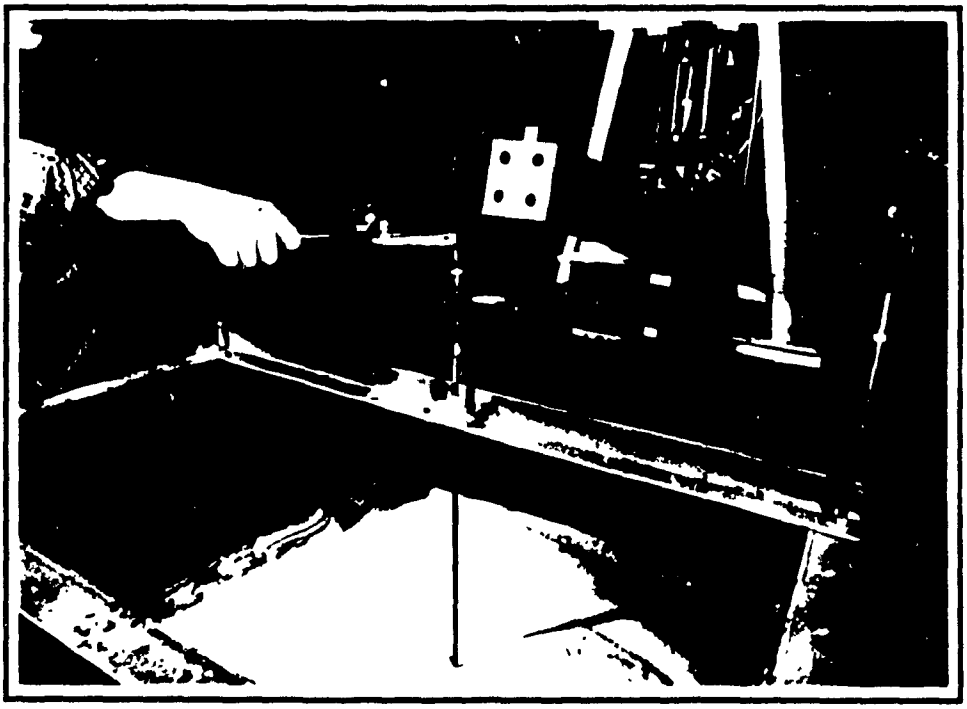

Plate 3.14: Torque-meter used for measuring the value of installation torque

and the tie rod was passed through the angles of the guide frame. This procedure was adopted to assure that the anchor advances vertically into the sand during torque application. Torque was provided by adjustable speed electrical drill and measured by sensitive torque meters for every 50 mm penetration depth (Plate 3.14 and Fig. 3.8). The tie rod was protected against friction with the angles of the guide frame by passing it through a rollar bearing fixed to the angles.

3.8 Test Program

Table 3.3 summarizes the tests conducted to study the behaviour of single screw anchors installed in dry sand.

3.9 Test Results and Discussion

Table 3.4 presents the test results of the tested five types of screw anchors installed in dense, medium, and loose sand. Typical pullout load versus upward displacement relationship is shown in Fig. 3.9. From this figure, it can be seen that as the depth of embedment of anchor increases, the pullout load and the upward displacement increases too. This behaviour was observed for all tested types of anchors and it gives an indication that the screw anchor configuration has little or no influence on the pullout load-upward displacement relationship. Also, a typical pullout load versus upward displacement relationship for a screw anchor installed in dense, medium, and loose sand is shown in Fig. 3.10. From this figure, it can be indicated that the sand mechanical characteristics have a significant effect on the load-displacement relationship. The higher the angle of shearing resistance (ϕ), the higher is the ultimate pullout load and the greater is the upward displacement.

In the present research study, failure was defined as the point at which no more increase in the pullout load is recorded, while there is further increase in the upward displacement. Based on this definition, the ultimate pullout load and the corresponding upward displacement were

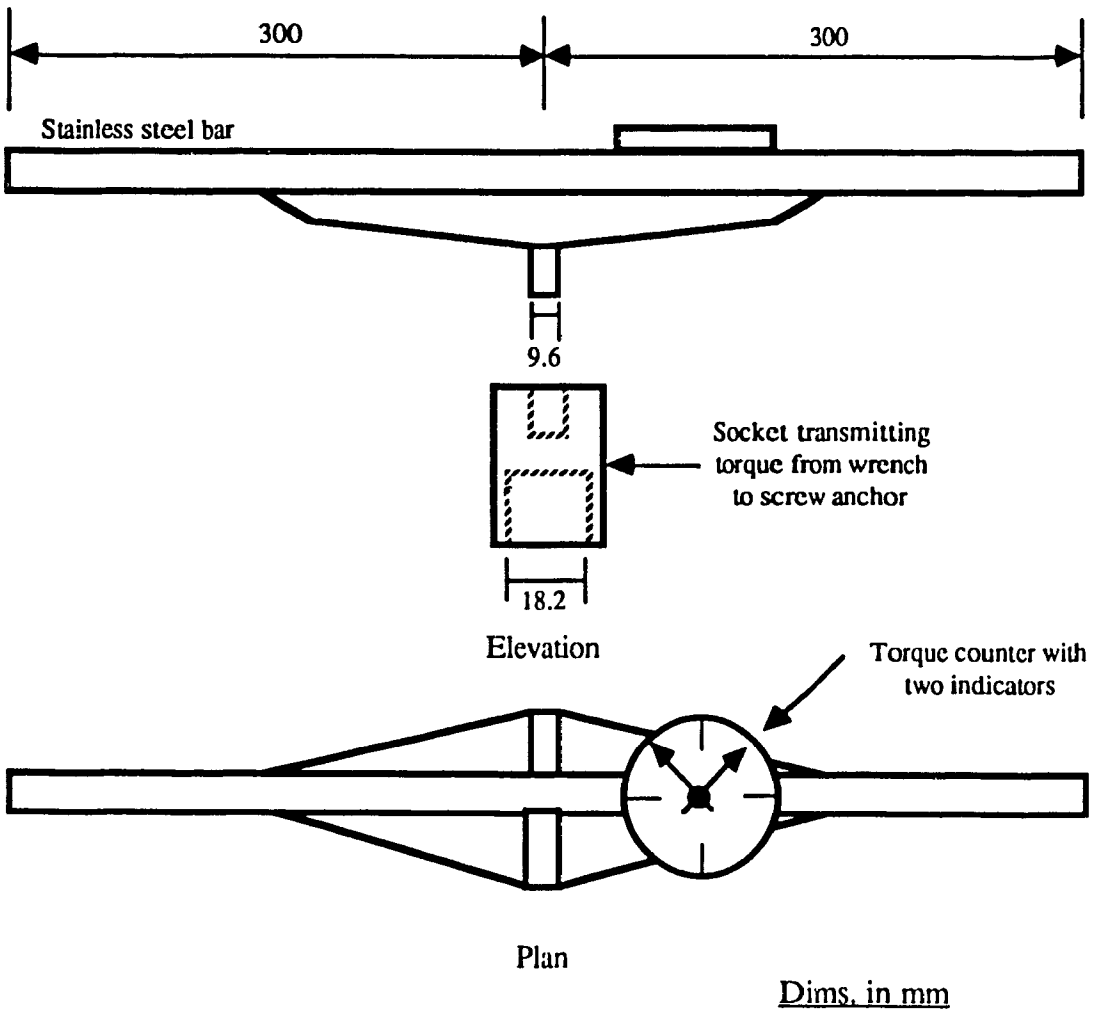

Fig. 3.8: Torque wrench used for producing and measuring torque.

Table 3.3: Test program on single screw anchors.

Screw Type	Dense Sand ($\phi = 42°$)	Medium Sand ($\phi = 36°$)	Loose Sand ($\phi = 31°$)
	H/B	H/B	H/B
1	4, 8, 12, 16	4, 8, 12, 16	4, 8, 12, 16
2	4, 8, 12, 16	4, 8, 12, 16	4, 8, 12, 16
3	4, 8, 12, 16	4, 8, 12, 16	4, 8, 12, 16
4	4, 8, 12, 16	4, 8, 12, 16	4, 8, 12, 16
5	4, 8, 12, 16	4, 8, 12, 16	4, 8, 12, 16

Table 3.4: Test results of tested types of single screw anchors.

H	H/B	ϕ°	Type 1 screw anchor		Type 2 screw anchor		Type 3 screw anchor		Type 4 screw anchor		Type 5 screw anchor	
			Qu (N)	Uu (mm)	Qu (N)	Uu (mm)	Qu (N)	Uu (mm)	Qu (N)	Uu (mm)	Qu (N)	Uu (mm)
0.2	4	31	171.8	1.887	179.0	1.912	182.4	2.001	181.3	1.875	172.5	2.002
0.4	8	31	659.2	2.591	686.3	2.631	698.7	2.702	678.2	2.509	693.4	2.629
0.6	12	31	1395.1	4.393	1420.2	4.427	1435.8	4.486	1453.6	4.401	1400.7	4.397
0.8	16	31	2188.7	6.670	2213.9	6.715	2243.5	6.793	2192.7	6.732	2234.8	6.738
0.2	4	36	229.9	2.325	232.8	2.470	245.7	2.508	213.6	2.511	219.9	2.486
0.4	8	36	1051.3	4.648	1079.5	4.663	1116.2	4.701	1108.4	2.696	1083.7	4.651
0.6	12	36	2076.4	6.509	2108.9	6.534	2187.1	6.584	2121.7	6.505	2116.4	6.548
0.8	16	36	3311.5	10.024	3336.3	10.097	3391.5	10.146	3352.8	10.073	3300.5	10.037
0.2	4	42	273.6	3.008	284.7	3.021	295.4	3.037	281.3	3.029	279.9	2.989
0.4	8	42	1412.3	6.701	1475.5	6.740	1493.2	6.759	1461.1	6.751	1453.8	6.495
0.6	12	42	2981.1	9.398	3039.2	9.416	3100.7	9.428	3058.4	9.432	3097.6	9.573
0.8	16	42	4112.3	12.716	4206.4	12.730	4282.2	12.744	4291.9	12.720	4165.5	12.612

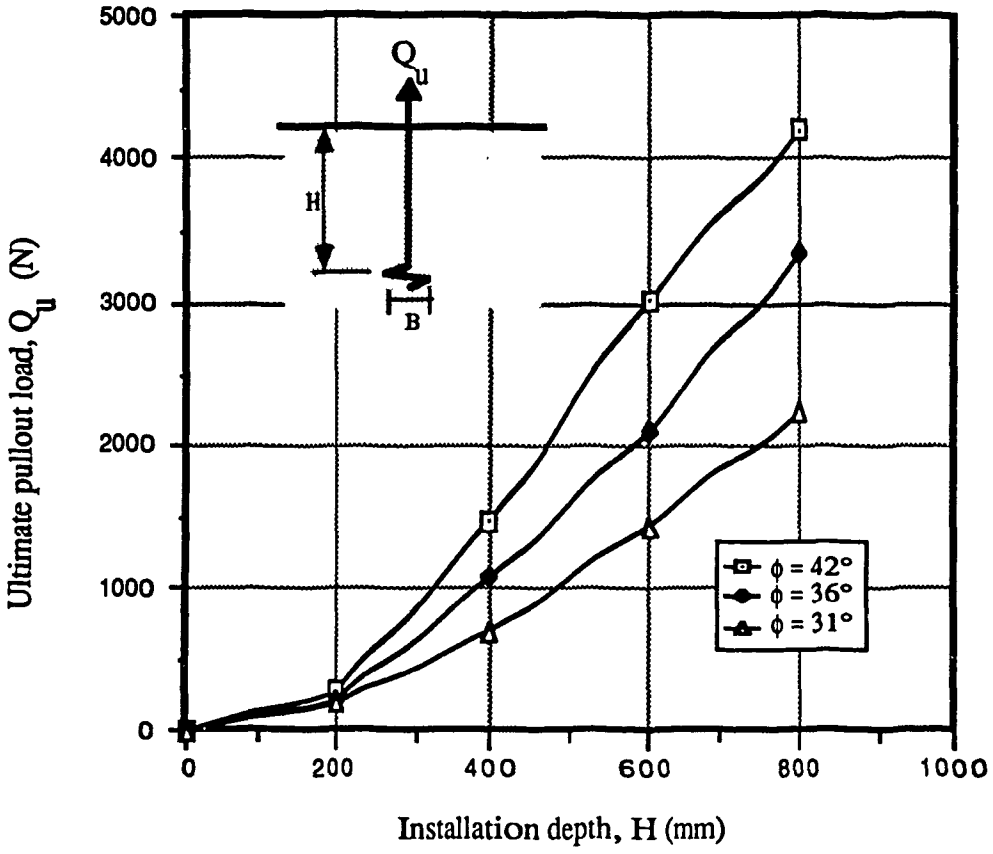

Fig. 3.9: Ultimate pullout load versus installation depth for dense, medium, and loose sand; experimental results.

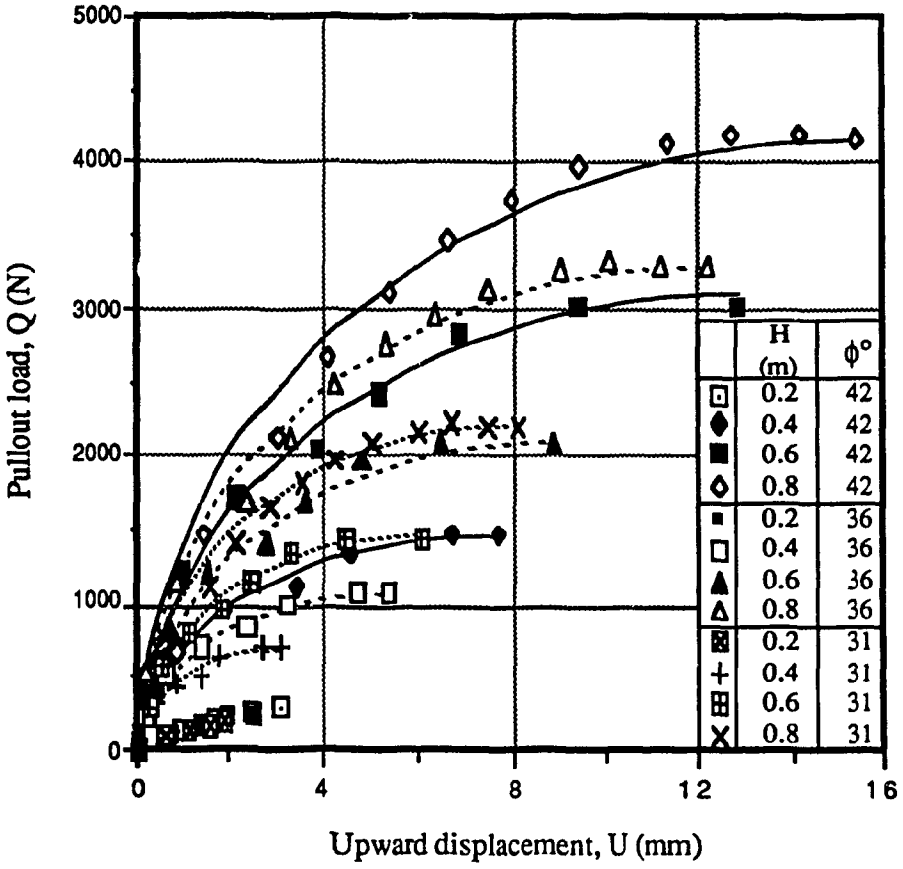

Fig. 3.10: Pullout load versus upward displacement in dense, medium, and loose sand.

determined from the load-displacement curves plotted for all the conducted tests. Figure 3.11 presents the relationship between the ultimate pullout load and installation depth for the tested types of screw anchors installed in dense sand. Similar relationships can be found in case of medium and loose sand. From this figure, it can be seen that the geometrical properties of the screw anchor has little or no influence on the recorded value of uplift capacity. Also, from Fig. 3.11 it can be observed that as the depth of installation increases, the differences between the ultimate pullout loads of the tested anchors become more significant. This can be attributed to the stress development in the sand during anchor installation.

Figure 3.12 shows the relationship of sand depth versus lateral stress in the sand after anchor installation. It is obvious from this figure that the shape (geometrical properties) of the screw anchor has a significant effect on the development of lateral stress in the sand layer during anchor installation. This effect becomes more significant in deep depths. It can also be observed that the ratio between the anchor's pitch (p) and the diameter of its first blade (B) is an important factor influencing the lateral stress development. For Type 1 screw anchor, pitch/diameter ratio (p/B) equals 0.2, it can be indicated from Fig. 3.12 that this type causes the smallest increase in the developed lateral stress due to installation. Type 3 screw anchor, ratio p/B = 0.4, causes the largest increase in the lateral stress due to installation, as compared with the other single pitch screw anchors (Type 1 and Type 2). This shows that the larger the pitch/diameter ratio, the greater is the developed lateral stresses in the sand layer due to anchor installation. The helix angle (ψ) of a screw anchor is dependent on the pitch/diameter ratio where $\psi^{\circ} = \tan^{-1} p/\pi B$. Based on this definition of the helix angle (ψ), a conclusion can be generalized for screw anchors with a single pitch: the greater the helix angle of a screw anchor, the greater is the developed lateral stress in the sand due to installation. Analyzing the behaviour of Type 4 and Type 5 screw anchors from Fig. 3.12, one may conclude that the parallel blades screw anchor (Type 5) develops lateral stresses during installation lower than those developed by the unsymmetrical screw anchor (Type 4). This can be explained in terms of the densification effect that each type causes to the sand deposit during installation. Both Type 4 and Type 5 screw anchors is a multi pitch screw; Type 4 is a screw with three equal

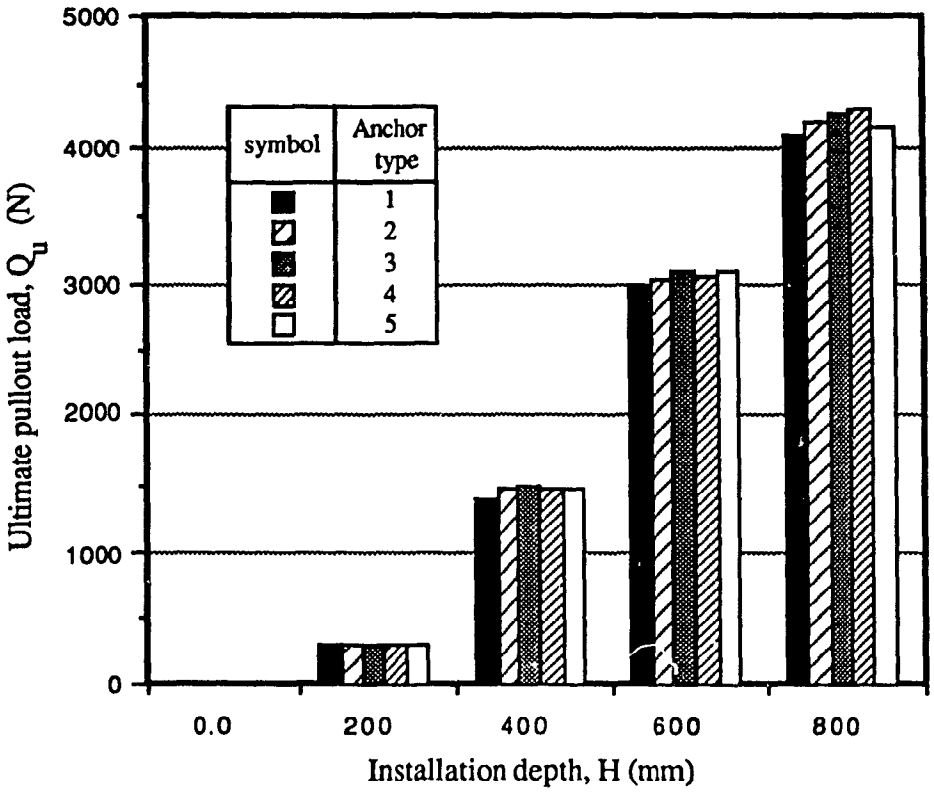

Fig. 3.11: Ultimate pullout load versus installation depth for tested types of anchors installed in dense sand; experimental results.

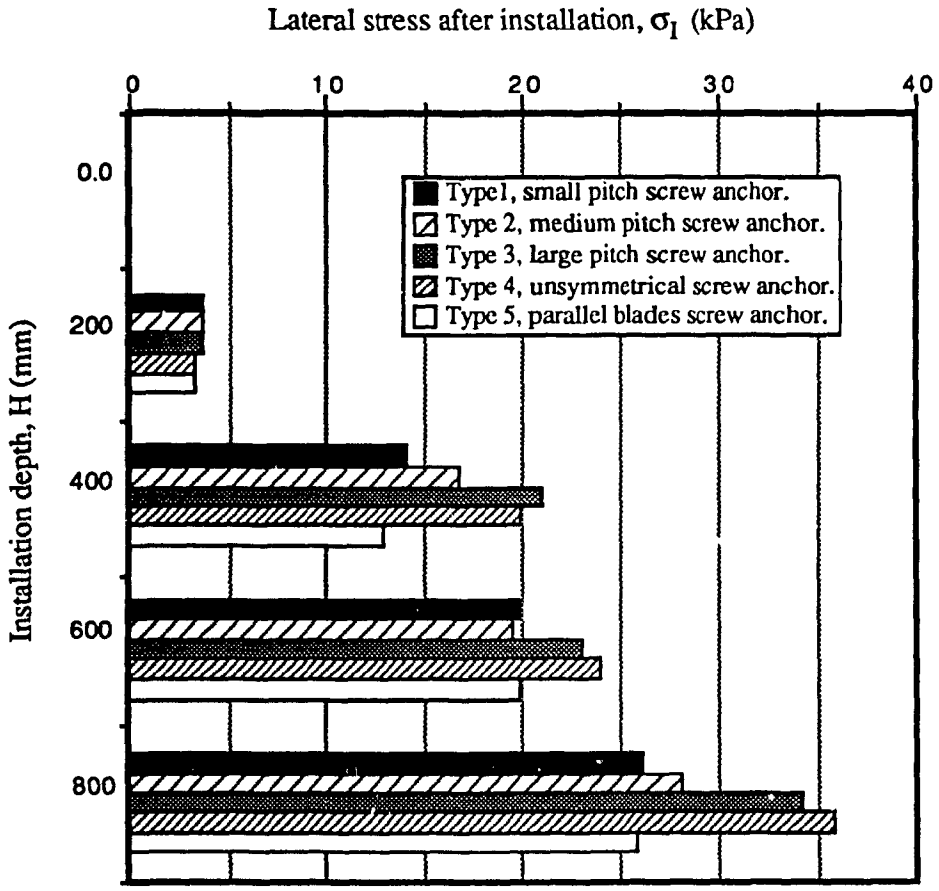

Fig. 3.12: Installation depth versus lateral stress after installation of screw anchors in dense sand.

pitchs and three different helix angles, while Type 5 is a screw with three variable pitchs but three equal helix angles. Also, this is due to the minimal densification effect of the parallel blades screw anchor on the sand deposit which is a result to the introductory effect of the screw's parallel blades conical end. Although the unsymmetrical screw anchor also has a conical end, the existence of this conical end results in more densification to the sand because it has three different helix angles, which is contrary to the case of the parallel blades screw anchor. Hence, the existence of equal helix angles conical end results in easier installation as well as lesser magnitude of the developed lateral stress due to installation, while the existence of a variable helix angles conical end results in an opposite effect. It should be mentioned that the relationship shown in Fig. 3.12 is for dense sand state, but a similar relationship can be observed for the case of medium and loose sand.

A typical relationship of sand depth versus the developed lateral stress in the sand at failure due to the application of the pullout load, is shown in Fig. 3.13. From this figure it can be seen that the initial state of stress developed in the sand layer due to anchor installation has a considerable effect on the lateral stress field produced by the same anchor at failure. Comparing between Fig. 3.12 and Fig. 3.13, one can conclude that the application of a pullout load to the anchor increases the lateral stresses around and in the near vicinity of the anchor. An almost equal amount of lateral stress increase is recorded for all tested types of anchors installed to a specific depth. This indicates that the screw anchor configuration has no effect on the development of the lateral stresses during the stage of uplifting load application. Furthermore, it can be observed from Fig. 3.13 that for anchors installed to a deep depth (H = 800 mm), there was a significant increase in the lateral stress at failure for the types of anchors showed low lateral stress after installation, (Types 1, 2, and 5), as compared with the types of anchors that showed high lateral stress after installation, (Types 4, and 5). This behaviour demonstrates the fact that the lateral stress at failure for different types of anchors installed in a sand with the same characteristics, is supposed to be the same for all, but the developed lateral stress after installation for every type of screw anchors remains a factor strongly affects the "after installation stage" (stage of loading). Similar observations can be observed in the case of

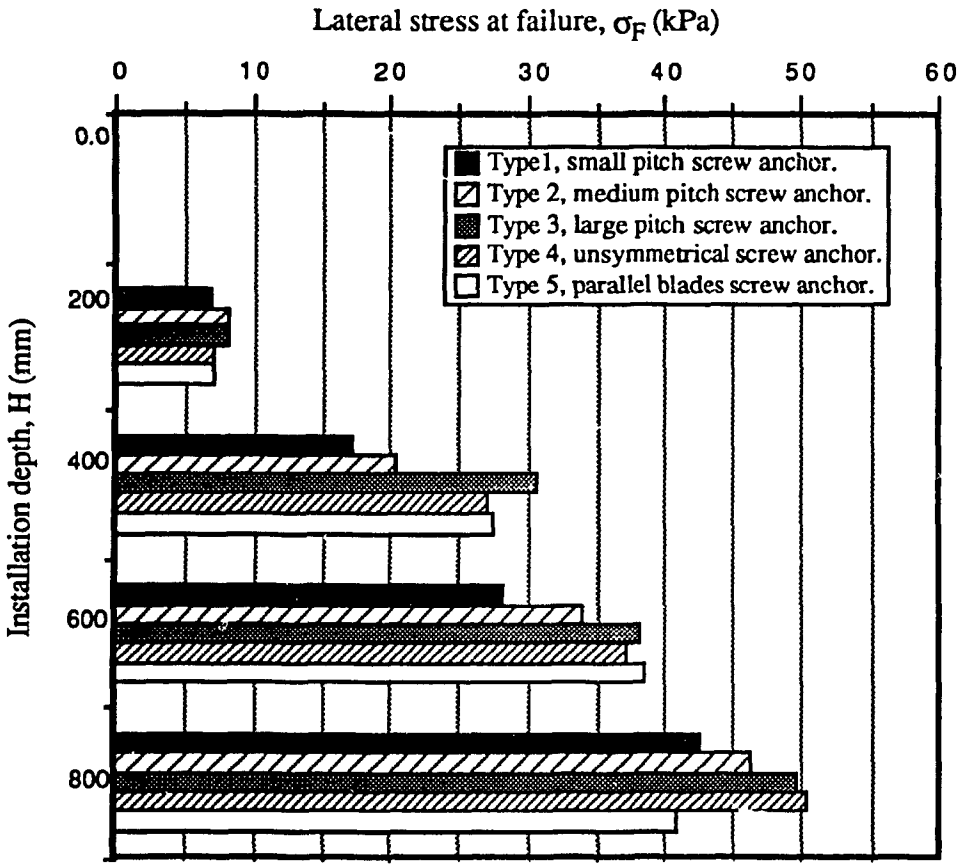

Fig. 3.13: Installation depth versus lateral stress at failure of screw anchors in dense sand.

medium and loose sand.

Figures 3.14 through 3.18 present the lateral stress development in the stress transducers located in the tested sand layer due to the advancement of the screw anchor inside the sand. Each figure shows the typical relationship between the installation depth and lateral stress during installation for one type of the tested anchors. Part (a) from each figure presents the influence line of stress development in the transducers located at 0.1m from the anchor's axis, and part (b) for stress transducers located at 0.2 m from the anchor's axis. It can be noticed from these figures that the influence lines of lateral stress development in the transducers due to the advancement of screw anchor in the sand deposit, are usually higher for stress transducers located nearer to the installation path. Also, it can be seen that the lateral stress in a given stress transducer increases as the anchor approaches the location of the stress transducers. This emphasizes the fact that the installation of a screw anchor in a sand layer creates a stress field around and in the near vicinity of the installation path. This stress field is created due to the densification effect caused by the installation process. The extent of this stress field away from anchor's axis depends primarily on the initial relative density of the sand layer. For higher value of initial relative density, a larger extent of densification effect is expected. Moreover, from Fig. 3.14 through 3.18 it can be indicated that the stress transducers located at relatively very shallow depth of embedment (H = 0.1 m) showed poor response to the advancement of the screw anchor in the sand, while those located at relatively deep depth of embedment (H = 0.7 m) showed the greatest response to the advancement of the screw anchor in the sand. This can be explained in terms of the overburden pressure acting on the top surface of the screw blade to withstand the relative upward movement of the sand wedge above the screw unit due to its rotation. In case of shallow installation depth, the low value of the overburden pressure is not sufficient to withstand the relative upward movement of the sand wedge above the screw unit, hence, stress development in the sand transfers into vertical surface upheave with neglected lateral effect. In case of deep installation depth, higher overburden pressure is involved in resisting the relative upward movement of the sand wedge above the screw unit. This results in a local densification of the sand around the anchor and extends several anchor

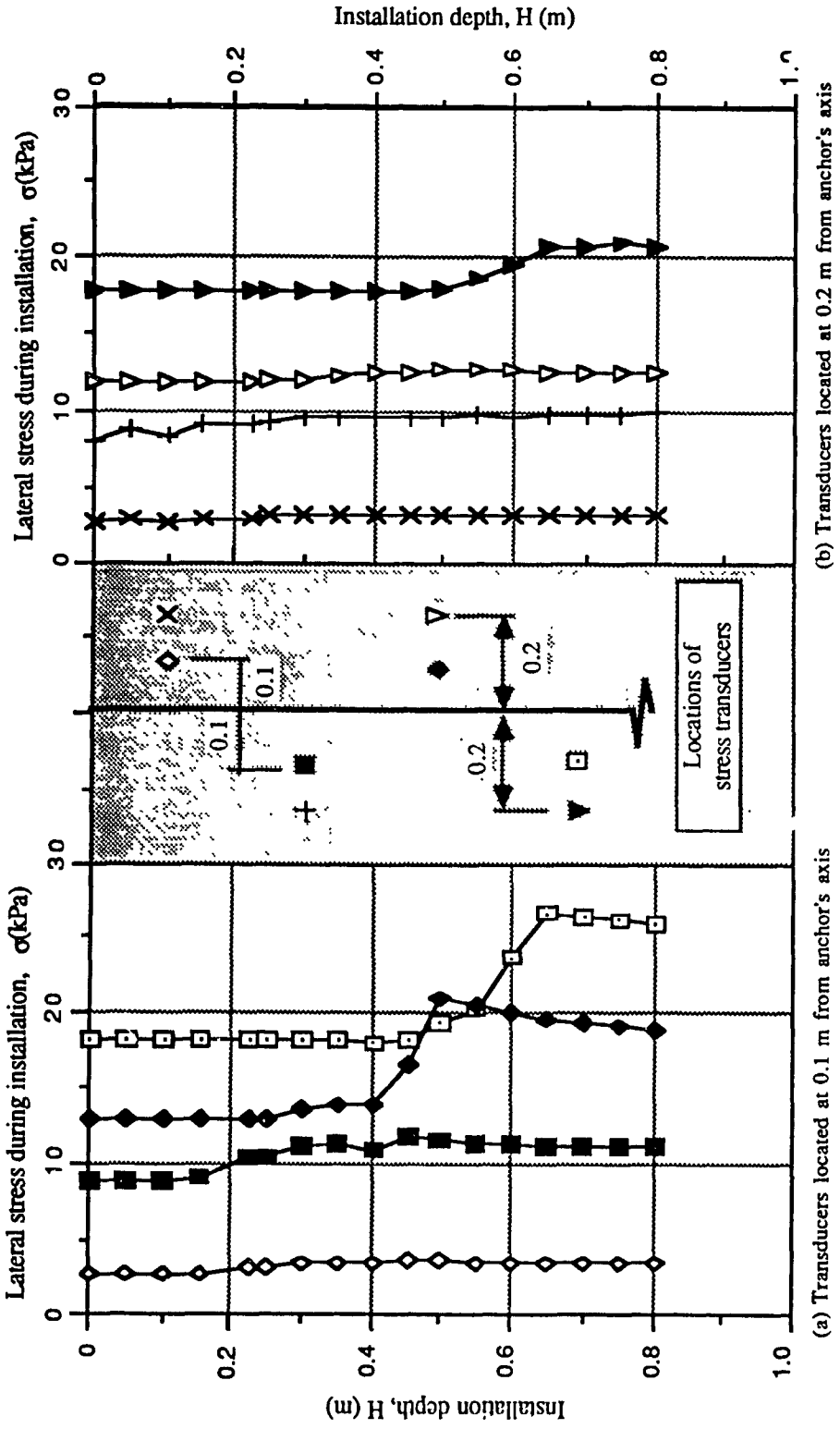

Fig. 3.14: Stress development in sand due to anchor installation. Type 1 screw anchor installed in dense sand; experimental results.

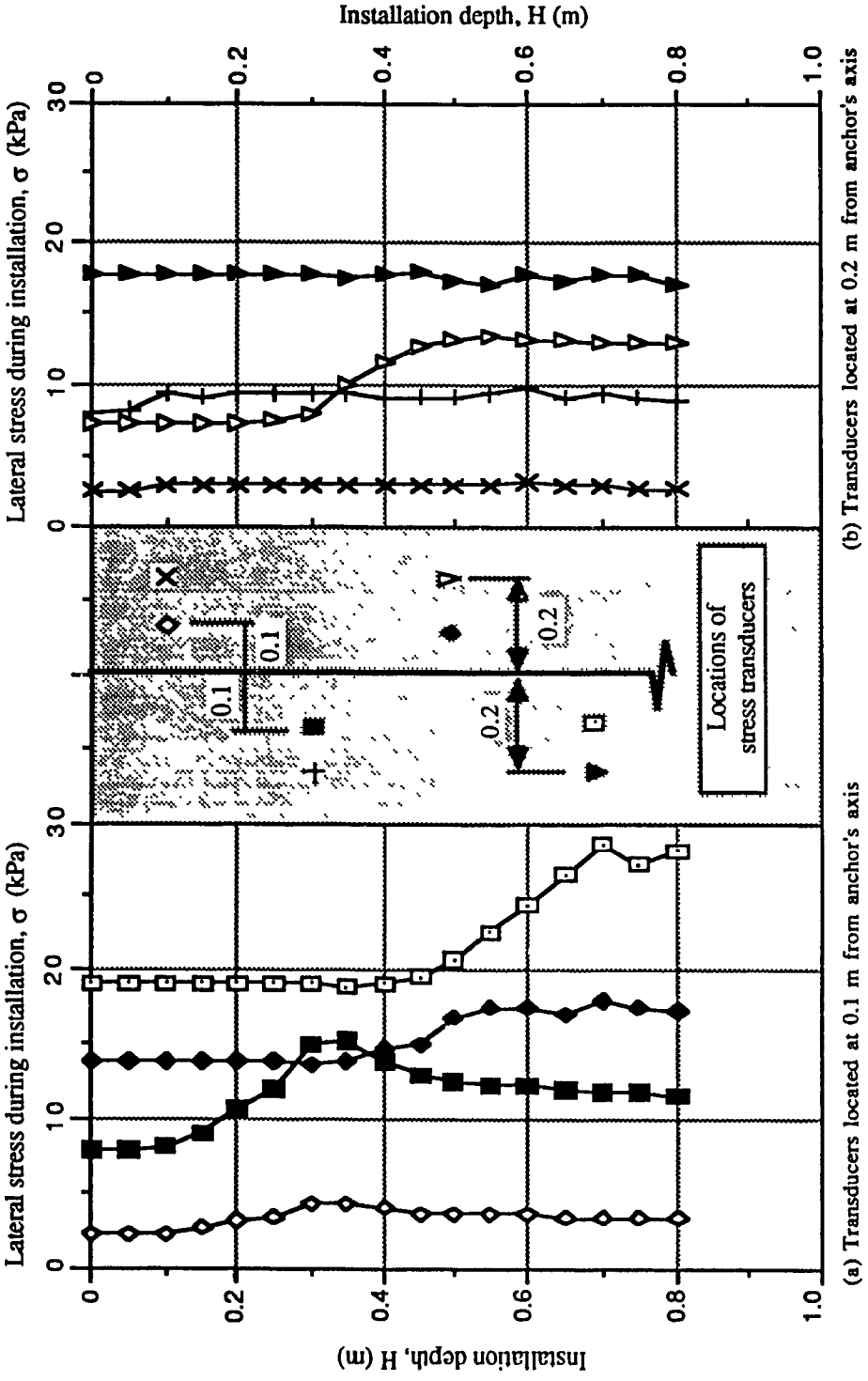

Fig. 3.15: Stress development in sand due to anchor installation. Type 2 screw anchor installed in dense sand; experimental results.

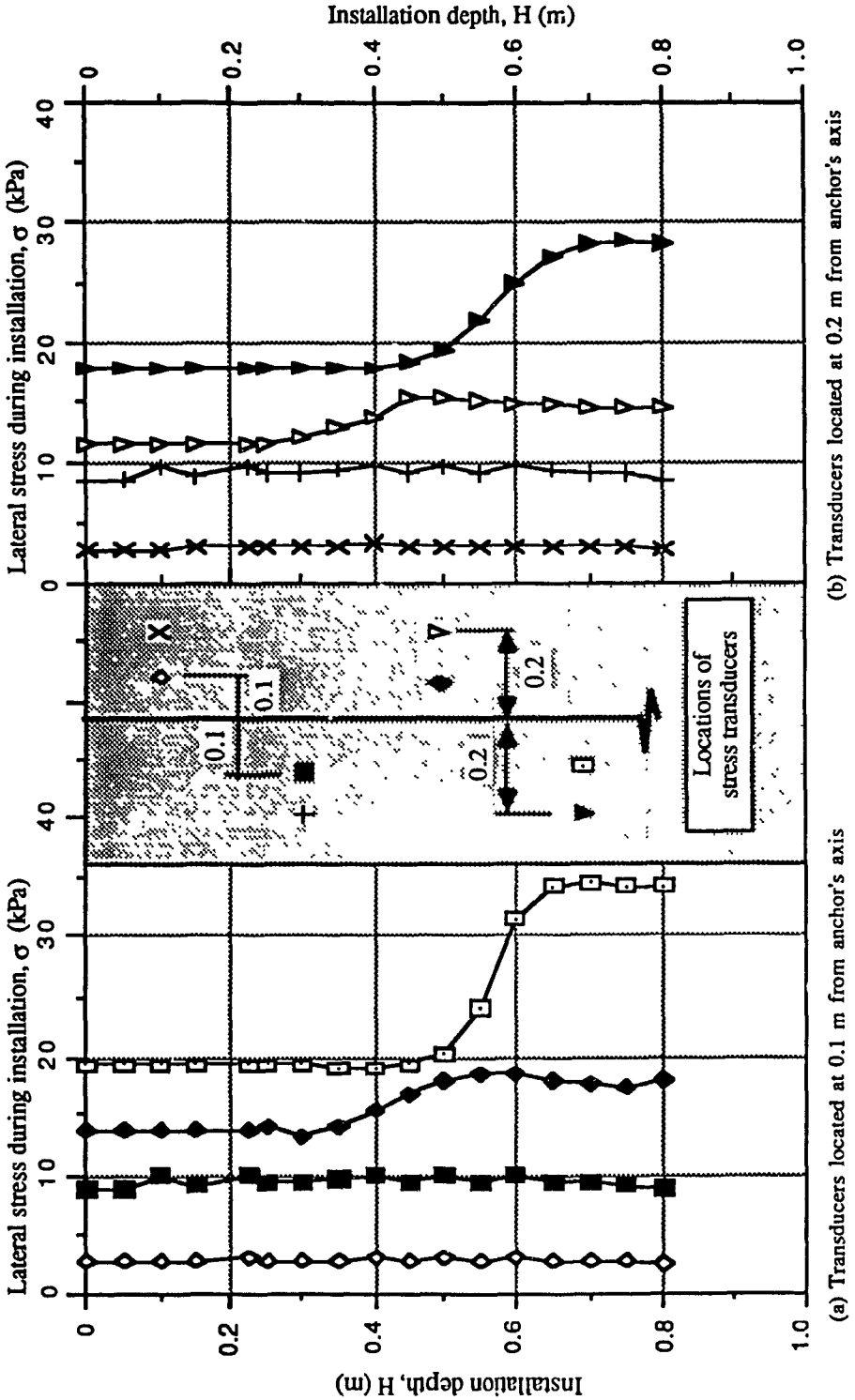

Fig. 3.16: Stress development in sand due to anchor installation. Type 3 screw anchor installed in dense sand; experimental results.

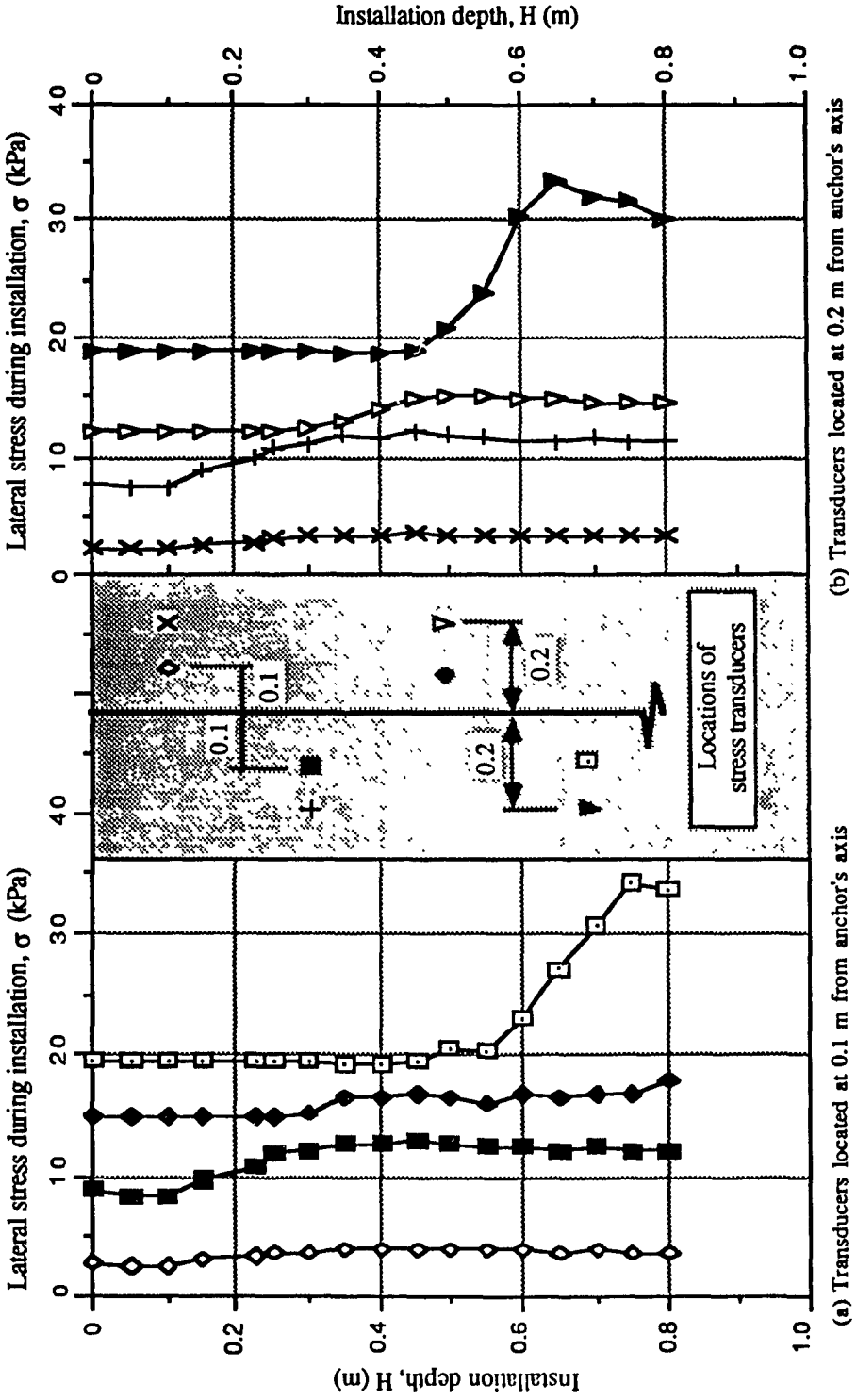

Fig. 3.17: Stress development in sand due to anchor installation. Type 4 screw anchor installed in dense sand; experimental results.

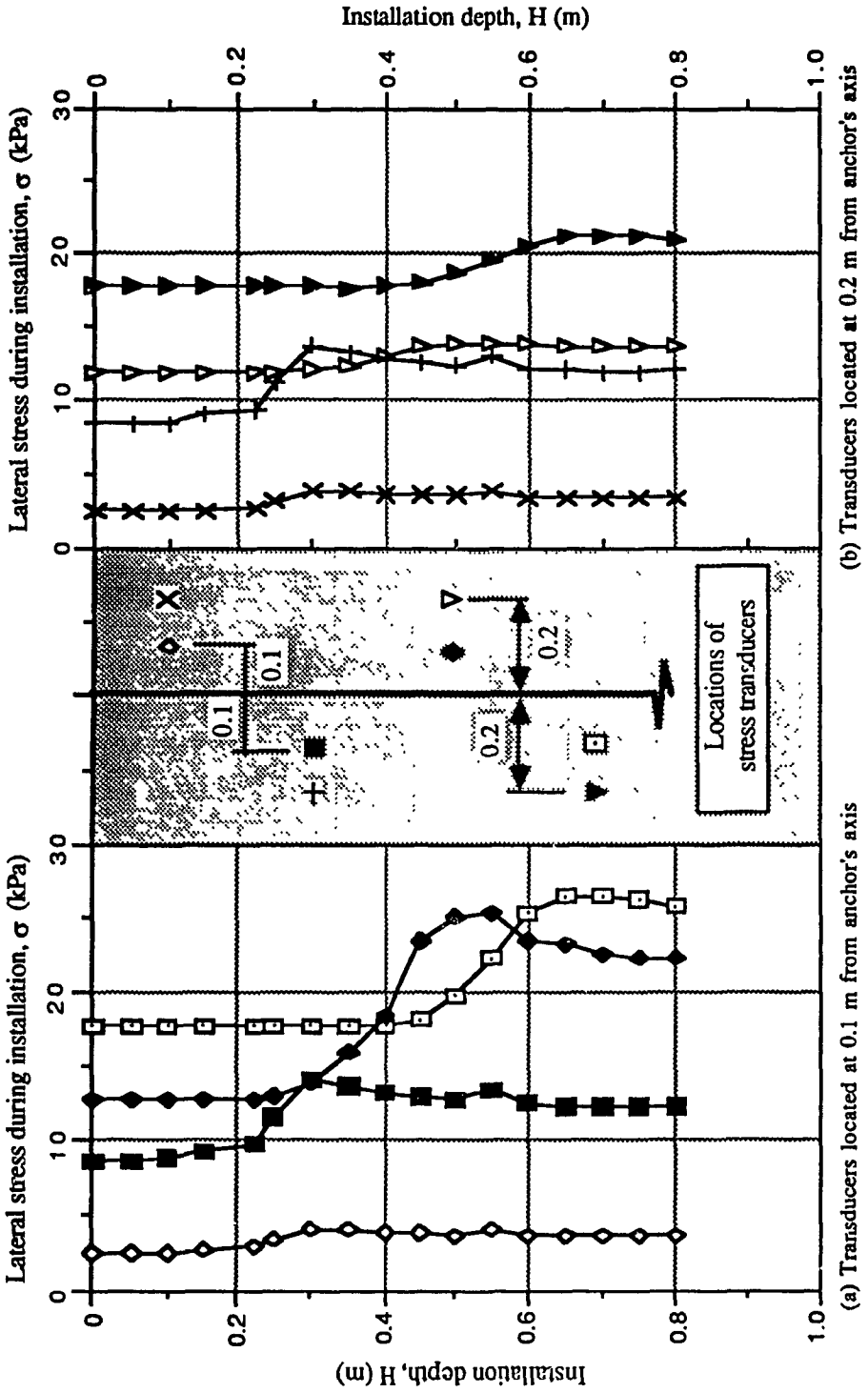

Fig. 3.18: Stress development in sand due to anchor installation. Type 5 screw anchor installed in dense sand; experimental results.

diameters laterally and, to a lesser extent, vertically.

A comparison between Fig. 3.14 through 3.18 indicates that, for single pitch screw anchors (Types 1, 2, and 3), the anchor with smallest pitch/diameter ratio (i.e., smallest helix angle) develops the lowest increase in the lateral stress during installation; while the anchor with largest pitch/diameter ratio (i.e., greatest helix angle) develops the highest increase in the lateral stress during installation. For multi pitch screw anchors (Types 4, and 5), it can be indicated that the parallel blades screw anchor with equal helix angles (Type 5) develops lateral stresses in the sand lower than those caused by the unsymmetrical screw anchor with variable helix angles (Type 4). Generally, a single pitch screw anchor with a small helix angle or a multi pitch screw anchor with parallel blades and consistant helix angles, are such type of screw anchors that develop the least increase in the lateral stress in the sand due to installation. Similar observations can be observed in the cases of medium and loose sand.

Typical relationships of pullout load versus lateral stress development in the sand during the pullout load application are shown in Fig. 3.19 through Fig. 3.23 for the tested five types of screw anchors. Each curve in the graphs represents the influence line of stress development in every stress transducer due to the progress in the applied pullout load. The first point on each curve represents the recorded lateral stress in the location of the stress transducer after installing the screw anchor. It can be observed from these figures that the stress transducers nearly located to the anchor's screw unit are significantly influenced by the pulling out process, and those which are located far from the screw unit are poorly affected by the progress of pullout load application. This can be explained in terms of the developed failure surface within the sand layer and the relative location of the stress transducer with respect to this failure surface. Taking into account that Fig. 3.19 through 3.23 are plotted for deeply installed anchor (relative depth ratio, H/B = 16), hence, the mode of failure is of a local nature. A closed sand wedge (bulb) is locally created above the upper surface of the top blade of screw unit, due to reaching the point of ultimate pullout load. If a stress transducer is located inside the created failure surface, a considerable increase in lateral stress will be recorded by this transducer as

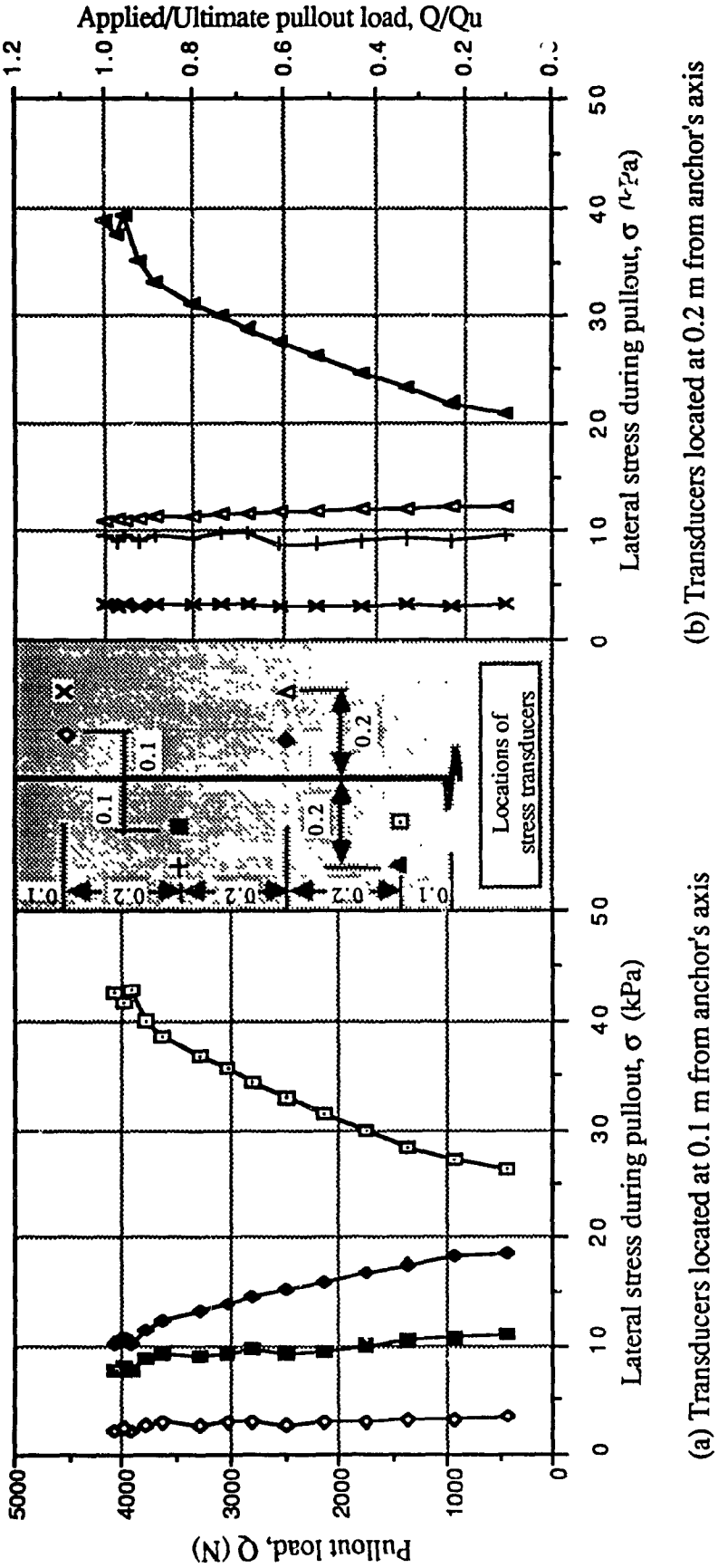

(a) Transducers located at 0.1 m from anchor's axis (b) Transducers located at 0.2 m from anchor's axis

Fig. 3.19: Stress development in sand during pullout load application. Type 1 screw anchor installed in dense sand; experimental results.

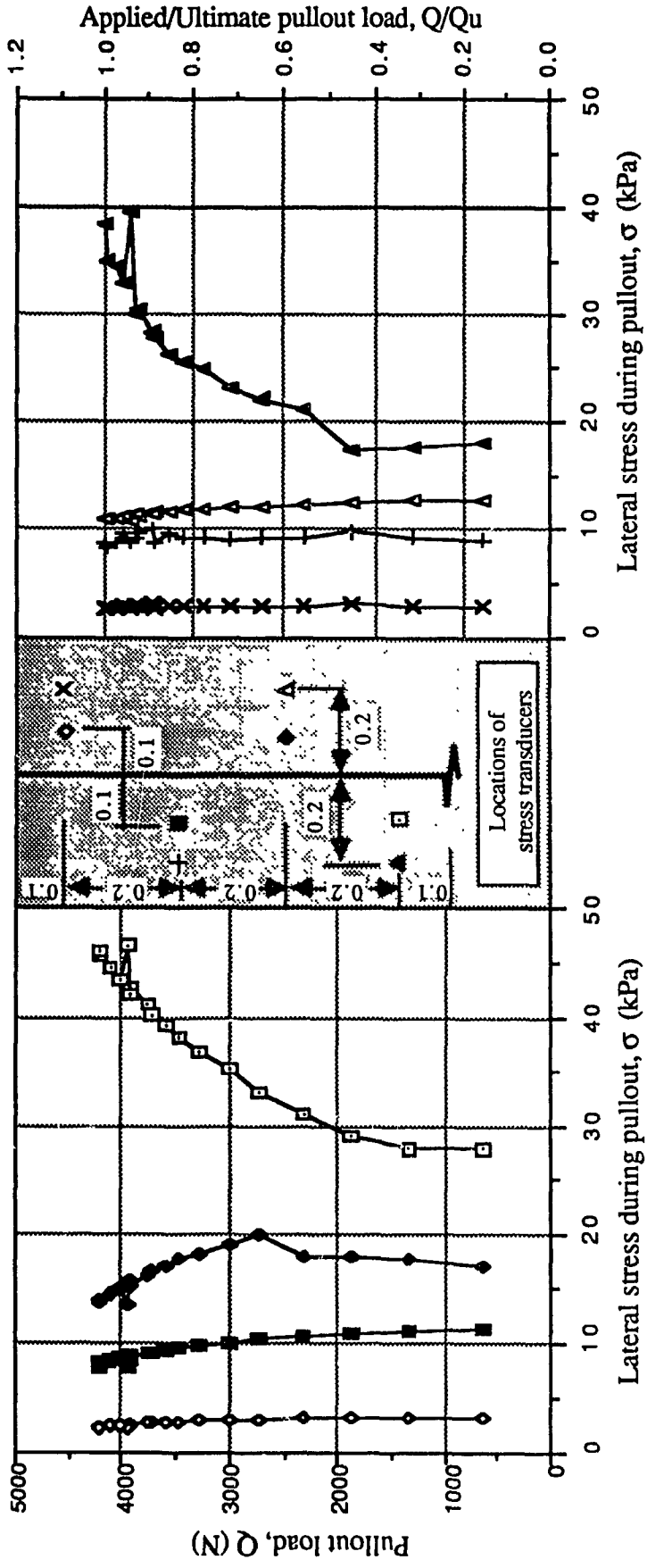

(a) Transducers located at 0.1 m from anchor's axis (b) Transducers located at 0.2 m from anchor's axis

Fig. 3.20: Stress development in sand during pullout load application. Type 2 screw anchor installed in dense sand; experimental results.

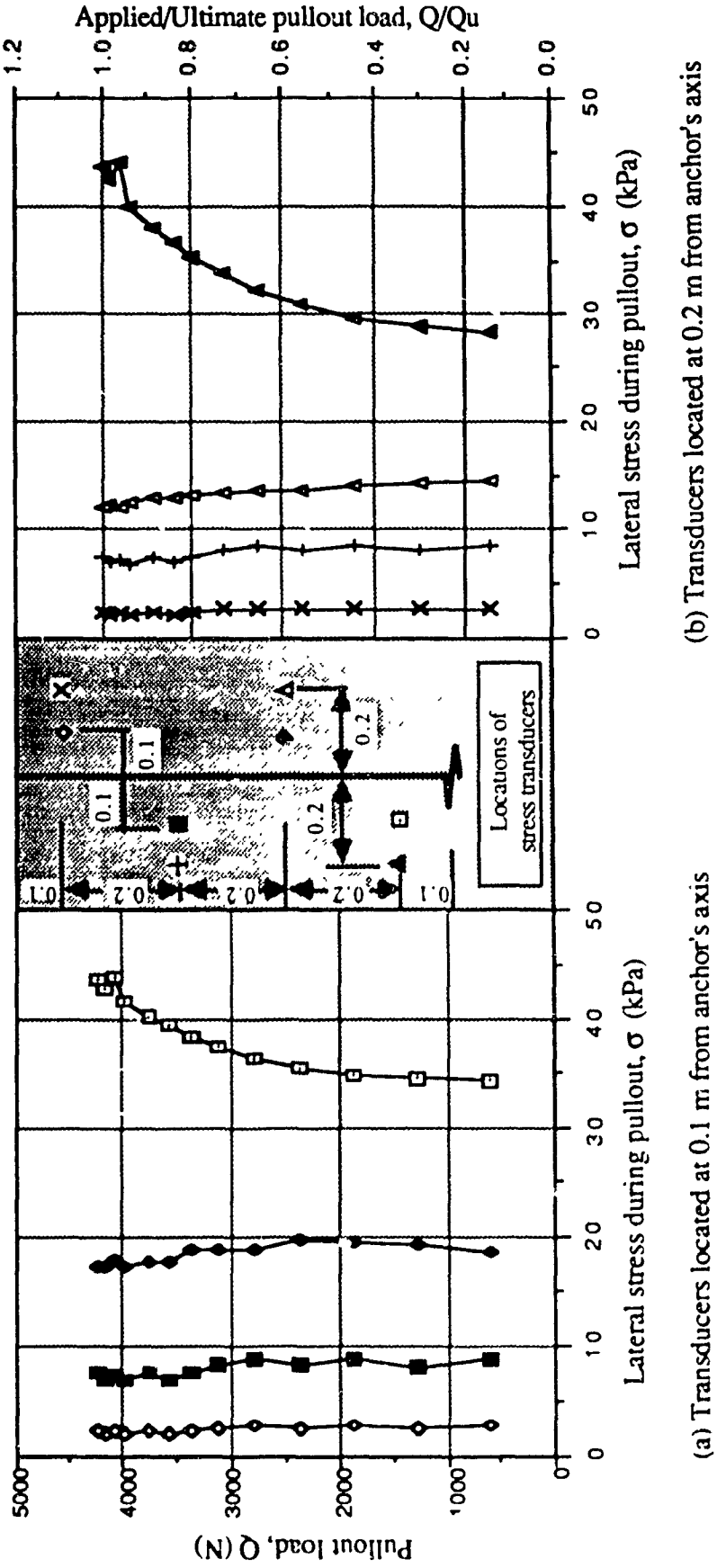

(a) Transducers located at 0.1 m from anchor's axis

(b) Transducers located at 0.2 m from anchor's axis

Fig. 3.21: Stress development in sand during pullout load application. Type 3 screw anchor installed in dense sand; experimental results.

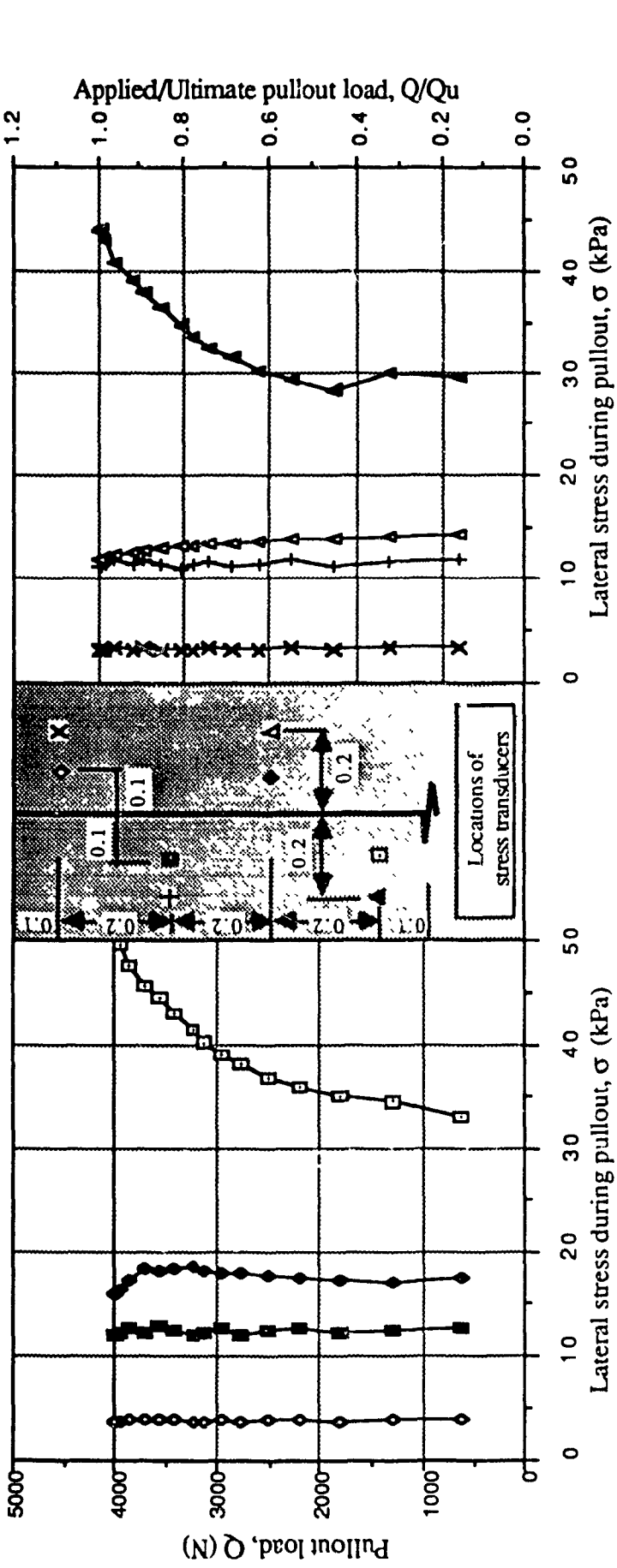

(a) Transducers located at 0.1 m from anchor's axis

(b) Transducers located at 0.2 m from anchor's axis

Fig. 3.22: Stress development in sand during pullout load application. Type 4 screw anchor installed in dense sand; experimental results.

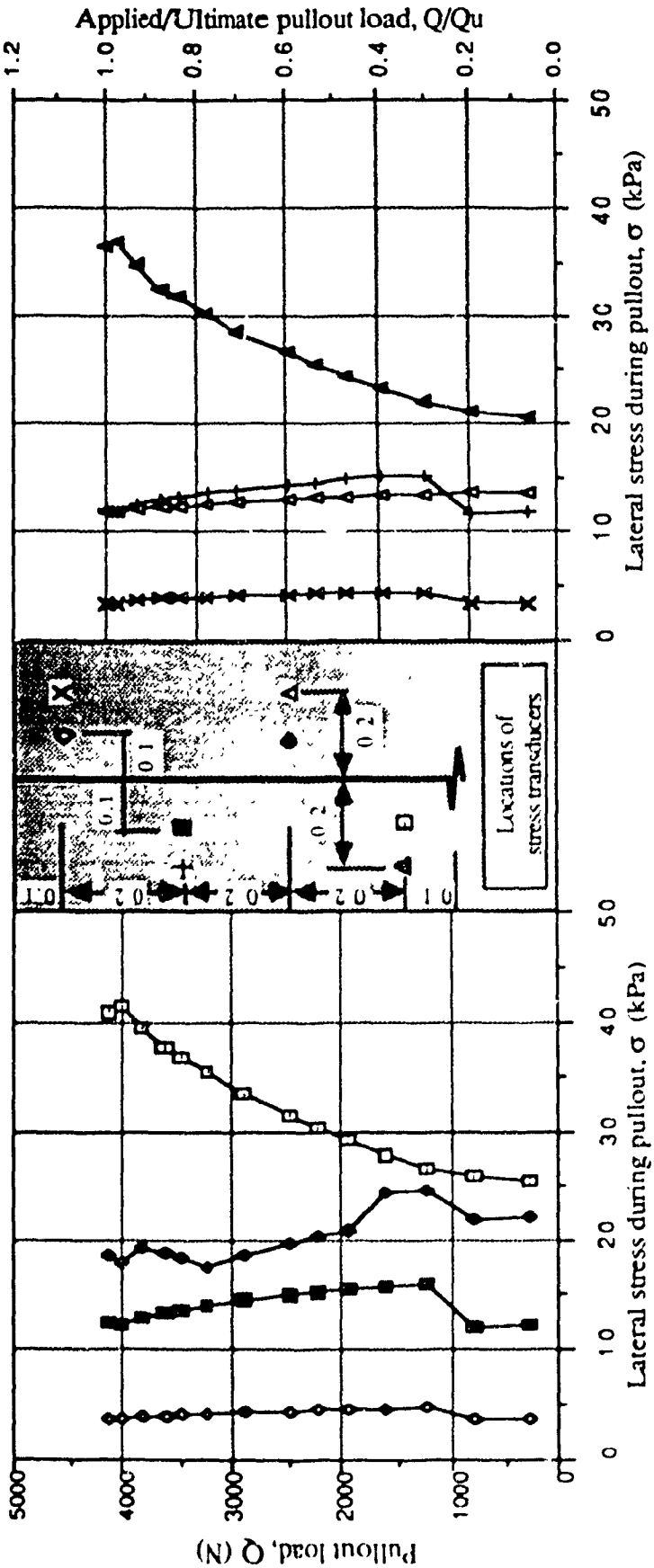

(a) Transducers located at 0.1 m from anchor's axis (b) Transducers located at 0.2 m from anchor's axis

Fig. 3.23: Stress development in sand during pullout load application. Type 5 screw anchor installed in dense sand; experimental results.

uplifting process progresses. This is due to the fact that the closed sand wedge becomes harder as the pullout load increases due to the increase of the compressive force acting upon this wedge. This sand wedge, together with the screw anchor act as one solid unit when failure becomes imminent. Contrarily is the behaviour of the stress transducers located outside and far from the created failure surface, where there is little or no influence from the applied pullout load on the developed stresses in these zones

From Fig. 3.19 through Fig. 3.23, it can be noticed that when the ratio of the applied load to the ultimate pullout load (Q/Q_u) is about 0.95, a considerable disturbance occurs in the sand zone surrounding the screw unit and irregular behaviour takes place. This reflects on the measured lateral stresses where sudden variations occur in a relatively very small stage of loading. It is of interest to report that these variations were not observative in the case of screw anchors with multi pitch (Type 4, and 5), (Fig. 3.22 and Fig. 3.23).

A typical lateral stress development plan in the sand layer due to the sand placing technique, screw anchor installation, and pullout load application is shown in Fig. 3.24. This figure demonstrates the fact that every progressive stage of testing, results in a variation in the magnitude of the measured lateral stress. After placing the sand, the value of the lateral stress (σ_S) is dependent on the depth of sand and the placing technique. As the test proceeds, the lateral stress increases from σ_S to σ_I which represents the measured lateral stress after installation. The value of σ_I is dependent on the geometrical characteristics of the screw anchor (pitch, diamter, and helix angle), and the method of installation. During the application of pullout load, the lateral stress developed in the sand deposit increases from σ_I till it reaches its maximum value at failure σ_F. For a given depth of sand, the value of σ_F depends mainly on the initial state of stress created after anchor installation and recorded before starting the uplifting process. From Fig. 3.24, the lateral stress development in a sand layer can be subdivided into three main zones; namely: (1) after sand placing, (2) during anchor installation, and (3) at failure.

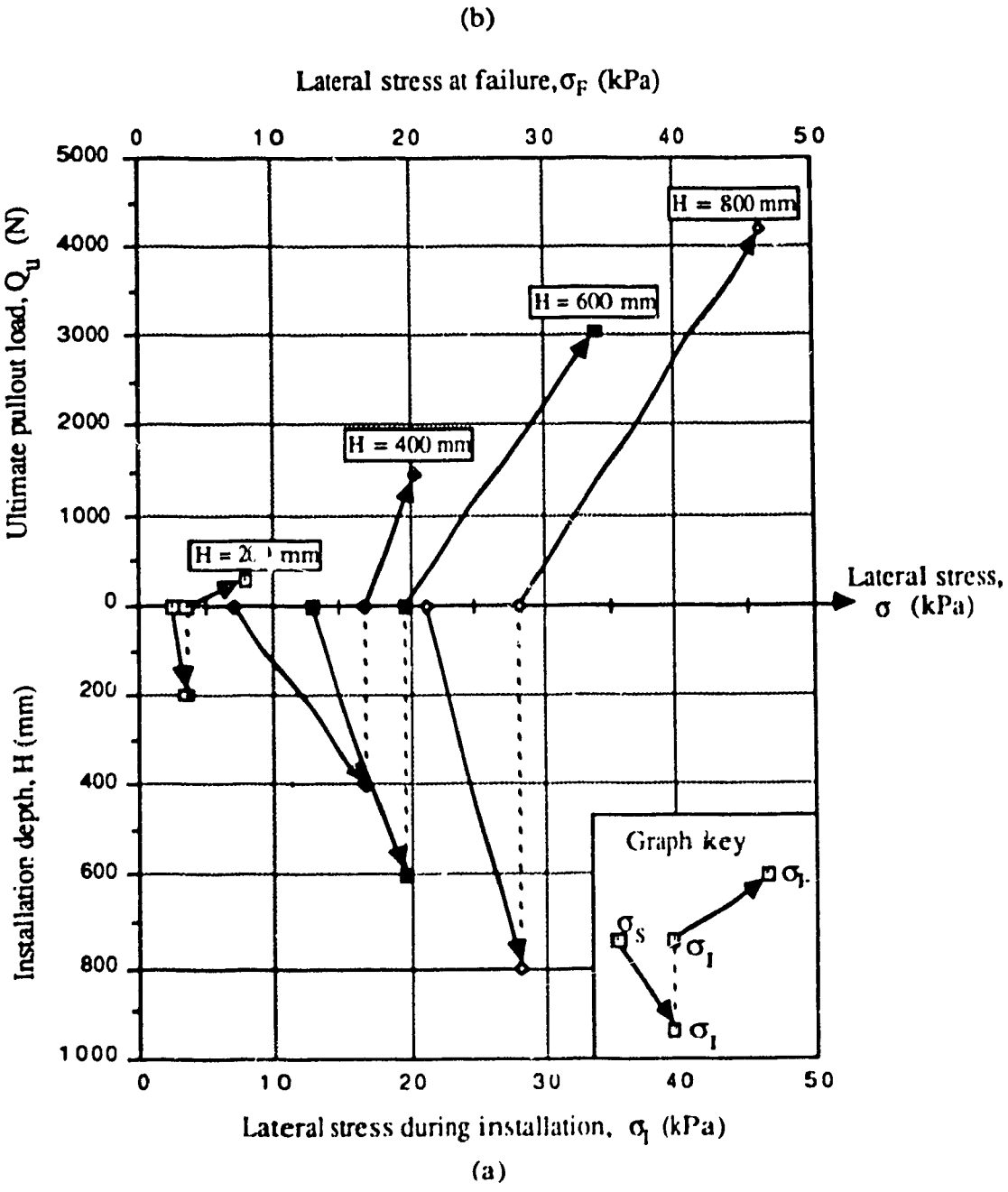

Fig. 3.24: Typical stress development in the sand after placing, during anchor installation, and at failure.

Figures 3.25a through 3.25e present typical relationships between anchor installation depth and the lateral earth pressure measured at that depth at rest condition, after sand placing, after anchor installation, at failure, and at passive state. Lateral stresses at rest condition (σ_O) were calculated based on the theoretical coefficient of lateral earth pressure at rest (K_O) given by Jaky (1944) [27],

$$K_O = 1 - \sin \phi \qquad ...(3.1)$$

where ϕ = angle of shearing resistance of the tested sand. The results of the experimental investigation plotted in Fig. 3.25 shows, however, that the lateral earth pressure at rest after placing the sand (σ_S) is higher than that calculated theoretically for normally consolidated (NC) sand. This indicates that high horizontal (lateral) stresses induced in the sand layer due to the applied impulsive effort during compaction procedure to obtain the high density. Similar observations were reported in other studies. Andreadis et al. (1981) [4], reported lateral stresses ranges between two to three times higher than the calculated theoretical values for dense sand compacted by vibration. Clemence and Pepe (1984) [11], showed that the lateral earth pressure at rest (σ_O) was approximately doubled with the use of a vibrating compactor to compact sand to relative density $D_r = 90\%$. Based on the above, it can be deduced that the use of a tamping technique to compact the sand to obtain high relative densities results in overconsolidated sand (OC).

The overconsolidated ratio (OCR) of sand depends on the applied compactive effort to the layer to obtain the required relative density. Also the OCR depends on the depth of the tested sand as the applied compaction to a certain sand layer affects the previous layers. The coefficient of lateral earth pressure of an overconsolidated sand layer at rest condition ($K_{O(OC)}$) is equal to the measured coefficient of lateral earth pressure after placing the sand (K_S). From the results of the present experimental investigation, K_S was calculated as the ratio between the measured lateral and vertical stresses at a given depth after placing the sand. Lateral stress at a

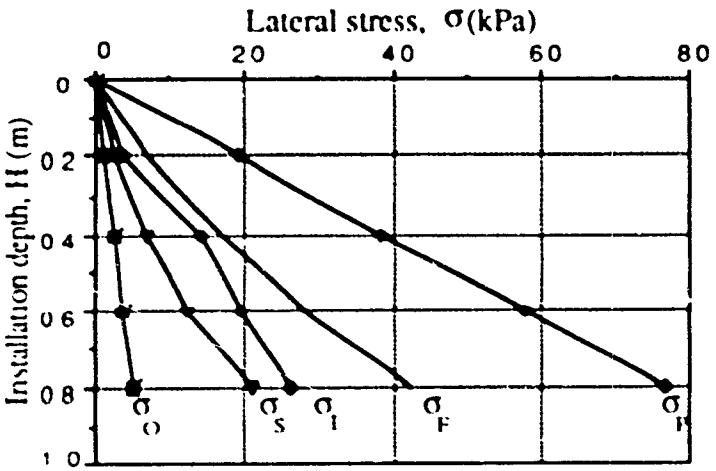

(a) - Type 1, small pitch screw anchor

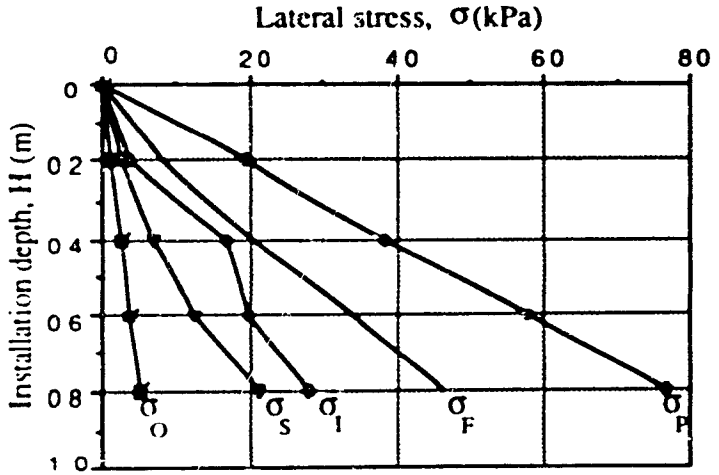

(b) - Type 2, medium pitch screw anchor

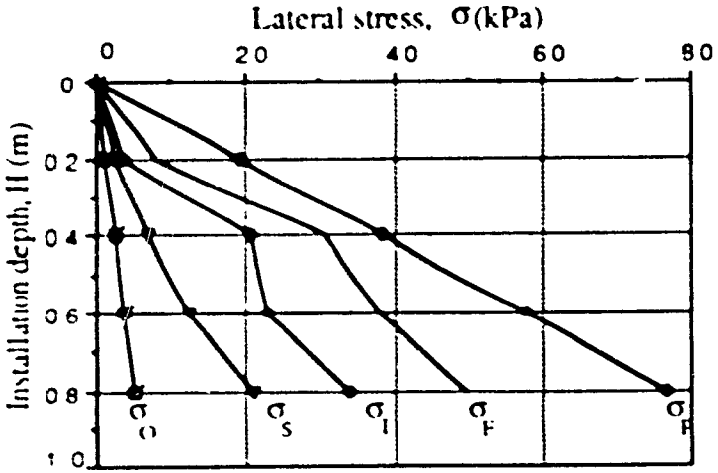

(c) - Type 3, large pitch screw anchor

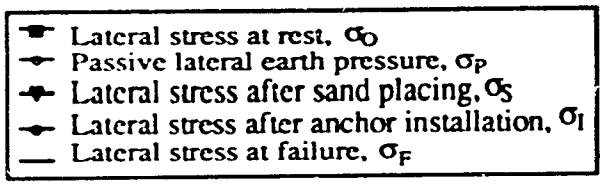

Fig. 3.25: Relationship between installation depth and lateral earth pressure in dense sand; experimental results.

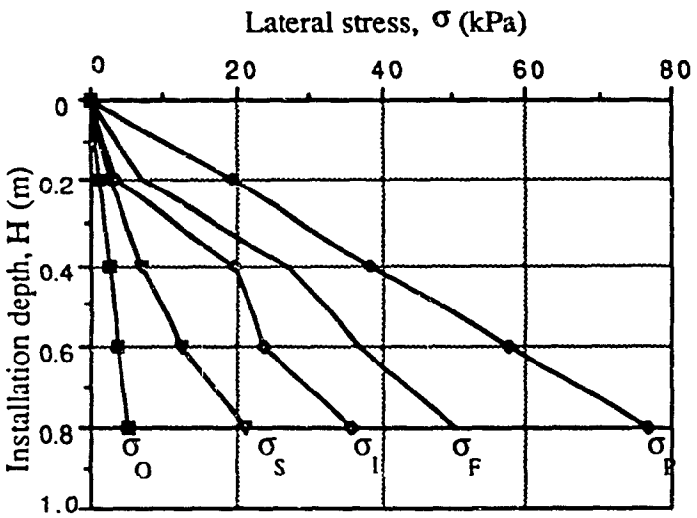

(d) - Type 4, unsymmetrical screw anchor

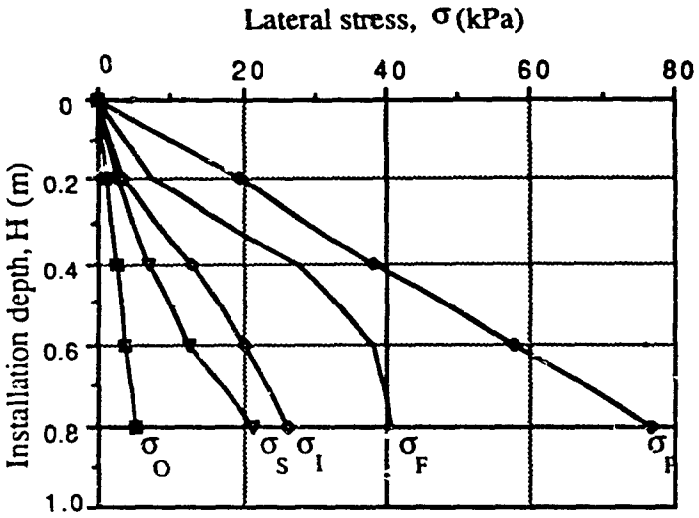

(e) - Type 5, parallel blades screw anchor

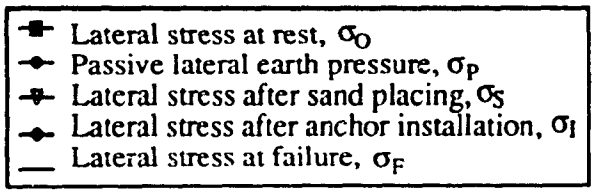

Fig. 3.25cont'd: Relationship between installation depth and lateral earth pressure in dense sand; experimental results.

given depth was calculated as the average of two measurements of two stress transducers placed above and below the point in question. Vertical stress was the average of four measurements of four stress transducers. The calculated averages of the measured stresses together with the coefficient of lateral earth pressure after placing the sand (K_S) are shown in Table 3.5.

Wroth (1972) [75], proposed a relationship from which the coefficient of lateral earth pressure at rest for overconsolidated granular soil can be determined by employing the known overconsolidation ratio. This expression reads as follows:

$$K_{O(OC)} = K_{O(NC)} \cdot OCR - (\mu/1-\mu)(OCR-1) \qquad ...(3.2)$$

Where $K_{O(OC)}$ and $K_{O(NC)}$ are the respective values of K_O for overconsolidated and normally consolidated soil, μ is Poisson's ratio, and OCR is the overconsolidation ratio.

This expression was employed in a reversed way in the present investigation to determine the value of the OCR. Since $K_{O(NC)}$ can be calculated from the theoretical expression given by Jaky's equation (eq. 3.1) and $K_{O(OC)}$ is the measured K_S from the experiment, hence, eq. (3.2) can be used to determine the OCR. Proper values were assumed for the Poisson's ratio (μ) for the tested sand. Identical values of μ for dense, medium, and loose sands are 0.2, 0.16, and 0.12, (Lambe and Whitman (1969) [36]). Calculated values of OCR are shown in Table 3.5.

From the data shown in Table 3.5, it can be observed that the higher the required relative density, the greater is the OCR calculated for a given depth of sand. Moreover, for a given relative density, the OCR increases with the increase of the compacted depth of sand. A comparison between the values of $K_{O(NC)}$ and $K_{O(OC)}$ indicates that there was a considerable

Table 3.5: Stresses after placing the sand and calculated overconsolidation ratio.

H (m)	H/B	$\phi°$	$K_{O(NC)}$	$K_{O(OC)}=\sigma_{Sexp.}/\sigma_{Vexp.}$		$K_{O(OC)}=K_S$	OCR
				$\sigma_{S\ exp.}$	$\sigma_{V\ exp.}$		
0.2	4	42	0.331	2.65	6.31	0.420	2.1
0.4	8	42	0.331	7.06	14.80	0.477	2.8
0.6	12	42	0.331	12.47	24.12	0.517	3.3
0.8	16	42	0.331	21.17	35.40	0.598	4.3
0.2	4	36	0.412	2.76	4.68	0.589	1.8
0.4	8	36	0.412	6.81	10.04	0.678	2.2
0.6	12	36	0.412	13.39	16.07	0.833	2.9
0.8	16	36	0.412	22.21	23.00	0.966	3.5
0.2	4	31	0.485	2.41	3.86	0.624	1.4
0.4	8	31	0.485	6.42	8.04	0.799	1.9
0.6	12	31	0.485	11.73	12.51	0.938	2.3
0.8	16	31	0.485	20.08	18.10	1.110	2.8

increase in the magnitude of the lateral earth pressure coefficient at rest due to overconsolidation. This increase becomes larger as the depth of embedment increases due to the increase of the OCR.

Figures 3.25a through 3.25e show also the measured values of lateral stresses in the sand after anchor installation. The test results show that the installation of screw anchors into the sand layer induces significant increase in the lateral stresses. This is due to the densification effect caused by screwing the anchor into the sand. During the application of a rotating moment (Torque) to the anchor's shaft, the anchor penetrates the sand causing it to displace in lateral and vertical directions. When the overburden pressure on the screw element is high enough to act against the vertical sand movement, the sand displaces laterally and this displacement results in sand densification which reflects on the measured lateral stress. Similar observations were reported by Clemence and Pepe (1984) [11]. It can be indicated from Fig. 3.25 that the installation depth and screw anchor configuration are the main factors affecting the value of lateral stress after anchor installation.

Lateral stresses during pullout load application and at failure were measured for all the tests conducted in this study. The "at failure" lateral stresses for the tested types of screw anchors were plotted in Fig. 3.25. It can be seen that as the anchor is loaded up to failure, a significant increase in the lateral stresses was recorded. This stress increase is attributed to the dilation and reorientation of soil particles as it is subjected to shearing force. The volume increase of the soil mass results in larger lateral stress along the yielding soil interface. The sand's relative density and the developed lateral stress due to installation are the main factors influencing the measured lateral stress at failure.

The passive lateral earth pressure is the upper limit of the pressures developed in the sand due to an applied shearing force. From Fig. 3.25, it can be noticed that the lateral stress at failure increases towards the passive state and approaches it but it never exceeds the passive condition. The ratio between the measured lateral earth pressure at failure for a given depth

(σ_F) and the theoretical computed value of σ_P at the same depth, produces a factor (F_r) specifies the amount of stress developed in the sand due to failure at the location of the stress transducer. The results of the present experimental study showed that, for a given sand depth, the value of the factor F_r increases with the increase of the angle of shearing resistance as well as with the relative density. Also, the present study suggests that, for a given sand characteristics, the F_r value slightly increases with the installation depth.

Typical deflection of sand surface at failure is shown in Fig. 3.26 for dense, medium, and loose sand. From this figure, it can be indicated that the relative depth ratio (H/B) affects the value of the sand surface deflection as well as the extent of this deflection. Also, this figure shows that the surface deflection is larger for higher values of angle of shearing resistance. Moreover, the relative depth ratio (H/B) after which no sand surface deflection was observed can be identified as the ratio at which the deep anchor behaviour takes place. Hence, for the tested dense, medium, and loose sands the critical relative depth ratios were, 10, 8, 6 respectively.

3.10 Shape of Rupture Surface

Special experiments were conducted on sand with coloured layers in order to determine experimentally the shape of rupture surface. A tank of perspex 1.0 x 0.55 x 0.12 m, length, depth, and width respectively was used to place the coloured sand layers, Plate 3.15. A guide frame was mounted on the top of the tank to keep the screw anchor in place during installation. Torque was applied to the anchor's shaft until the required installation depth was reached. Vertical pullout load was then applied in increaments to allow photographing the progress of the rupture surface. It was observed that the final shape of the rupture surface takes place at about 95% of the ultimate pullout load and any further application of pullout load results in moving the failing mass confined by the rupture surface in an upward direction. Observations recorded in the sand layered system as well as surface deflections suggest that the rupture

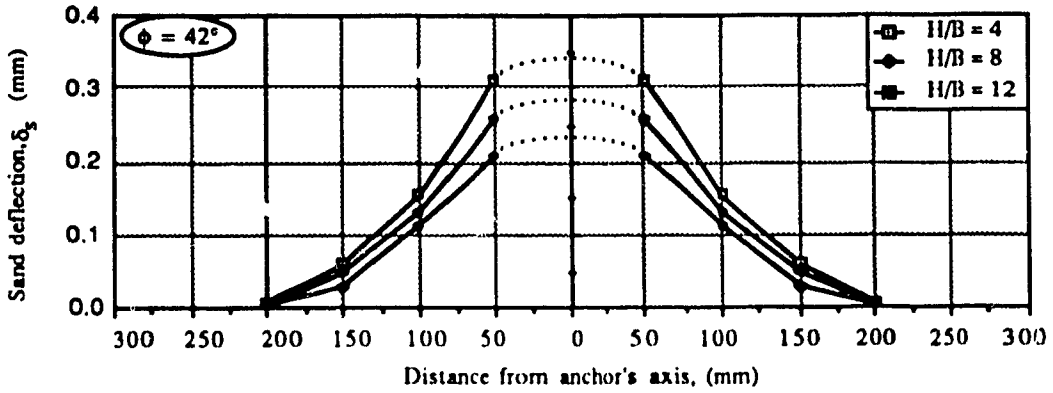

(a)

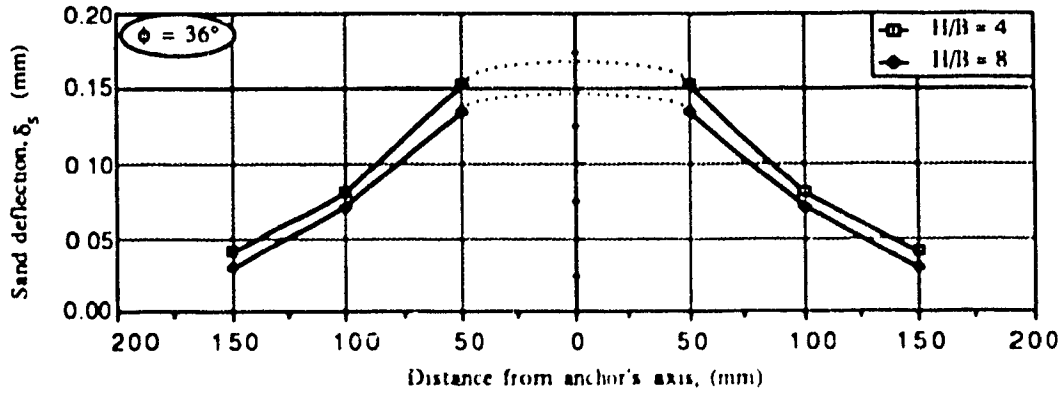

(b)

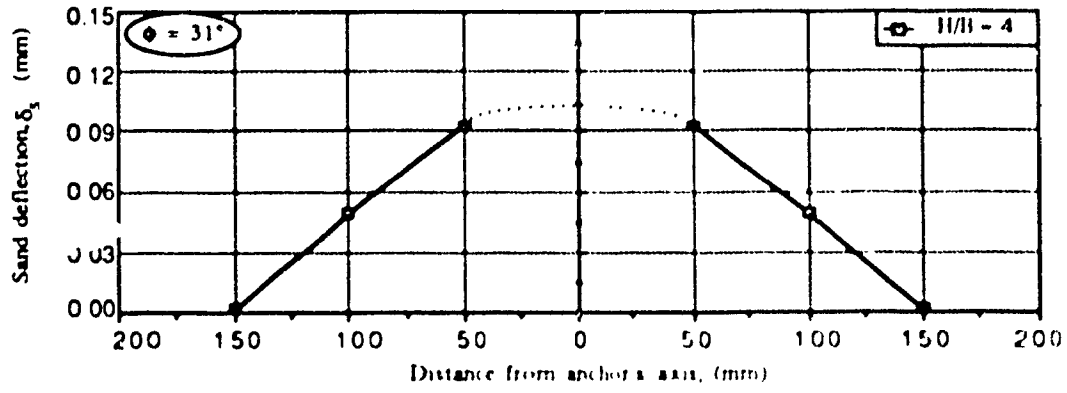

(c)

Fig. 3.26. Typical deflection of sand surface at failure

surface can be closely approximated to a logarithmic spiral curve. A tangent to the log-spiral curve at the anchor's level makes an angle of 90° with the screw unit, and the curve intersects the sand surface at an angle of $(\pi/4 - \phi/2)$ due to the development of the passive state in the sand at failure. A unique sliding surface exists for a given embedment depth ratio of the anchor and relative density of the sand.

The above mentioned boundary conditions are used to fix the geometrical position of the segment of the log-spiral representing the rupture surface.

Similar observations regarding the shape of rupture surface were reported by Khadilkar et al. (1971) [32]. They observed, experimentally, that a log-spiral curve can represent the rupture surface for under-reamed piles subjected to tension forces.

Curved rupture surface has been observed by numerous number of investigators, Balla (1961), Adams and Hayes (1967), Meyerhof and Adams (1968), Larnach and McMullan (1974), Wang and Wu (1980), Sutherland et al. (1983), Ghaly (1986), etc. However, due to the difficulty encountered in calculating the uplift resistance components (soil weight and shear force) on curved rupture surface, it was usually approximated to a plane failure surface. In the present investigation, however, the analysis will be performed considering the actual observed surface of rupture.

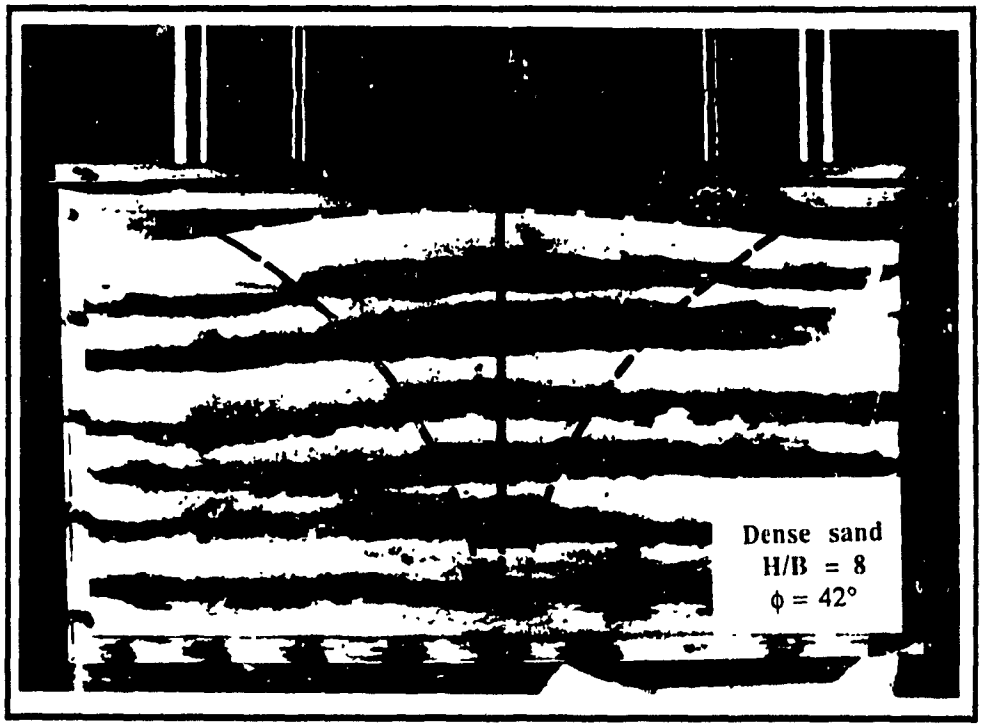

Plate 3.15: The logarithmic spiral surface of rupture observed experimentally.

CHAPTER 4

Group Action of Screw Anchors

4.1 Concept

Experimental tests on group action of screw anchors in sand incorporated a variety of variables and factors influencing the group performance. Group configuration, center-to-center spacing between anchors, group size, installation technique, order of installation, embedment depth ratio, and distribution of uplift load amongst the individual anchors of the group are examples of such factors. In the present investigation a trial has been made to study the effect of the above mentioned factors on group performance.

An experimental set-up was instrumented to allow measuring the total uplift capacity and upward displacement of a group as well as of every single anchor in the group. This was achieved by a system of load cells mounted on top of the anchors' shafts. Also, the average upward displacement of the group as well as the relative (differential) upward displacement of the individual anchors were measured by dial gages.

4.2 Experimental Set-Up

The same set-up described before in Section 3.2 was used to conduct the experimental tests on the group action of screw anchors. The stress transducer units were removed from the inside of the tank to provide clear sand layer for the pupose of group installation. The loading system

was provided by a proving ring 50 kN capacity to measure the expected high uplift resistance of a group of great number of anchors installed into great depth. For small number of anchors group installed in loose sand or into shallow depth, the total pullout capacity of the group was measured by means of load cell 10 kN capacity, mounted in the place of the proving ring. This system was adopted to guarantee that the uplift capacity is measured with a good accuracy. Caps were made of steel plates 10 mm thick, and provided with holes located at distances according to the proposed spacings, Plates 4.1, 4.2, 4.3, and 4.4. These groups' caps were found to behave as rigid slabs. Pullout load was applied to the group of anchors at the central point of the cap, however, for large number group installed in dense sand to great depth, pullout load was applied at four points lying at very small equal distances from the central point.

4.3 Model Screw Anchors

Nine models of Type 2 screw anchor, Fig. 3.6b and Plate 3.12b, were fabricated to be used for the experimental investigation on group action of screw anchors. The choice of this type was based on test results of the single action of the tested five types of model screw anchors. These results showed that the configuration of screw anchors with the same diameter, has little or no influence on the uplift behaviour although it has significant influence on the stress development in the sand layer. Hence, a single pitch screw anchor is selected for the tests on the group action because this type of anchor is easy to manufacture for practical purposes as well as for laboratory modelling. Moreover, it is easy to analyze the stresses developed on its single blade as installation process takes place. Furthermore, this type of screw anchor represents an intermediate pitch/diameter ratio of the tested screw anchors, hence, the behaviour of a screw anchor with higher or lower pitch/diameter ratio can be predicted.

4.4 Group Configuration

Figure 4.1 shows the configurations of the tested groups in the present research program. Four arrangements of anchors group were tested and the performance of each group was

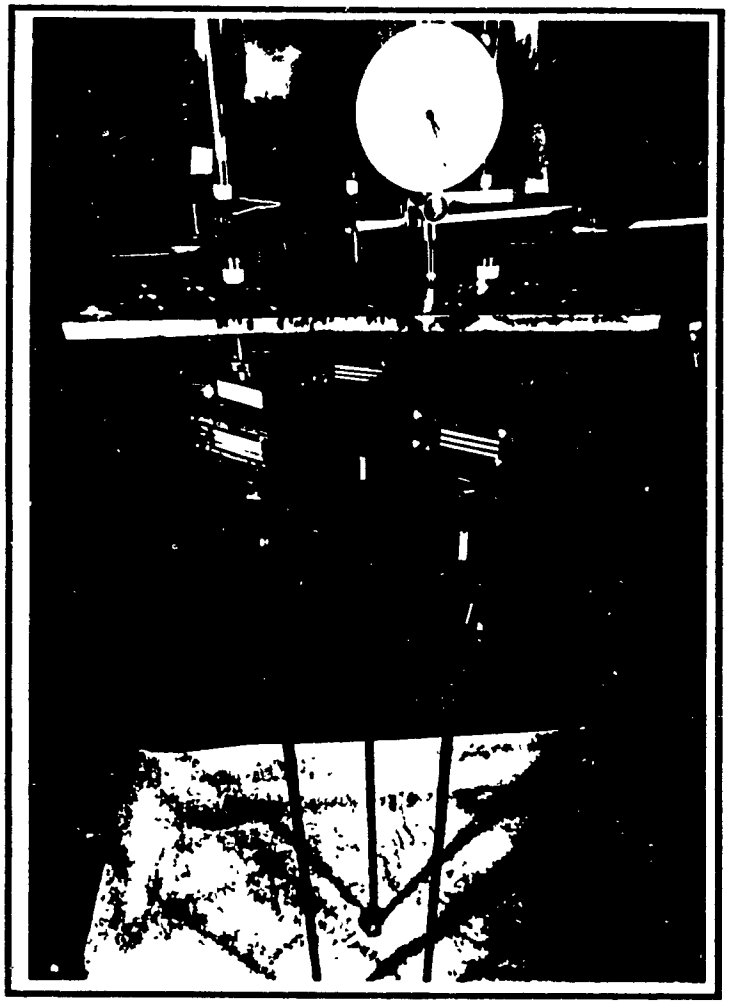

Plate 4.1: Triangular configuration of anchors group (3 anchors).

Plate 4.2: Square configuration of anchors group (4 anchors).

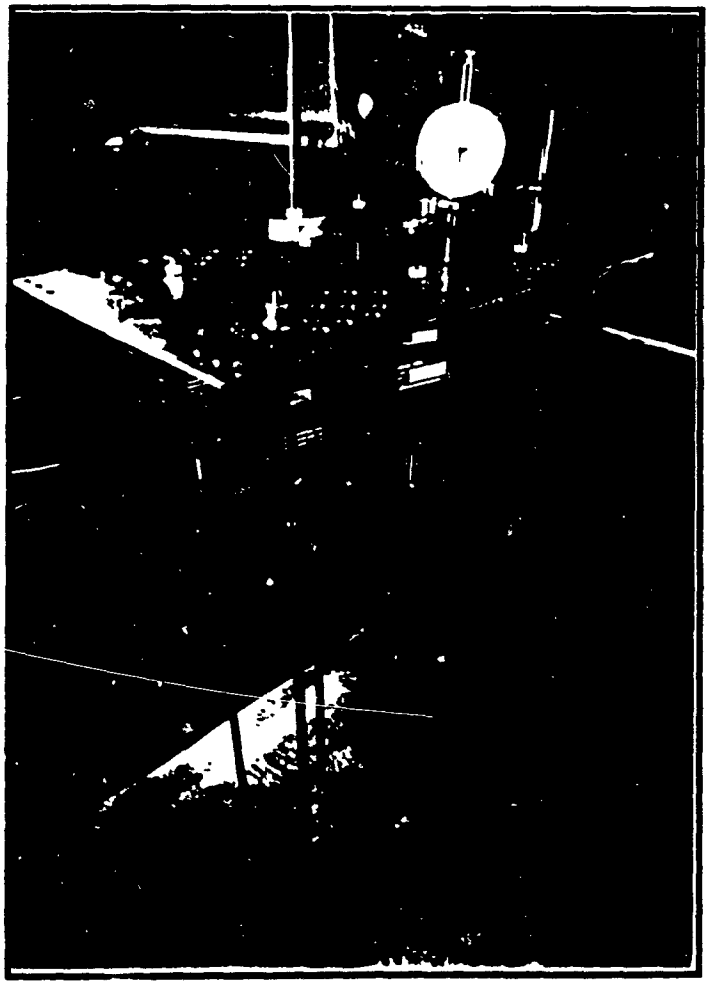

Plate 4.3: Rectangular configuration of anchors group (6 anchors).

Plate 4.4: Square configuration of anchors group (9 anchors).

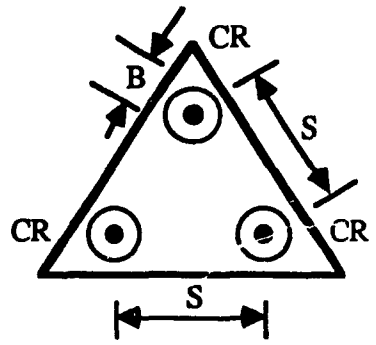

1x3 group, Triangular

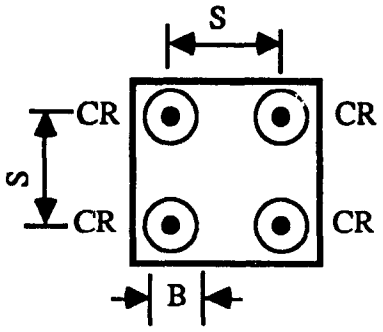

2x2 group, Square

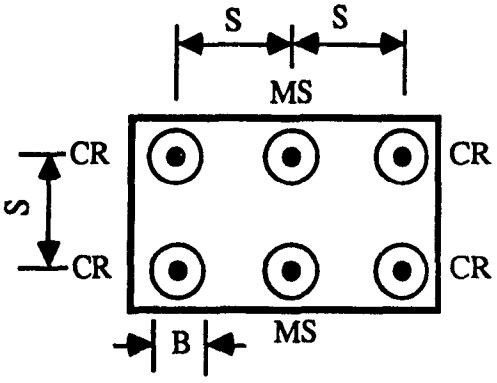

2x3 group, Rectangular

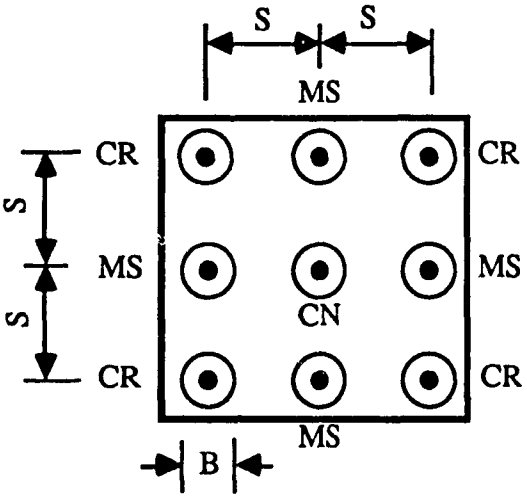

3x3 group, Square

CR = Corner anchor; MS = Midside anchor; CN = Center anchor.	S = Spacing between anchors. B = Anchor diameter.

Fig. 4.1: Tested group configurations and anchors identification.

examined at three different spacing/diameter ratios. The corner, midside, and center anchors in a given group were symboled as CR, MS, and CN respectively (Fig. 4.1). This was achieved to facilitate describing the behaviour of the similarly positioned anchors in different groups.

4.5 Testing Program

The anchors of the above mentioned groups were spaced at spacing/diameter ratio (S/B) of 3, 4, and 5 installed to embedment depth ratio (H/B) of 4, 8, 12, and 16 into dense, medium, and loose sand. A summary of the testing program on the group action of screw anchors is given in Table 4.1.

4.6 Test Procedure

A sand placing technique similar to that described in Section 3.5 was adopted to obtain the required mechanical properties of the tested dense, medium, and loose sand (see Table 3.1 for sand characteristics). After placing the sand in the testing tank, the anchors were carefully located on the sand surface in predetermined positions, according to the spacing, controlled by the group cap. Then they were screwed in the sand deposit by applying a torque to the shaft of each anchor. A roller bearing was used to reduce the friction between the anchors and the cap. The torque required for installation was measured regularly for every 50 mm penetration depth for every single anchor in the group. Load cells 5 kN capacity each were mounted on top of the anchors' shafts to measure the pullout load of every individual anchor in the group. For 1 x 3 and 2 x 2 anchors group, load cells were mounted on top of all the anchors of the group. For 2 x 3 and 3 x 3 group configuration, load cells were mounted on at least two typical anchors in the group, for example, two CR anchors or two MS anchors. This was achieved to assure that similar types of anchors in a group are equally loaded. For 3 x 3 anchors group, a load cell was mounted on the unique central anchor (CN) to measure the share of this anchor in resisting the uplift load.

Table 4.1: Test program on group action of screw anchors.

Group Size	Group Configuration	Dense Sand, $\phi = 42°$		Medium Sand, $\phi = 36°$		Loose Sand, $\phi = 31°$	
		Embedment Ratio (H/B)	Spacing Ratio (S/B)	Embedment Ratio (H/B)	Spacing Ratio (S/B)	Embedment Ratio (H/B)	Spacing Ratio (S/B)
1 x 1	Single	4, 8, 12	--------	4, 8, 12	--------	4, 8, 12	--------
1 x 3	Triangular	4, 8, 12	3, 4, 5	4, 8, 12	3, 4, 5	4, 8, 12	3, 4, 5
2 x 2	Square	4, 8, 12	3, 4, 5	4, 8, 12	3, 4, 5	4, 8, 12	3, 4, 5
2 x 3	Rectangular	4, 8, 12	3, 4, 5	4, 8, 12	3, 4, 5	4, 8, 12	3, 4, 5
3 x 3	Square	4, 8, 12	3, 4, 5	4, 8, 12	3, 4, 5	4, 8, 12	3, 4, 5

Pullout load was then applied vertically to the central point of the group's cap. The total pullout load of the group was measured as well as the portion that every individual anchor resists. Total upward displacement was measured by means of dial gage located as near as possible to the central point of the cap. Every test was started with a level group's cap. Knowing the average upward displacement and comparing the new level of the cap's corners after the group's failure, with the level of a given datum, the differential upward displacement can be obtained. Results of the tests on group action of screw anchors are summarized in Table 4.2.

4.7 Test Results and Discussion

Figures 4.2, 4.3, and 4.4 show a typical relationship of pullout load (Q) versus upward displacement (U) for a single anchor and for an anchor representing the average of the total load of a group installed in dense, medium, and loose sand respectively. It can be noticed from these figures that, for a given applied level of uplift load, the upward displacement in the case of a group of anchors is generally greater than that of a single anchor. This was observed for all group configuration and all tested depths. Furthermore, for a given upward displacement, an average anchor representing a group of a certain number of anchors showed resistance against uplift higher than a group with greater number of anchors. This appears to be clearer for anchors installed to relatively deep depths. The behaviour shown in Figs. 4.2, 4.3, and 4.4 is for spacing/diameter ratio (S/B) of 3 and similar behaviour can be observed from the other tested S/B ratios (4 and 5).

Figures 4.5, 4.6, 4.7, and 4.8 show pullout load versus upward displacement for groups of 3, 4, 6, and 9 anchors respectively. These figures demonstrate the effect of the sand characteristics on the load-displacement relationship. It can be seen that the shear strength of the sand deposit has an appreciable influence on the group performance in uplift, and this influence

Table 4.2: Summary of testing program and results of group action.

Group configuration			1x3 group, triangular		2x2 group, square		2x3 group,rectangular		3x3 group, square	
Depth H (mm)	Spacing S = x B	ϕ (°)	Uplift capacity Qu (N)	Displacement at failure, U (mm)	Uplift capacity Qu (N)	Displacement at failure, U (mm)	Uplift capacity Qu (N)	Displacement at failure, U (mm)	Uplift capacity Qu (N)	Displacement at failure, U (mm)
200	3	42	841	1.631	1105	3.530	1553	3.296	2228	1.558
400	3	42	4917	11.789	6452	10.671	9291	9.914	13406	11.788
600	3	42	11427	20.522	14706	20.522	19254	21.344	30123	19.390
800	3	42	17580	26.774	22853	31.960	32451	32.058	48267	35.164
200	4	42	884	1.714	1127	3.602	1587	3.368	2140	1.497
400	4	42	4873	11.684	6390	12.456	9291	9.316	13540	11.905
600	4	42	10786	19.090	14094	19.660	18413	20.412	27928	17.050
800	4	42	16449	25.244	21509	30.080	30189	30.030	44504	33.688
200	5	42	892	1.730	1196	3.821	1638	3.478	2407	1.684
400	5	42	4962	11.899	6390	12.456	9193	8.830	13272	11.670
600	5	42	10053	17.794	13244	19.017	17049	18.300	29240	16.550
800	5	42	14942	23.206	19828	27.730	27418	27.551	40729	31.661
200	3	36	624	1.210	791	2.529	1130	2.399	1633	1.142
400	3	36	2851	6.838	3636	6.088	5116	5.358	6992	6.148
600	3	36	5580	9.877	7087	10.360	9257	10.263	13489	11.235
800	3	36	8264	14.175	10526	14.720	14561	15.039	20340	16.311
200	4	36	667	1.292	866	2.766	1200	2.547	1716	1.201
400	4	36	2981	7.148	3895	6.594	5373	6.577	7671	6.745
600	4	36	6025	10.664	7840	10.930	9843	10.912	15012	12.165
800	4	36	9062	15.255	11856	16.582	15961	16.293	22424	17.983
200	5	36	716	1.388	931	4.659	1283	2.723	1842	1.289
400	5	36	3176	7.615	4155	7.100	5763	6.909	8254	7.258
600	5	36	6470	11.451	8518	11.442	10547	11.693	16339	12.975
800	5	36	10320	16.538	13060	18.264	17759	16.903	24532	19.673
200	3	31	464	0.922	594	1.323	848	1.824	1143	1.896
400	3	31	1751	3.242	2257	3.425	3170	3.737	4321	3.830
600	3	31	3503	5.215	4429	6.350	5683	6.303	8190	6.078
800	3	31	5287	8.153	6721	9.446	9269	8.314	11909	9.550
200	4	31	504	1.617	631	2.122	902	2.331	1257	2.323
400	4	31	1826	3.651	2388	3.923	3293	4.128	4508	4.242
600	4	31	3746	5.522	4884	6.571	6646	8.316	8911	8.730
800	4	31	5775	8.513	7236	9.824	9543	10.414	12902	12.675
200	5	31	536	2.129	679	2.318	954	2.911	1320	2.736
400	5	31	1996	3.812	2607	3.050	3559	4.524	4816	5.224
600	5	31	4090	6.415	5341	7.227	6886	10.305	9853	10.089
800	5	31	6022	9.337	7849	10.644	10462	13.317	14089	14.753

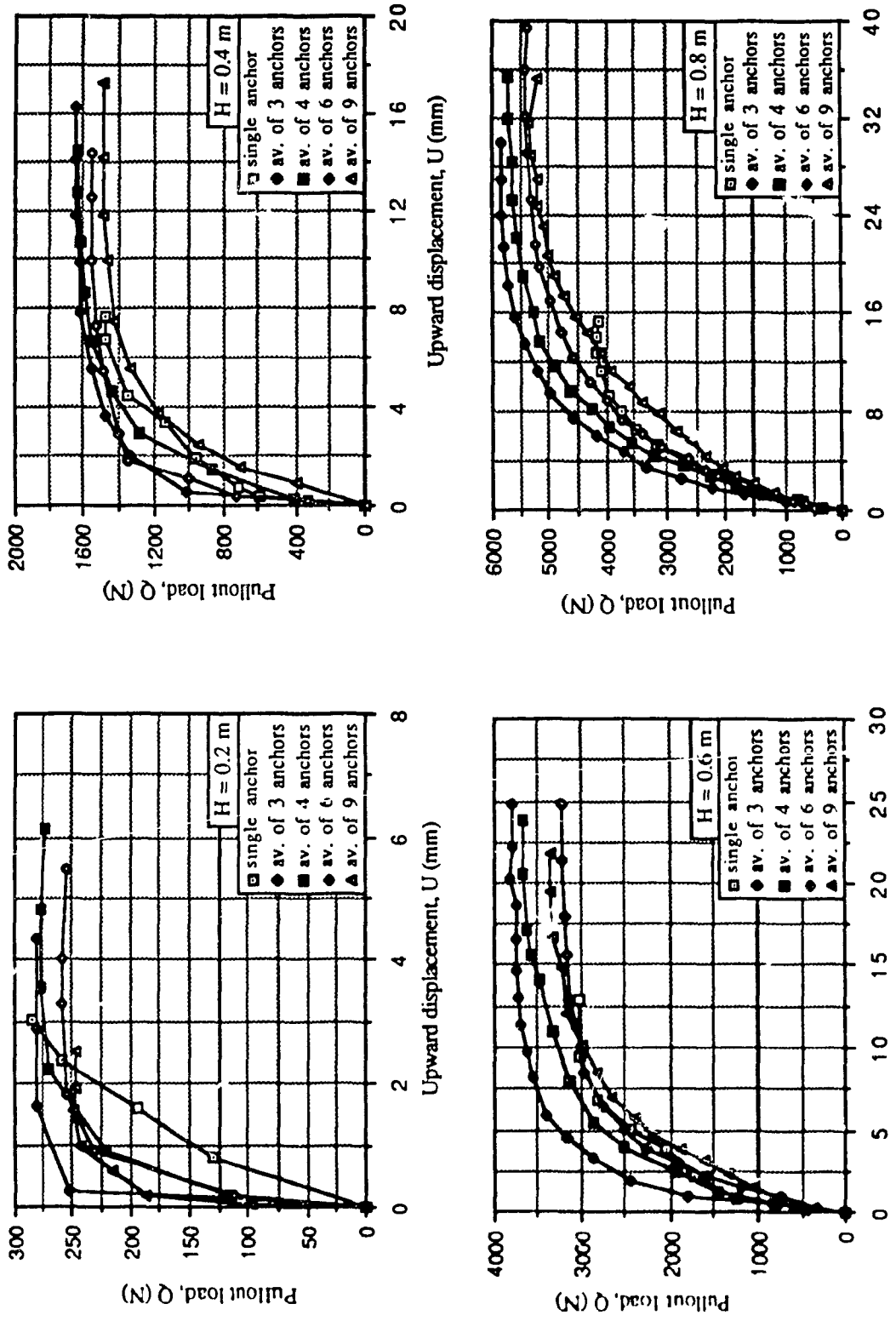

Fig. 4.2: Pullout load versus upward displacement for anchor groups installed in dense sand and spaced at S=3B.

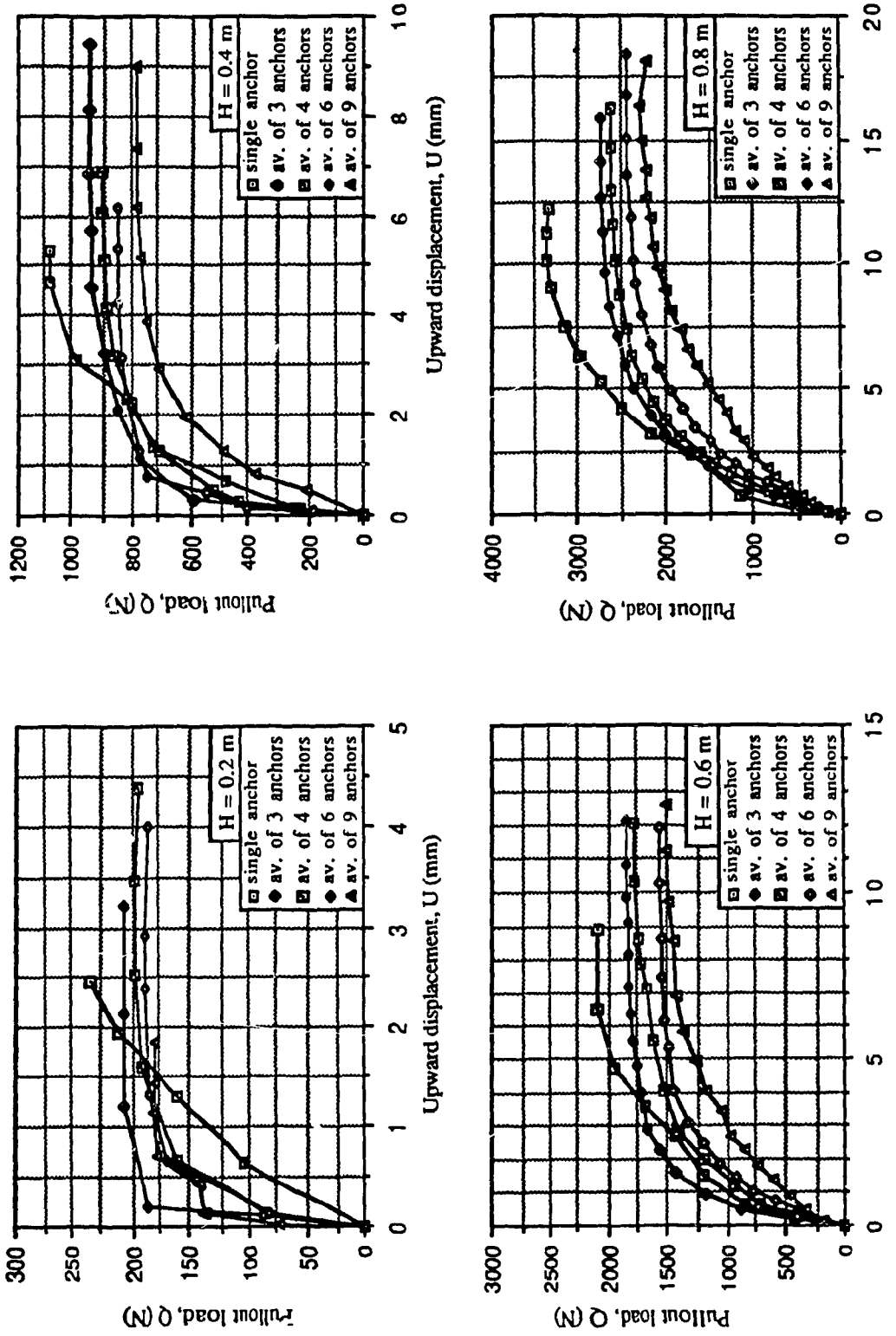

Fig. 4.3: Pullout load versus upward displacement for anchor groups installed in medium sand and spaced at S=3B.

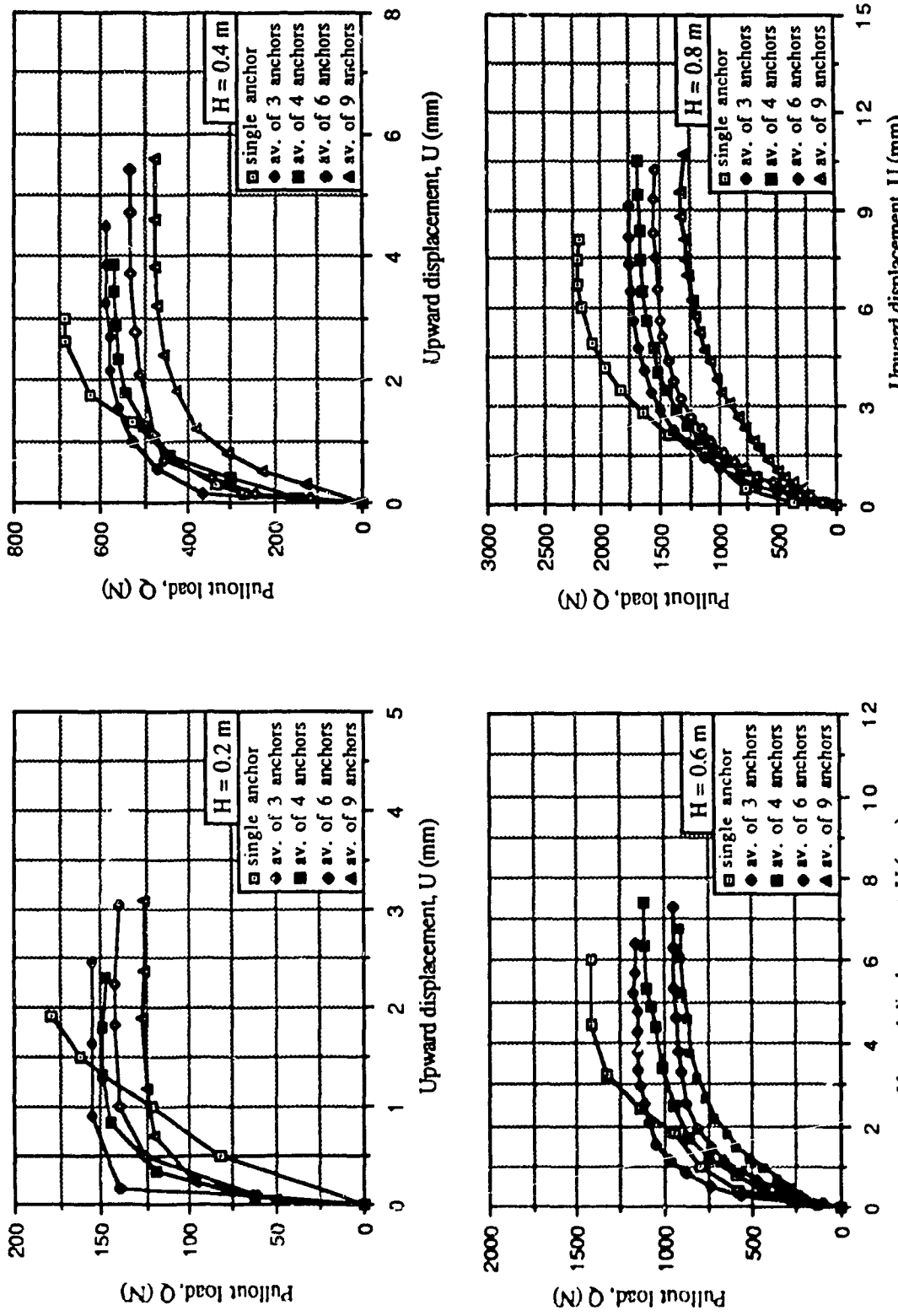

Fig. 4.4: Pullout load versus upward displacement for anchor groups installed in loose sand and spaced at S=3B.

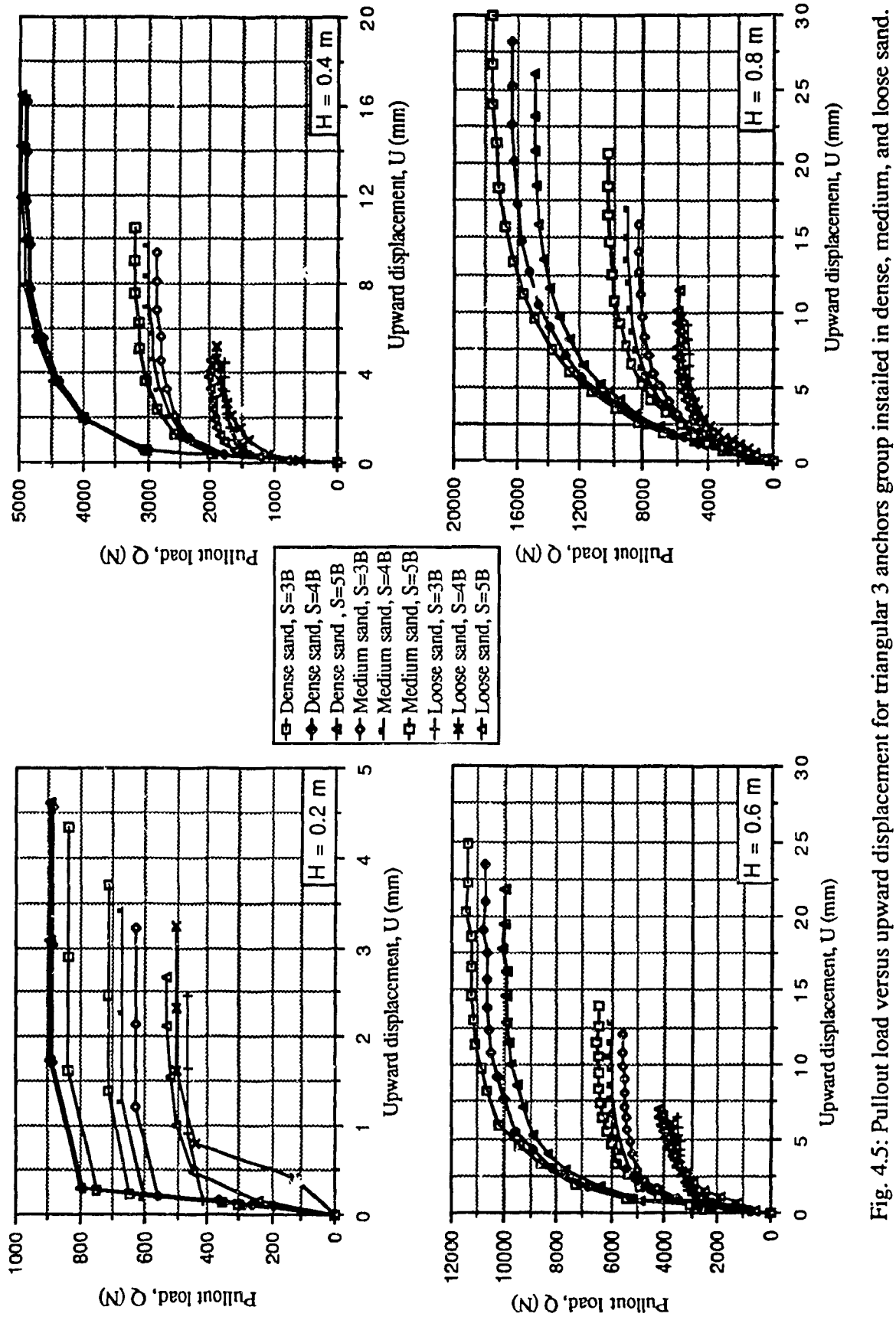

Fig. 4.5: Pullout load versus upward displacement for triangular 3 anchors group installed in dense, medium, and loose sand.

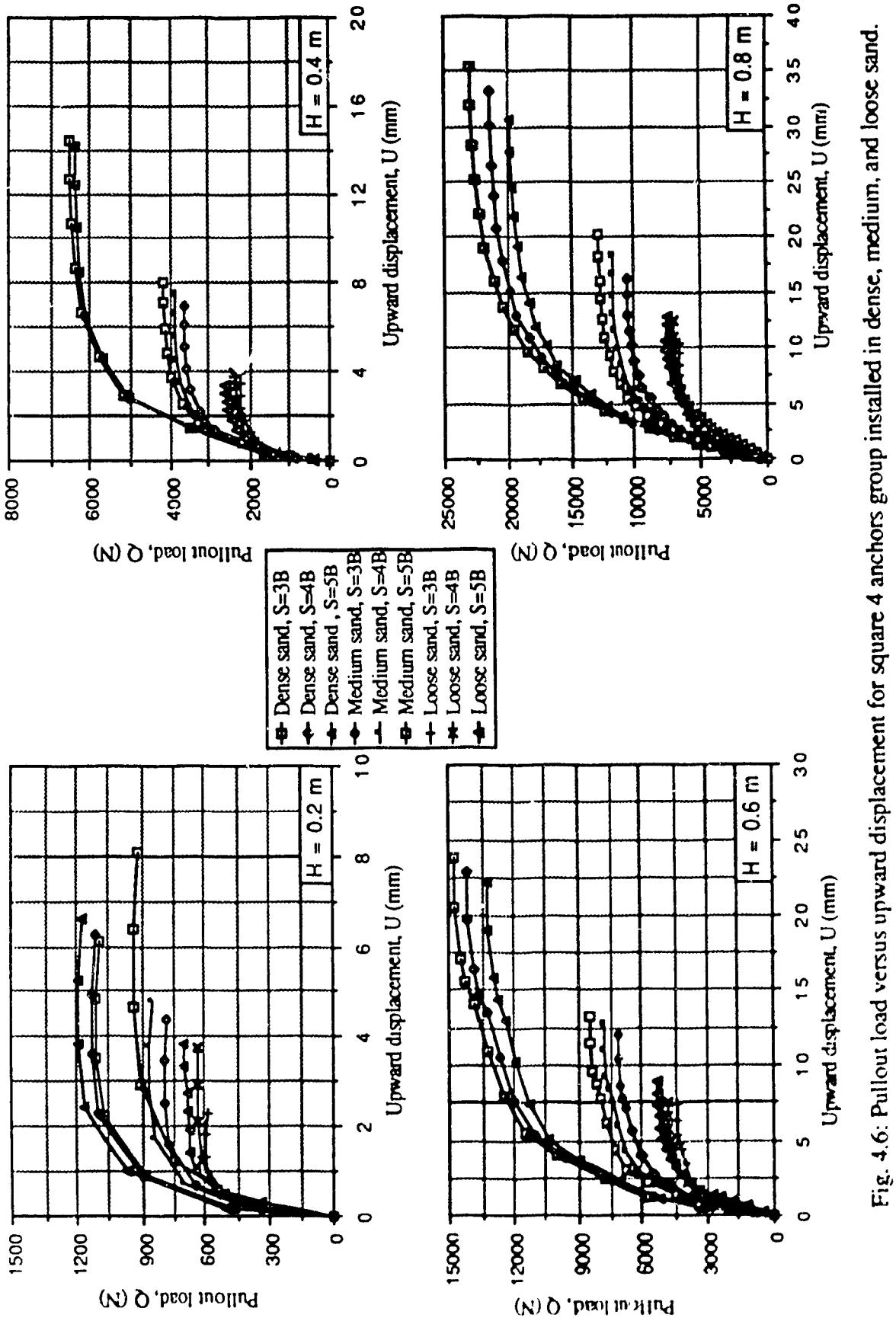

Fig. 4.6: Pullout load versus upward displacement for square 4 anchors group installed in dense, medium, and loose sand.

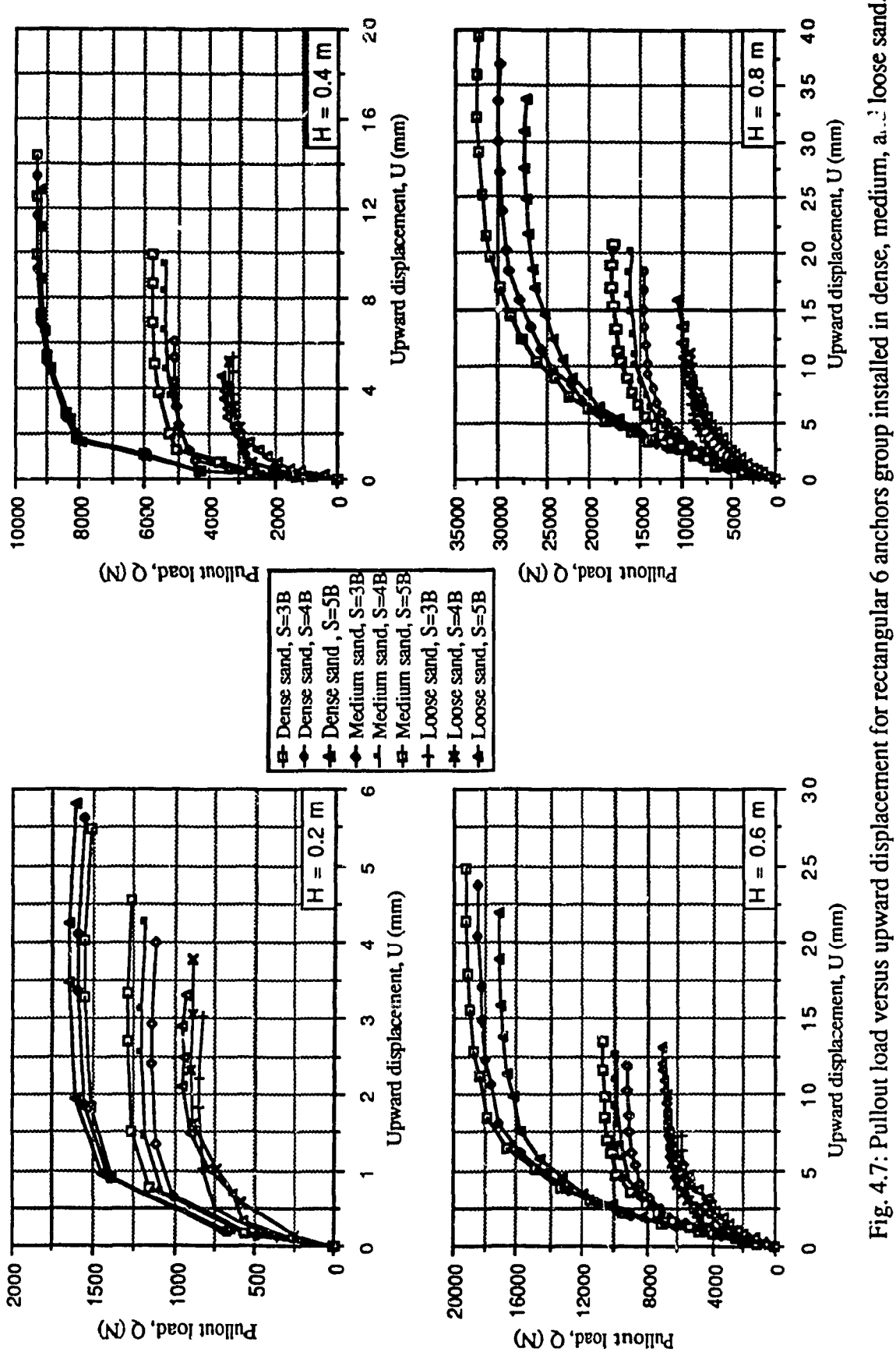

Fig. 4.7: Pullout load versus upward displacement for rectangular 6 anchors group installed in dense, medium, and loose sand.

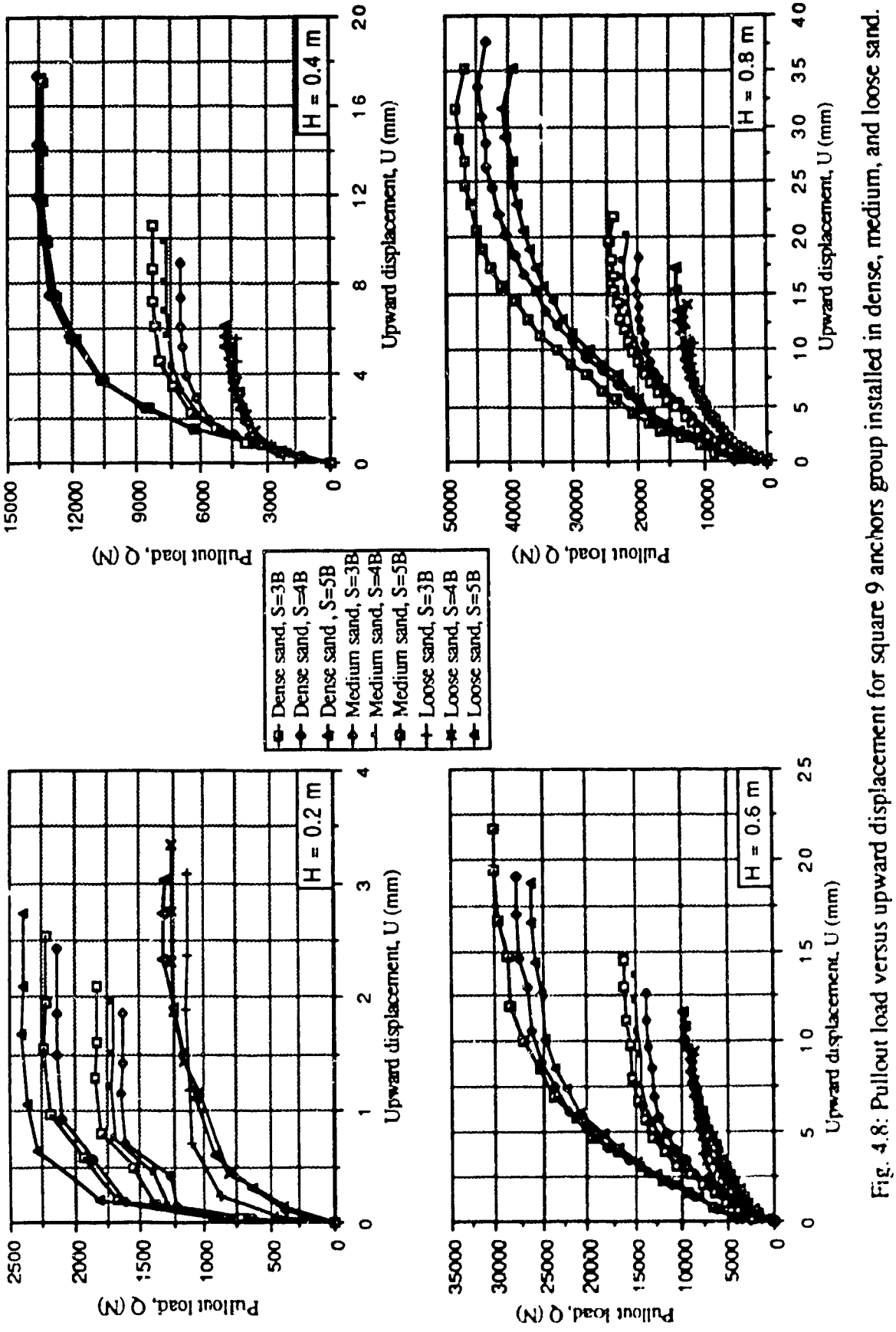

Fig. 4.8: Pullout load versus upward displacement for square 9 anchors group installed in dense, medium, and loose sand.

becomes clearer as the embedment depth increases. Also, it can be noticed that the effect of the spacing variation on the pullout load of a group is more significant as the embedment depth increases. Also, from these figures, it can be seen that the upward displacement increases with the increase of the pullout load. This observation is valid for all of the tested group configurations. Although the uplift performance of the tested groups is almost identical, the effect of group size appears to be more significant for groups with large number of anchors (Fig. 4.8).

Figures 4.9, 4.10, and 4.11 show the relationship between the ultimate pullout load (Q_u) and the embedment depth for a single anchor as well as for groups installed in dense, medium, and loose sand respectively. These figures demonstrate the effect of the group size and installation depth on the uplift capacity. As the group size increases and/or installation depth, the uplift capacity increases, also.

The load distribution amongst the individual anchors within a group is shown in Figs. 4.12, 4.13, and 4.14 for 2 x 3 anchors group of anchors installed in dense, medium, and loose sand respectively; and in Figs. 4.15, 4.16, and 4.17 for 3 x 3 anchors group. These figures are plotted as a relationship of load on a group as a percentage of load at failure versus the load on an anchor as a percentage of the load on the group at failure. It can be noticed from these figures that at low uplift load level, the CN anchor (symbols to identify anchors are shown in Fig. 4.1) usually experiences a higher portion of uplift load than the CR one, while the MS anchor resists the uplift load in an almost constant rate, increases with the increase of the uplift load. As failure approaches, the uplift resistance of the CN anchor decreases rapidly while that of the CR anchor increases rapidly and an almost equal amount of uplift is resisted by each differently located anchor at failure. It has to be mentioned that the group cap in these experiments was a rigid one, to allow for such discrimination between the performance of the anchors within the group.

Furthermore, it is worth noting that the upward displacement of the different spots of the group cap was a direct function in the uplift load that was being resisted by an anchor located at a

given spot, i.e., when a greater portion of uplift load is resisted by this anchor, greater displacement was recorded. When failure takes place and the uplift load is almost equally distributed, the upward displacement becomes more or less the same for all the spots of the cap. This behaviour can be attributed to the fact that at low level of uplift load, the surface of rupture is not created yet and the shear resistance on this surface is not fully mobilized, hence, the anchor directly located below the point of uplift load application (CN anchor) takes the greatest portion of the uplift load whereas the other types of anchors (MS and CR anchors) resist portions of uplift load appear to be proportional to their distances from the point of the pullout load application. When failure occurs, the group behaves as one unit and the CN anchor becomes the axis of the central core. Meanwhile, the shear force on the surface of failure is fully mobilized, hence, an equal portion of uplift is resisted by each anchor.

From the present test results, it was noticed that the order of anchors installation in a group has a significant influence on the load distribution amongst the individual anchors of the group. It was found that when the load on the group was relatively small as compared to the failure load, the anchors that had been installed earlier carried less load than those that have been installed later. When the failure load of the group approaches, the influence of the installation order appears significantly, and the primary load distribution amongst the individual anchors of the group reflects its effect on the differential upward displacement of the group cap. The spot of the cap at which an anchor resists higher uplift load is located, experiences greater displacement as compared to the average upward displacement of the group. The order of the anchors installation is the main factor controlling the differential upward displacement specially for closely spaced anchors and for large size group.

The criteria that should be followed in group installation is a complex one and it requires good engineering judgement and experience, however, based on the present observations, the differential upward displacement can be reduced by installing the anchors in an order that permits no creation of a closed zone some anchors will be installed in later on. It is always recommended to first install the central core of anchors then to install the anchors located on the perimeter of the

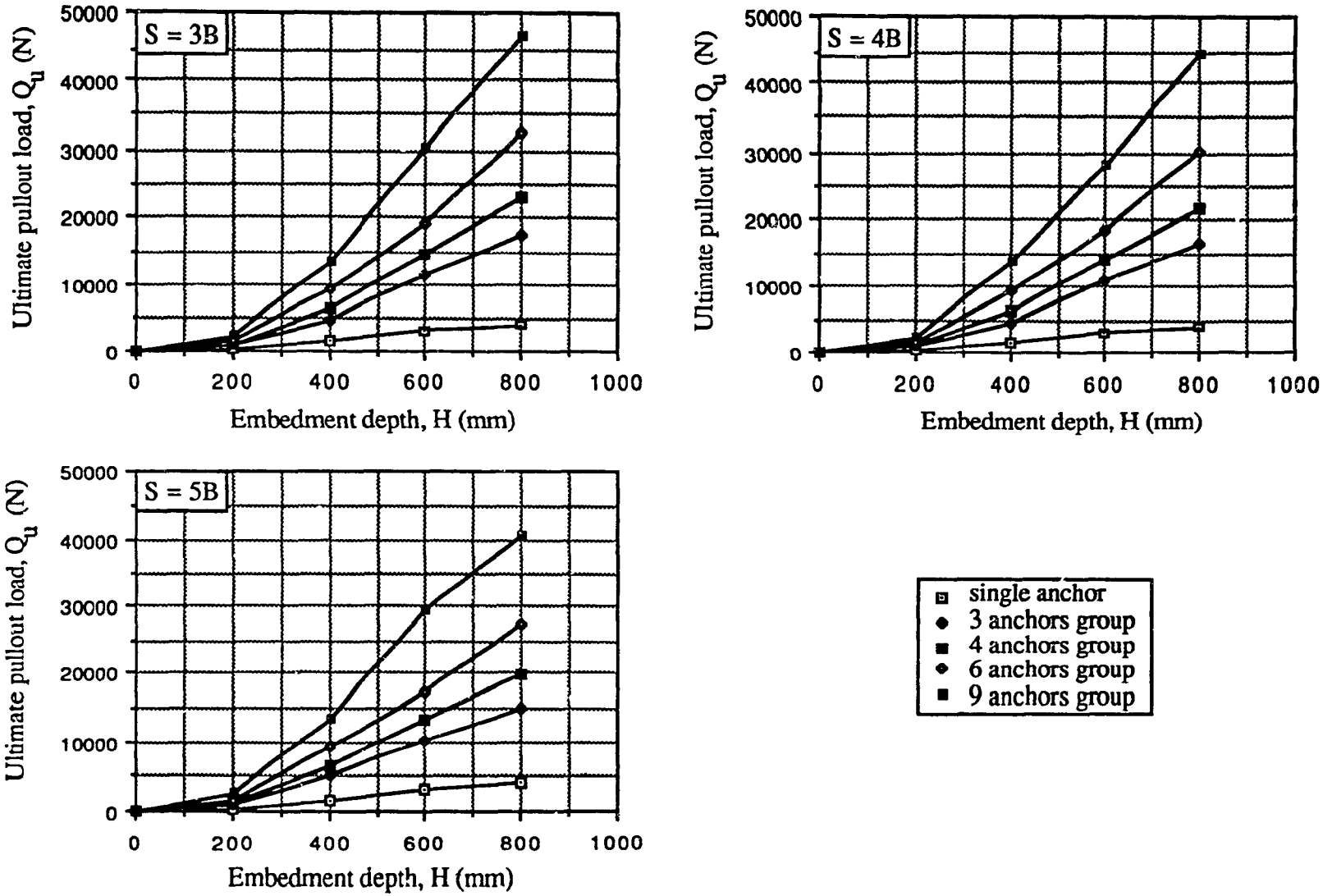

Fig. 4.9: Relationship between ultimate pullout load and embedment depth for single and group of anchors installed in dense sand.

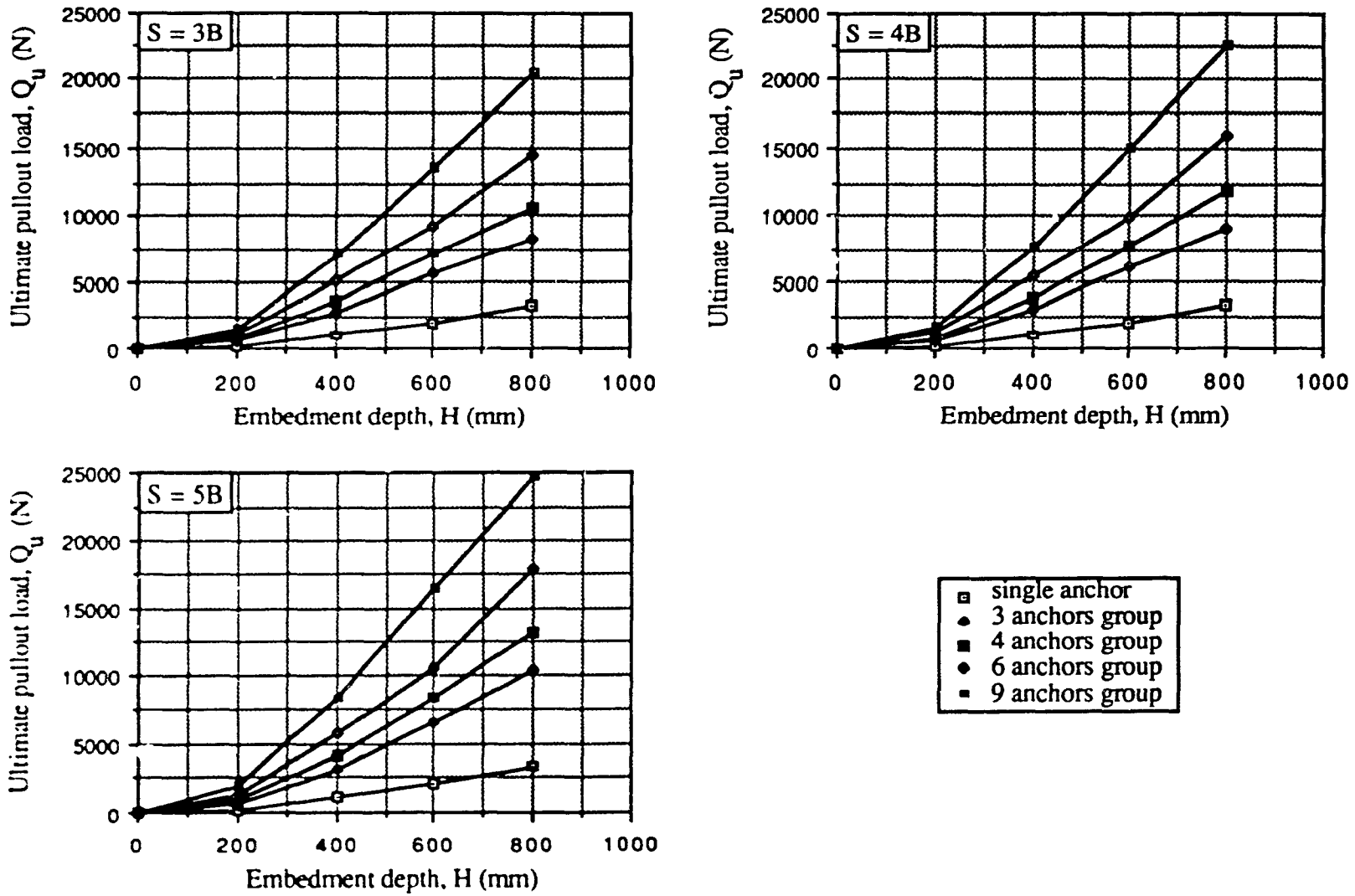

Fig. 4.10: Relationship between ultimate pullout load and embedment depth for single and group of anchors installed in medium sand.

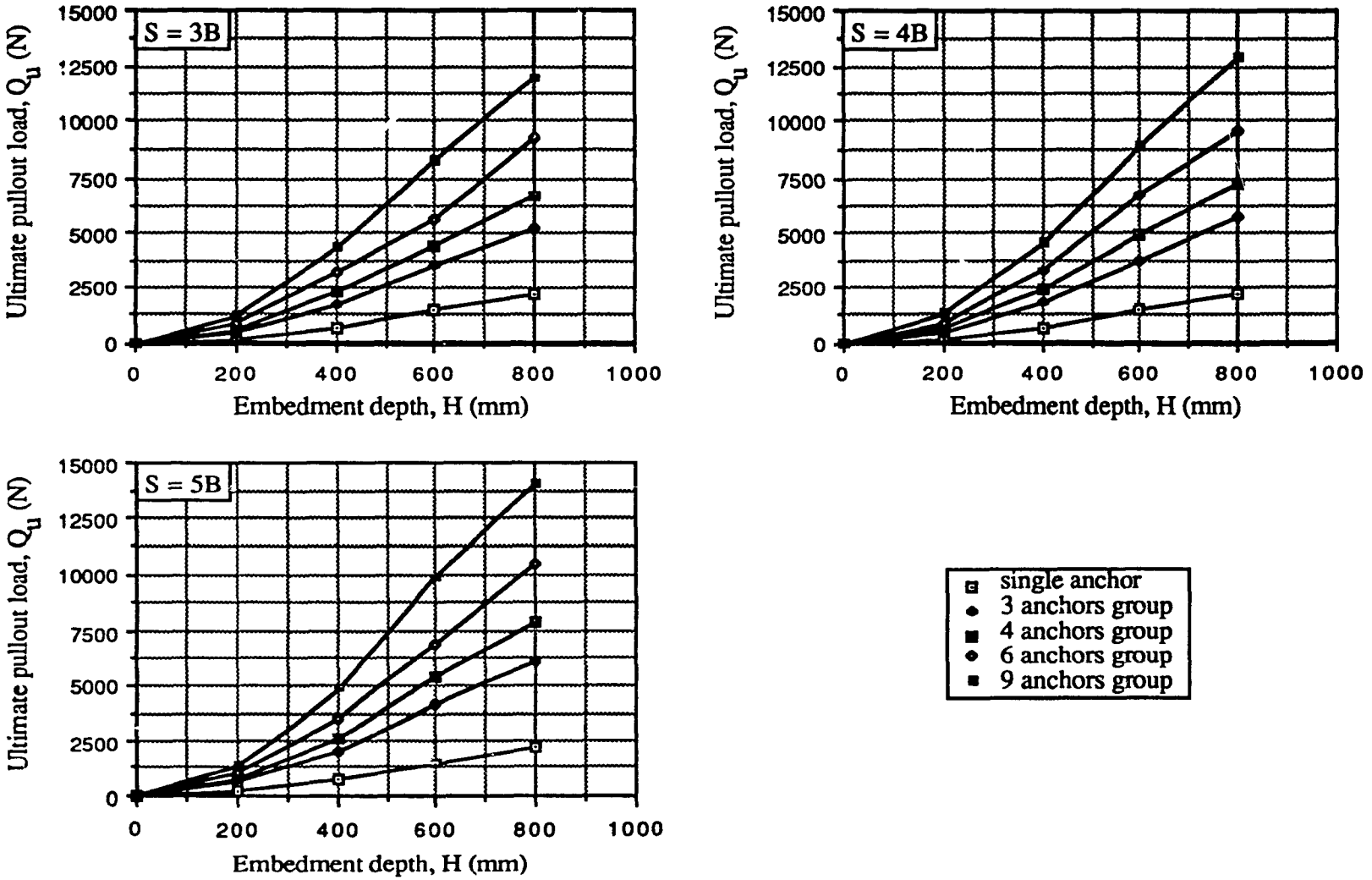

Fig. 4.11: Relationship between ultimate pullout load and embedment depth for single and group of anchors installed in loose sand.

group. This arrangement of placing a group of anchors may be called cobweb installation.

The efficiency of a group of anchors (E) is calculated as the ratio between the uplift capacity of the group and the total uplift capacities of identical number of single anchors. The calculated efficiencies of the tested group configurations are listed in Table 4.3. Figure 4.18 demonstrates the influence of the group configuration, installation depth, spacing, and angle of shearing resistance of the sand, on the group efficiency. From this figure it can be indicated that, for loose and medium sand, the efficiency increases with the increase of the spacing but it slightly decreases with the increase of installation depth. Also, for a given spacing and installation depth, a larger group size results in a reduction in the efficiency (E). It can be noticed that the efficiency calculated for groups installed in loose and medium sand is generally less than 100%. This can be attributed to the interference effect between the action of each single anchor within the group. This interlock effect is reduced as the spacing increases due to the establishment of the isolation behaviour for every individual anchor of a group. For small size groups (1 x 3 and 2 x 2), it can be seen that the efficiency is almost 100% when the spacing/diameter ratio (S/B) is 5. This behaviour was observed in all tested installation depths. These findings agree well with those reported by Hanna et al. (1972) [20] and Das and Jin (1987) [12] for embedded anchor plates in medium sand.

The calculated values of group efficiency in dense sand showed trends different from those observed in loose and medium sand. For all tested group configurations installed to relatively shallow depth (200 mm and 400 mm), the efficiency was slightly influenced by the spacing. The efficiency (E) exceeded 100% for all group configurations installed to 400 mm (H/B = 8) in dense sand. For deeper depths (600 mm and 800 mm), the efficiency was quite higher than 100% at closely spaced anchors (S = 3B) and decreased with the increase of the spacing (S = 4B and S = 5B). This behaviour is attributed to the lateral stresses that the installation of screw anchors induces in the sand deposit around and in the near vicinity of the installation path. These lateral stresses appear to be so large in the case of closely spaced anchor groups installed to deep depths in dense sand due to the high initial relative density (D_r = 90%). These lateral stresses reflect their

Table 4.3: Efficiency of anchor groups.

Installation depth (mm)	Group configuration	Efficiency E, (%)			Efficiency E, (%)			Efficiency E, (%)		
		$\phi = 31°$			$\phi = 36°$			$\phi = 42°$		
		Spacing, S			Spacing, S			Spacing, S		
		3B	4B	5B	3B	4B	5B	3B	4B	5B
200	1x3	0.86	0.94	1.00	0.89	0.95	1.02	0.98	1.03	1.04
200	2x2	0.83	0.88	0.97	0.85	0.93	1.00	0.97	0.99	1.05
200	2x3	0.79	0.84	0.89	0.81	0.86	0.92	0.91	0.93	0.96
200	3x3	0.71	0.78	0.82	0.78	0.82	0.88	0.87	0.91	0.94
400	1x3	0.85	0.91	0.97	0.88	0.92	0.98	1.11	1.10	1.12
400	2x2	0.82	0.87	0.95	0.84	0.90	0.96	1.10	1.08	1.08
400	2x3	0.77	0.80	0.87	0.79	0.83	0.89	1.05	1.05	1.04
400	3x3	0.70	0.73	0.78	0.72	0.79	0.85	1.01	1.02	1.00
600	1x3	0.82	0.88	0.96	0.88	0.95	1.02	1.25	1.18	1.10
600	2x2	0.78	0.86	0.94	0.84	0.93	1.01	1.21	1.16	1.09
600	2x3	0.72	0.78	0.82	0.79	0.84	0.90	1.14	1.09	1.01
600	3x3	0.64	0.70	0.74	0.71	0.79	0.86	1.10	1.02	0.96
800	1x3	0.80	0.87	0.91	0.83	0.91	1.04	1.40	1.31	1.19
800	2x2	0.76	0.82	0.89	0.79	0.89	0.98	1.36	1.28	1.18
800	2x3	0.70	0.72	0.79	0.73	0.80	0.89	1.29	1.20	1.09
800	3x3	0.60	0.65	0.71	0.68	0.75	0.82	1.28	1.18	1.08

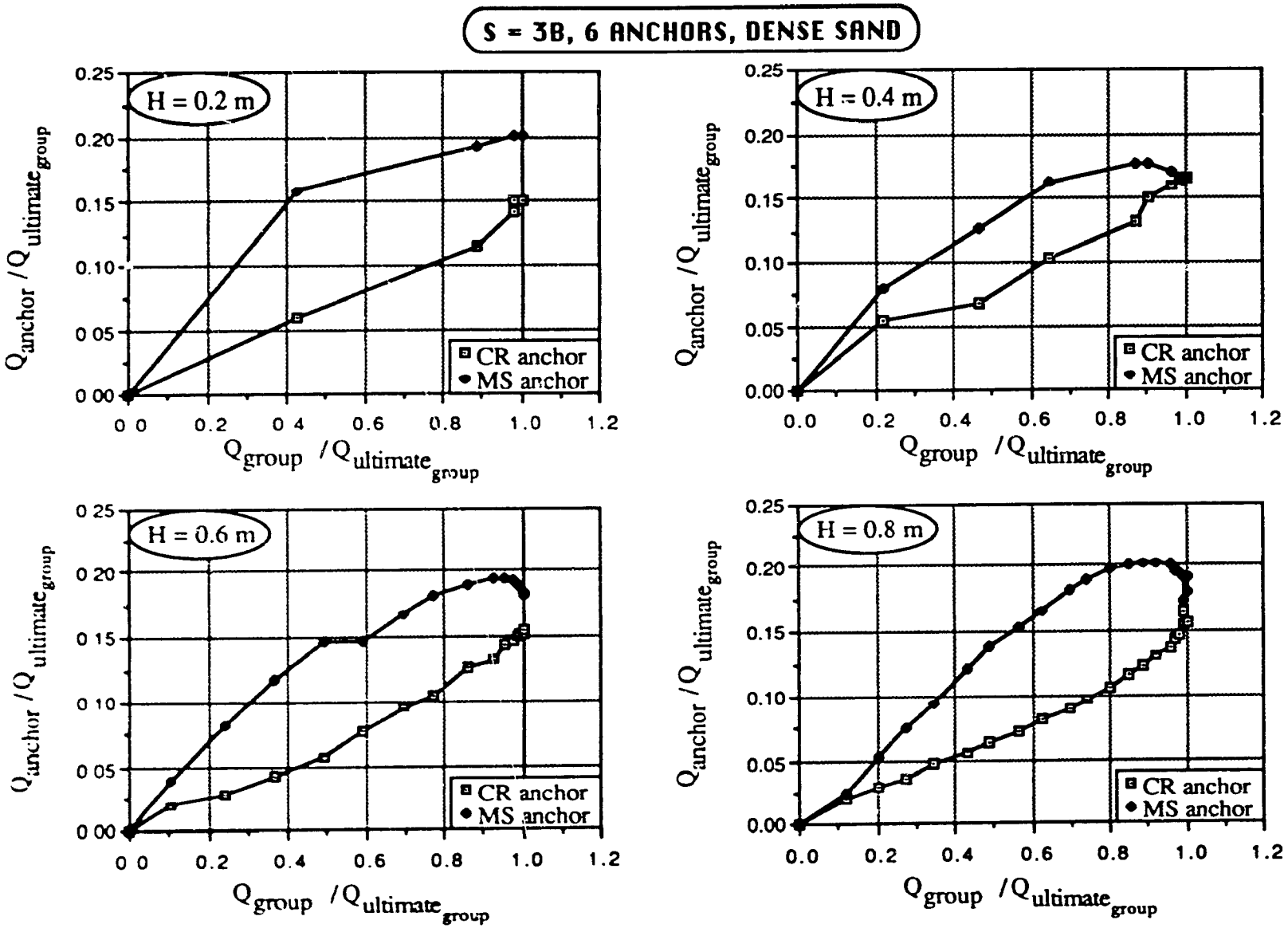

Fig. 4.12: Load on a group as a percentage of load at failure versus load on anchor as a percentage of the load on the group at failure.

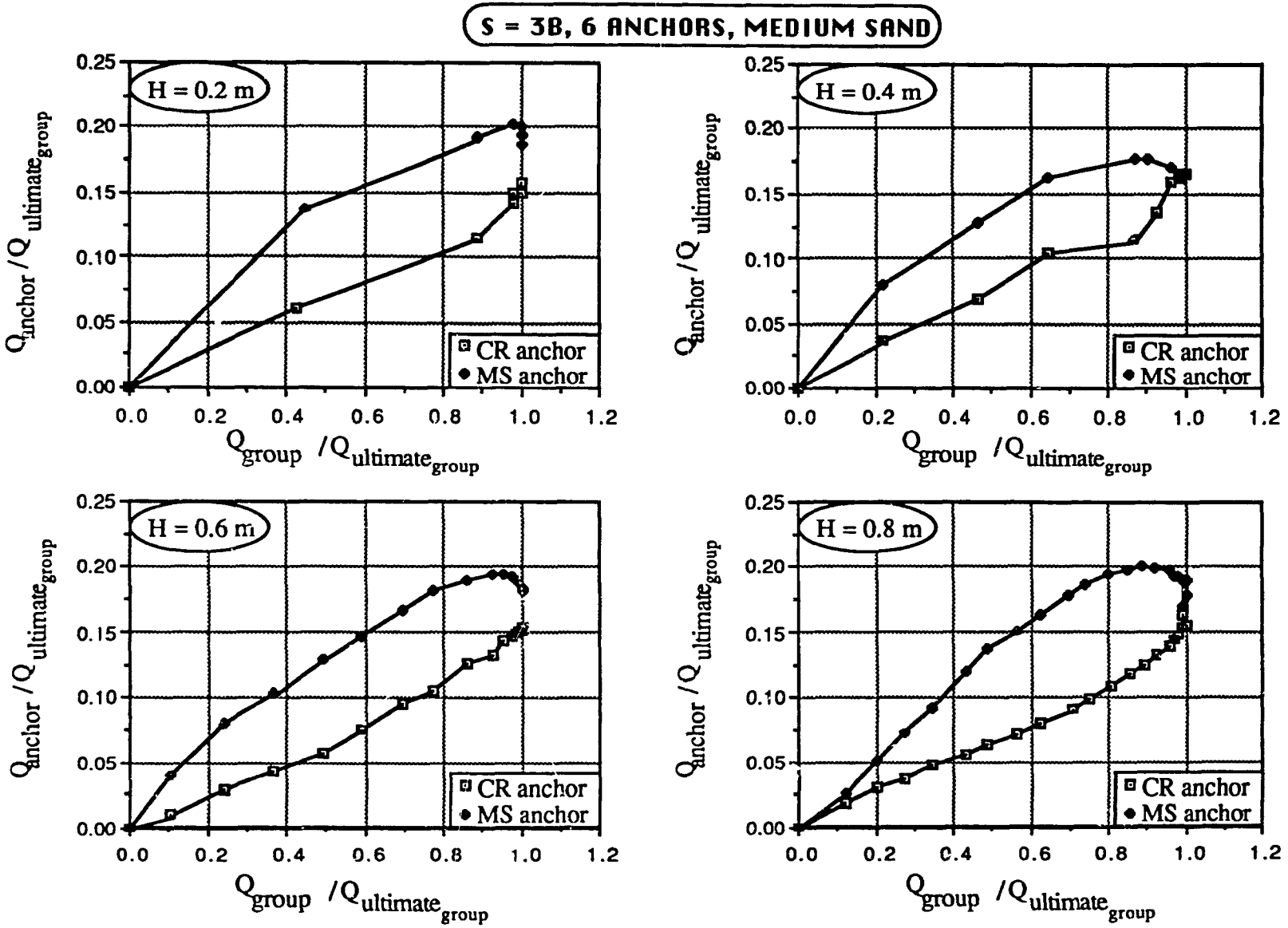

Fig. 4.13: Load on a group as a percentage of load at failure versus load on anchor as a percentage of the load on the group at failure.

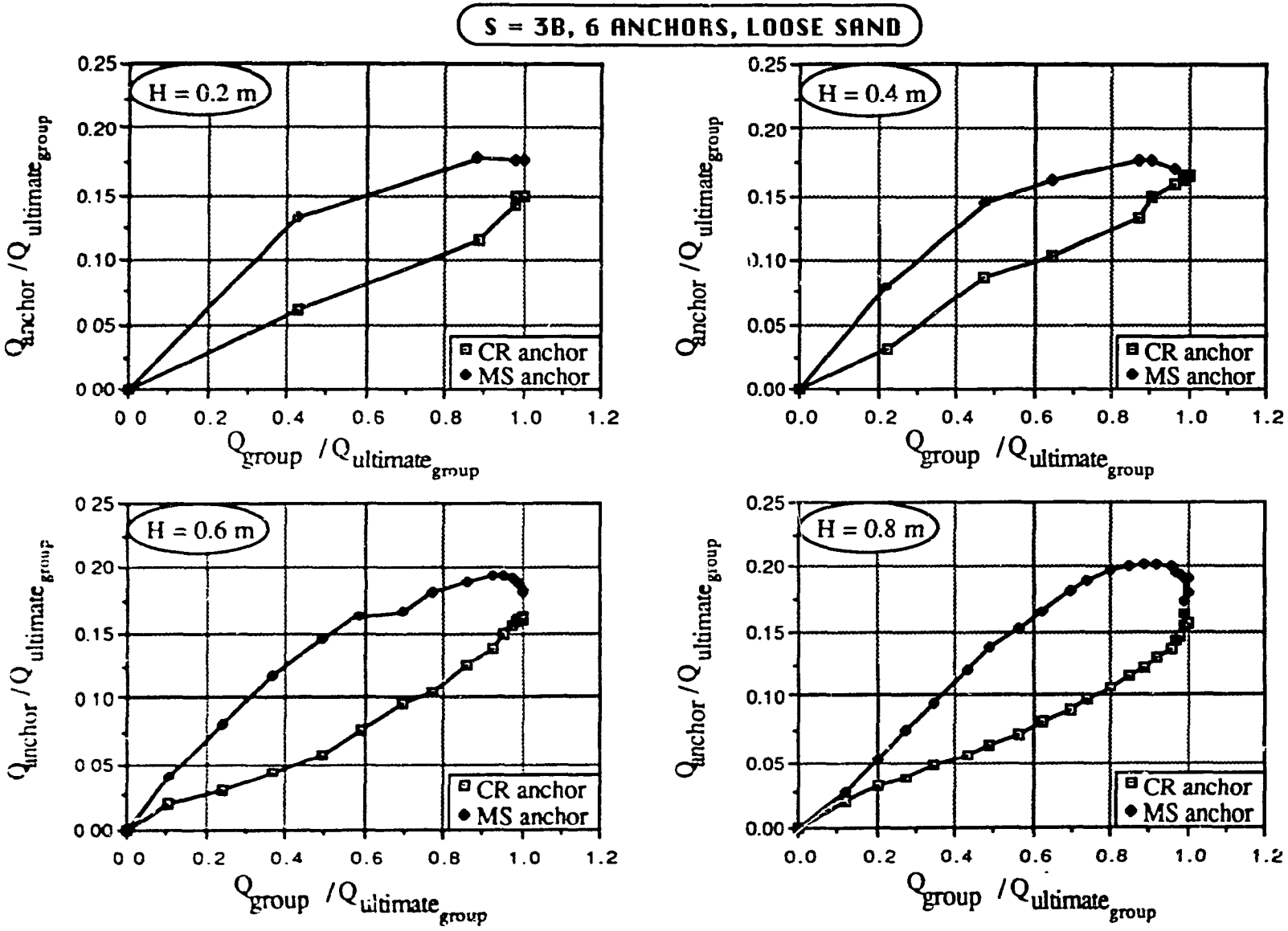

Fig. 4.14: Load on a group as a percentage of load at failure versus load on anchor as a percentage of the load on the group at failure.

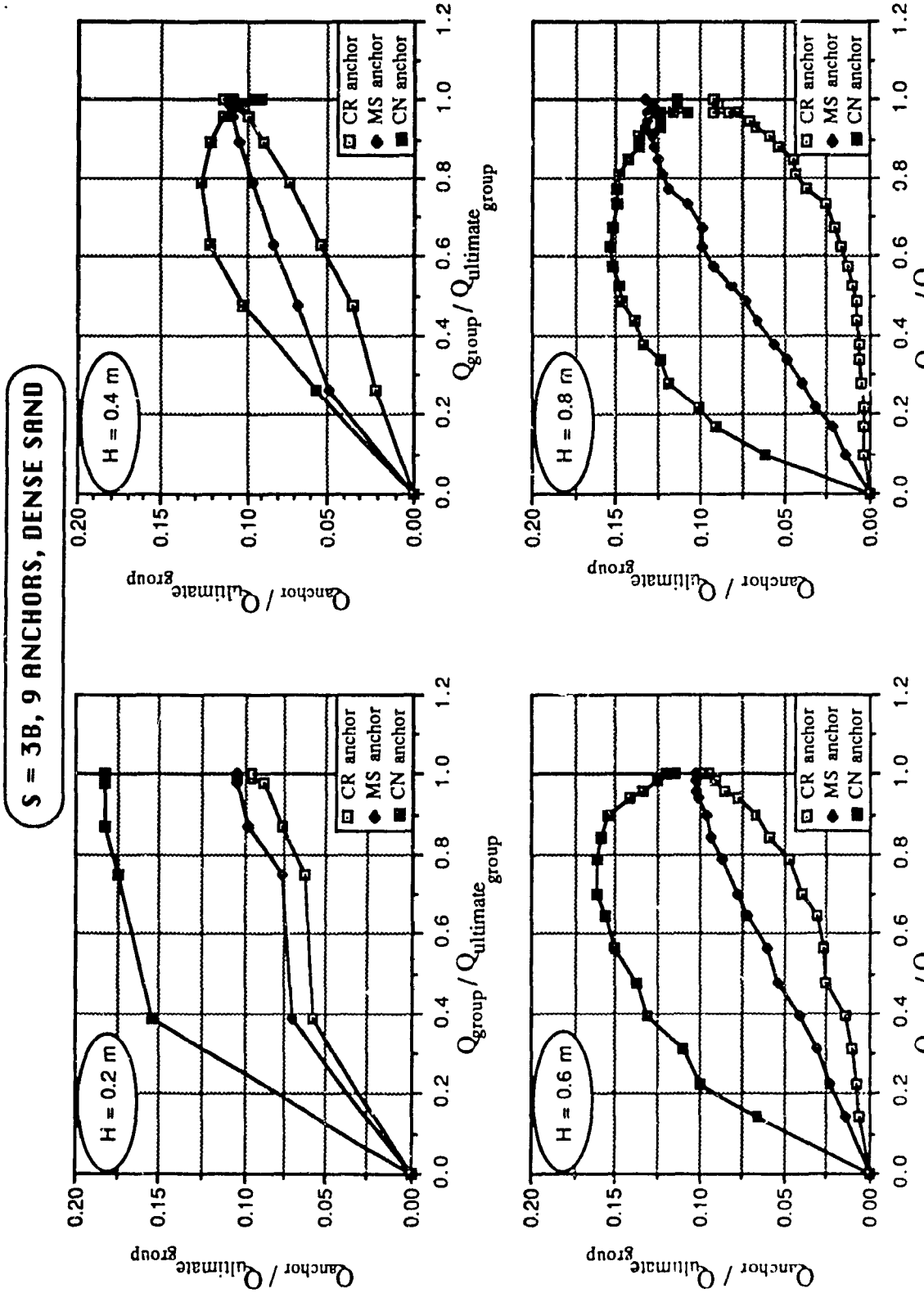

Fig. 4.15: Load on a group as a percentage of load at failure versus load on anchor as a percentage of the load on the group at failure.

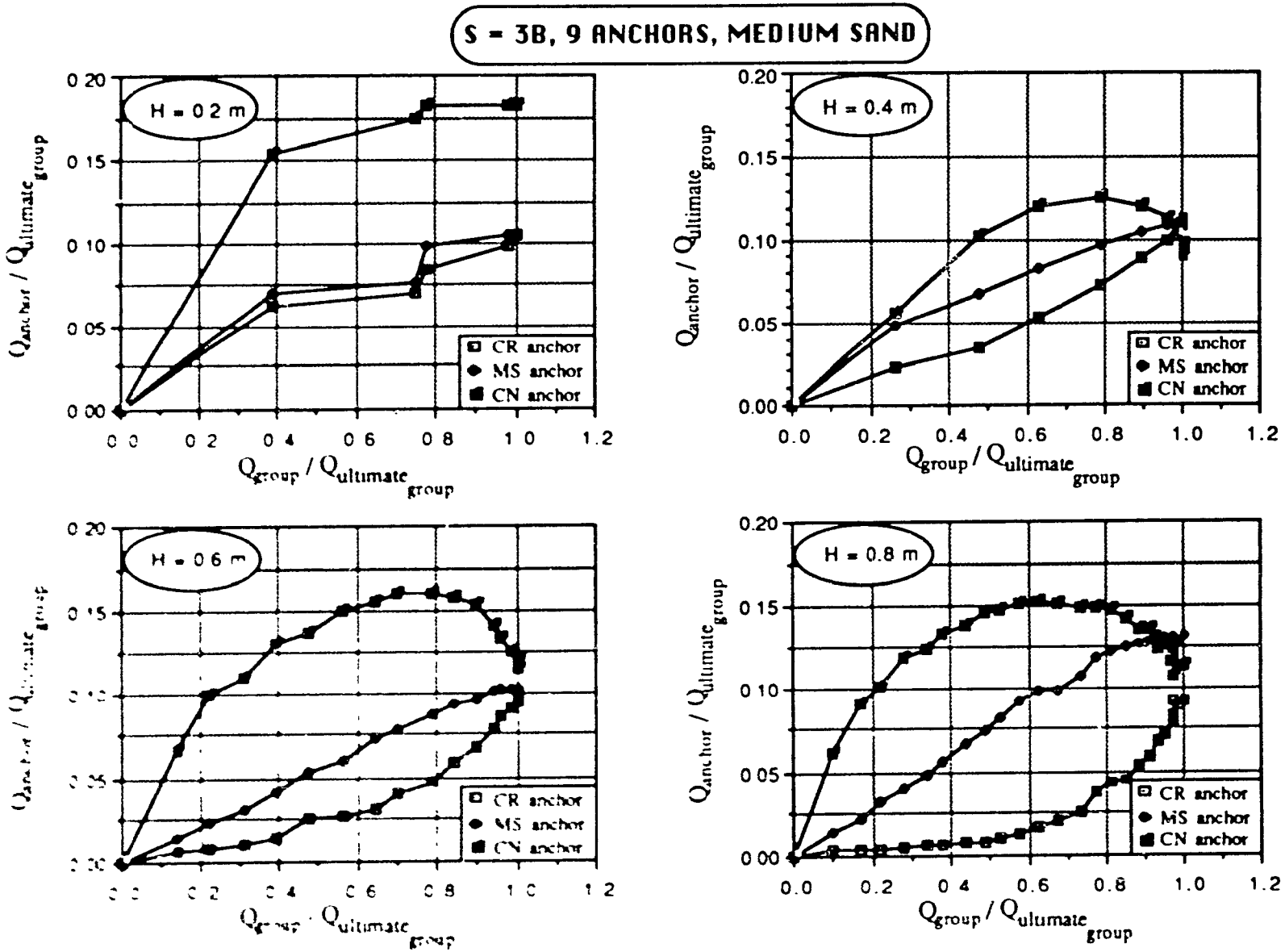

Fig. 4.16 Load on a group as a percentage of load at failure versus load on anchor as a percentage of the load on the group at failure.

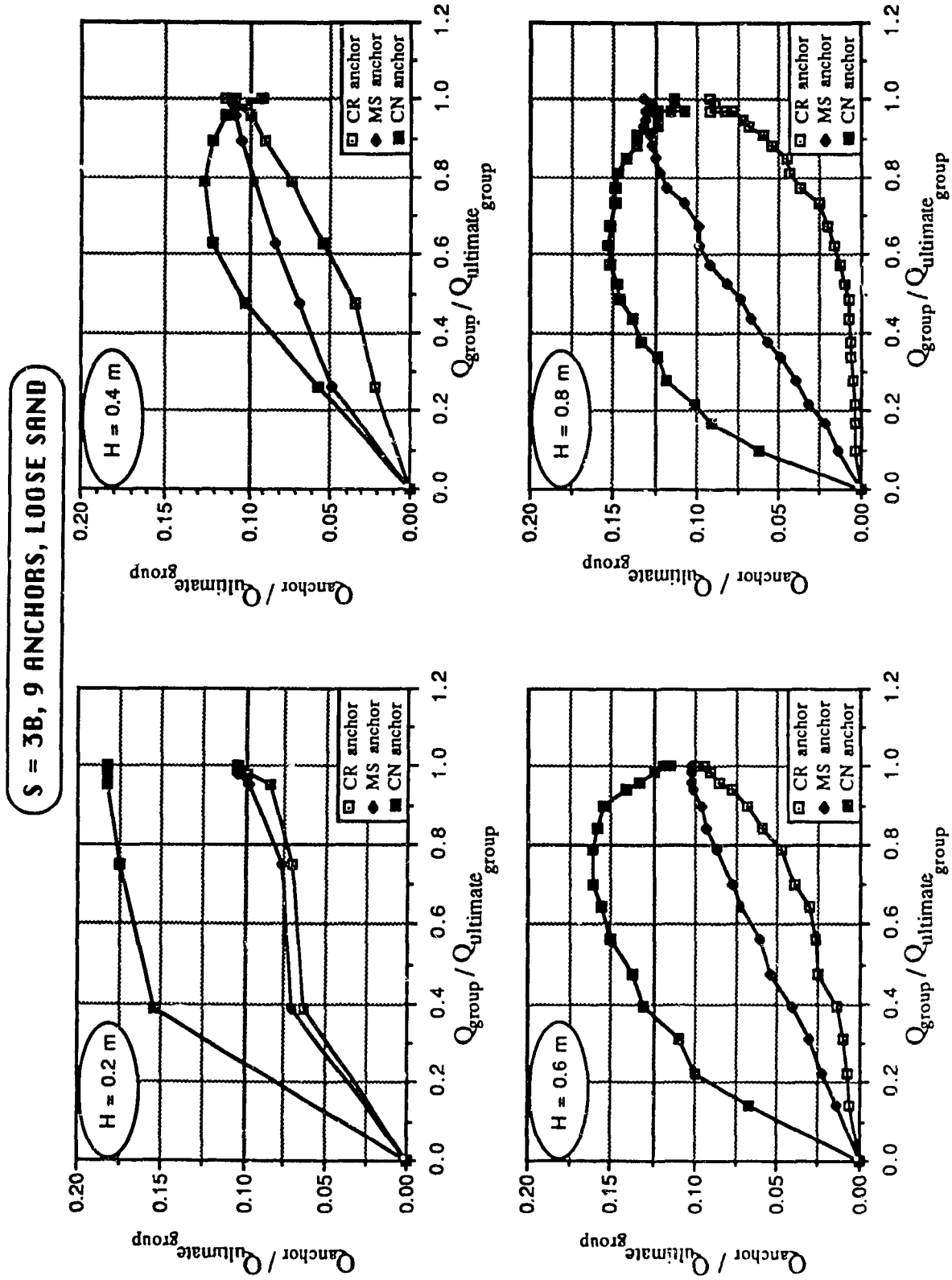

Fig. 4.17: Load on a group as a percentage of load at failure versus load on anchor as a percentage of the load on the group at failure.

influence on the uplift performance of the group. For widely spaced anchors (S = 5B), the developed lateral stresses during installation are of magnitude lower than that developed in the case of closely spaced anchor. Although it is expected that the isolation behaviour that takes place at widely spaced anchors increases the group efficiency, it was found that the effect of the developed lateral stresses during installation is much stronger than the effect of the isolated behaviour. Moreover, the overconsolidation state that developed in the sand due to the applied sand compaction technique yielded high overconsolidation ratio (OCR) of 4.3 for 800 mm sand depth which significantly contributed to the efficiency. Hanna et al. (1972 [20], compared test results of normally consolidated sand with those of corresponding overconsolidated sand. They reported that the overconsolidation ratio (OCR) has an appreciable effect on the measured pullout load of the overconsolidated sand. They indicated that at high OCR values (OCR>3), the effect of the overconsolidation state on the ultimate pullout load is significantly larger than its effect when it has a value lower than 3. These observations by Hanna et al. support the results of the present investigation.

It is worth noting that for a given installation depth and spacing ratio, the effect of the group size on the calculated efficiency of groups installed in dense sand is similar to that in medium and loose sand, i.e., efficiency decreases with the increase of the number of anchors in the group

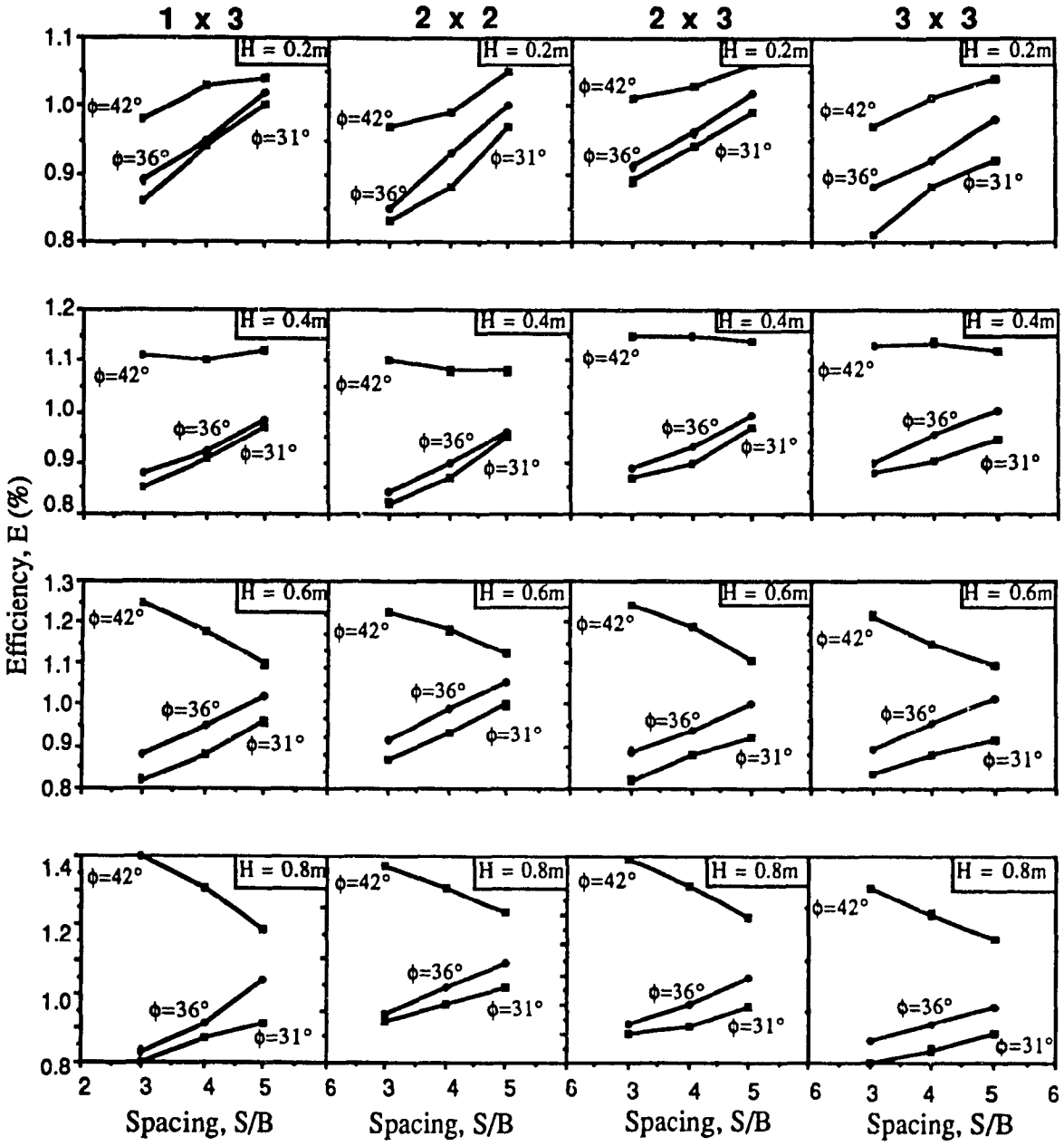

Fig. 4.18: Efficiency of group of anchors versus spacing.

CHAPTER 5

Theoretical Analysis

5.1 Single Anchors

5.1.1 Shallow single anchors

The observed log-spiral rupture surface was employed together with the limiting equilibrium method of analysis to develop a theoretical model to calculate the uplift capacity of screw anchors installed in sand deposits. The geometrical properties of the segment of the log spiral are shown in Fig. 5.1. The equation representing a log-spiral curve is as follows

$$r_\omega = r_0 \cdot e^{\omega \cdot \tan \phi} \qquad (5.1)$$

where r_ω = radius of log-spiral at an angle ω

r_0 = initial radius of log-spiral at ω equal to zero

ω = angle of revolution

ϕ = angle of shearing resistance of the sand

For shallow single anchors, the uplift resistance is of three components namely, the self weight of the anchor, the dead weight of the soil mass involved within the rupture surface and the vertical component of the shearing resistance mobilized along the rupture surface. The self

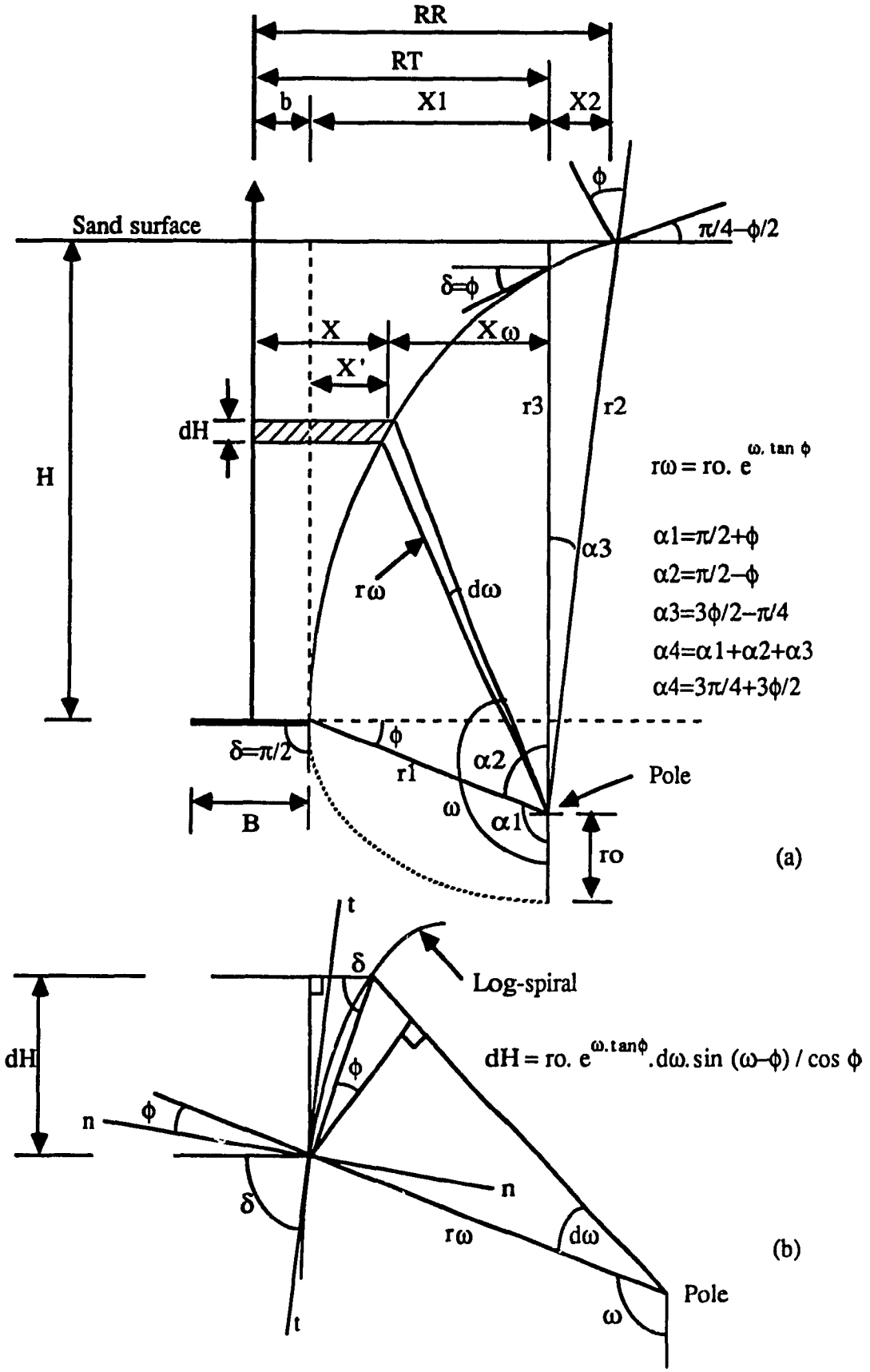

Fig. 5.1: Geometrical properties of rupture surface of shallow anchors.

weight of the anchor can be disregarded as it is a very small fraction as compared with the other two components. The volume (V) of the breaking out sand mass can be calculated by integrating an elemental circular area of radius of revolution (X) on the total height (H) of the log-spiral. (Fig. 5.1a).

$$V_{ss} = \int_0^H \pi \cdot X^2 \cdot dH \qquad \ldots (5.2)$$

$$X = X' + b \qquad \ldots (5.3)$$

where V_{ss} = volume of breaking out sand mass of shallow single anchor

X = radius of revolution of elemental circular area

X' = distance between log-spiral segment and anchor's edge

b = radius of anchor.

$$X' = X_1 - X_\omega$$

$$X' = r_1 \cdot \cos \phi - r_\omega \cdot \cos (\omega - \pi/2) \qquad \ldots (5.4)$$

$$H = r_2 \cdot \cos \alpha_3 - r_1 \cdot \sin \phi \qquad \ldots (5.5)$$

$$r_2 = r_0 \cdot e^{\alpha_4 \cdot \tan \phi} \qquad \ldots (5.5a)$$

$$r_1 = r_0 \cdot e^{\alpha_1 \cdot \tan \phi} \qquad \ldots (5.5b)$$

$$\text{put } e^{\alpha_1 \cdot \tan \phi} = \alpha \qquad (5.6a)$$

$$\text{and } e^{\alpha_4 \cdot \tan \phi} = \beta \qquad (5.6b)$$

$$\text{Hence } r_1 = \alpha \cdot r_0 \qquad (5.7a)$$

$$r_2 = \beta \cdot r_0 \qquad (5.7b)$$

$$H = r_0 \cdot \beta \cdot \cos \alpha_3 \cdot r_0 \ \alpha \cdot \sin \phi$$

$$r_0 = H/(\beta \cdot \cos \alpha_3 - \alpha \cdot \sin \phi) \quad \text{... (5.8)}$$

Where $\alpha_1 = \pi/2 + \phi$ ... (5.8a)

$$\alpha_2 = \pi/2 - \phi \quad \text{... (5.8b)}$$

$$\alpha_3 = 3\phi/2 - \pi/4 \quad \text{... (5.8c)}$$

$$\alpha_4 = 3\pi/4 + 3\phi/2 \quad \text{... (5.8d)}$$

substituting the values of r_1 and r_ω in eq. (5.4):

$$X' = \alpha \cdot r_0 \cdot \cos \phi - e^{\omega \cdot \tan \phi} \cdot \cos (\omega - \pi/2) \quad \text{... (5.9)}$$

From which the value of X can be calculated from eq. (5.3) (Fig. 5.1b),

$$dH = (r_\omega \cdot d\omega) \cdot \sin \delta/\cos \phi \quad \text{... (5.10)}$$

$$\delta = \pi - (\omega - \phi)$$

$$dH = r_0 \cdot e^{\omega \cdot \tan \phi} \cdot [\sin(\omega - \phi)/\cos \phi]\, d\omega \quad \text{... (5.11)}$$

From equations (5.3), (5.9), and (5.11), the integration in eq. (5.2) yields the following equation:

$$V_{ss} = \pi \int_{\alpha_1}^{\alpha_4} [r_0^2 \cdot \alpha^2 \cdot \cos^2 \phi + r_0^2 \cdot e^{2\omega \cdot \tan \phi} \cdot \sin^2 \omega - 2\alpha \cdot r_0^2 \cdot \cos \phi \cdot e^{\omega \cdot \tan \phi} \cdot \sin \omega$$

$$+ b^2 + 2b \cdot r_0 \cdot \alpha \cdot \cos \phi - 2b \cdot r_0 \cdot e^{\omega \cdot \tan \phi} \cdot \sin \omega] [r_0 \cdot e^{\omega \cdot \tan \phi} \cdot \sin \omega$$

$$- r_0 \cdot \tan \phi \cdot e^{\omega \cdot \tan \phi} \cdot \cos \omega]\, d\omega \quad \text{... (5.12)}$$

Putting

$$K1 = \int_{\alpha_1}^{\alpha_4} e^{\omega \cdot \tan\phi} \cdot \sin\omega \, d\omega \qquad \ldots(5.13)$$

$$K2 = \int_{\alpha_1}^{\alpha_4} e^{\omega \cdot \tan\phi} \cdot \cos\omega \, d\omega \qquad \ldots(5.14)$$

$$K3 = \int_{\alpha_1}^{\alpha_4} e^{2\omega \cdot \tan\phi} \cdot \sin\omega \, d\omega \qquad \ldots(5.15)$$

$$K4 = \int_{\alpha_1}^{\alpha_4} e^{3\omega \cdot \tan\phi} \cdot \sin\omega \, d\omega \qquad \ldots(5.16)$$

$$K5 = \int_{\alpha_1}^{\alpha_4} e^{2\omega \cdot \tan\phi} \cdot \cos\omega \, d\omega \qquad \ldots(5.17)$$

$$K6 = \int_{\alpha_1}^{\alpha_4} e^{3\omega \cdot \tan\phi} \cdot \cos\omega \, d\omega \qquad \ldots(5.18)$$

$$K7 = \int_{\alpha_1}^{\alpha_4} e^{2\omega \cdot \tan\phi} \cdot \cos 2\omega \, d\omega \qquad \ldots(5.19)$$

$$K8 = \int_{\alpha_1}^{\alpha_4} e^{2\omega \cdot \tan\phi} \cdot \sin^2\omega \, d\omega \qquad \ldots(5.20)$$

$$K9 = \int_{\alpha_1}^{\alpha_4} e^{3\omega \cdot \tan\phi} \cdot \sin^3\omega \, d\omega \qquad \ldots(5.21)$$

$$K10 = \int_{\alpha_1}^{\alpha_4} e^{3\omega \cdot \tan\phi} \cdot \cos^3\omega \, d\omega \qquad \ldots(5.22)$$

$$K11 = \int_{\alpha_1}^{\alpha_4} e^{3\omega \cdot \tan\phi} \, d\omega \qquad (5.23)$$

$$K12 = \int_{\alpha_1}^{\alpha_4} e^{3\omega \cdot \tan\phi} \cdot \sin 2\omega \, d\omega \qquad (5.24)$$

$$K13 = \int_{\alpha_1}^{\alpha_4} e^{4\omega \cdot \tan\phi} \cdot \sin\omega \, d\omega \qquad (5.25)$$

$$K14 = \int_{\alpha_1}^{\alpha_4} e^{2\omega \tan\phi} \cdot \cos^2\omega \, d\omega \qquad (5.26)$$

$$K15 = \int_{\alpha_1}^{\alpha_4} e^{4\omega \tan\phi} \cos\omega \, d\omega \qquad (5.27)$$

$$K16 = \int_{\alpha_1}^{\alpha_4} e^{3\omega \cdot \tan\phi} \cdot \sin^2 \omega \, d\omega \qquad ...(5.28)$$

$$K17 = \int_{\alpha_1}^{\alpha_4} e^{4\omega \cdot \tan\phi} \cdot \sin^2 \omega \, d\omega \qquad ...(5.29)$$

$$K18 = \int_{\alpha_1}^{\alpha_4} e^{4\omega \cdot \tan\phi} \cdot \sin 2\omega \, d\omega \qquad ...(5.30)$$

where α_1 and α_4 are the angles of revolution at the beginning and at the end of the log-spiral segment respectively.

After integration and doing contractions, the final expression that equation (5.9) produces is:

$$V_{ss} = r_0^3 \cdot \pi \, [(\alpha^2 \cdot \cos^2\phi + C^2 + 2\alpha \cdot C \cdot \cos\phi) \cdot K1$$

$$- (\alpha^2 \cdot \cos^2\phi \cdot \tan\phi + C^2 \cdot \tan\phi + 2\alpha \cdot C \cdot \cos\phi) \cdot K2$$

$$- (\tan\phi) \cdot K6 + (\alpha \cdot \cos\phi \cdot \tan\phi + C \cdot \tan\phi) \cdot K7$$

$$- (2\alpha \cdot \cos\phi + 2C) \cdot K8 + K9 + (\tan\phi) \cdot K10] \qquad ... (5.31)$$

where $C = b/r_0$ ... (5.32)

Weight of the breaking out sand of shallow single screw anchor (W_{ss}) is:

$$W_{ss} = \gamma \cdot V_{ss} \qquad ...(5.33)$$

Where γ = unit weight of the sand.

Expressing r_0 in terms of sand height (H) over the anchor by substituting eq. (5.8) in eq. (5.31):

$$W_{ss} = \gamma \cdot H^3 \cdot FW_{ss} \qquad ... (5.34)$$

Where FW_{ss} is a weight factor depending on the sand's angle of shearing resistance (ϕ) and embedment depth ratio (H/B).

A computer program was developed to calculate the weight factor (FW_{ss}) for a range of ϕ values between 30° and 46°, and for H/B ratios varying from 2 to 10. Computed factors are given in Table 5.1 and they are plotted in a from of design chart shown in Fig. 5.2.

Determination of shear force participating in resisting the uplifting force requires the evaluation of the shear stresses acting on the observed log-spiral rupture surface. The variation of shear stress along the rupture surface can be obtained by using Kotter's differential equation. This equation expresses the relationship between the resultant stress acting on the observed rupture surface at the critical state of limit equilibrium, and the radius of curvature of this surface. The following simplifying assumptions have been made:

1. The sand is at the state of limit equilibrium; that is Mohr-Coulomb failure criterion is satisfied

   ($\tau = \sigma_n \cdot \tan \phi$) where τ and σ_n are shear stress and normal stress respectively.

2. A plane stress condition is considered; that is the stresses acting on the rupture surface depend on two coordinates in a semi-infinite mass, namely, depth and distance from the anchor's axis.

3. As the problem of anchor pulling out is a three dimensional axi symmetrical problem in physical reality, a full solution can be obtained by integrating the resulting stress from the plane stress condition around the axis of the anchor

Kotter's differential equation in case of uplifting load involving passive resistance of lateral earth pressure, has the following form

Table 5.1: Weight factor FW_{SS} for shallow single anchors.

$\phi°$	Embedment depth ratio, H/B				
	2	4	6	8	10
30	0.741	0.438	0.359	-------	-------
31	0.754	0.448	0.368	-------	-------
32	0.766	0.458	0.377	-------	-------
33	0.779	0.468	0.387	-------	-------
34	0.793	0.479	0.397	-------	-------
35	0.807	0.491	0.407	0.369	-------
36	0.822	0.503	0.418	0.380	-------
37	0.837	0.515	0.430	0.391	-------
38	0.853	0.528	0.442	0.402	-------
39	0.870	0.542	0.454	0.415	-------
40	0.887	0.556	0.467	0.427	0.404
41	0.905	0.571	0.481	0.441	0.417
42	0.924	0.587	0.496	0.455	0.431
43	0.945	0.603	0.511	0.469	0.446
44	0.966	0.621	0.528	0.485	0.461
45	0.988	0.639	0.545	0.502	0.477
46	1.012	0.659	0.563	0.519	0.494

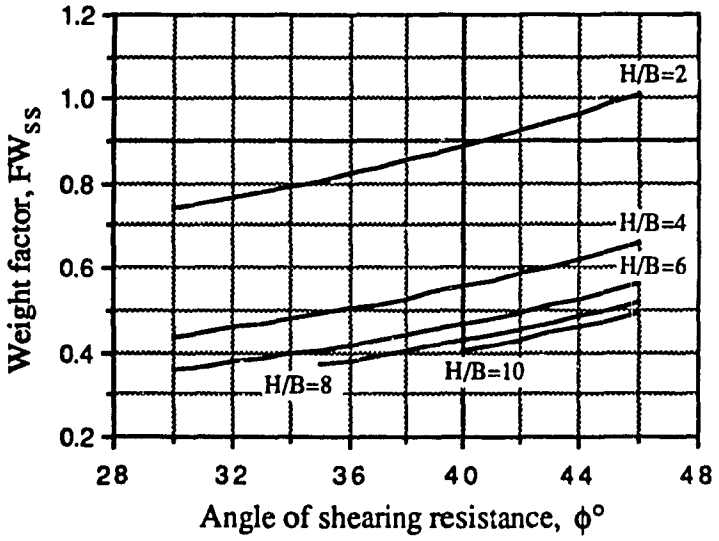

Fig. 5.2: Weight factor for shallow single anchors versus angle of shearing resistance.

$$\frac{d\tau}{d\delta} + 2(\tan\phi)\,\tau = \gamma \sin\phi \cdot \sin(\delta + \phi) \cdot \rho \qquad \ldots (5.35)$$

Where τ = shear stress along the rupture surface

δ = angle between the horizontal and rupture surface

ϕ = angle of shearing resistance of the sand

ρ = radius of curvature of rupture surface.

For log-spiral rupture surface, the radius of curvature (ρ) is given by the following expression:

$$\rho = r_0 \cdot e^{\omega \cdot \tan\phi}\left(\sqrt{1+\tan^2\phi}\right) = \frac{r_\omega}{\cos\phi} \qquad \ldots(5.36)$$

Also from the geometry of the rupture surface shown in Fig. 5.3, it can be seen that

$\delta = \omega - \pi + 2\delta - \phi$

from which $\delta = \pi - \omega + \phi$

differentiating with respect to ω, hence $d\delta = -d\omega$.

Equation (5.35) can be written in the following form:

$$\frac{d\tau}{d\omega} - 2(\tan\phi)\,\tau = -\gamma \cdot r_\omega \cdot \tan\phi \cdot \sin(\omega - 2\phi) \qquad \ldots (5.37)$$

Where r_ω is as given by eq. (5.1). The solution of eq. (5.37) is:

$$\tau = c_1 e^{\omega \tan\phi} \cdot \cos(\omega - 3\phi) - c_1 \cdot c_2 \cdot e^{2\omega \tan\phi} \qquad \ldots (5.38)$$

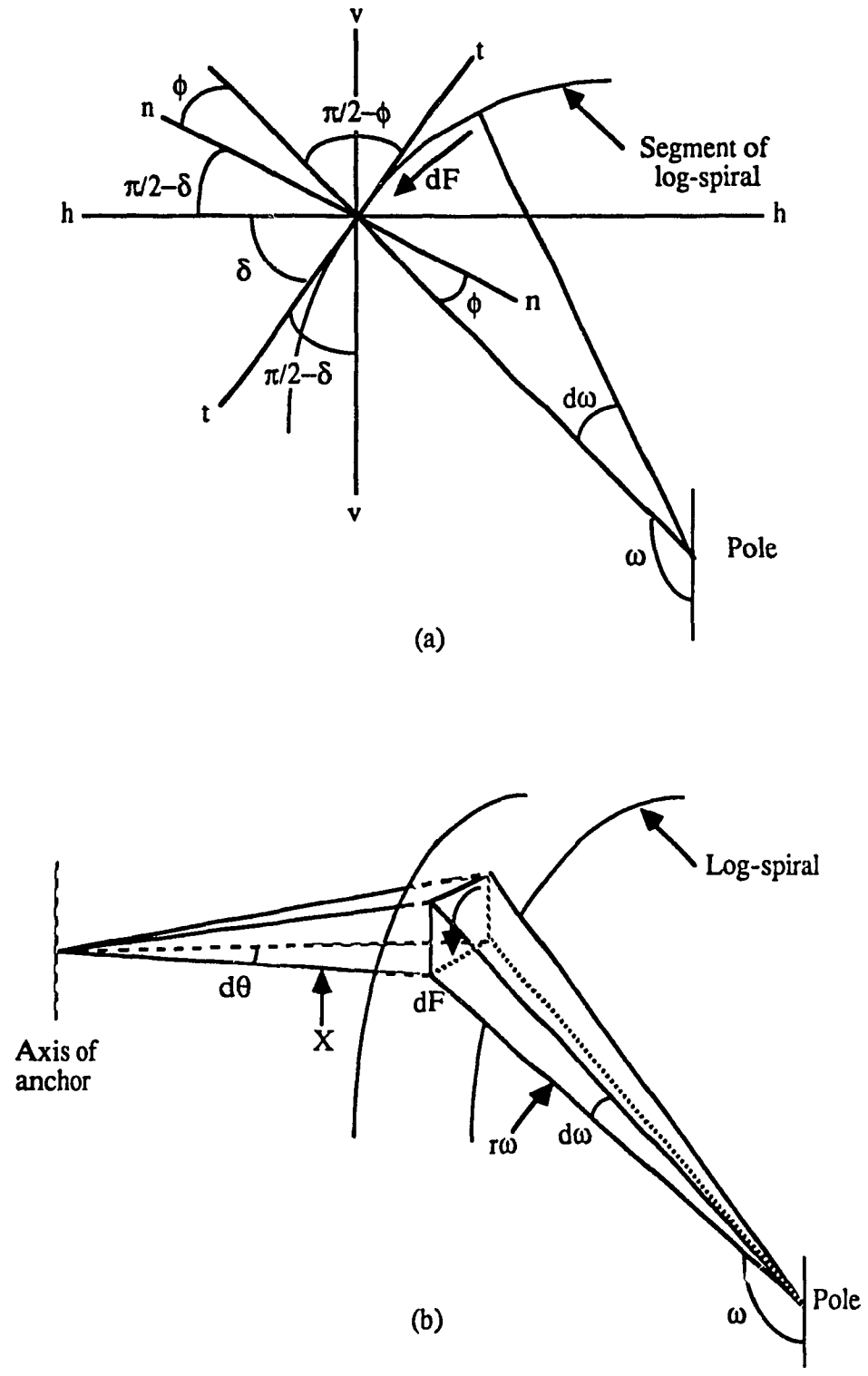

Fig. 5.3: Schematic representation of shearing force acting on rupture surface of shallow anchors.

Where $c_1 = \gamma \cdot r_0 \cdot \sin \phi$ ... (5.38a)

$$c_2 = \frac{1}{\beta} \cdot \cos \left(\frac{3\pi}{4} - \frac{3\phi}{2}\right) \quad \text{... (5.38b)}$$

The vertical component of the shearing resistance of shallow single anchor (F_{ss}) acting on the rupture surface can be calculated by considering the shearing resistance acting on an elemental area on the surface of the log-spiral (Fig. 5.3):

$$dF_{ss} = \tau \cdot \sec \phi \cdot (r_\omega \cdot d\omega) \cdot (X \cdot d\theta) \cdot \sin \delta \quad \text{... (5.39)}$$

$$\sin \delta = \sin (\pi - \omega + \phi) = \sin (\omega - \phi) \quad \text{... (5.40)}$$

Substituting the values of τ, X, and $\sin \delta$ from equations (5.38), (5.3), (5.9), and (5.40) in eq. (5.39); the shearing resistance of vertically pulled single shallow screw anchor is given by the following equation:

$$F_{ss} = \int_0^{2\pi} \int_{\alpha_1}^{\alpha_4} d F_{ss} \cdot d\omega \cdot d\theta \quad \text{... (5.41)}$$

This integration yields the following equation:

$$F_{ss} = 2\pi \cdot \gamma \cdot r_0^3 \cdot \tan \phi \{\alpha \cdot \cos^2 \phi (0.5 \cdot \cos 3\phi \cdot K7 + \sin 3\phi \cdot K8 - c_2 \cdot K4)$$

$$- \cos \phi (\cos 3\phi \cdot K6 - \cos 3\phi \cdot K10 + \sin 3\phi \cdot K9 - c_2 \cdot K17)$$

$$+ C \cdot \cos \phi (0.5 \cdot \cos 3\phi \cdot K7 + \sin 3\phi \cdot K8 - c_2 \cdot K4)$$

$$- \alpha \sin \phi \cos \phi (\cos 3\phi \cdot K14 + 0.5 \cdot \sin 3\phi \cdot K7 - c_2 \cdot K6)$$

$$+ \sin \phi (\cos 3\phi \cdot K4 - \cos 3\phi \cdot K9 + \sin 3\phi \cdot K6 - \sin 3\phi \cdot K10 - 0.5 \cdot c_2 \cdot K18)$$

$$- C \cdot \sin \phi \, (\cos 3\phi \cdot K14 + 0.5 \cdot \sin 3\phi \cdot K7 + c_2 \cdot K6)] \qquad \ldots (5.42)$$

The above equation can be reduced to the following equation:

$$F_{ss} = \gamma \cdot H^3 \cdot FF_{ss} \qquad \ldots (5.43)$$

Where FF_{ss} is a shear factor of shallow single anchor, its value depends on the angle of shearing resistance of the sand (ϕ) and the depth/diameter ratio (H/B) of the anchor. Values of FF_{ss} for angle ϕ ranging between 30° and 46°, and for H/B ratio varying from 2 to 10, are given in Table 5.2, they are also plotted in Fig. 5.4. Ultimate pullout load of single shallow anchor (QU_{ss}) is given by the following equation:

$$QU_{ss} = W_{ss} + F_{ss} \qquad \ldots (5.44)$$

5.1.2 Deep single anchors

It has been stated by a number of investigators that the mode of failure of deep anchors is of a local nature [18, 22, 37, 42, 43, 47, 48, 50, 57, 67]. Meyerhof and Adams (1968) [42], observed a rupture surface in the form of inverted cone with curved side walls (Fig. 2.4). However, they performed their theoretical analysis on an assumed plane surface of rupture. Mitsch and Clemence (1985) [43], reported several local surfaces of rupture, each of them is created on the top of every individual helix of a multi helical screw anchor. Ghaly (1986) [18], observed a local closed bulb created on the top of the helical unit of the screw anchor, however, he conducted the theoretical analysis on an equivalent simplified conical surface of rupture.

Measurements of sand surface deflections and lateral and vertical stresses in the sand medium

Table 5.2: Shear factor FF_{ss} for shallow single anchors.

$\phi°$	Embedment depth ratio, H/B				
	2	4	6	8	10
30	0.530	0.352	0.293	.....	.....
31	0.568	0.376	0.312	.....	.....
32	0.610	0.403	0.334	.....	.....
33	0.654	0.431	0.357	.....	.....
34	0.702	0.462	0.382	.....	.....
35	0.753	0.494	0.408	0.365	.....
36	0.806	0.529	0.436	0.390	.....
37	0.862	0.565	0.466	0.416	.....
38	0.921	0.603	0.497	0.444	.....
39	0.982	0.642	0.529	0.472	.....
40	1.045	0.683	0.562	0.502	0.466
41	1.110	0.725	0.596	0.532	0.494
42	1.177	0.768	0.632	0.564	0.523
43	1.245	0.812	0.668	0.596	0.553
44	1.316	0.858	0.705	0.629	0.583
45	1.387	0.904	0.743	0.663	0.614
46	1.460	0.951	0.782	0.697	0.646

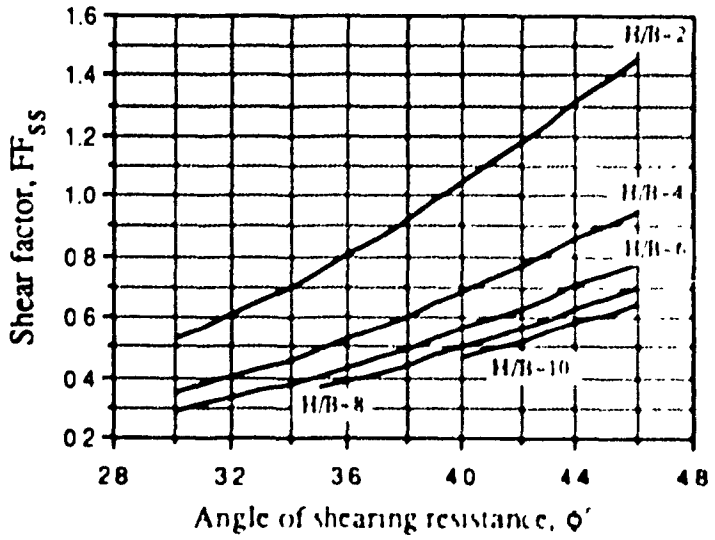

Fig 5.4: Shear factor for shallow single anchors versus angle of shearing resistance

for deeply installed screw anchor in the present investigation, emphasized the fact that the rupture surface is of a local nature. Based on the experimental results, it was observed that the shallow mode of failure does not take place beyond H/B ratios of 7, 9, and 11 for the tested loose, medium, and dense sand respectively. An analysis of the extent of the stress field, vertically and laterally away from the anchor's helical unit, indicated that the mode of failure of deeply installed anchors is a segment of log-spiral and its geometry depends on the angle of shearing resistance of the sand (ϕ) and on the relative embedment depth of the anchor (H/B). Typical rupture surface of deep anchors is shown in Fig. 5.5a. The rupture surface has a horizontal tangent at the anchor's level and it intersects the anchor's shaft at an angle of ($\pi/4 - \phi/2$) with the horizontal. The height of the local bulb (h) was determined experimentally and it was 6B, 5B, and 4B for $\phi = 31°$, 36°, and 42° respectively. It is worth noting that the height (h) of the bulb was constant for a given type of sand even with deeper depth of installation of the screw anchor.

For deep single anchors, the uplift capacity consists of four components, namely the self weight of the anchor, the dead weight of the sand mass within the rupture bulb, the vertical component of the shearing resistance mobilized along the rupture surface, and the surcharge pressure acting on the upper surface of the failure bulb. To simplify calculating the surcharge pressure, it will be considered as a uniformly distributed load acting on the imaginary surface i - i (Fig. 5.5a). The self weight of the anchor is negligible as compared with the other three components. The volume (V_{ds}) of the breaking out sand mass of deeply installed single screw anchor can be calculated by considering an elemental circular area of radius of revolution (X) and height (dh) (Fig. 5.5a):

$$V_{ds} = \int_0^h \pi \cdot X^2 \cdot dh \qquad \ldots (5.45)$$

$$X' = X_\omega - X_1$$

$$X = r_\omega \cdot \sin \omega + r_2 \cdot \sin \alpha_3 \qquad \ldots (5.46)$$

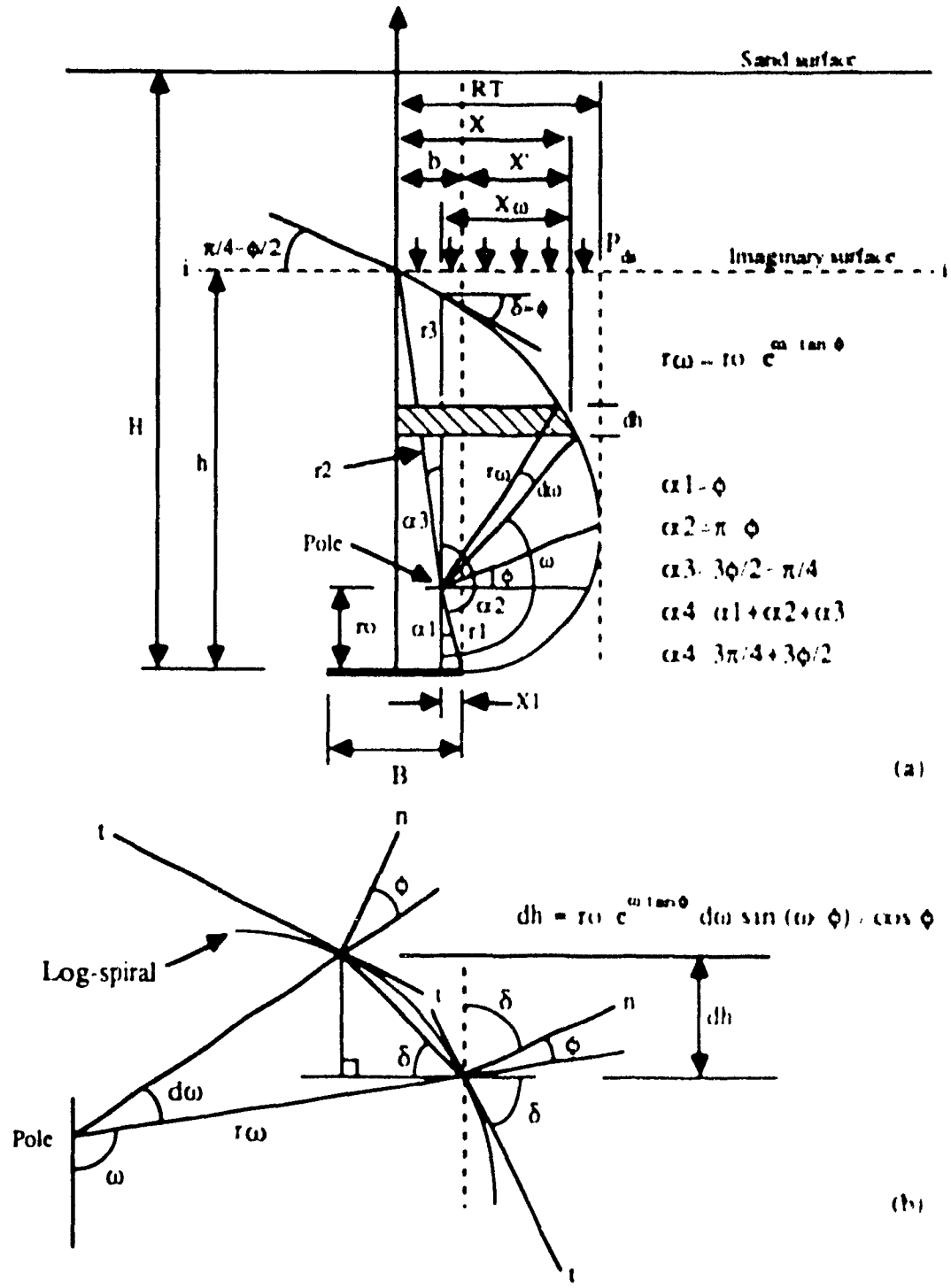

Fig 5.5 Geometrical properties of rupture surface of deep anchors

$$h = r_1 \cdot \cos \alpha_1 + r_2 \cdot \cos \alpha_3 \quad \text{...(5.47)}$$

$$r_2 = r_0 \cdot e^{\alpha_4 \cdot \tan \phi} \quad \text{...(5.47a)}$$

and $$r_1 = r_0 \cdot e^{\alpha_1 \cdot \tan \phi} \quad \text{...(5.47b)}$$

put $$e^{\alpha_1 \cdot \tan \phi} = \alpha \quad \text{...(5.6a)}$$

and $$e^{\alpha_4 \cdot \tan \phi} = \beta \quad \text{...(5.6b)}$$

$$r_0 = h / (\alpha \cdot \cos \alpha_1 + \beta \cdot \cos \alpha_3) \quad \text{... (5.48)}$$

Where $\alpha_1 = \phi$ ... (5.48a)

$$\alpha_2 = \pi - \phi \quad \text{... (5.48b)}$$

$$\alpha_3 = 3\phi/2 - \pi/4 \quad \text{... (5.48c)}$$

$$\alpha_4 = 3\pi/4 + 3\phi/2 \quad \text{... (5.48d)}$$

Substituting the values of r_ω and r_2 in eq. (5.46):

$$X = r_0 \cdot e^{\omega \cdot \tan \phi} \cdot \sin \omega + \beta \cdot r_0 \cdot \sin \phi \quad \text{... (5.49)}$$

$$dh = (r_\omega \cdot d\omega) \cdot \sin \delta / \cos \phi \quad \text{... (5.50)}$$

$$\sin \delta = \sin (\pi - \omega + \phi) = \sin (\omega - \phi) \quad \text{... (5.40)}$$

$$dh = r_0 \cdot e^{\omega \cdot \tan \phi} \cdot [\sin (\omega - \phi) / \cos \phi] \, d\omega \quad \text{... (5.51)}$$

From equations (5.49), and (5.51), the integration in eq. (5.44) can be evaluated:

$$V_{ds} = \pi \cdot r_0^3 [K9 - \tan\phi\,(K6 - K10)$$

$$+ \beta \cdot \sin\alpha_3\,(2 \cdot K8 - K7 \cdot \tan\phi)$$

$$+ (\beta \cdot \sin\alpha_3)^2\,(K1 - K2 \cdot \tan\phi)] \qquad \ldots (5.52)$$

Weight of the breaking out sand of deep single screw anchor (W_{ds}) is:

$$W_{ds} = \gamma \cdot V_{ds} \qquad \ldots (5.53)$$

Expressing r_0 in terms of bulb height (h) over the anchor by substituting eq. (5.24) in eq (5.28):

$$W_{ds} = \gamma \cdot h^3 \cdot FW_{ds} \qquad \ldots (5.54)$$

Where FW_{ds} is a weight factor of single deep anchor, its value depends on sand's angle of shearing resistance (ϕ) and ratio between the rupture bulb height and anchor diameter (H/B). Computed values of FW_{ds} for ϕ varying between 30° and 46° are given in Table 5.3. These values were calculated for h = 6B if $30° \leq \phi \leq 34°$, h = 5B if $35° \leq \phi \leq 39°$, and h = 4B if $40° \leq \phi \leq 46°$. Computed values of FW_{ds} are plotted in the chart shown in Fig. 5.6. It should be mentioned that the bulb height (h) is not expected to be constant throughout a given range of ϕ. This approximation has been made due to the lack of information about the anchor behaviour in the other non-tested values of ϕ, and this problem requires further investigation.

The resultant of shearing stress acting on the bulb rupture surface can be determined by using Kotter's differential equation given in eq. (5.37) and applying the proper boundary conditions due to the bulb embedment below the sand surface. In case of deep single anchor, the solution of eq (5.37) is:

Table 5.3: Weight factor FW_{ds} for deep single anchors.

$\phi°$	Failure bulb height-diameter ratio, h/B		
	6	5	4
30	0.311	-------	-------
31	0.331	-------	-------
32	0.352	-------	-------
33	0.374	-------	-------
34	0.397	-------	-------
35	-------	0.423	-------
36	-------	0.450	-------
37	-------	0.478	-------
38	-------	0.509	-------
39	-------	0.541	-------
40	-------	-------	0.576
41	-------	-------	0.612
42	-------	-------	0.652
43	-------	-------	0.693
44	-------	-------	0.738
45	-------	-------	0.786
46	-------	-------	0.838

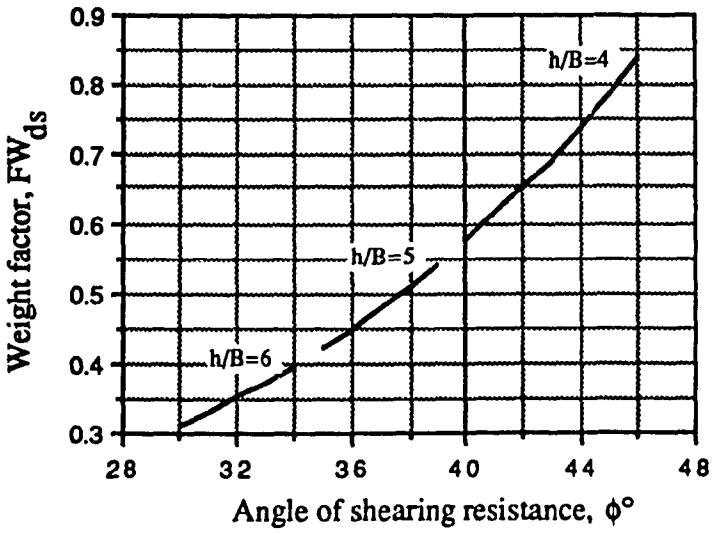

Fig. 5.6: Weight factor for deep single anchors versus angle of shearing resistance.

$$\tau = c_1 e^{\omega \cdot \tan\phi} \cdot \cos(\omega - 3\phi) + (c_3 - c_1 \cdot c_2) e^{2\omega \cdot \tan\phi} \quad \ldots (5.55)$$

Where $c_1 = \gamma \cdot r_0 \cdot \sin\phi$ ... (5.55a)

$$c_2 = \frac{1}{\beta} \cdot \cos\left(\frac{3\pi}{4} - \frac{3\phi}{2}\right) \quad \ldots (5.55b)$$

$$c_3 = \frac{1}{\beta^2} \cdot [\gamma \cdot (H - h) \cdot K_P \cdot \tan\phi] \quad \ldots (5.55c)$$

$$K_P = (1 + \sin\phi) / (1 - \sin\phi) \quad \ldots (5.55d)$$

Considering the shearing stress acting on an elemental area on the bulb surface (Fig. 5.7) and integrating this area on the total surface area of the bulb, the vertical component of the shearing resistance (F_{ds}) acting on the rupture surface can be calculated

$$dF_{ds} = \tau \cdot \sec\phi \cdot (r_\omega \cdot d\omega) \cdot (X \cdot d\theta) \cdot \sin\delta \quad \ldots (5.56)$$

$$\sin\delta = \sin(\pi - \omega + \phi) = \sin(\omega - \phi) \quad \ldots (5.40)$$

Substituting the values of τ, X, and $\sin\delta$ from equations (5.55), (5.49), and (5.40) in eq (5.31), the shearing resistance of vertically pulled single deep screw anchor is given by the following equation:

$$F_{ds} = \int_0^{2\pi} \int_{\omega_i}^{\omega_u} dF_{ds} \; d\omega \; d\theta \quad (5.57)$$

The integration yields the following equation

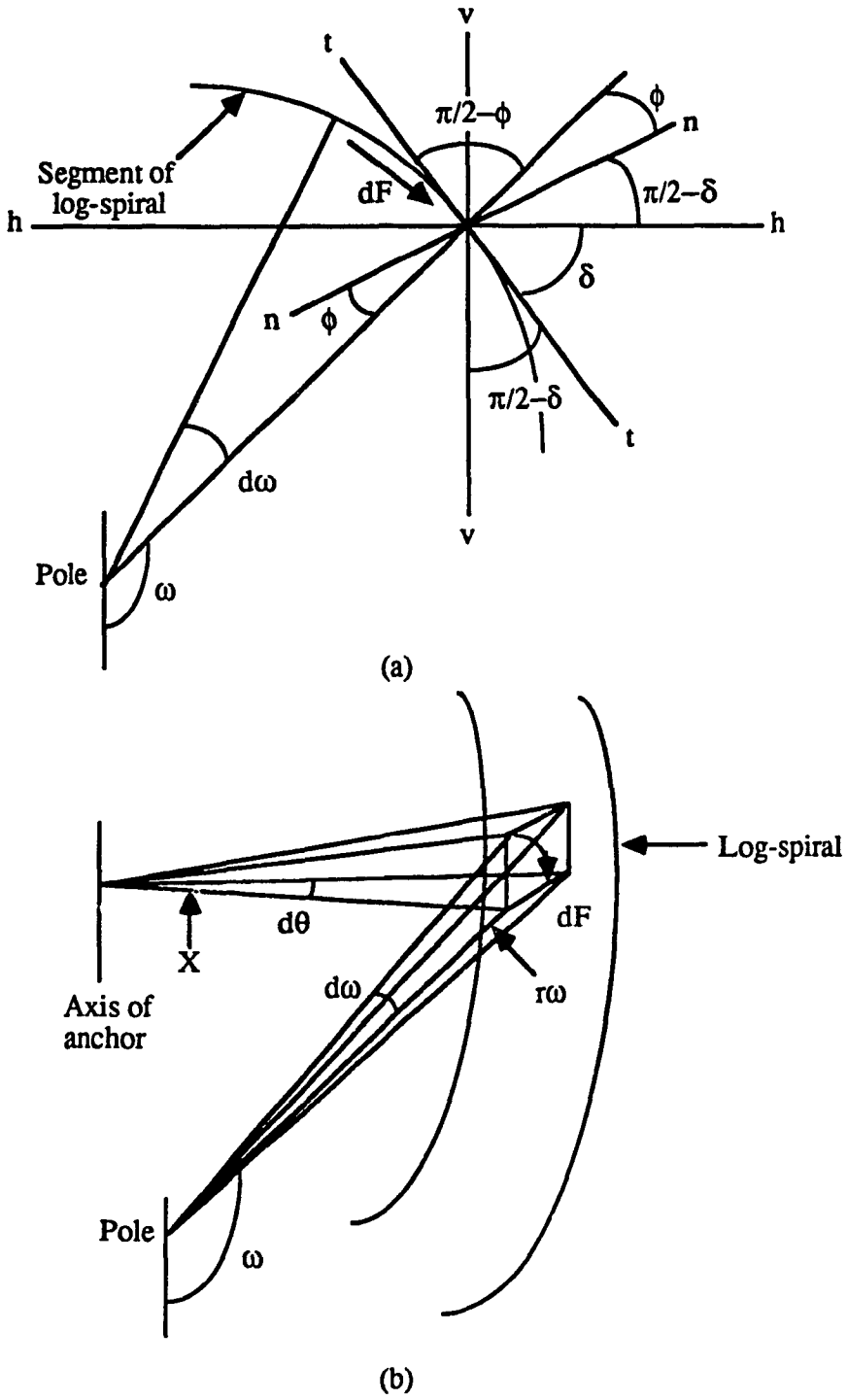

Fig. 5.7: Schematic representation of shearing force acting on rupture surface of deep anchors.

$$F_{ds} = 2\pi \cdot \gamma \cdot r_0^3 \cdot \tan\phi \{ \cos\phi [\cos 3\phi\ (K6 - K10) + \sin 3\phi \cdot K9 + \beta \cdot \sin\alpha_3\ (0.5 \cdot \cos 3\phi \cdot K7 + \sin 3\phi \cdot K8)]$$

$$- \sin\phi\ [\cos 3\phi\ (K4 - K9) + \sin 3\phi\ (K6 - K10) + \beta \cdot \sin\alpha_3\ (\cos 3\phi \cdot K14 + 0.5 \cdot \sin 3\phi \cdot K7)]$$

$$+ (c_4 - c_2) \cos\phi\ [K17 + \beta \cdot \sin\alpha_3 \cdot K4]$$

$$- (c_4 - c_2) \sin\phi\ [0.5 \cdot K18 + \beta \cdot \sin\alpha_3 \cdot K6] \} \quad \ldots (5.58)$$

Where $c_4 = c_3/c_1$ ... (5.58a)

The above equation can be reduced to the following equation:

$$F_{ds} = \gamma \cdot h^3 \cdot FF_{ds} \quad \ldots (5.59)$$

Where FF_{ds} is a shear factor of deep single anchor, its value depends on the sand's angle of shearing resistance (ϕ), ratio between the rupture bulb height and anchor diameter (h/B), and boundary conditions on the rupture bulb. Computed values of FF_{ds} for ϕ varies between 30° and 46° and for deep anchors installed at H/B ratio up to 16, are given in Table 5.4 and plotted in Fig. 5.8. As mentioned before, these values were obtained based on bulb dimensions of h = 6B for $30° \le \phi \le 34°$, h = 5B for $35° \le \phi \le 39°$, and h = 4B for $40° \le \phi \le 46°$.

The surcharge pressure acting on the upper surface of the rupture bulb of deeply installed single anchor (P_{ds}), can be calculated from the following equation (Fig. 5.5a):

$$P_{ds} = \gamma \cdot \pi \cdot RT^2 \cdot (H - h) \quad (5.60)$$

Table 5.4: Shear factor FF_{ds} for deep single anchors.

$\phi°$	h/B	Embedment depth ratio, H/B				
		8	10	12	14	16
30	6	0.706	1.101	1.495	1.890	2.285
31	6	0.759	1.193	1.626	2.059	2.492
32	6	0.816	1.291	1.766	2.241	2.716
33	6	0.875	1.395	1.916	2.436	2.956
34	6	0.938	1.507	2.076	2.645	3.214
35	5	-------	2.249	2.995	3.741	4.487
36	5	-------	2.434	3.249	4.063	4.877
37	5	-------	2.634	3.522	4.411	5.299
38	5	-------	2.849	3.818	4.786	5.755
39	5	-------	3.082	4.137	5.193	6.249
40	4	-------	-------	6.208	7.646	9.084
41	4	-------	-------	6.738	8.304	9.870
42	4	-------	-------	7.313	9.019	10.726
43	4	-------	-------	7.940	9.799	11.658
44	4	-------	-------	8.624	10.650	12.676
45	4	-------	-------	9.373	11.582	13.791
46	4	-------	-------	10.194	12.604	15.013

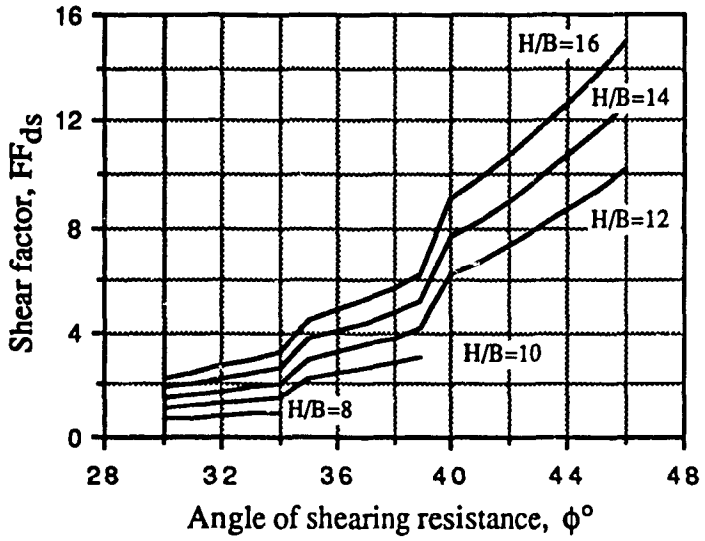

Fig. 5.8: Shear factor for deep single anchors versus angle of shearing resistance.

Where RT = radius of circle produced from the intersection of vertical tangent to the rupture bulb with the imaginary surface i - i.

$$RT = r_0 [e^{\pi/2 \cdot \tan \phi} \cdot \cos \phi + \beta \cdot \sin (3\phi/2 - \pi/4)] \quad \ldots (5.61)$$

Ultimate pullout load of single deep anchor (QU_{ds}) is given by the following equation:

$$QU_{ds} = W_{ds} + F_{ds} + P_{ds} \quad \ldots (5.62)$$

5.1.3 Transit single anchors

It is believed that the conversion from shallow anchor mode of failure to a deep anchor one does not occur suddenly, but it takes place gradually through a transition zone. In the present investigation, however, this zone was recognised and experimentally determined for loose, medium, and dense sand. This transit phase was clearly observed for tests conducted on dense and loose sand. However, it was less obvious in the case of medium sand, and this may be attributed to the large differences between the tested H/B ratios (4, 8, 12 & 16), i.e., transit zone might took place in an intermediate H/B ratio, hence, it was not recorded. However, the medium sand is expected to behave similar to the dense and loose sand as regards the existence of a transit zone. The features that accompanied the appearance of the failure surface of an anchor installed to a transit zone, were as follows:

a) No sand surface deflections and no stress increase in the transducers located at the upper half of the sand deposit, up to about 90% of failure load.

b) Significant sand surface deflections and stress increase in the stress transducers, located at the upper half of the sand layer, were recorded when the pullout load exceeded 90% of

failure load and continued up to failure.

c) Maximum diameter of the circle representing the sand surface deflections is smaller than that expected for pure shallow anchor behaviour.

Analysis of test results indicated that a combined shallow-deep behaviour takes place in the transition zone (Fig. 5.9). Comparison of the dimensions of radius of maximum surface deflection (RR) (Fig. 5.9) with the relevant results of shallow anchors installed in a similar sand layer, indicated that the radius RR is comparable with a radius of failure circle of shallow anchor installed to half of the depth of the transit anchor.

Based on these observations, it was indicated that a deep anchor behaviour takes place in the lower half of the sand layer while a shallow one takes place in the upper half (Fig. 5.9). Employing the principle of superposition, the total uplift capacity of a transit single anchor (QU_{ts}) can be expressed as the summation of the forces acting on the rupture surface and contributing to the resistance against uplift. Considering the lower part of deep behaviour, the forces acting against uplift can be expressed as the following:

$$W_{tds} = \gamma \cdot FW_{ds} \cdot (H/2)^3 \quad \text{... (5.63)}$$

$$F_{tds} = \gamma \cdot FF_{ds} \cdot (H/2)^3 \quad \text{... (5.64)}$$

$$P_{tds} = \gamma \cdot \pi \, (RT^2 - b^2) \cdot H/2 \quad \text{... (5.65)}$$

Where FW_{ds} and FF_{sd} are weight and shear factors, respectively, for a deep single anchor, its bulb dimensions and sand elevation, over the bulb, are comparable with the deep mode of failure of the transit anchor in question. Radius RT is given by eq. (5.61). W_{tds}, F_{tds}, and P_{tds} represent the weight, shear, and earth pressure values, respectively, that constitute the portion of the deep

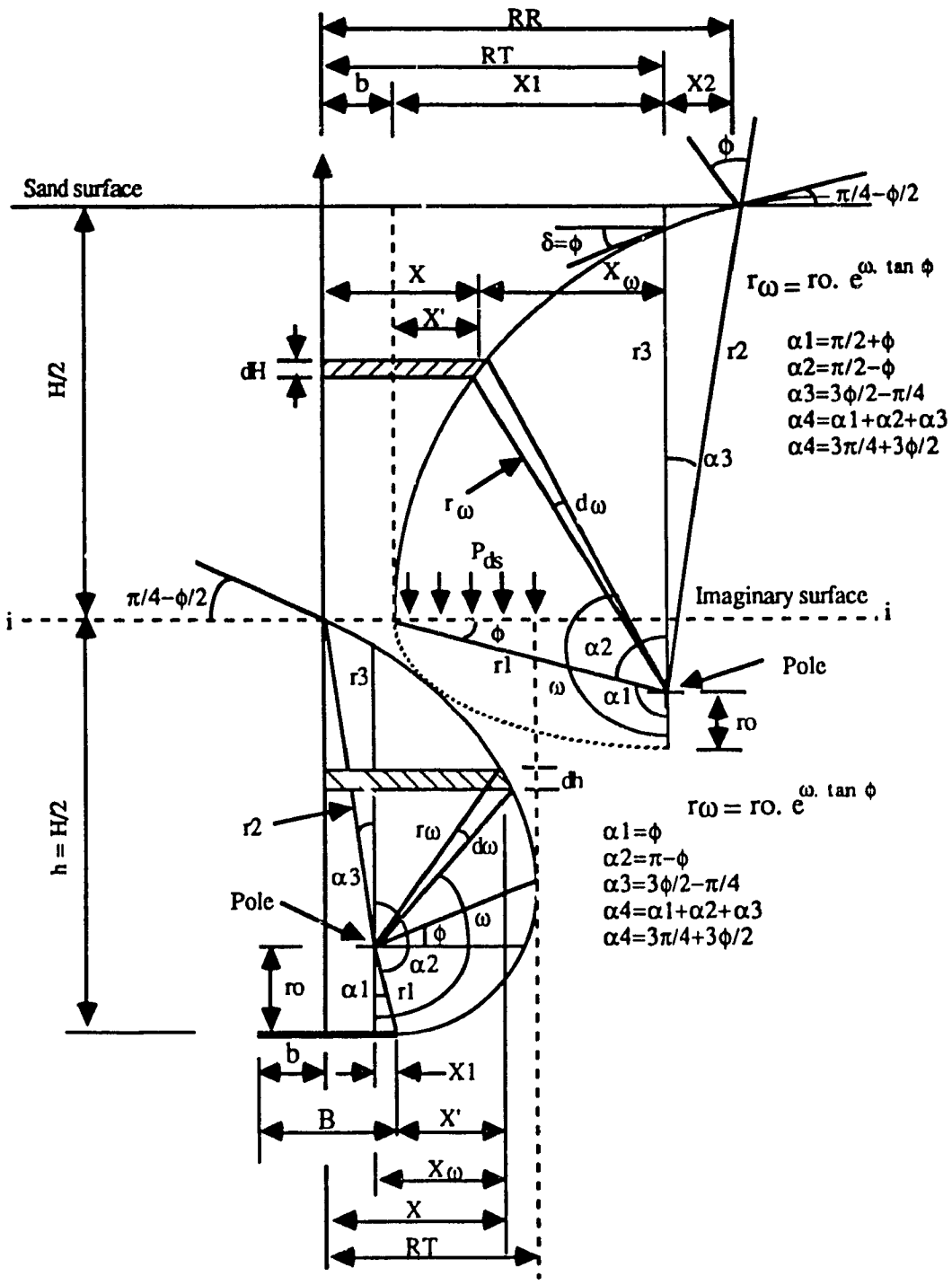

Fig. 5.9: Geometrical properties of rupture surface of transit anchors.

phase of a transit single anchor against uplift.

Considering the upper part of shallow behaviour, the forces acting against uplift are given by the following equations:

$$W_{tss} = \gamma \cdot FW_{ss} \cdot (H/2)^3 \quad \text{... (5.66)}$$

$$F_{tss} = \gamma \cdot FF_{ss} \cdot (H/2)^3 \quad \text{... (5.67)}$$

Where FW_{ss} is the weight factor and FF_{ss} is the shear factor for a shallow single anchor, its depth of installation is half of the total depth of the transit anchor and installed in comparable conditions. W_{tss}, F_{tss}, and P_{tss} represent the weight, shear, and earth pressure values, respectively, that constitute the portion of the shallow phase of a transit single anchor against uplift.Values of factors required for evaluating equations (5.63) through (5.67) can be obtained from Tables 5.1 through 5.4 or from the relevant design charts.

Hence, the total uplift capacity of a single transit anchor (QU_{ts}) is:

$$QU_{ts} = W_{tds} + F_{tds} + P_{tds} + W_{tss} + F_{tss} \quad \text{... (5.68)}$$

5.2 Group of Anchors

5.2.1 Shallow square or rectangular group of anchors

The observed mechanism of rupture for single shallow anchor was utilized to establish the form of the rupture surface for shallow group of anchors. Figure 5.10a shows an isometry of surface of rupture for square shallow group of anchors. From Fig. 5.10b, it can be indicated that the pullout capacity of a shallow group of anchors consists of self weight of the anchors, weight of sand involved within the rupture surface, and vertical component of shearing resistance mobilized along the rupture surface. Dimensions of the log-spiral rupture surface depends on the

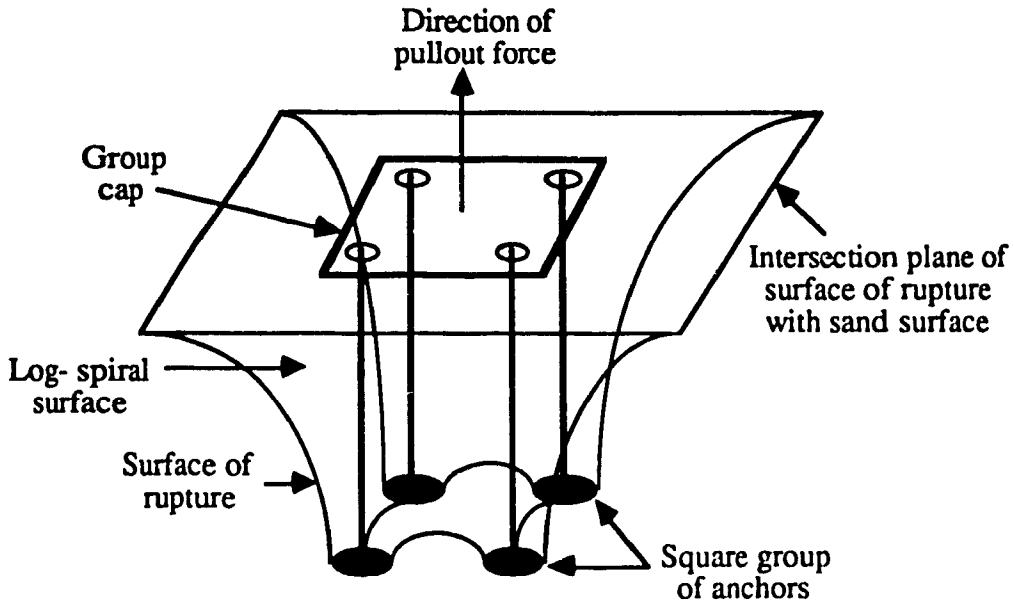

(a) Isometry of surface of rupture for shallow square group of anchors.

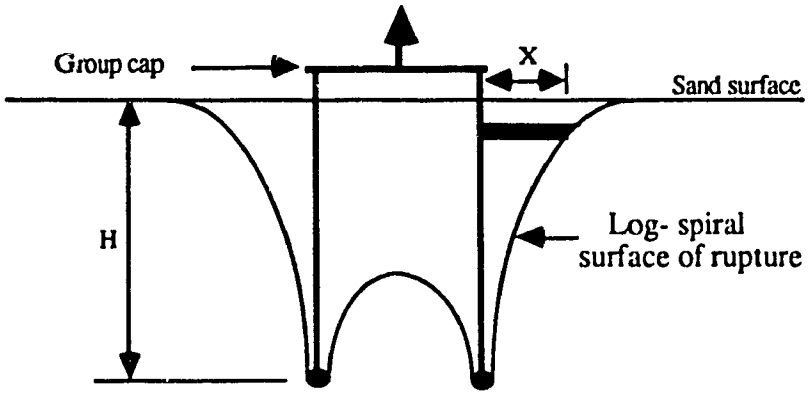

(b) Elevation of rupture mechanism for shallow square group of anchors.

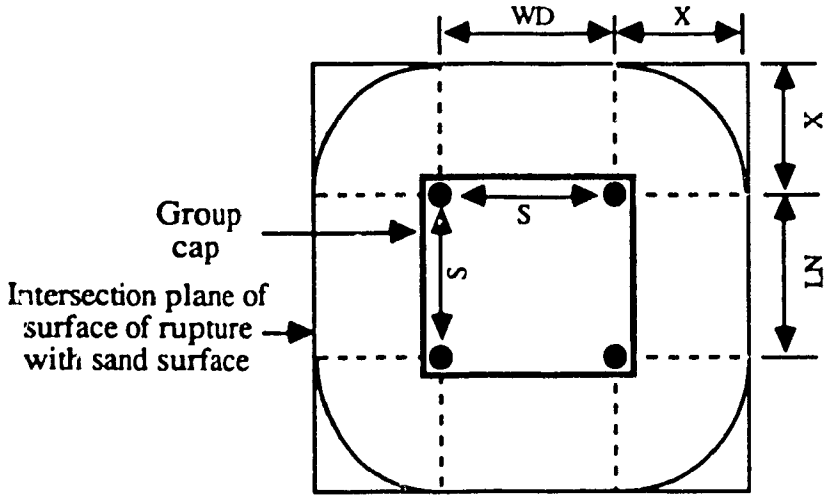

(c) Plan of rupture mechanism for shallow square group of anchors.

Fig. 5.10: Geometry of rupture mechanism for shallow square group of anchors.

angle of shearing resistance of the sand and the relative depth ratio H/B of anchors located at the outer perimeter of the group. Also, zone of interference of the single action of every individual anchor of the group depends on the spacing between anchors as well as on the geometrical properties of the rupture surface. Self weight of the anchors group can be neglected as it constitutes a very small fraction as compared with the total uplift capacity. The weight of the breaking out sand mass (W_{sg}) consists of the weight of the sand between the individual anchors of the group (W1), in addition to the weight of the sand between the rupture surface and the outer perimeter of the anchor group (W2).

$$A_g = LN \cdot WD \quad \text{... (5.69)}$$

$$P_g = 2\,(LN + WD) \quad \text{... (5.70)}$$

Where A_g, P_g, LN, and WD are area, perimeter, length, and width of the anchors group respectively.

$$W1 = \gamma \cdot A_g \cdot H \quad \text{... (5.71)}$$

$$W2 = \gamma \cdot P_g \int_0^H X \cdot dH + W_{ss} \quad \text{... (5.72)}$$

Where $X = X' + b$ ... (5.3)

$$X' = \alpha \cdot r_0 \cdot \cos\phi - e^{\omega \cdot \tan\phi} \cdot \cos(\omega - \pi/2) \quad \text{... (5.9)}$$

$$\alpha = e^{(\pi/2 + \phi) \cdot \tan\phi}$$

$$W_{ss} = \gamma \cdot H^3 \cdot FW_{ss} \quad \text{... (5.34)}$$

$$dH = r_0 \cdot e^{\omega \cdot \tan\phi} \cdot [\sin(\omega - \phi)/\cos\phi]\, d\omega \quad \text{... (5.11)}$$

$$\int_0^H X \cdot dH = r_0^2 [(C + \alpha \cdot \cos\phi)(K1 - K2 \cdot \tan\phi) - K8 + 0.5 \cdot \tan\phi \cdot K7] \quad \ldots (5.73)$$

Where $C = b/r_0$ ... (5.32)

Expressing r_0 in terms of H by using eq. (5.8), the weight W2 can be determined from the following equation:

$$W2 = \gamma \cdot P_g \cdot H^2 \cdot FW_{sg} + \gamma \cdot H^3 \cdot FW_{ss} \quad \ldots (5.74)$$

Where FW_{ss} is the weight factor for shallow single anchor, its value can be obtained from Table 5.1 or the chart in Fig. 5.2. FW_{sg} is the weight factor for shallow group of anchors, its value depends on the angle of shearing resistance of the sand (ϕ) and the relative depth ratio H/B. Computed values of FW_{sg} are given in Table 5.5 and plotted in Fig. 5.11. Hence, W_{sg} can be given by:

$$W_{sg} = W1 + W2 \quad \ldots (5.75)$$

The vertical component of shearing resistance of shallow group of anchors (F_{sg}) acting on the rupture surface can be calculated by considering an elemental area on the surface of the log-spiral. An equation similar to equation (5.39) can be written for shallow anchors group (Fig. 5.10a & b):

$$dF_{sg} = \tau \cdot \sec\phi \cdot (r_\omega \cdot d\omega) \cdot P_f \cdot \sin\delta \quad \ldots (5.76)$$

Where τ and δ are as given by equation (5.38) and (5.40) respectively.

Table 5.5: Weight factor FW_{sg} for shallow group of anchors.

$\phi°$	Embedment depth ratio, H/B				
	2	4	6	8	10
30	0.449	0.324	0.282	-------	-------
31	0.452	0.327	0.285	-------	-------
32	0.455	0.330	0.288	-------	-------
33	0.458	0.333	0.292	-------	-------
34	0.461	0.337	0.295	-------	-------
35	0.465	0.340	0.298	0.277	-------
36	0.468	0.344	0.302	0.281	-------
37	0.472	0.347	0.306	0.285	-------
38	0.476	0.351	0.309	0.289	-------
39	0.480	0.355	0.313	0.292	-------
40	0.484	0.359	0.317	0.296	0.284
41	0.488	0.363	0.321	0.301	0.288
42	0.492	0.367	0.326	0.305	0.293
43	0.497	0.372	0.330	0.310	0.297
44	0.502	0.377	0.335	0.314	0.302
45	0.507	0.382	0.340	0.319	0.307
46	0.512	0.387	0.345	0.324	0.312

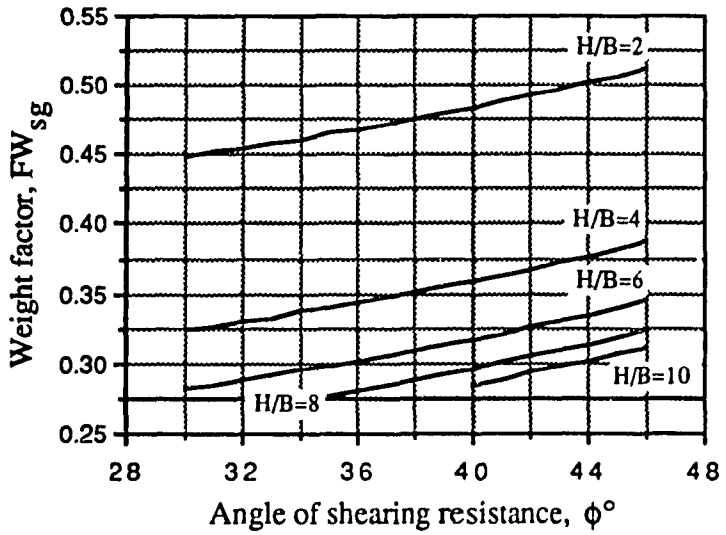

Fig. 5.11: Weight factor for shallow group of anchors versus angle of shearing resistance.

P_f = perimeter of failed group

$= 2\,[(LN + 2X) + (WD + 2X)]$

$= 2\,(LN + WD) + 8X$

$$P_f = P_g + 8X \qquad \ldots (5.77)$$

From eq. (5.75) and eq. (5.74), the following equation can be written:

$$\int dF_{sg} = P_g \int_{\alpha_1}^{\alpha_4} \tau \cdot \sec\phi \cdot \sin\delta \cdot r_\omega \cdot d\omega + 8 \int_{\alpha_1}^{\alpha_4} \tau \cdot \sec\phi \cdot \sin\delta \cdot X \cdot r_\omega \cdot d\omega \quad \ldots (5.78)$$

This integration yields the following expression:

$$F_{sg} = \gamma \cdot H^2 \cdot P_g \cdot FF_{sg} + (8/2\pi) \cdot \gamma \cdot H^3 \cdot FF_{ss} \qquad \ldots (5.79)$$

Where FF_{ss} is the shear factor for shallow single anchor and is given by Table 5.2 or Fig. 5.4. FF_{sg} is the shear factor for the shallow group of anchors and is given by the following expression:

$$FF_{sg} = r_0^2 \cdot \tan\phi\,[\cos 3\phi\,(0.5 \cdot \cos\phi \cdot K7 - \sin\phi \cdot K14)$$
$$+ \sin 3\phi\,(\cos\phi \cdot K8 - 0.5 \cdot \sin\phi \cdot K7)$$
$$- c_2\,(\cos\phi \cdot K4 - \sin\phi \cdot K6)] \qquad \ldots (5.80)$$

$$\text{Where } c_2 = \frac{1}{\beta} \cdot \cos\left(\frac{3\pi}{4} - \frac{3\phi}{2}\right) \qquad \text{... (5.80a)}$$

$$\beta = e^{\alpha_4 \cdot \tan\phi} = e^{(3\pi/4 + 3\phi/2)\cdot \tan\phi} \qquad \text{...(5.80b)}$$

FF_{sg} is a shear factor its value depends on the angle of shearing resistance of the sand (ϕ) and H/B ratio. Computed values for FF_{sg} are listed in Table 5.6 and plotted in Fig. 5.12. The total uplift capacity of shallow group of anchors (QU_{sg}) can be given by the following equation:

$$QU_{sg} = W_{sg} + F_{sg} \qquad \text{... (5.81)}$$

5.2.2 Shallow triangular group of anchors

The behaviour of shallow triangular group of anchors is similar to that of square or rectangular but with different geometry for the rupture surface (Fig. 5.13). Using the same notation that was used for shallow square and rectangular anchors group, the final equations to determine the uplift capacity of shallow triangular group of anchors can be given directly as:

$$A_g = 0.5\,(LN)^2 \cdot \sin 60° \qquad \text{... (5.82)}$$

$$P_g = 3\,(LN) \qquad \text{... (5.83)}$$

W1, W2, and W_{sg} are as given by equations (5.71), (5.74), and (5.75) respectively.

$$P_f = P_g + 6X \cdot \cot 30° \qquad \text{... (5.84)}$$

$$F_{sg} = \gamma \cdot H^2 \cdot P_g \cdot FF_{sg} + (6\,.\,\cot 30°) \cdot \gamma \cdot H^3 \cdot FF_{ss} \qquad \text{... (5.85)}$$

Table 5.6: Shear factor FE_{sg} for shallow group of anchors.

$\phi°$	Embedment depth ratio, H/B				
	2	4	6	8	10
30	0.226	0.226	0.226	-------	-------
31	0.231	0.231	0.231	-------	-------
32	0.236	0.236	0.236	-------	-------
33	0.241	0.241	0.241	-------	-------
34	0.245	0.245	0.245	-------	-------
35	0.249	0.249	0.249	0.249	-------
36	0.253	0.253	0.253	0.253	-------
37	0.257	0.257	0.257	0.257	-------
38	0.260	0.260	0.260	0.260	-------
39	0.263	0.263	0.263	0.263	-------
40	0.266	0.266	0.266	0.266	0.266
41	0.269	0.269	0.269	0.269	0.269
42	0.271	0.271	0.271	0.271	0.271
43	0.274	0.274	0.274	0.274	0.274
44	0.276	0.276	0.276	0.276	0.276
45	0.278	0.278	0.278	0.278	0.278
46	0.279	0.279	0.279	0.279	0.279

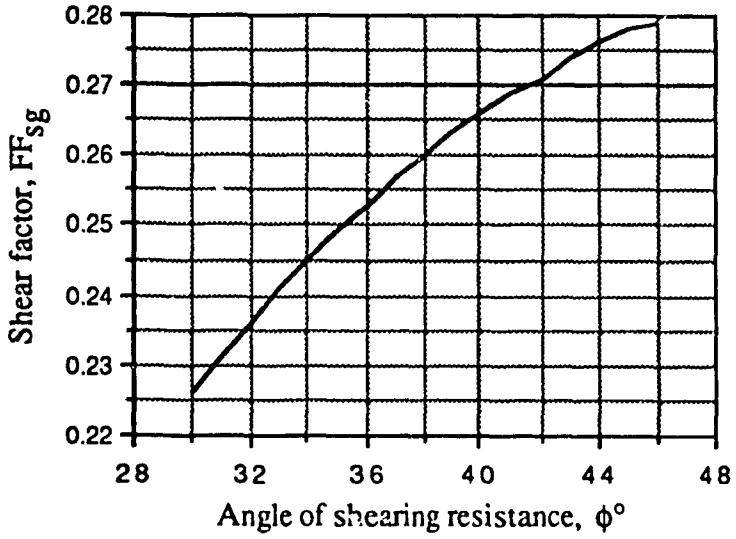

Fig. 5.12: Shear factor for shallow group of anchors versus angle of shearing resistance.

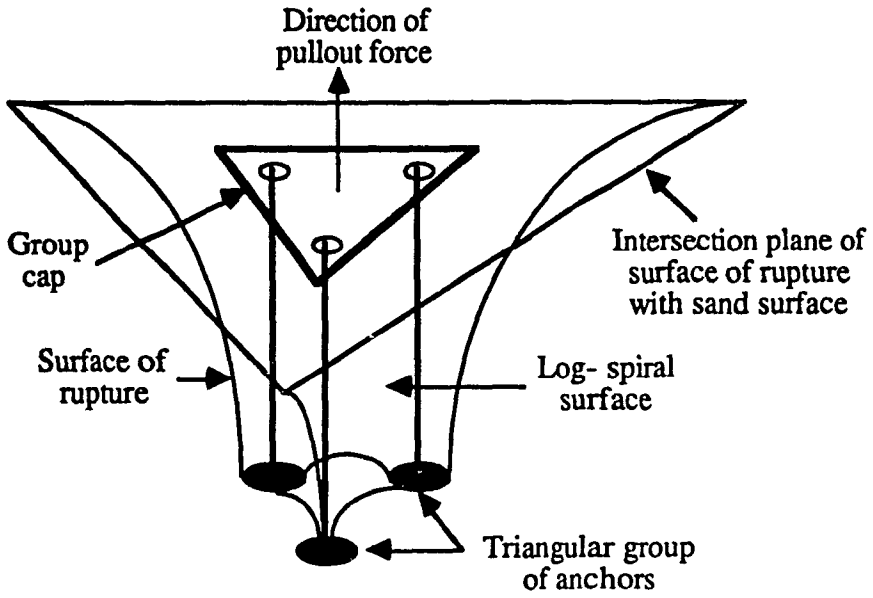

(a) Isometry of surface of rupture for shallow triangular group of anchors.

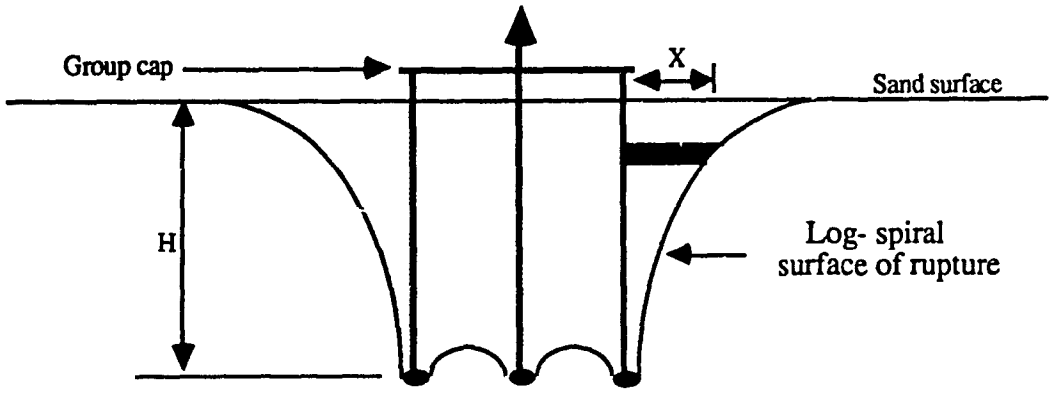

(b) Elevation of rupture mechanism for shallow triangular group of anchors.

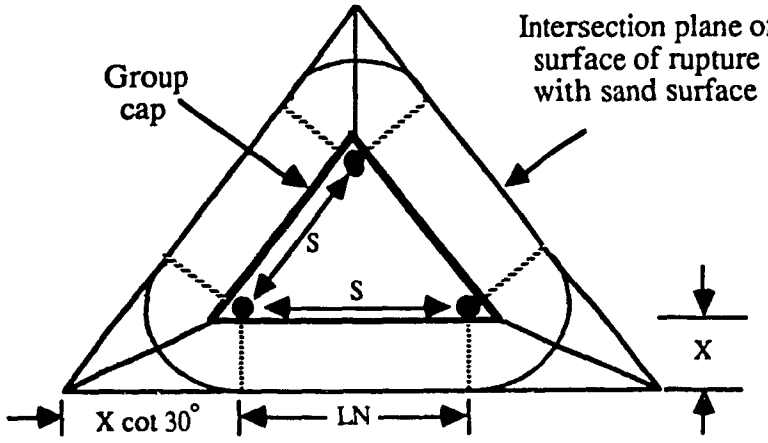

(b) Plan of rupture mechanism for shallow triangular group of anchors.

Fig. 5.13: Geometry of surface of rupture for shallow triangular group of anchors.

$$QU_{sg} = W_{sg} + F_{sg} \qquad \ldots (5.81)$$

Weight and shear factors FW_{ss}, FW_{sg}, FF_{ss}, and FF_{sg} are as given in Table 5.1, 5.5, 5.2, and 5.6 respectively or from the relevant charts.

5.2.3 Deep square or rectangular group of anchors

The form of the rupture surface for deep group of anchors was established by utilizing the observed mechanism of rupture for single deep anchor. Figure 5.14a shows an isometry of the surface of rupture for square deep group of anchors. The pullout capacity of a deep group of anchors consists of self weight of the anchors, weight of the sand involved within the rupture surface, vertical component of shearing resistance mobilized along the rupture surface, and the surcharge pressure acting on the upper surface of the failed mass of sand. Self weight of anchors can be neglected. Weight of breaking out sand mass (W_{dg}) is of two components, namely, weight of the sand between the individual anchors of the group (W1), and weight of sand between the rupture surface and the outer perimeter of the anchors group (W2) (Fig. 5.14b & c).

$$A_g = LN \cdot WD \qquad \ldots (5.69)$$

$$P_g = 2\,(LN + WD) \qquad \ldots (5.70)$$

$$W1 = \gamma \cdot A_g \cdot h \qquad \ldots (5.86)$$

$$W2 = \gamma \cdot P_g \int_0^h X \cdot dh + W_{ds} \qquad \ldots (5.87)$$

$$X = r_0 \cdot e^{\omega \cdot \tan \phi} \cdot \sin \omega + \beta \cdot r_0 \cdot \sin \phi \qquad \ldots (5.49)$$

$$\alpha = e^{\phi \cdot \tan \phi}$$

$$W_{ds} = \gamma \cdot h^3 \cdot FW_{ds} \quad \ldots (5.54)$$

$$dh = r_0 \cdot e^{\omega \cdot \tan \phi} \cdot [\sin (\omega - \phi) / \cos \phi] \, d\omega \quad \ldots (5.51)$$

Expressing r_0 in terms of h by using eq. (5.48), the weight W2 can be determined from the following equation:

$$W2 = \gamma \cdot P_g \cdot h^2 \cdot FW_{dg} + \gamma \cdot h^3 \cdot FW_{ds} \quad \ldots (5.89)$$

Where FW_{ds} is the weight factor for deep single anchors and given in Table 5.3 or the chart in Fig. 5.6. FW_{dg} is the weight factor for deep group of anchors, its value depends on the angle of shearing resistance of the sand (ϕ) and the ratio (h/B). Computed values of FW_{dg} are given in Table 5.7 and plotted in Fig. 5.15. Hence, W_{dg} is given by:

$$W_{dg} = W1 + W2 \quad \ldots (5.90)$$

The vertical component of shearing resistance of deep group of anchors (F_{dg}) acting on the rupture surface can be calculated by considering an elemental area on the surface of the log-spiral. An equation similar to eq. (5.76) can be written:

$$dF_{dg} = \tau \cdot \sec \phi \cdot (r_\omega \cdot d\omega) \cdot P_f \cdot \sin \delta \quad \ldots (5.91)$$

Where τ, P_f, and δ are given by equations (5.55), (5.77), and (5.40) respectively. Substituting the values of τ, P_f, and δ in eq. (5.91) and integrating, the vertical component of shearing resistance of deep group of anchors, F_{dg} can be given by the following equation:

$$F_{dg} = \gamma \cdot h^2 \cdot P_g \cdot FF_{dg} + (8/2\pi) \cdot \gamma \cdot h^3 \cdot FF_{ds} \quad \ldots (5.92)$$

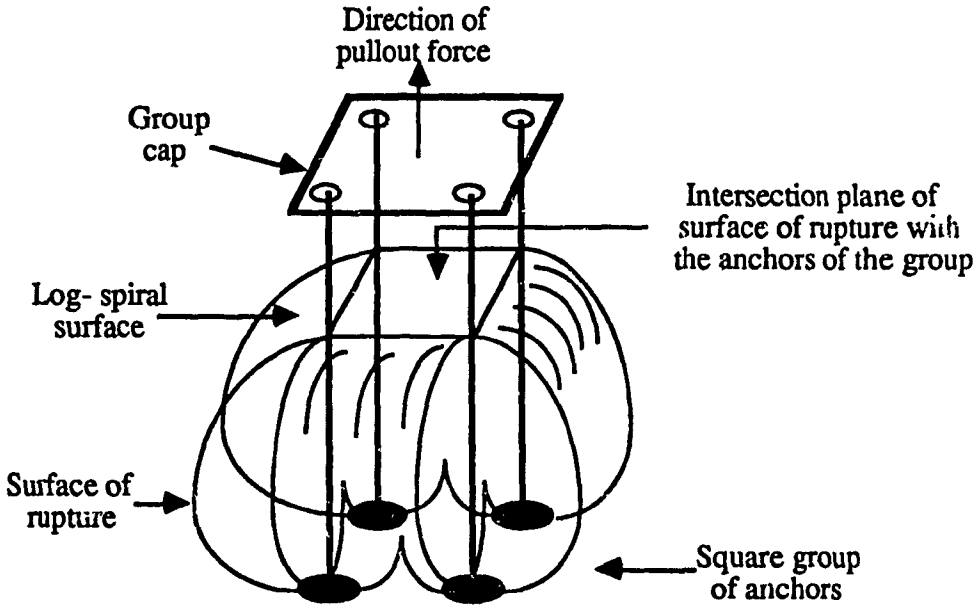

(a) Isometry of surface of rupture for deep square group of anchors.

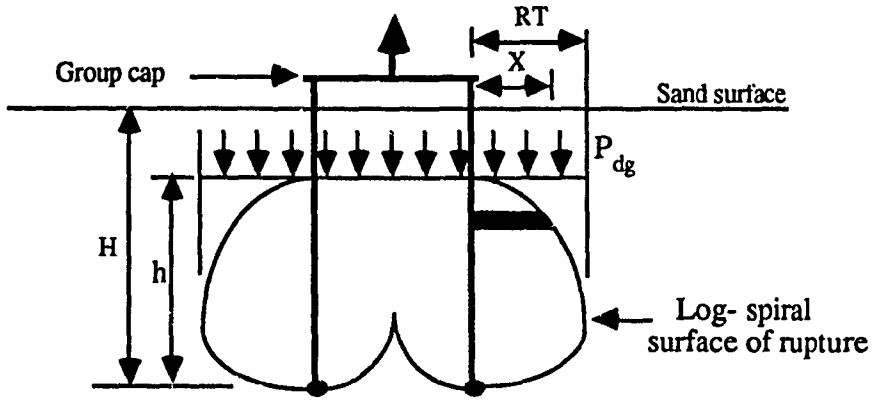

(b) Elevation of rupture mechanism for deep square group of anchors.

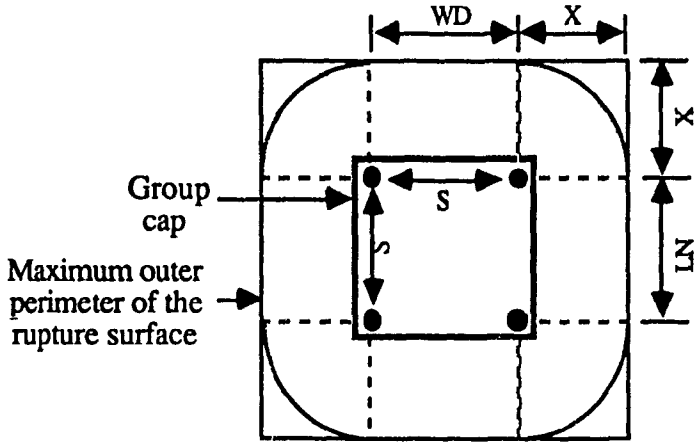

(c) Plan of rupture mechanism for deep square group of anchors.

Fig. 5.14: Geometry of rupture mechanism for deep square group of anchors.

Table 5.7: Weight factor FW_{dg} for deep group of anchors.

$\phi°$	Failure bulb height-diameter ratio, h/B		
	6	5	4
30	0.337	-------	-------
31	0.340	-------	-------
32	0.341	-------	-------
33	0.341	-------	-------
34	0.340	-------	-------
35	-------	0.336	-------
36	-------	0.332	-------
37	-------	0.325	-------
38	-------	0.317	-------
39	-------	0.307	-------
40	-------	-------	0.296
41	-------	-------	0.282
42	-------	-------	0.267
43	-------	-------	0.249
44	-------	-------	0.230
45	-------	-------	0.209
46	-------	-------	0.185

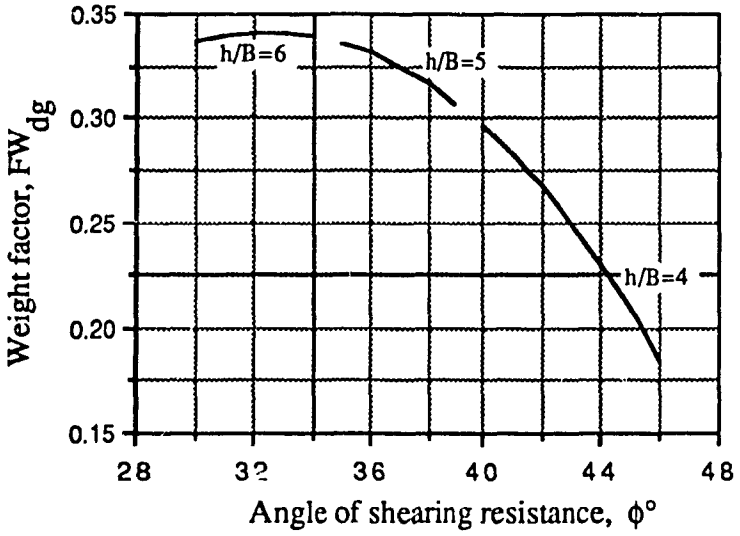

Fig. 5.15: Weight factor for deep group of anchors versus angle of shearing resistance.

Where FF_{ds} is the shear factor for deep single anchor and is given by Table 5.4 or Fig. 5.8. FF_{dg} is the shear factor for deep group of anchors and is given by the following expression:

$$FF_{dg} = r_0^3 \cdot \tan\phi \, [0.5 \cdot K7 \, (\cos 3\phi \cdot \cos\phi - \sin\phi) - K14 \cdot \sin\phi + K8 \cdot \sin 3\phi \cdot \cos\phi + (c_4 - c_2) \, (K4 \cdot \cos\phi - K6 \cdot \sin\phi)] \quad \ldots (5.93)$$

Where c_2 and c_4 are constants given by equations (5.55b) and (5.58a) respectively.

The shear factor for deep group of anchors (FF_{dg}) depends on the sand's angle of shearing resistance (ϕ), the ratio h/B, and boundary conditions on the rupture surface. Computed values of FF_{dg} are given in Table 5.8 and Fig. 5.16.

The surcharge pressure acting on the failed sand body of the anchors group (P_{dg}) can be calculated from the following equation (Fig. 5.14b & c):

$$P_{dg} = \gamma \cdot (H - h) \, (LN + 2RT) \, (WD + 2RT) \quad \ldots (5.94)$$

Where RT is given by eq. (5.61). The ultimate pullout load of deep group of anchors (QU_{dg}) is given by the following equation:

$$QU_{dg} = W_{dg} + F_{dg} + P_{dg} \quad \ldots (5.95)$$

Table 5.8: Shear factor FF_{dg} for deep group of anchors.

ϕ°	h/B	Embedment depth ratio, H/B				
		8	10	12	14	16
30	6	0.393	0.637	0.881	1.125	1.369
31	6	0.409	0.667	0.925	1.183	1.442
32	6	0.427	0.700	0.973	1.245	1.518
33	6	0.445	0.733	1.022	1.311	1.599
34	6	0.464	0.769	1.075	1.380	1.685
35	5	-------	1.130	1.518	1.906	2.294
36	5	-------	1.189	1.600	2.010	2.421
37	5	-------	1.252	1.686	2.121	2.556
38	5	-------	1.318	1.779	2.240	2.700
39	5	-------	1.390	1.878	2.366	2.855
40	4	-------	-------	2.761	3.409	4.056
41	4	-------	-------	2.923	3.610	4.298
42	4	-------	-------	3.097	3.827	4.558
43	4	-------	-------	3.284	4.061	4.838
44	4	-------	-------	3.487	4.314	5.140
45	4	-------	-------	3.706	4.587	5.468
46	4	-------	-------	3.944	4.884	5.824

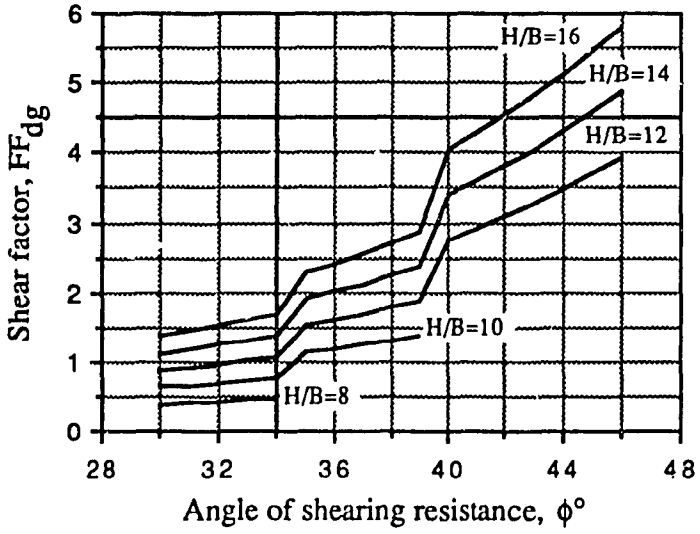

Fig. 5.16: Shear factor for deep group of anchors versus angle of shearing resistance.

5.2.4 Deep triangular group of anchors

Figure 5.17 shows the rupture surface of a deep triangular group of anchors. It can be noticed that the failure mechanism is similar to that of square or rectangular group, however, the group configuration affects its geometry.

Final equations to determine the uplift capacity of deep triangular group of anchors are given in the following, using the same notation used for deep square and rectangular groups of anchors:

$$A_g = 0.5\ (LN)^2 \cdot \sin 60° \qquad \ldots (5.82)$$

$$P_g = 3\ (LN) \qquad \ldots (5.83)$$

W1, W2, and W_{dg} are as given by equations (5.86), (5.88), and (5.90) respectively.

$$F_{dg} = \gamma \cdot h^2 \cdot P_g \cdot FF_{dg} + (6\ .\ \cot 30°) \cdot \gamma \cdot h^3 \cdot FF_{ds} \qquad \ldots (5.96)$$

$$P_{dg} = 0.5\ \gamma\ (H - h)\ (LN + 2RT \cdot \cot 30°)^2 \cdot \sin 60° \qquad \ldots (5.97)$$

Where RT is as given by eq. (5.61).

$$QU_{dg} = W_{dg} + F_{dg} + P_{dg} \qquad \ldots (5.95)$$

Weight and shear factors FW_{ds}, FW_{dg}, FF_{ds}, and FF_{dg} are as given in Table 5.3, 5.7, 5.4, and 5.8 or from the relevant charts.

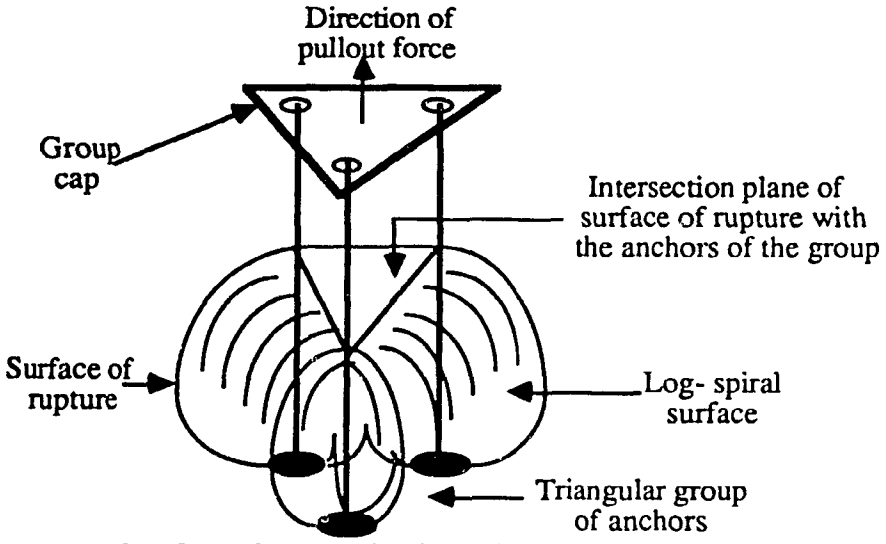

(a) Isometry of surface of rupture for deep triangular group of anchors.

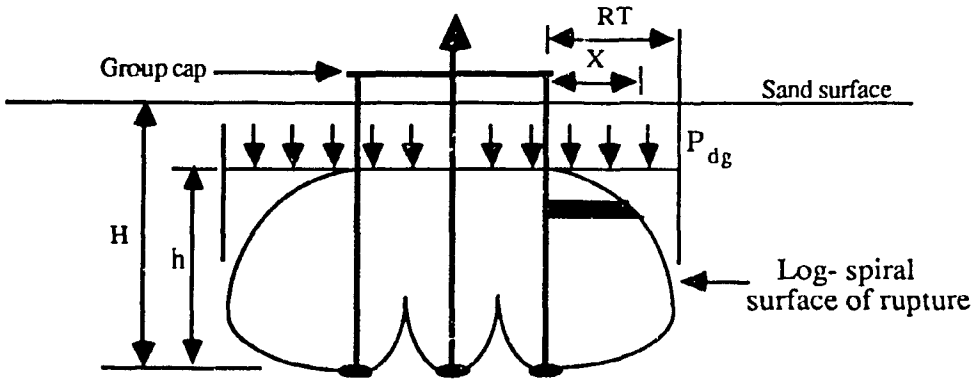

(b) Elevation of rupture mechanism for deep triangular group of anchors.

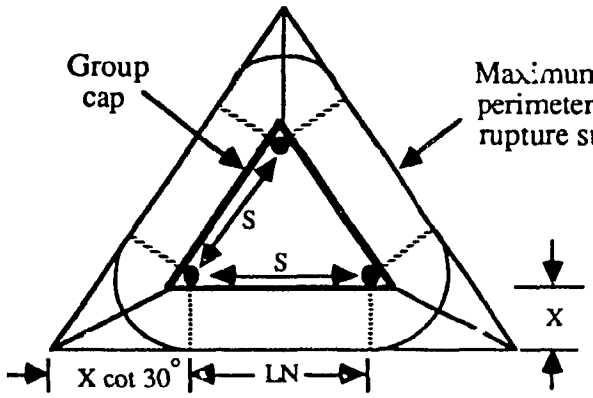

(b) Plan of rupture mechanism for deep triangular group of anchors.

Fig. 5.17: Geometry of surface of rupture for deep triangular group of anchors.

5.2.5 Transit square or rectangular group of anchors

Figure 5.18 shows a typical surface of rupture of square group installed to a transition depth. With reference to notations given in section 5.1.3, the following equations are given to determine the uplift capacity of transit square or rectangular group of anchors:

$$W_{tdg} = \gamma \cdot A_g \cdot (H/2) + g \cdot P_g \cdot (H/2)^2 \cdot FW_{dg} + \gamma \cdot (H/2)^3 \cdot FW_{ds} \quad \ldots (5.98)$$

Where A_g and P_g are as given by equations (5.70) and (5.71). FW_{dg} and FW_{ds} are as given by Talbes 5.7 and 5.3 or relevant charts.

$$F_{tdg} = \gamma \cdot (H/2)^2 \cdot P_g \cdot FF_{dg} + (8/2\pi) \cdot \gamma \cdot (H/2)^3 \cdot FF_{ds} \quad \ldots (5.99)$$

Where FF_{dg} and FF_{ds} are as given by Tables 5.8 and 5.4 or relevant charts.

$$P_{tdg} = \gamma \cdot (H/2) \cdot [(LN + 2RT)(WD + 2RT) - A_g] \quad \ldots(5.100)$$

Where RT is as given by eq. (5.61).

$$W_{tdg} = \gamma \cdot A_g \cdot (H/2) + \gamma \cdot P_g \cdot (H/2)^2 \cdot FW_{sg} + \gamma \cdot (H/2)^3 \cdot FW_{ss} \quad \ldots(5.101)$$

Where FW_{sg} and FW_{ss} are as given by Tables 5.5 and 5.1 or relevant charts.

$$F_{tsg} = \gamma \cdot (H/2)^2 \cdot P_g \cdot FF_{sg} + (8/2\pi) \cdot \gamma \cdot (H/2)^3 \cdot FF_{ss} \quad \ldots(5.102)$$

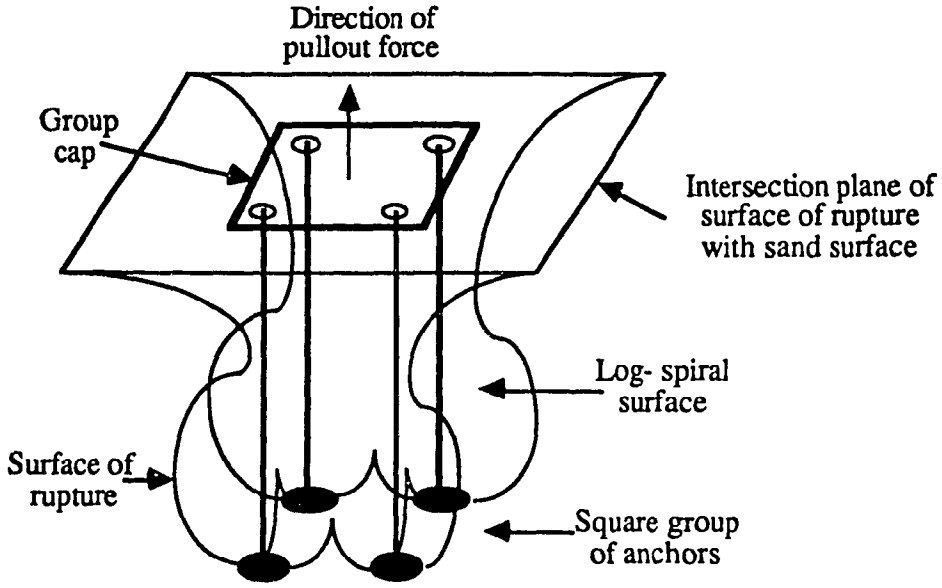

(a) Isometry of surface of rupture for transit square group of anchors.

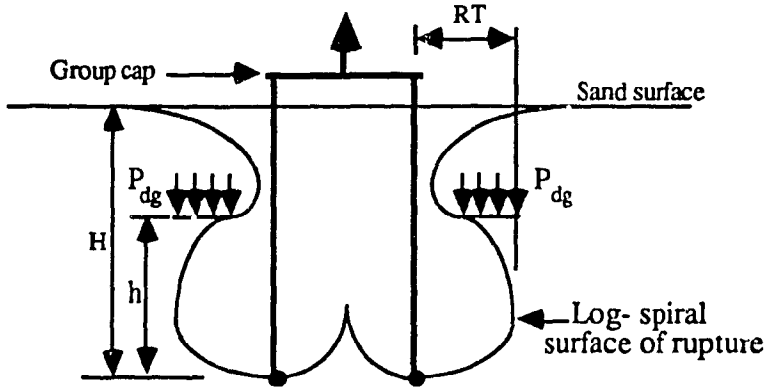

(b) Elevation of rupture mechanism for transit square group of anchors.

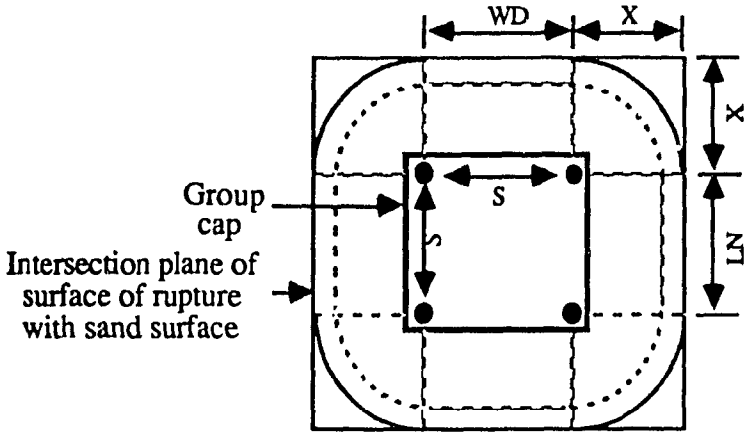

(c) Plan of rupture mechanism for transit square group of anchors.

Fig. 5.18: Geometry of rupture mechanism for transit square group of anchors.

Where FF_{sg} and FF_{ss} are as given by Tables 5.6 and 5.2 or relevant charts.

Hence, the total uplift capacity of transit square or rectangular group of anchors can be given by the following equation:

$$QU_{tg} = W_{tdg} + F_{tdg} + P_{tdg} + W_{tsg} + F_{tsg} \qquad ...(5.103)$$

5.2.6 Transit triangular group of anchors

Figure 5.19 shows a typical surface of rupture of triangular group of anchors installed to a transition depth. Area and perimeter of the group (A_g) and (P_g) are as given by equations (5.81) and (5.56). W_{tdg} and W_{tsg} are as given by equations (5.98) and (5.101).

$$F_{tdg} = \gamma \cdot (H/2)^2 \cdot P_g \cdot FF_{dg} + (6 \cdot \cot 30°) \cdot \gamma \cdot (H/2)^3 \cdot FF_{ds} \qquad ...(5.104)$$

$$P_{tdg} = \gamma \cdot (H/2) \cdot [0.5\,(LN + 2RT \cdot \cot 30°)^2 \cdot \sin 60° - A_g] \qquad ...(5.105)$$

$$F_{tsg} = \gamma \cdot (H/2)^2 \cdot P_g \cdot FF_{sg} + (6 \cdot \cot 30°) \cdot \gamma \cdot (H/2)^3 \cdot FF_{ds} \qquad ...(5.106)$$

Then, by using eq. (5.103), the ultimate pullout load of a transit triangular group of anchors can be determined.

5.3 Effect of Overconsolidation on Uplift Capacity

Hanna and Carr (1971) [20] and Hanna et al. (1972) [22], reported test results on normally consolidated sand as well as overconsolidated one. They stated that the increase of the overconsolidation ratio (OCR) significantly increases the pullout capacity of the anchor. Tests

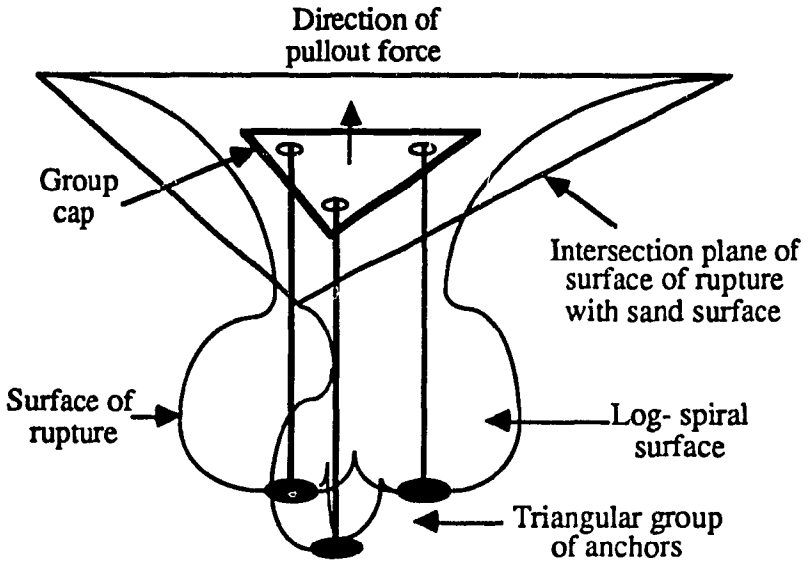

(a) Isometry of surface of rupture for transit triangular group of anchors.

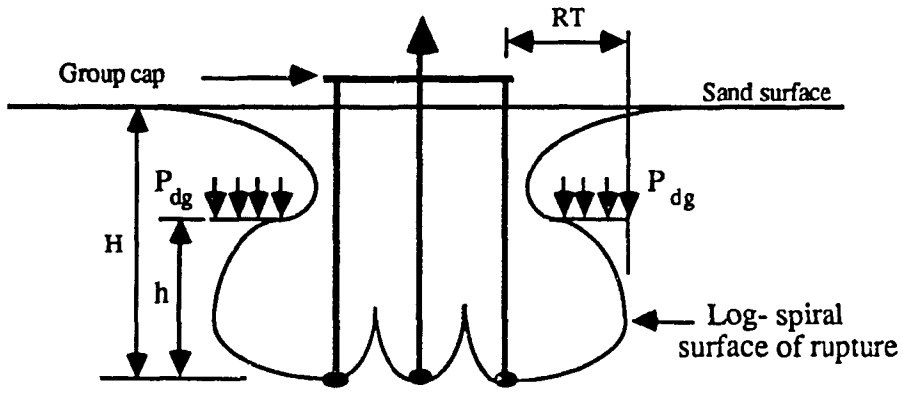

(b) Elevation of rupture mechanism for transit triangular group of anchors.

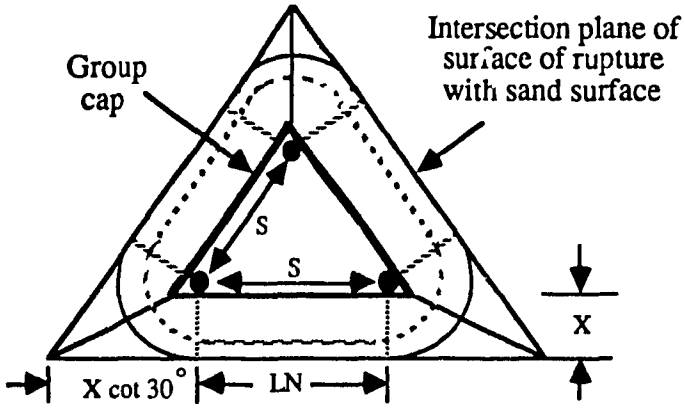

(b) Plan of rupture mechanism for transit triangular group of anchors.

Fig. 5.19: Geometry of surface of rupture for transit triangular group of anchors.

were conducted up to OCR of 14. They presented sets of data, out of which the relationship between the uplift capacity of the anchor plate and the OCR for constant depth of sand was plotted. This relationship is shown in Fig. 5.20. No trial has been made by the authors to quantify mathematically the effect of OCR on the uplift capacity. In the present analysis, however, an attempt has been made to relate the uplift capacity to the OCR. The uplift capacities given in Fig. 5.20 were reduced by a value representing the dead weight of the breaking out sand mass participating in uplift resistance. Hence, the remaining quantity represents the share of shearing resistance against uplift.

Shearing resistance is the fraction that is affected by overconsolidation. The best fitting curve for the relationship between the vertical component of shearing resistances and the corresponding OCR values can be given by the following equation:

$$VSR_{(OC)} = VSR_{(NC)} \sqrt{OCR} \qquad \ldots (5.107)$$

Where $VSR_{(OC)}$ and $VSR_{(NC)}$ are the vertical components of shearing resistance against uplift for overconsolidated and normally consolidated sand respectively. Normally consolidated sand in this equation is defined as a sand of an OCR of 1.

5.4 Comparison of Experimental and Theoretical Results

Equation (5.107) was used to adjust the shearing resistance calculated from the theory (shearing resistance of normally consolidated sand) according to the OCR of the tested sand. Modified values of the theoretical vertical component of shearing resistance are the values used in the following comparisons between theoretical and experimental results. Figure 5.21 shows comparison of experimental and theorectical results for single screw anchor installed in dense, medium, and loose sand. It can be indicated that good agreement exists between experimental and theoretical results. Also, this figure shows the lines separating between shallow, transit, and deep zones. It can be seen that the theory predicts well the ultimate pullout load of anchors

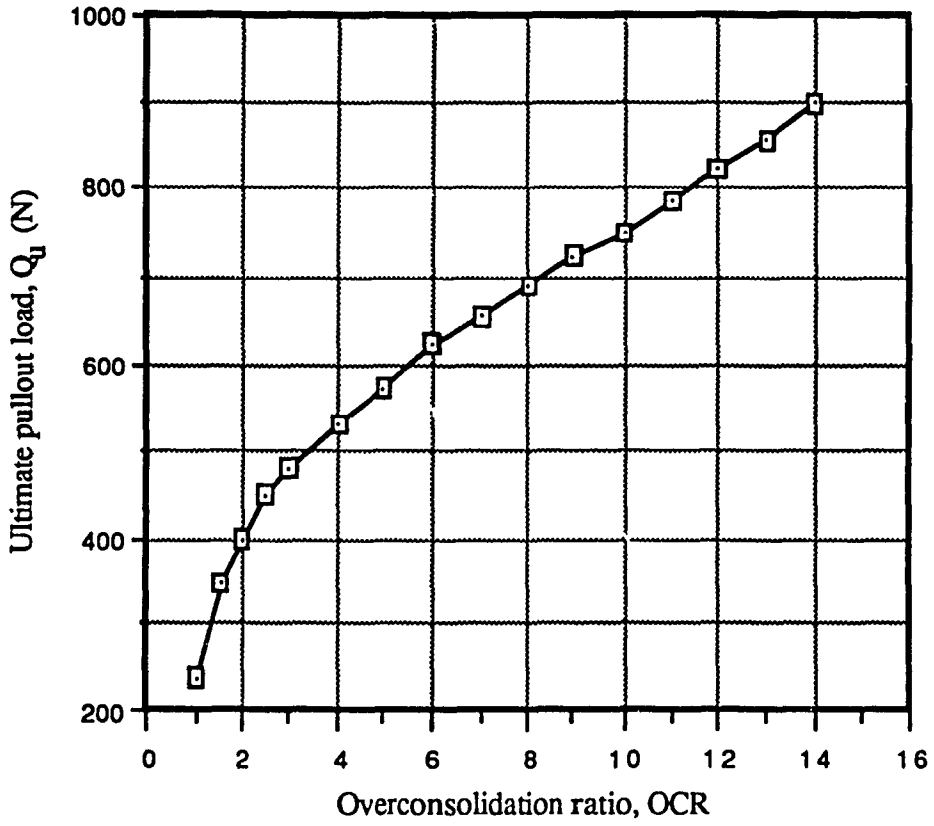

Fig. 5.20: Relationship between ultimate pullout load and overconsolidation ratio for anchor installed at constant depth of sand; after Hanna et al., (1971).

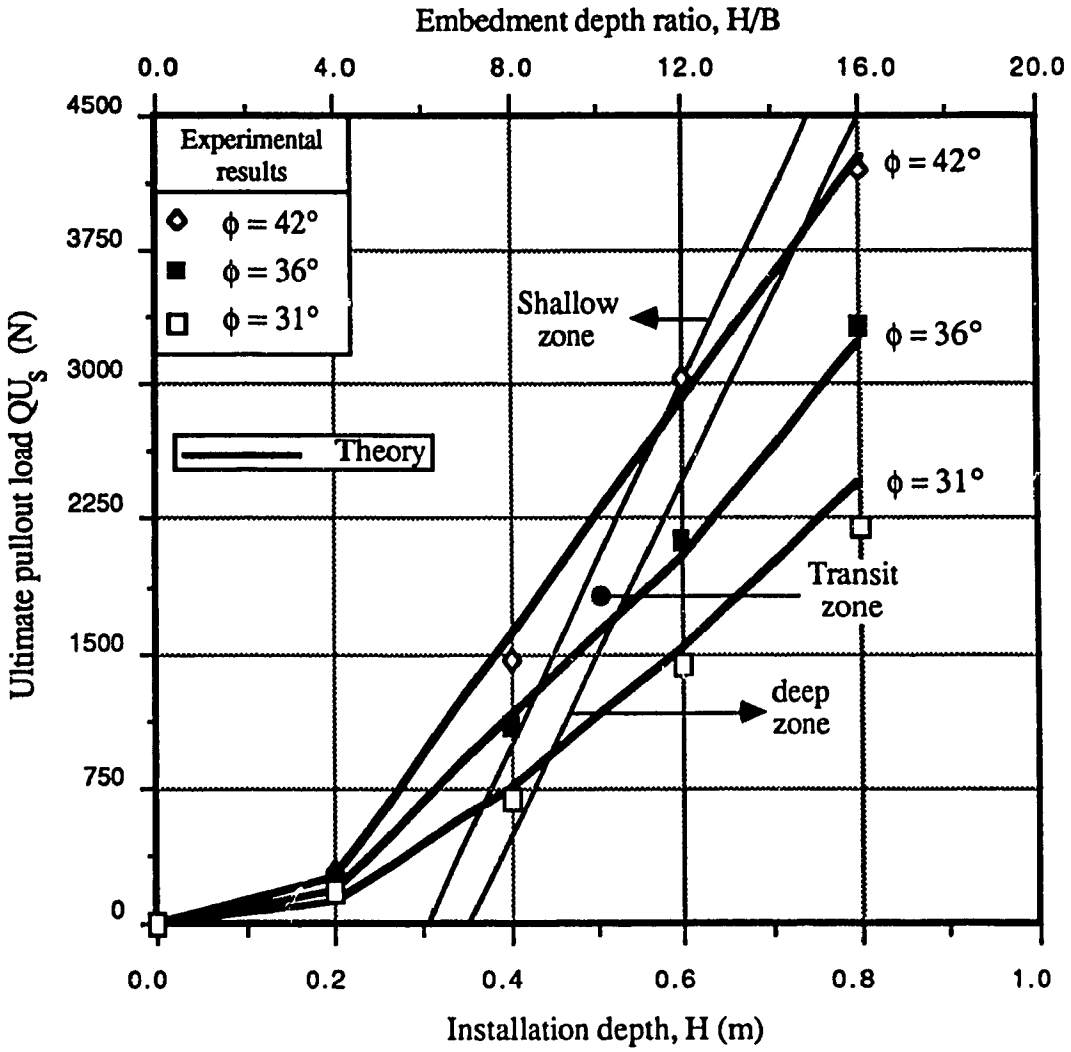

Fig. 5.21: Comparison of experimental and theoretical results for single anchors installed in dense, medium, and loose sand.

installed in any of the above mentioned zones.

Comparisons of experimental and theoretical results for groups of anchors installed in loose, medium, and dense sand are shown in Fig. 5.22, 5.23, and 5.24 respectively. From these figures, good agreement can generally be reported between experimental and theoretical results. However, for closely spaced large number of anchors groups (6 and 9 anchors groups spaced at S = 3B ans S = 4B), installed in dense sand, $\phi = 42°$, large discrepancy can be seen between the theory and the experimental results. This disagreement vanishes at widely spaced groups (S = 5B (Fig. 5.24)). This behaviour can be attributed to the fact that, a closely spaced group of anchors significantly densifies the sand during the installation procedure. This reflects its influence on the initial properties of the sand (unit weight and angle of shearing resistance). A comparison between the experimental results and theoretical values calculated for sands with angles of shearing resistance higher than the tested sands indicated that good agreement can be observed between the theoretical and experimental results for closely spaced anchors group if the effect of densification is taken into account. An analysis of the problem of densification led to a conclusion that, for a given sand, the increase in the value of the angle of shearing resistance (ϕ) due to group installation depends on the original value of ϕ before installation, spacing/diameter ratio (S/B), and a coefficient representing the degree of densification (c_d). Figure 5.25 shows the value of the coefficient of densification (c_d) for different group configurations. The value of c_d is defined by the maximum number of circles of influence that interfere together in one location. This interference results in sand densification and an increase of the uplift capacity. An empirical formula is given in the following to determine, numerically, the amount of increase in the angle of shearing resistance (ϕ) due to group installation:

$$\phi' = \left[\frac{c_d}{(S/B)}\right]\left[\frac{\phi^4}{10^6}\right] \qquad \ldots (5.108)$$

Where ϕ' = the increase in the angle of shearing resistance due to group installation (degrees).

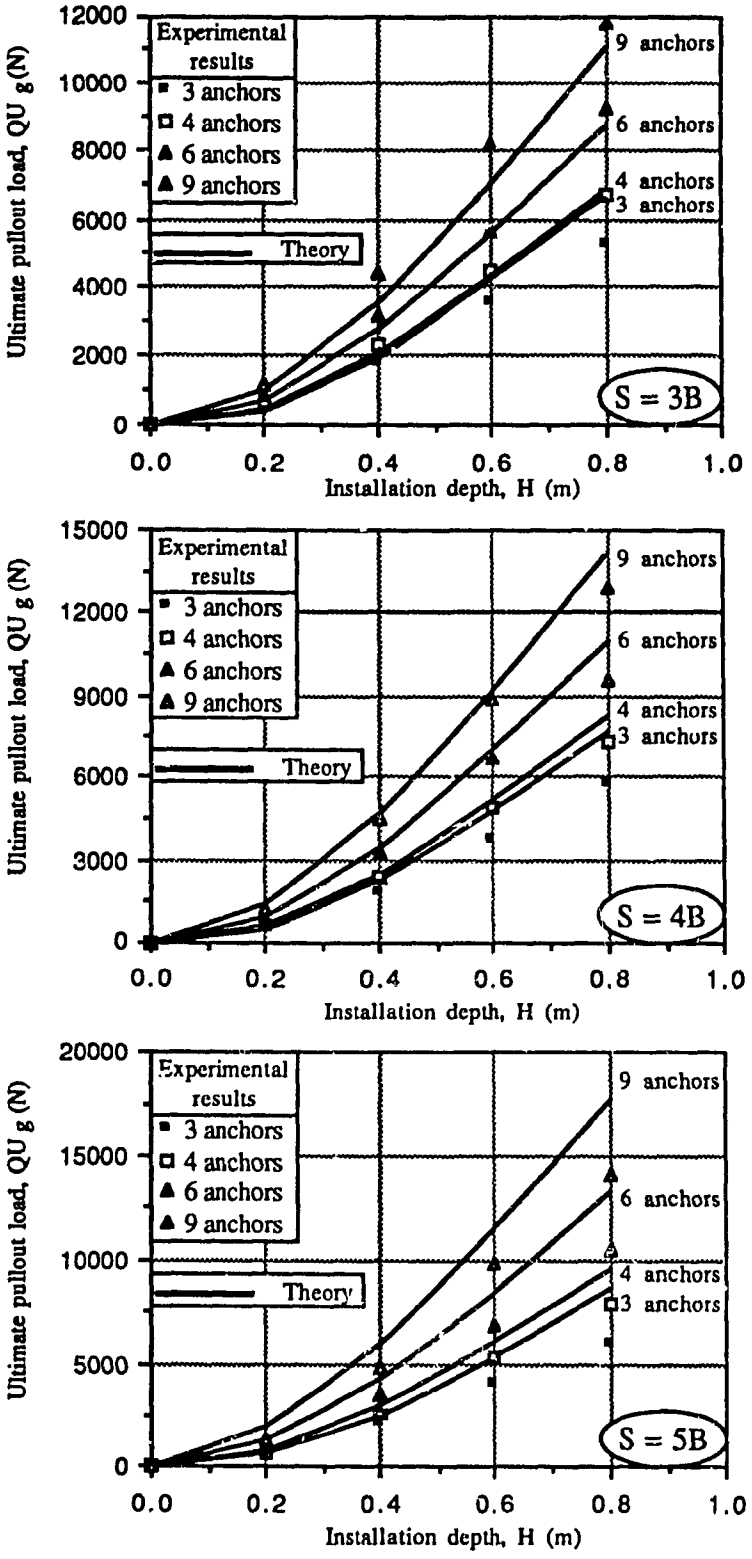

Fig. 5.22: Comparison of experimental and theoretical results for groups of anchors installed in loose sand.

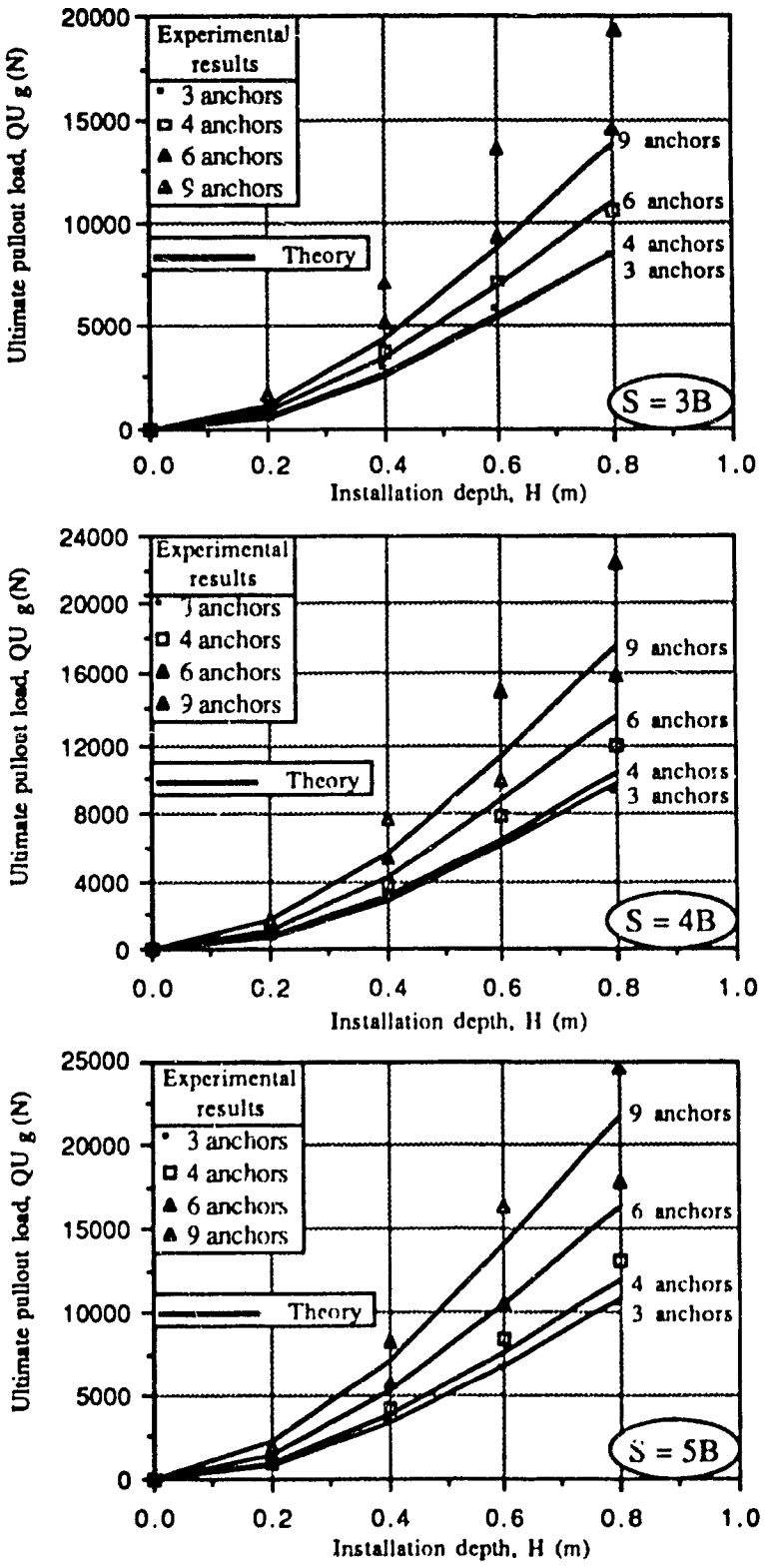

Fig. 5.23: Comparison of experimental and theoretical results for groups of anchors installed in medium sand.

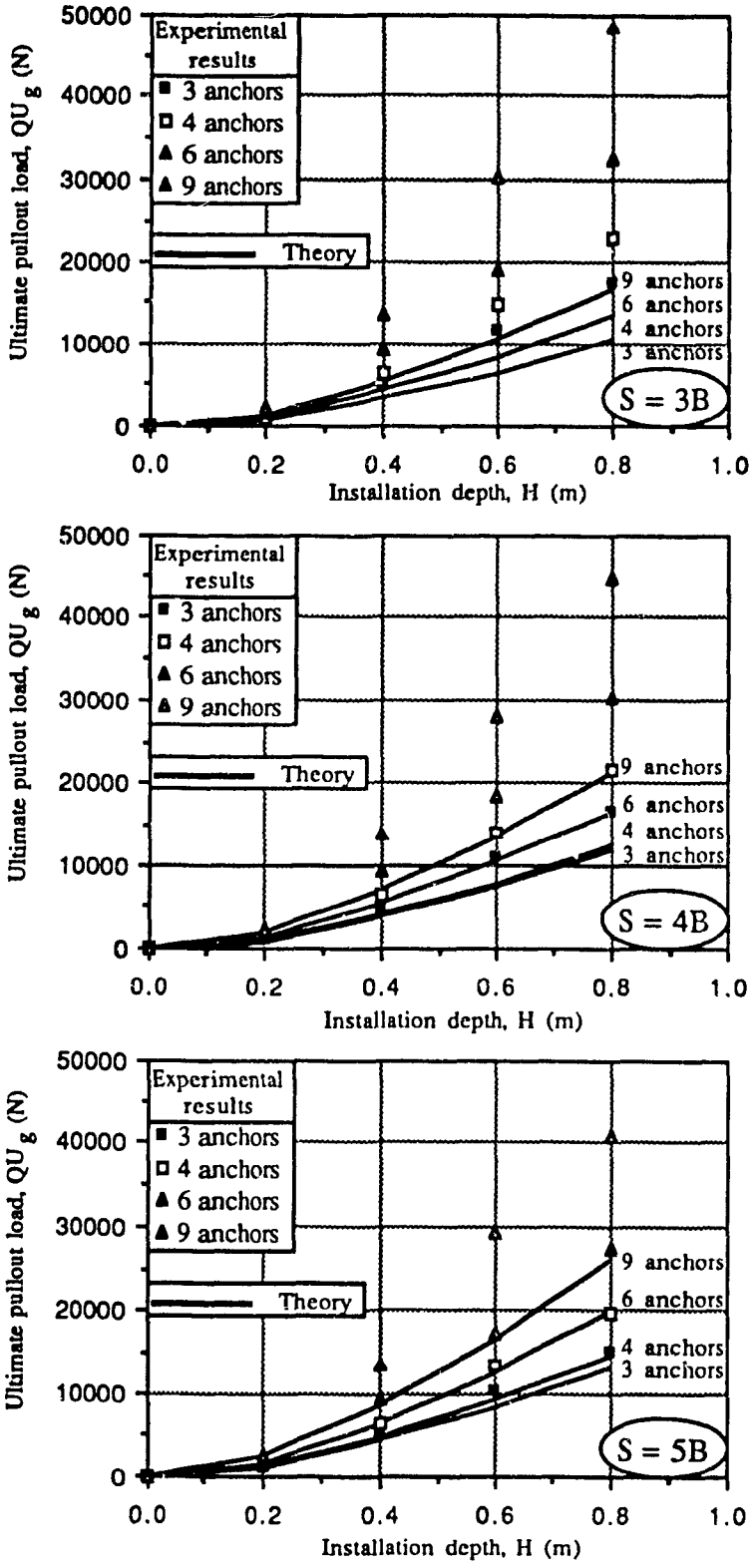

Fig. 5.24: Comparison of experimental and theoretical results for groups of anchors installed in dense sand.

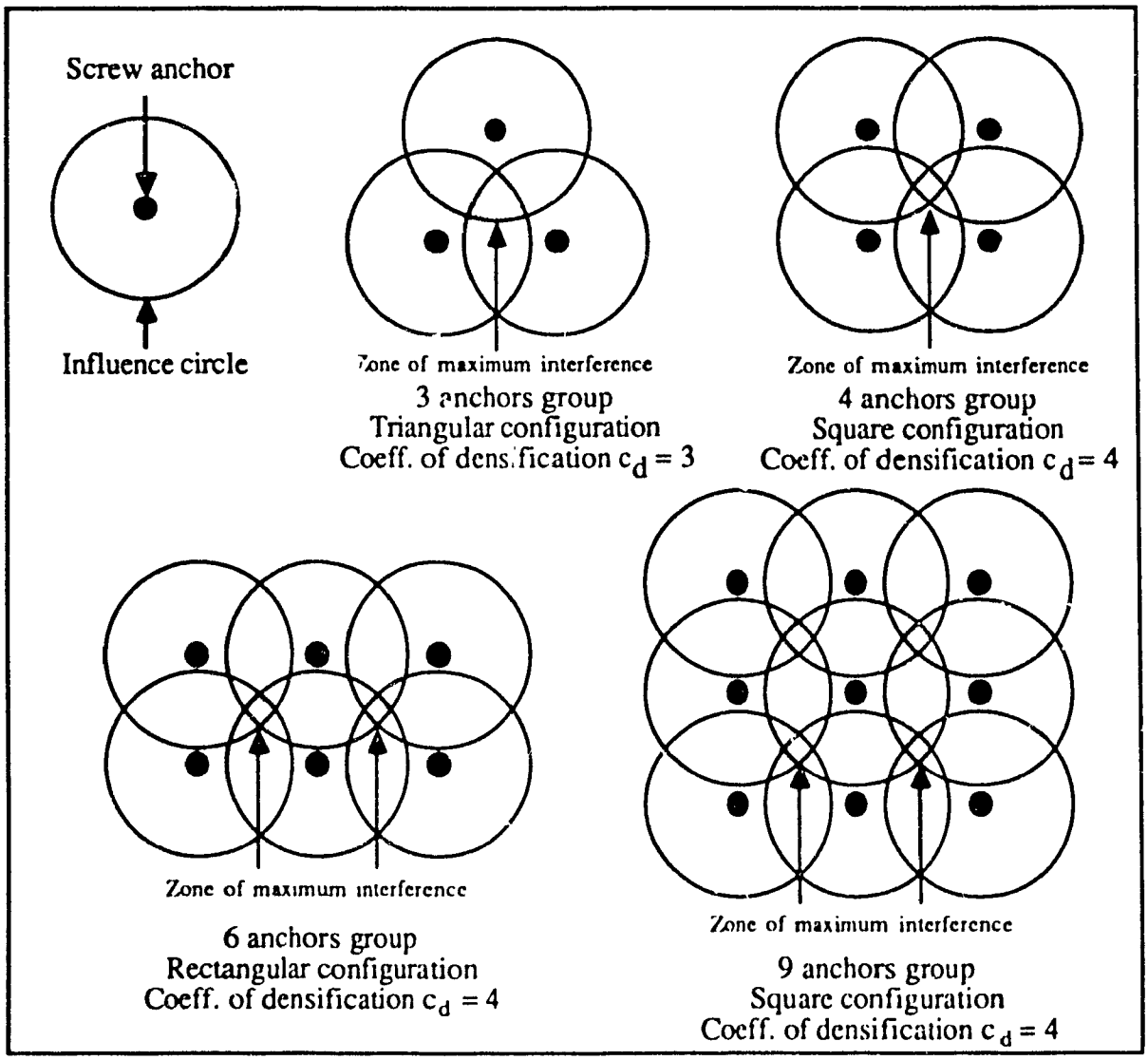

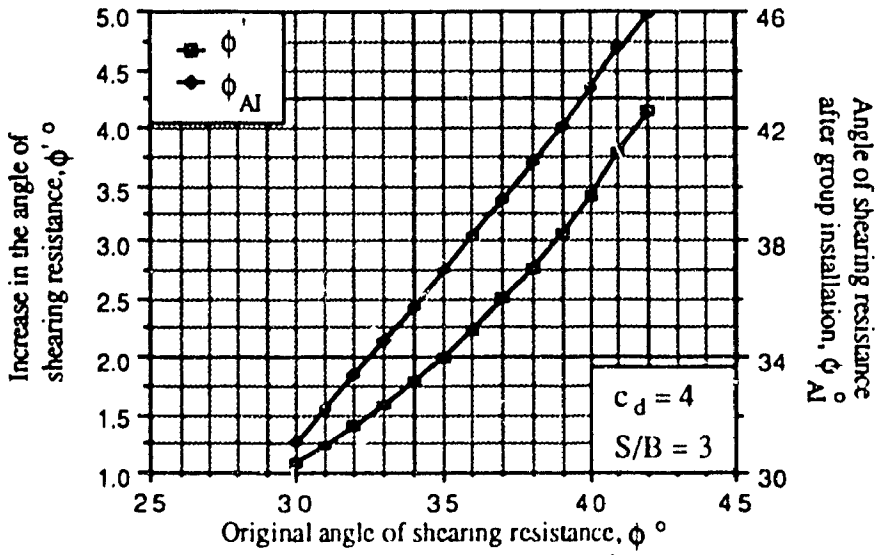

Typical relationship of ϕ versus ϕ' and ϕ_{AI} .

Fig. 5.25: Values of coefficient of densification for the tested group configurations.

c_d = coefficient of densification.

S/B= spacing / diameter ratio.

ϕ = original angle of shearing resistance (degrees).

Then $\phi_{AI} = \phi + \phi'$ ... (5.109)

Where ϕ_{AI} = angle of shearing resistance of the sand after group installation.

Using this formula provides good base for uplift capacity determination for a group of anchors taking into account the densification effect that the group installation causes to the sand. Figures 5.26, 5.27, and 5.28 show comparison of experimental results and theoretical values calculated for densified sand. From these figures, good agreement between experimental and theoretical results can be reported.

5.5 Comparison of Theoretical and Field Results

Figure 5.29 shows a comparison between the present theory and field results reported in the literature. Since no information about the stress history of the field soils is given, they were considered normally consolidated soils. Good agreement can be noticed between the theoretical and experimental field values of uplift capacity factor.

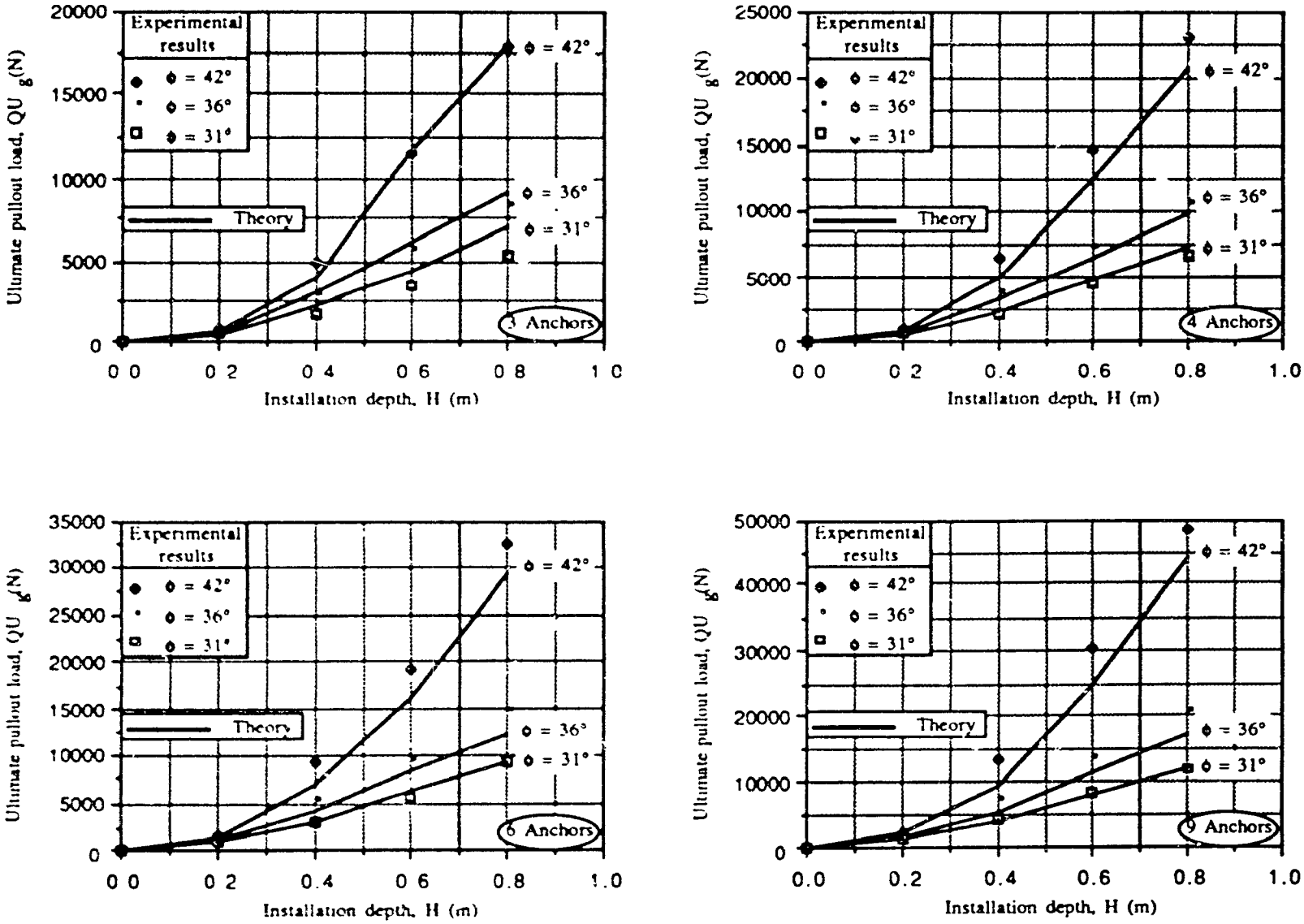

Fig. 5.26: Comparison of experimental and theoretical results for groups of anchors spaced at S=3B.

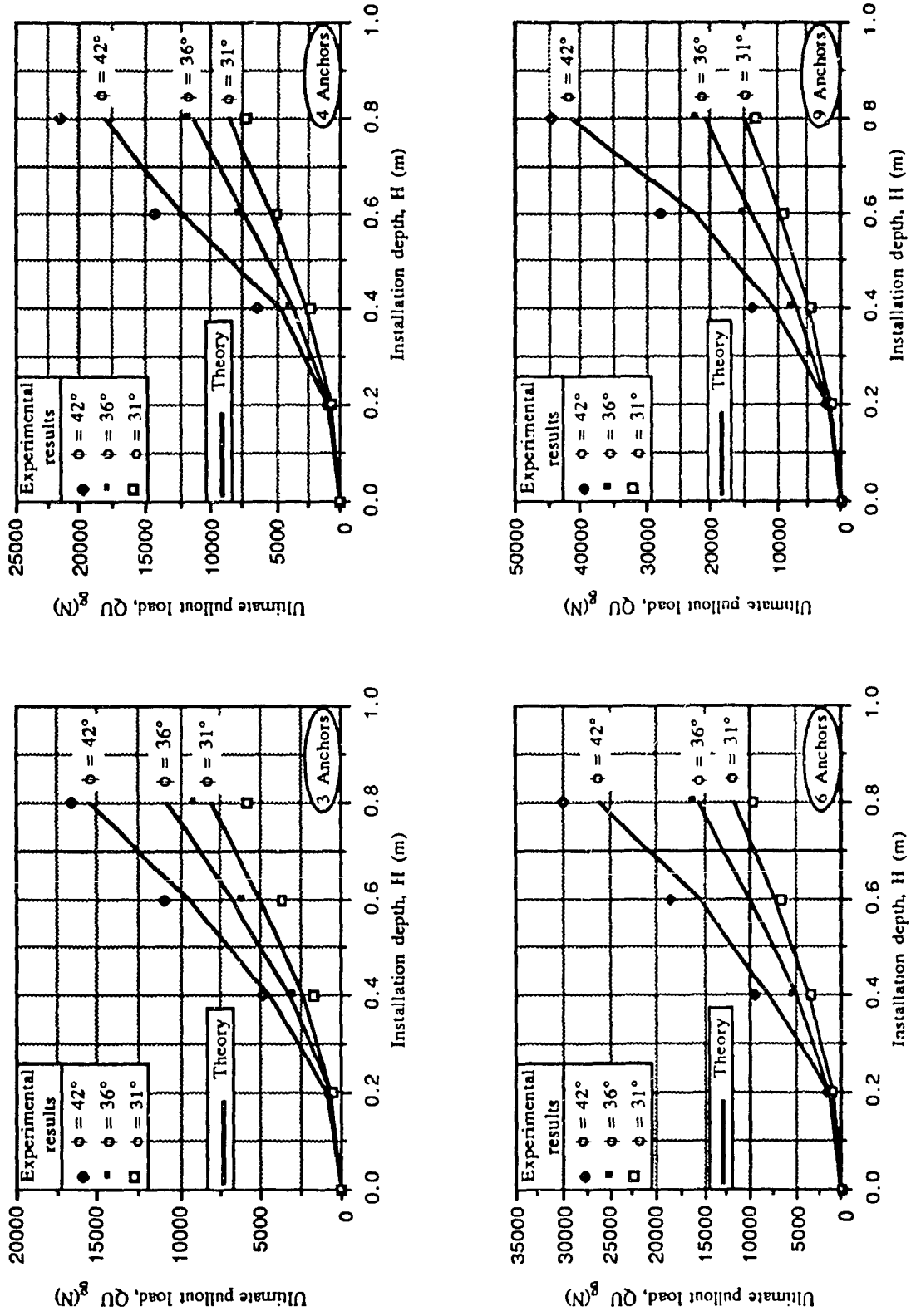

Fig. 5.27: Comparison of experimental and theoretical results for groups of anchors spaced at S=4B.

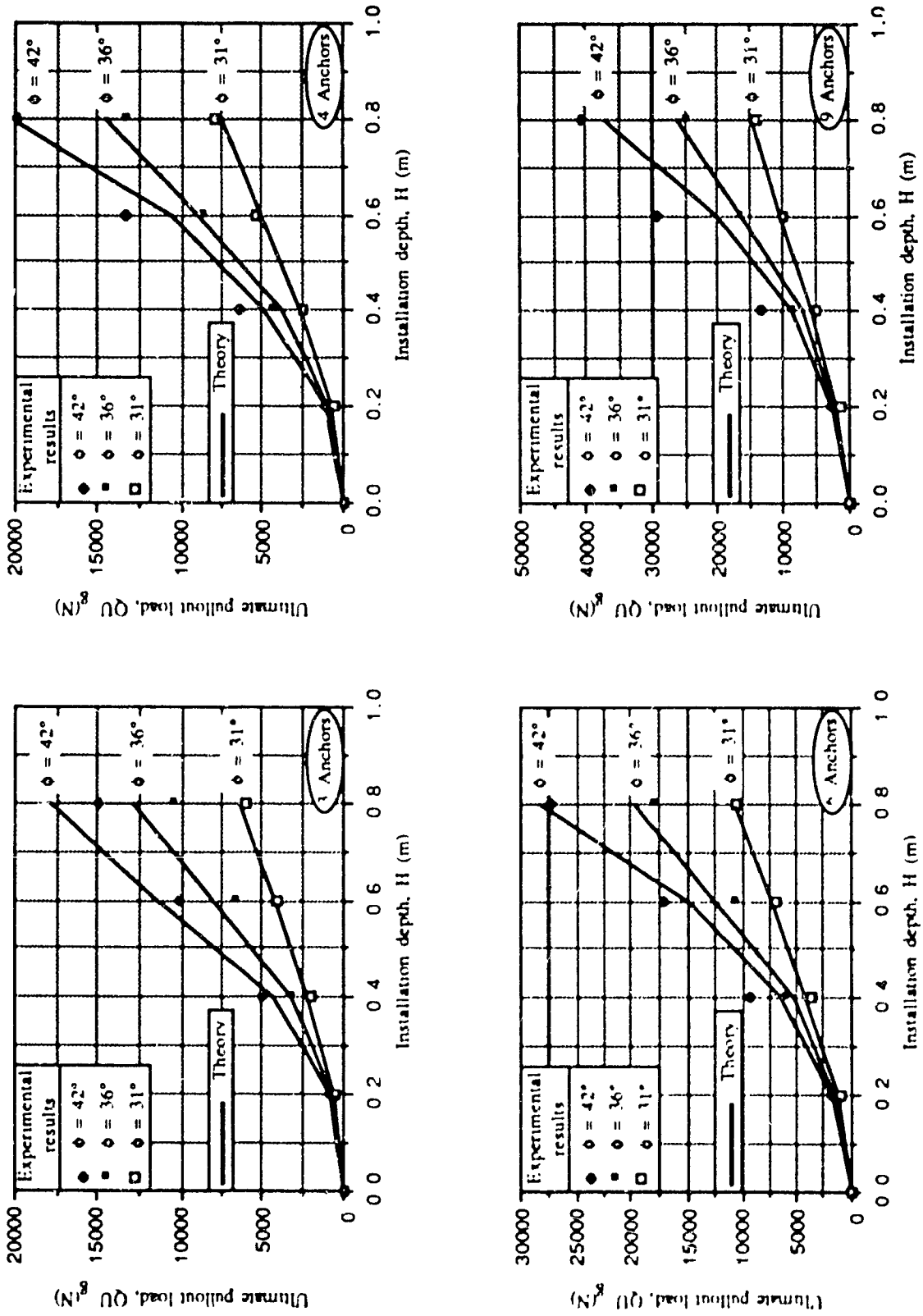

Fig. 5.28: Comparison of experimental and theoretical results for groups of anchors spaced at S=5B.

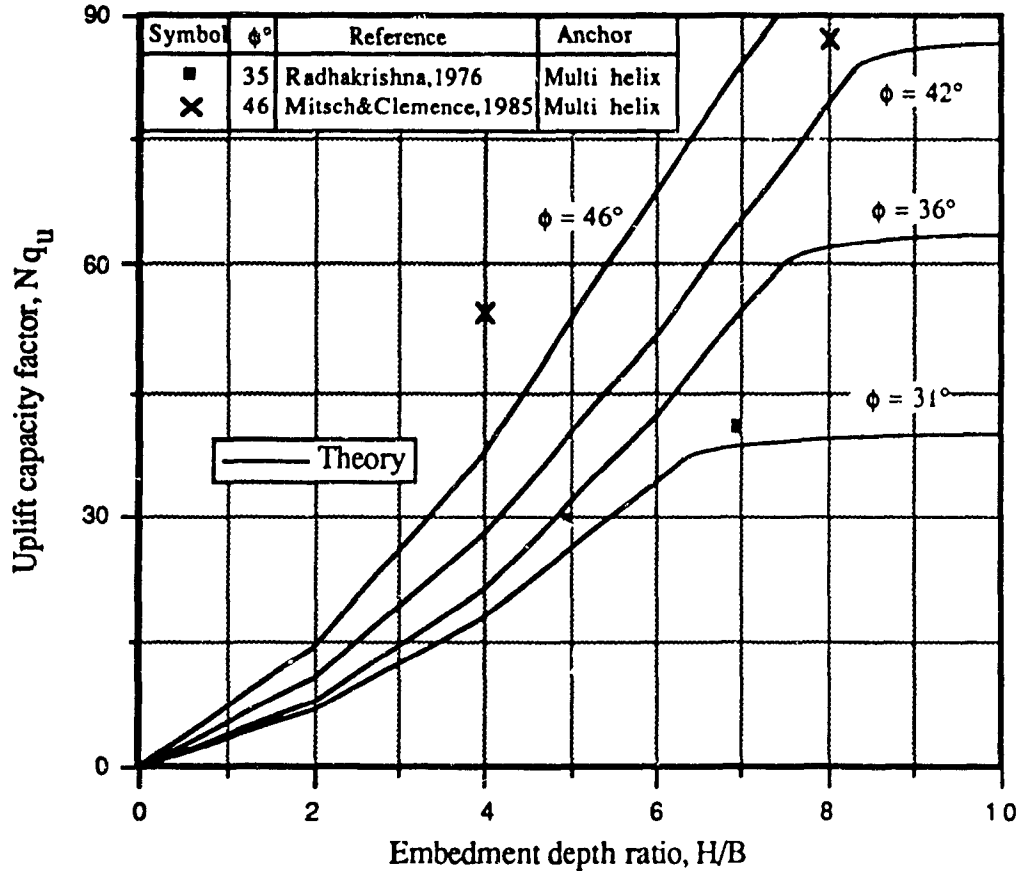

Fig. 5.29: Comparison of present theoretical results and field results reported in the literature.

CHAPTER 6

Installation Torque of Screw Anchors

6.1 General

The installation technique of screw anchors is accomplished in the field by applying torque to the shaft of the anchor by power auger or other suitable means. An axial load may be applied to the anchor's shaft to assure a steady advancement of the anchor into the soil equal to anchor's pitch per revolution. Due to the anchor rotation, when applying torque, drag forces are generated on the screw blades and the anchor penetrates the soil and advances downward. In the present investigation, however, a similar technique was used to install the tested model anchors.

This chapter presents the torque experimental results of the five screw-shaped tested model anchors, Fig. 3.6 a, b, c, d, e and Plate 3.12 a, b, c, d, e. The effect of screw shape and geometrical characteristics on the installation torque value was studied and compared. The parameters affecting the installation torque magnitude were identified. A theoretical model was developed from which the required installation torque value can be predicted. Utilizing the results of the theory of uplift capacity prediction, together with that of installation torque prediction, a correlation has been developed from which the uplift capacity can be predicted from the recorded installation torque value.

6.2 Test Results and Discussion

Table 6.1 summarizes a test program and results of installation torque value of the tested types of screw anchors installed into dense, medium, and loose sand. Figure 6 1 shows the installation torque value obtained experimentally versus installation depth for tested types of screw anchors installed in dense, medium, and loose sand. From this figure, it can be seen that, for a given type of screw anchor, the installation torque increases with installation depth as well as with the angle of shearing resistance of the sand. Also, for a given type of sand, the installation torque increases with the pitch/diameter ratio of the screw anchor, i.e , with the helix angle ψ ($\psi^\circ = \tan^{-1} p/\pi B$) of the screw element. From Fig. 6.1, it can be seen that, for a given type of sand, the small pitch screw anchor, Type 1 (Fig. 3 6a), required the least torque value as compared with the other types, to be installed to a certain depth, while the large pitch screw anchor, Type 3 (Fig. 3.6c), required the greatest torque. Other types of anchors (Types 2, 4, and 5) required torque values greater than those of Type 1 and smaller than those of Type 3. This behaviour can be explained in terms of the pitch/diameter ratios (p/B) of the tested model anchors. Type 1 screw anchor has the least p/B ratio when compared to the other types, whereas Type 3 has the largest one. Types 2, 4, and 5 have p/B ratios of intermediate values lying between those of Types 1 and 3. The pitch/diameter ratio is the main factor affecting the installation torque required to install a screw anchor. With an increase of p/B ratio, a larger surface area of the screw blades is subjected to sand resistance during installation. Also, the tangential component of the lateral earth pressure acting on the screw blades considerably increases with the screw's helix angle. This behaviour is consistent for single pitch screw anchors. For multi equal pitch (Type 4) and multi variable pitch (Type 5) screw anchors, additional factors influence significantly the screw behaviour during installation. Although the ratio between the upper blade's pitch and its diameter of Types 4 and 5 screw anchors is equivalent to the p/B ratio of Type 2, these three types did not show the same performance during installation. The torque required to install the unsymmetrical screw anchor (Type 4) was about 10 - 15% higher as that required to install the medium pitch screw anchor (Type 2),

Table 6.1: Installation torque for tested types of anchors.

Sand type	Depth H (m)	H/B	Installation torque, T (N.m)				
			Type 1 screw anchor	Type 2 screw anchor	Type 3 screw anchor	Type 4 screw anchor	Type 5 screw anchor
Dense sand, ϕ = 42°	0.1	2	0.48	0.55	0.68	0.60	0.53
	0.2	4	1.62	1.85	2.30	2.05	1.81
	0.3	6	3.40	3.89	4.84	4.31	3.81
	0.4	8	5.82	6.65	8.29	7.36	6.53
	0 5	10	8.88	10.16	12.66	11.25	9.97
	0.6	12	12.58	14.41	17.96	15.96	14.15
	0.7	14	16.92	19.39	24.17	21.48	19.03
	0.8	16	21.91	25.10	31.30	27.81	24.64
Medium sand, ϕ = 36°	0.1	2	0.29	0.31	0.39	0.34	0.28
	0.2	4	1.19	1.04	1.29	1.15	0.93
	0.3	6	2.01	2.18	2.72	2.41	1.96
	0.4	8	3.45	3.74	4.65	4.14	3.37
	0.5	10	5.27	5.71	7.11	6 33	5.14
	0.6	12	7.46	8 10	10.08	8.98	7.30
	0.7	14	10.05	10.89	13.56	12.07	9.82
	0.8	16	13.01	14.10	17.57	15.63	12.71
Loose sand, ϕ = 31°	0.1	2	0.23	0.19	0.23	0 21	0 17
	0.2	4	0.57	0.64	0.81	0.71	0.57
	0.3	6	1.13	1.35	1.71	1.51	1.21
	0.4	8	1.96	2.30	2.95	2 57	2.07
	0.5	10	3.32	3.52	4.49	3.94	3.16
	0.6	12	4.36	5.00	6.37	5.60	4.50
	0.7	14	5.65	6.72	8 58	7.53	6.04
	0.8	16	7.07	8.71	10.58	9.76	7.84

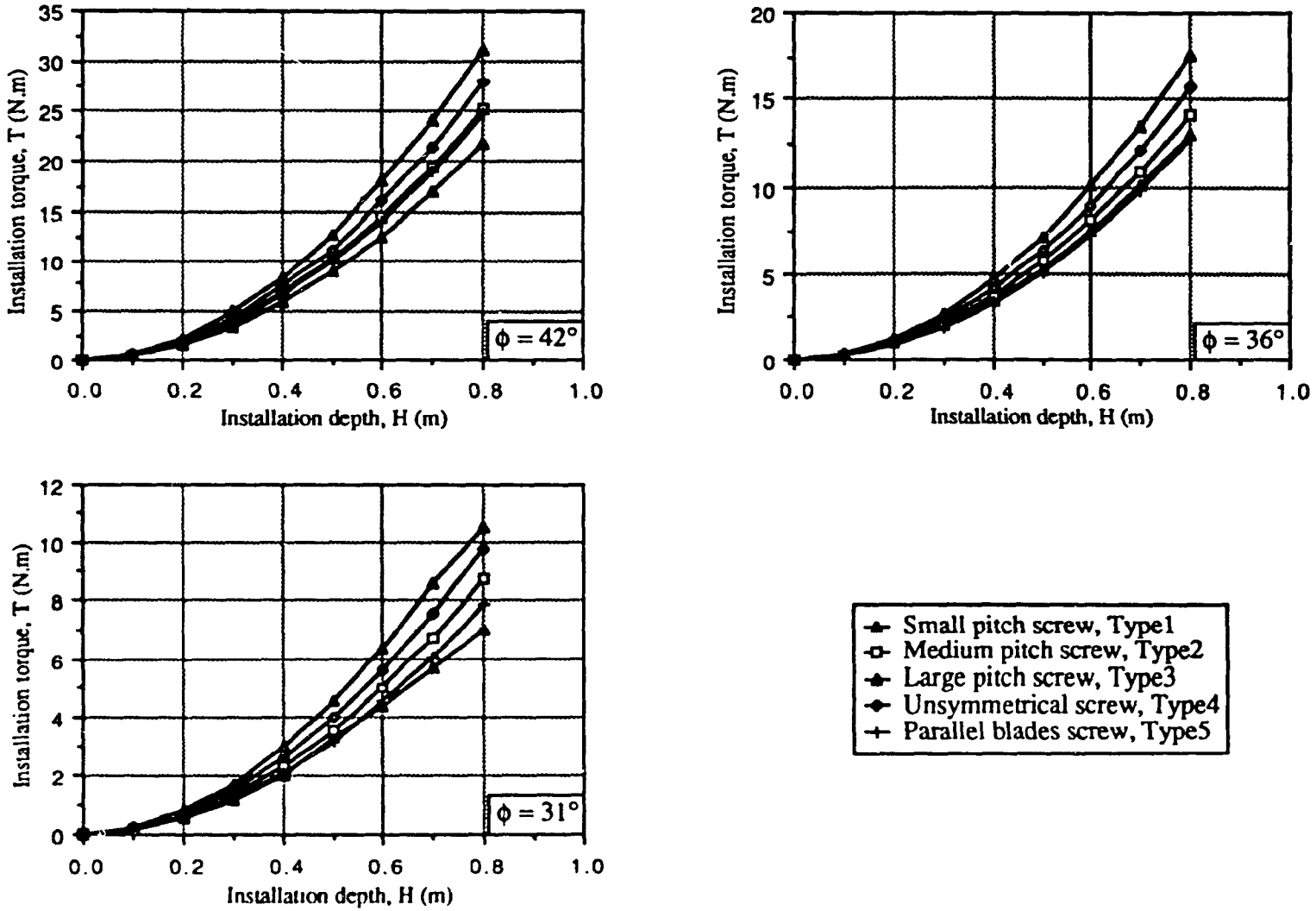

Fig. 6.1: Installation torque versus installation depth for tested types of anchors installed in dense, medium, and loose sand.

while it was about 10 - 15% lower for the parallel blades screw anchor (Type 5). This behaviour can be explained in terms of the effect of the conical end configuration of the multi pitch screw anchor. For the unsymmetrical screw anchor (Type 4), the helix angle increases with every progressive pitch due to the diameter reduction with constant pitch, hence, higher torque value was required to overcome the negative effect of helix angle increase. The helix angle (ψ) is constant in the case of parallel blades screw anchor (Type 5), hence, the tangential component of the lateral earth pressure acting on the screw blades is being resisted by a constant blades' slope. The introductory effect of the sloped conical end of the parallel blades screw anchor (Type 5) reflected its influence in facilitating installation as a reduction in the required installation torque value.

It is of interest to report that, for a single pitch screw anchor, the number of turns required to install the anchor to a certain depth increases with the decrease of the anchor's pitch. For multi pitch screw anchors, the number of turns is a function of the average p/B ratio comparable with single pitch anchor.

Based on field test results, Radhakrishra (1976) [48] indicated that the configuration of the screw anchor (single helix, uniform multi helix with constant helix angle, or tapered multi helix with increasingly helix angle) has a great influence on the installation torque value and consequently on the uplift capacity of the anchor. He reported that the tapered multi helix anchor (Fig 2.9) required about 25% more torque than the uniform multi helix anchor (Fig. 2.9) for installation to the same depth. He explained this behaviour in terms of the soil disturbance caused by the anchor installation. In the case of tapered multi helix anchor, less soil disturbance is expected than that in the case of tapered multi helix anchor. Radhakrishna stated that when the diameter of the bottom helix plate is less than those of the top two faces, this results in less soil disturbance than that of the case of uniform multi helix screw anchors. He also showed that this has a direct reflection on the uplift capacity of the anchor. The tapered multi helix anchor exhibited a higher uplift capacity than the anchor of uniform plate sizes and this behaviour is attributed to the fact that the top two helixes, in the case of the uniform helix

plate arrangement that are located entirely in soil, has been disturbed by the leading helix, whereas in the case of the tapered plate arrangement, the soil surrounding the top two helixes is subjected to less disturbance. Furthermore, Radhakrishna observed that the diameter of the extension pipe has a great effect on the measured torque value. When large extension pipes (100 to 200 mm) were used, the anchors were not installed to relatively deep depths because of the rapid build-up of the installation torque due to pipe friction. He showed that these anchors with large extension pipe diameter did not show superior performance in resisting uplift loads as compared with anchors with small diameter extension pipes.

Figures 6.2 through Fig. 6.6 show typical stress development in the sand due to the applied installation torque to the tested types of model screw anchor. From these figures, it can be seen that the shape of the screw anchor (geometry, pitch/diameter ratio, number of pitches) influences significantly the measured installation torque value (T) as well as the lateral stress in the sand during torque application. As discussed before and as illustrated by Fig. 6.2 through Fig. 6.6, the installation torque as well as the developed lateral stress during installation, increase with the anchor's pitch/diameter ratio and with the increase of the helix angle for multi pitch screw anchors.

Mitsch and Clemence (1985) [43] reported similar results on stress development in a sand deposit during the installation process. They performed an experimental study on uniform multi helix model anchors, one-third of the prototype dimensions. Based on the measured stresses of stress cells located in the sand layer, they reported that the installation of helical anchors results in a disturbance to the soil mass and induces significant stress changes in the deposit. They demonstrated that the soil distrubance has an appreciable influence on the anchor installation and uplift behaviour as well as on the observed failure surface. This results in a densification of the sand, and this densification changes from one location to another within the soil mass. The magnitude of the resulted densification depends on the initial relative density, the applied downward pressure to install the anchor, and the relative depth ratio of the anchor.

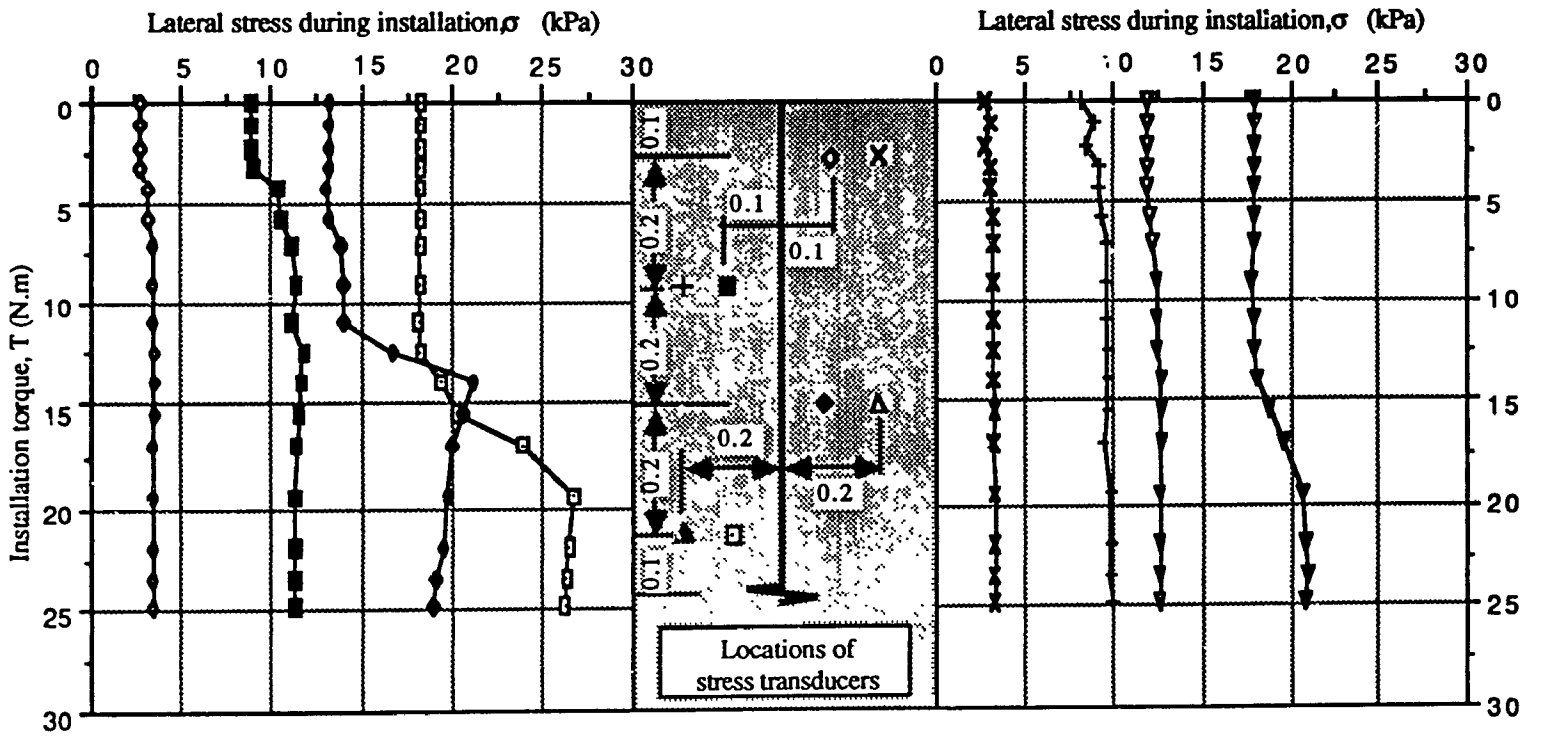

(a) Transducers located at 0.1 m from anchor's axis

(b) Transducers located at 0.2 m from anchor's axis

Fig. 6.2: Stress development in sand due to the applied installation torque. Type 1 screw anchor installed in dense sand; experimental results.

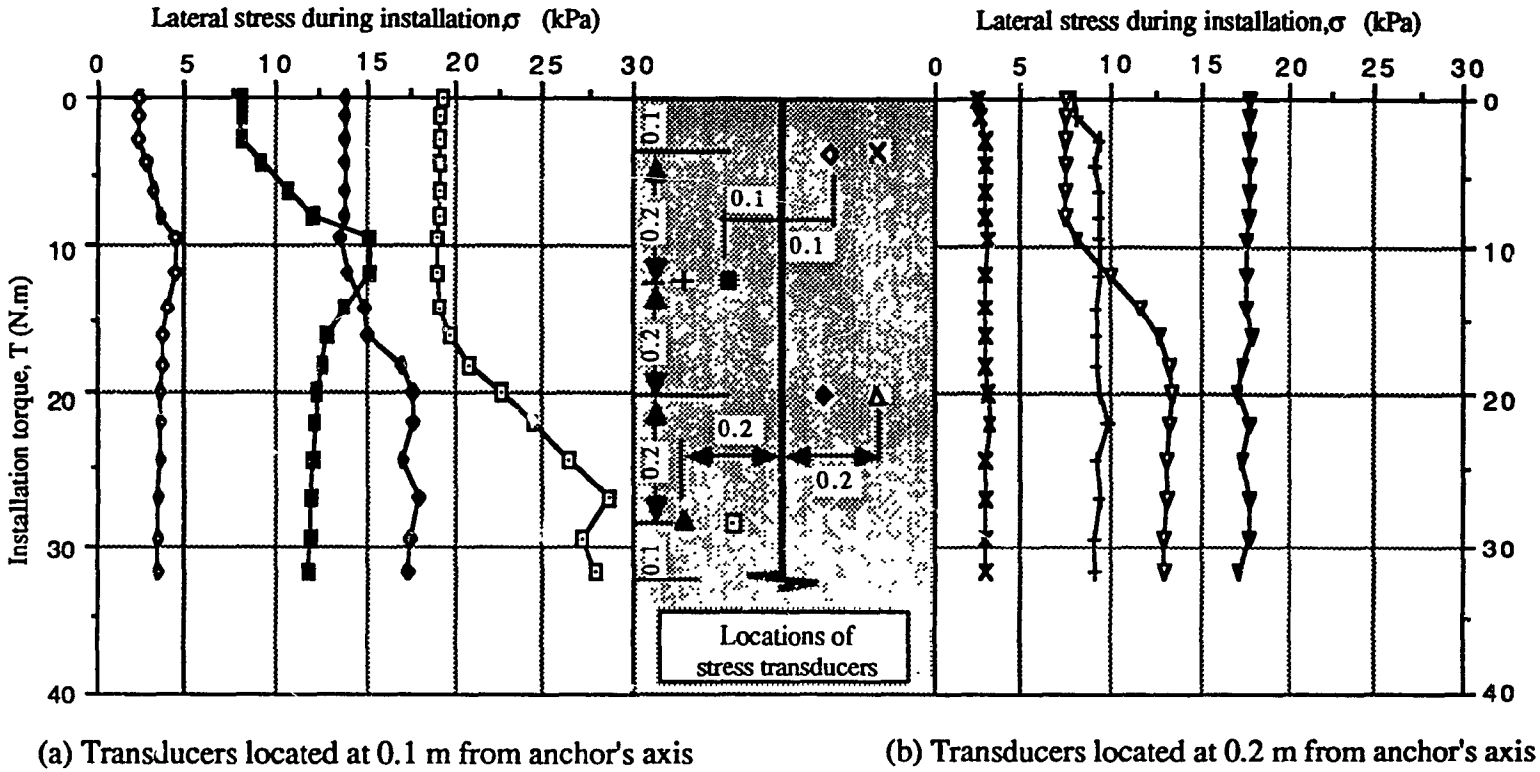

(a) Transducers located at 0.1 m from anchor's axis

(b) Transducers located at 0.2 m from anchor's axis

Fig. 6.3: Stress development in sand due to the applied installation torque. Type 2 screw anchor installed in dense sand; experimental results.

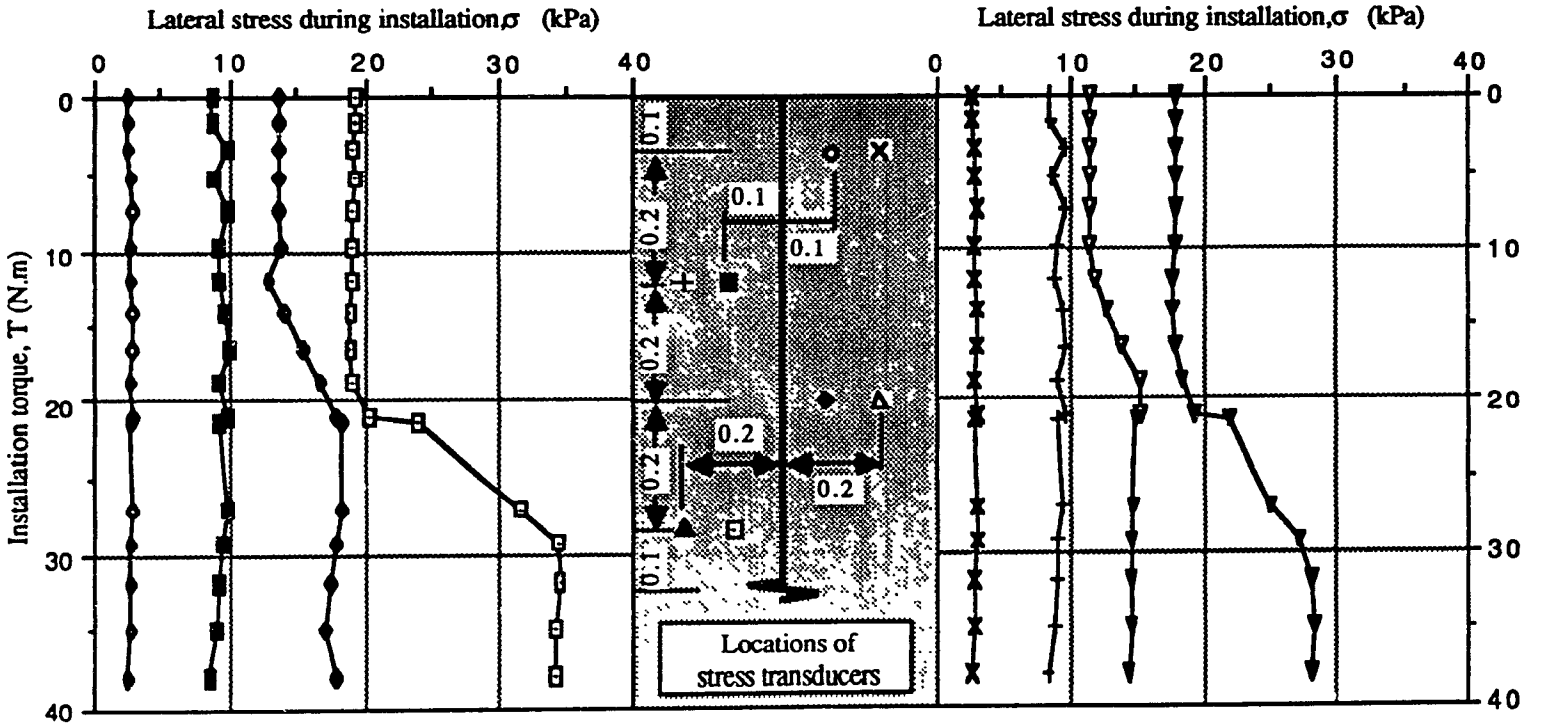

(a) Transducers located at 0.1 m from anchor's axis

(b) Transducers located at 0.2 m from anchor's axis

Fig. 6.4: Stress development in sand due to the applied installation torque. Type 3 screw anchor installed in dense sand; experimental results.

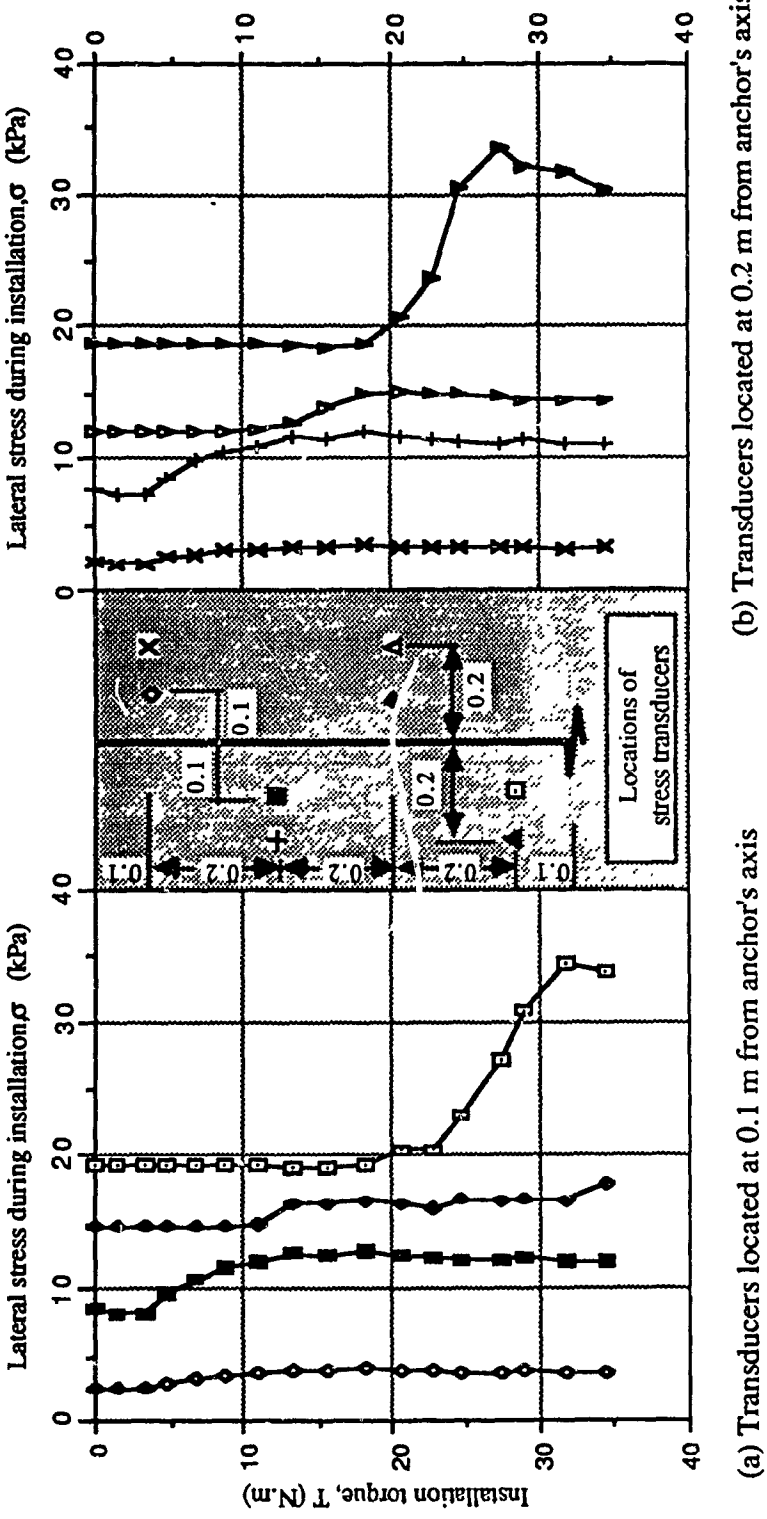

(a) Transducers located at 0.1 m from anchor's axis (b) Transducers located at 0.2 m from anchor's axis

Fig. 6.5: Stress development in sand due to the applied installation torque. Type 4 screw anchor installed in dense sand; experimental results.

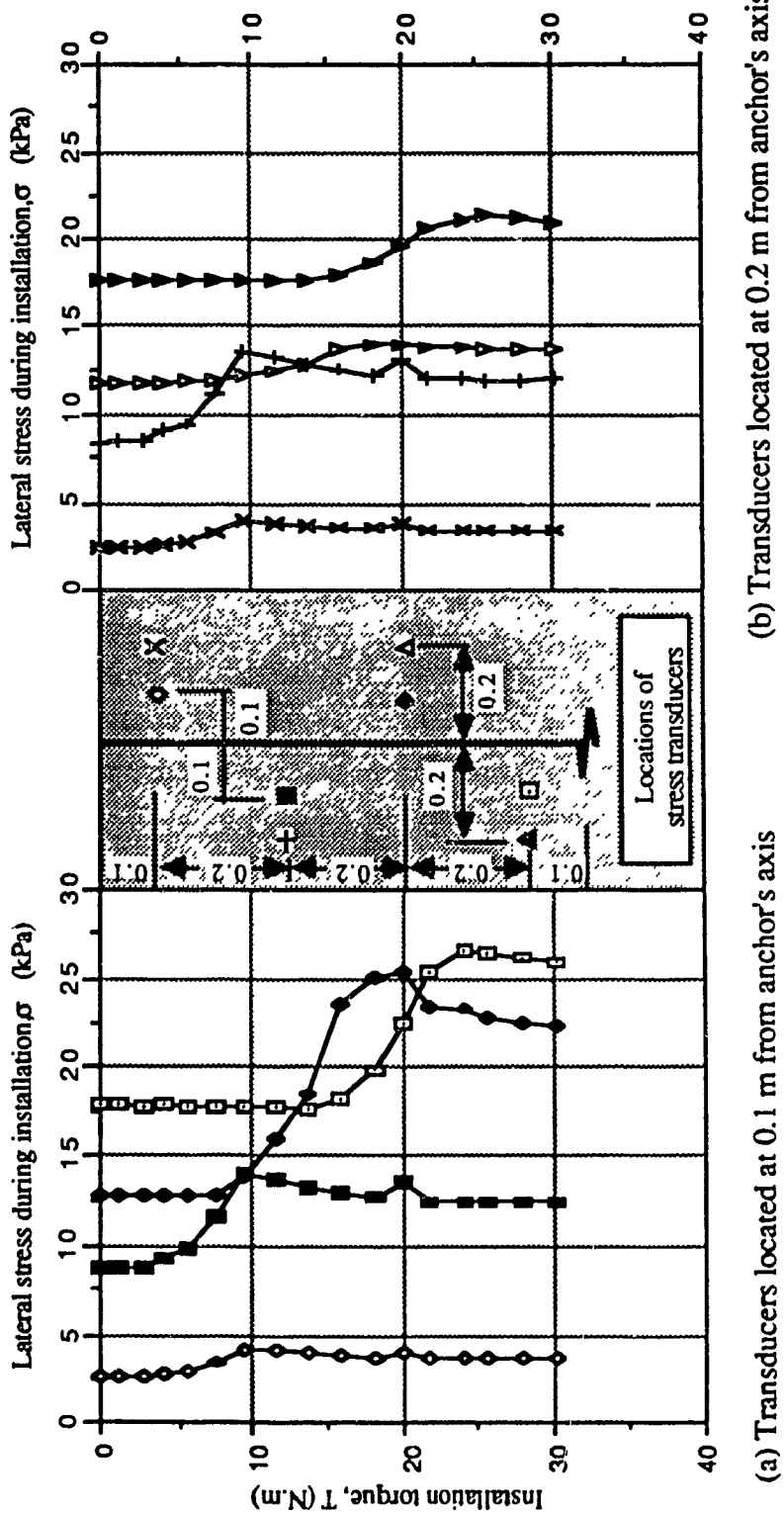

(a) Transducers located at 0.1 m from anchor's axis (b) Transducers located at 0.2 m from anchor's axis

Fig. 6.6: Stress development in sand due to the applied installation torque. Type 5 screw anchor installed in dense sand; experimental results.

An axial vertical downward force was applied to the anchor's shaft during the installation procedure to ensure regular advancement of the anchor into the sand equal to anchor's pitch per revolution. Due to the application of this downward force, an inverted void cone was observed on the sand surface after installing the anchor into the sand (Fig. 6.7). This inverted void cone was accompanied by a sand up-heave on the perimeter of the cone's base. The observed inverted void cone and the sand surface up-heave can be attributed to local compaction of the sand accompanied by lateral movement due to the extension of the developed displacement field resulted from installation process. The sand moves laterally and in upward direction due to the lack of surcharge preventing the upward movement. The extent of up-heave area as well as the amount of surface up-heave are dependent on the initial relative density of the sand as well as on the applied rate of installation. Figure 6.8 presents typical void cone and sand surface up-heave as observed from the present experimental investigation. It is worth noting that the dimensions of the inverted void cone as well as the sand surface up-heave increase with the initial relative density of the sand and the applied rate of installation. Also, it was noticed that, a column of sand concentric with the anchor's shaft was strongly affected by the shaft's rotation and it was partially involved in the rotation process at an angular velocity considerably less than the shaft's angular velocity. The diameter of the sand column involved in the angular rotation was a function of the initial relative density of the tested sand; the higher the initial relative density, the greater the diameter of the sand column. In addition, this angular rotation of the sand column was accompanied by a constant depression of the sand column. This can be explained in terms of the densification effect of the anchor installation process on the sand layer and beneath the anchor's blade due to the applied downward load.

An attempt has been made to define, experimentally, the shape of distortion that the screw anchor causes to the sand during installation. Thin flax strings were painted by silicone sealent, then they were placed in a pan containing sand to let the sand stick to them. After a period of time (1-2 hours), the sand strings were sprayed by a dark colour. These flexible

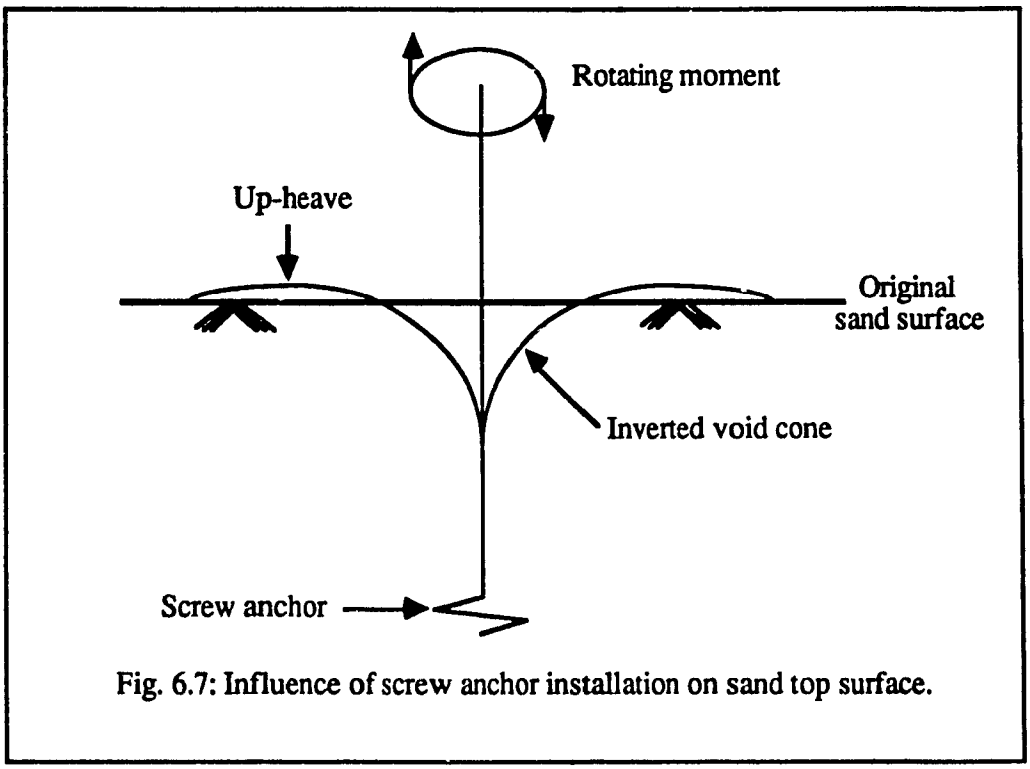

Fig. 6.7: Influence of screw anchor installation on sand top surface.

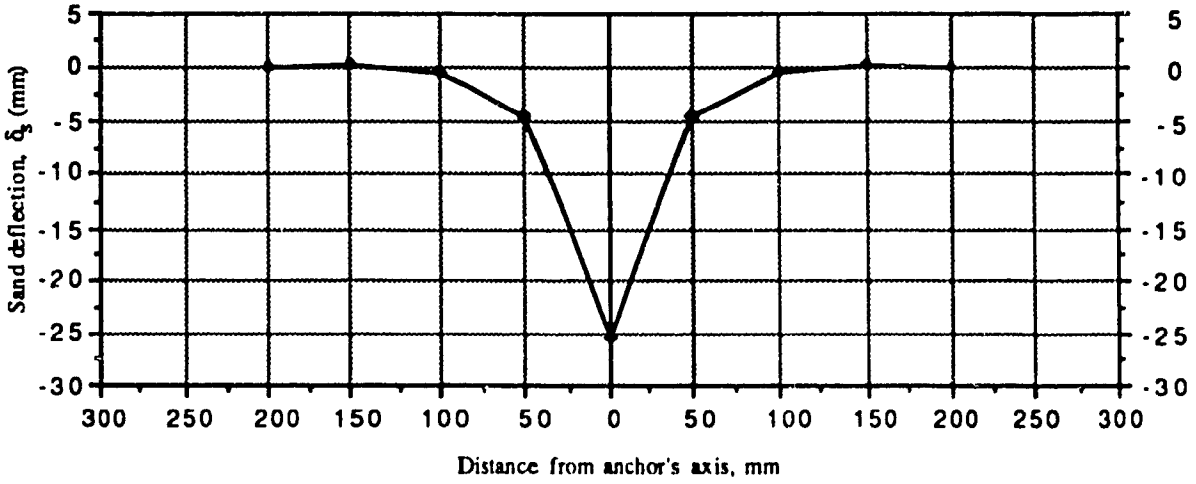

Fig. 6.8: Typical configuration of sand surface after the installation of the screw anchor.

coloured sandy strings were placed vertically on the internal perimeter of a 70 mm internal diameter plxiglass tube provided with a special base suitable for holding the strings vertically in position during the sand placement and anchor installation techniques (Plate 6.1). Care was given to sand placement process such that the strings remain vertical after placing the sand.The effect of screw installation on the strings can be seen in Plate 6.3 where these strings were shifted from the vertical position and they were pulled towards the central axis of the anchor due to the rotation process. This shows that a local compaction takes place during installation and this results in an increase in the lateral stresses. The effect of the local compaction caused by screw installation to the sand layer can also be seen in Plate 6.4 where coloured layers of sand were placed in 70 mm internal diameter plxiglass tube, in medium dense state. It is worth noting that thc torque magnitude required to install Type 2 screw anchor to deep depth (H > 500 mm) inside this tube, was significantly larger than that required to install the same anchor into a similar sand deposit placed in the testing tank. This can be attributed to the confinement role that the tube plays against the sand dilatancy in the lateral direction. This effect does not exist in the case of screw installation in an unconfined sand deposit where the sand has the freedom to displace vertically and laterally.

The ultimate pullout load (Q_u) of a screw anchor installed to a given depth of sand is plotted versus the final installation torque value (T) measured at the same depth. This relationship is shown in Fig. 6.9 for the tested types of model anchors installed in dense, medium, and loose sand. From this figure, it can be observed that an increase of installation torque value required to install a screw anchor to a given depth results in relatively higher pullout capacity of the anchor. This figure also demonstrates the effect of the pitch/diameter ratio (p/B) of the screw and its general configuration on the Q_u-T relationship, where higher torque was required to install the anchor with larger p/B ratio while the ultimate pullout load was poorly affected by this ratio. Moreover, Fig. 6.9 shows that, for relatively shallow anchors (up to H/B = 6), the influence of the screw anchor's geometrical characteristics on the Q_u -T relationship is insignificant.

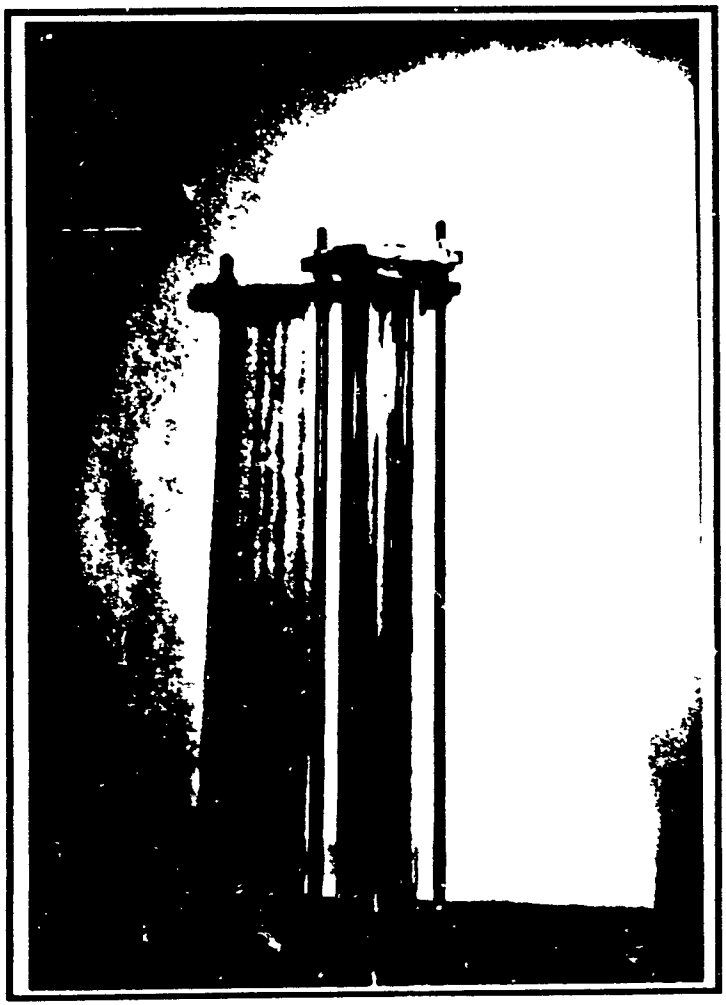

Plate 6.1: General view of sand strings before placing the sand inside the tube

Plate 6.2: General view of sand strings after placing the sand inside the tube

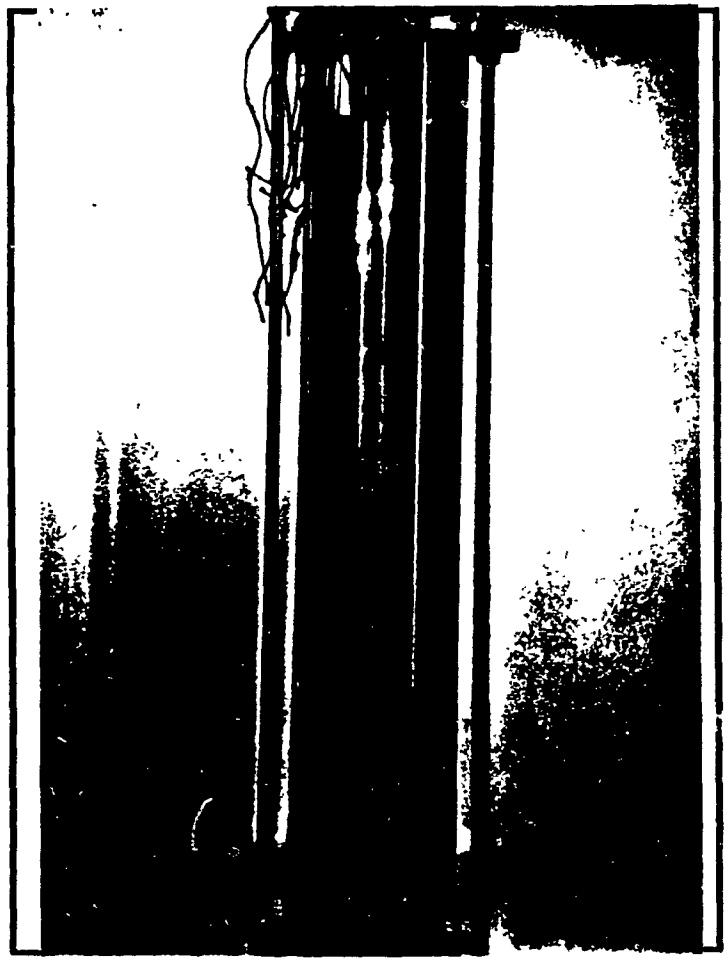

Plate 6.3: Effect of screw installation on the vertical sandy strings placed on the inner perimeter of the testing tube.

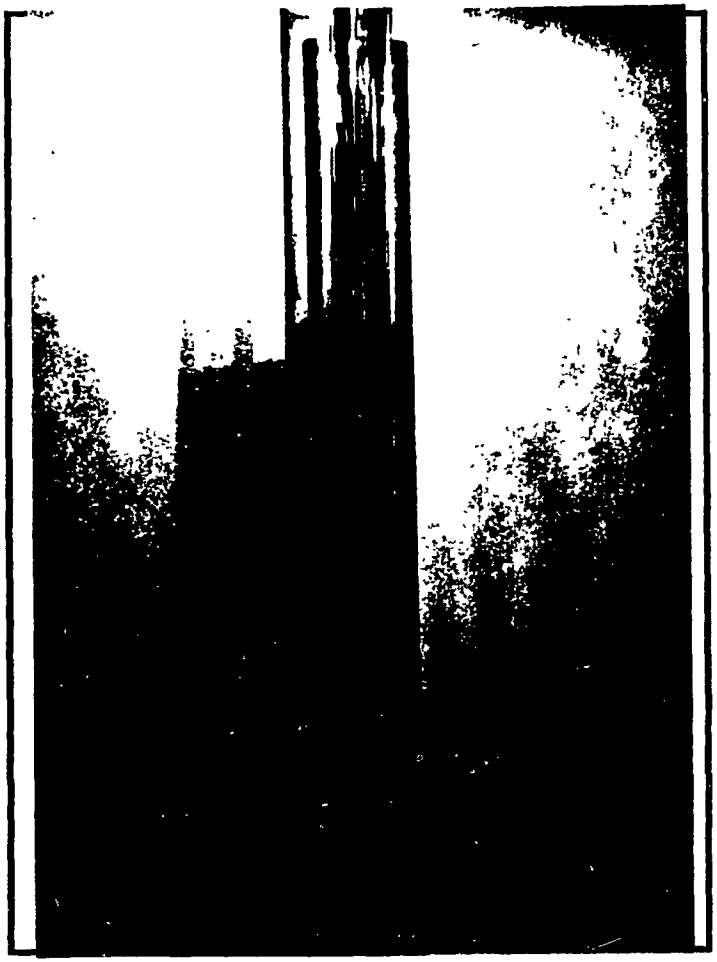

Plate 6.4: Effect of screw installation on horizontal coloured layers of sand.

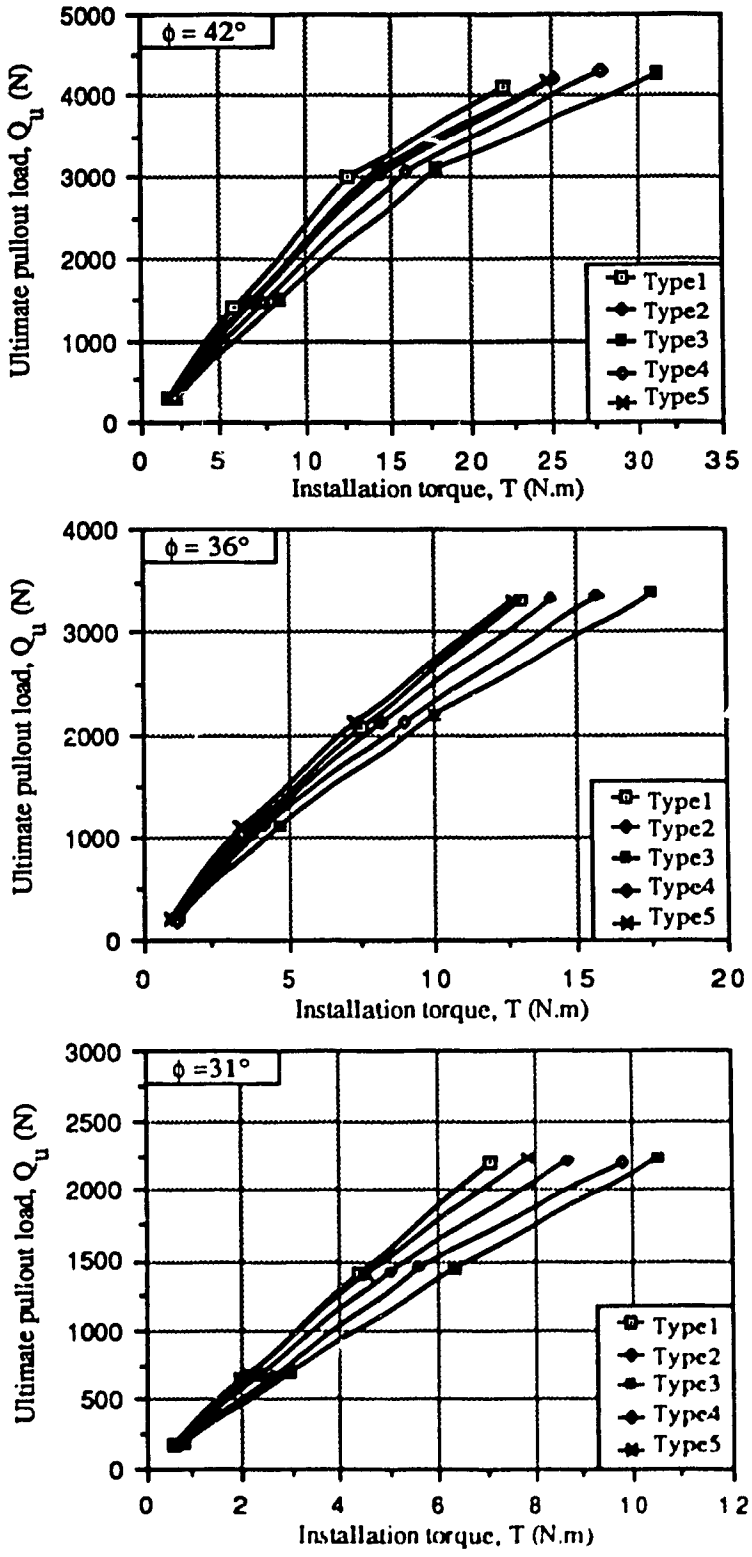

Fig. 6.9: Ultimate pullout load versus installation torque for tested types of anchors installed in loose, medium, and dense sand.

6.3 Theoretical Model

The performance of screw anchors during installation process is influenced by several factors that should be taken into consideration. These factors are summarized in the following:

1. The diameter of the upper blade.
2. The pitch of the screw anchor.
3. The helix angle(s).
4. The diameter of the stem or the shaft.
5. The general configuration of the screw anchor (single pitch, multi equal pitch, multi variable pitch, multi uniform helixes, mult uniform helixes with variable pitch, multi tapered helixes with constant helix angle, multi tapered helixes with variable helix angle, etc.).
6. The thickness of the screw blades.
7. The shape of the cutting edge of the screw blades (flat, knifed, V-shaped, square-shaped).
8. The method used in manufacturing the screw anchor (one unit, assembled, welded, bolted, riveted, etc.).
9. The anchor's material and surface roughness.
10. The anchor's end state whether it is conical or flat.

The above mentioned factors affect the performance of the screw anchor during installation to different degrees. Some of these factors have an appreciable effect on the instalaltion torque value (T) while others have little influence. In the present investigation, however, the study has concentrated on the effect of the pitch/diameter ratio, helix angle, and general screw configuration, on the required installation torque value (T). The effect of other factors of the above list is eliminated by considering a proper design and by fabricating the tested screw models as one piece with no assembled parts.

The installation of screw anchors encounters frictional and bearing resistances exerted on the blades of the screw unit, and on the anchor's shaft. Summation of frictional resistances acting on the screw surface area as well as its shaft yields the force that produces moment acting against the applied installation torque. Similarly, summation of bearing resistances acting on the screw blades produces the force that resists the downward advancement of the anchor. These bearing forces have components acting on the screw blades as frictional forces contribute to the resisting moment against the applied torque. A vertical downward force should be applied to the anchor's shaft to overcome the forces acting against installation. In the following, a theoretical model is developed to calculate the required installation torque (T) and the vertical downward force (V).

6.3.1 Single pitch screw anchor

Figure 6.10 shows the system of forces acting on the anchor's screw element and its shaft due to the application of an installation torque. Normal and lateral earth pressures are exerted on the anchor's body as a result of the forced rotation and the applied pushing down force. Forces shown in this figure produce resistance against the motion in the shown directions. Forces acting against rotation can be listed as follows:

1. Passive lateral earth pressure exerted on the entire embedded height of the anchor's shaft (P_1). This force has two components (P_{1x} and P_{1y}) of frictional resistance, the first component produces moment acting on the shaft resisting its rotation (T_1), and the second one produces frictional moment acting on the anchor's blade (T_2).
2. Force (P_2) acting on the cylindrical column of the sand overlying the screw blade. This force appears due to the local compaction that the screw anchor installation causes to the sand layer. The force (P_2) has two components (P_{2x} and P_{2y}), the first component produces no torsional resistance, while the second one reflects its influence as a frictional

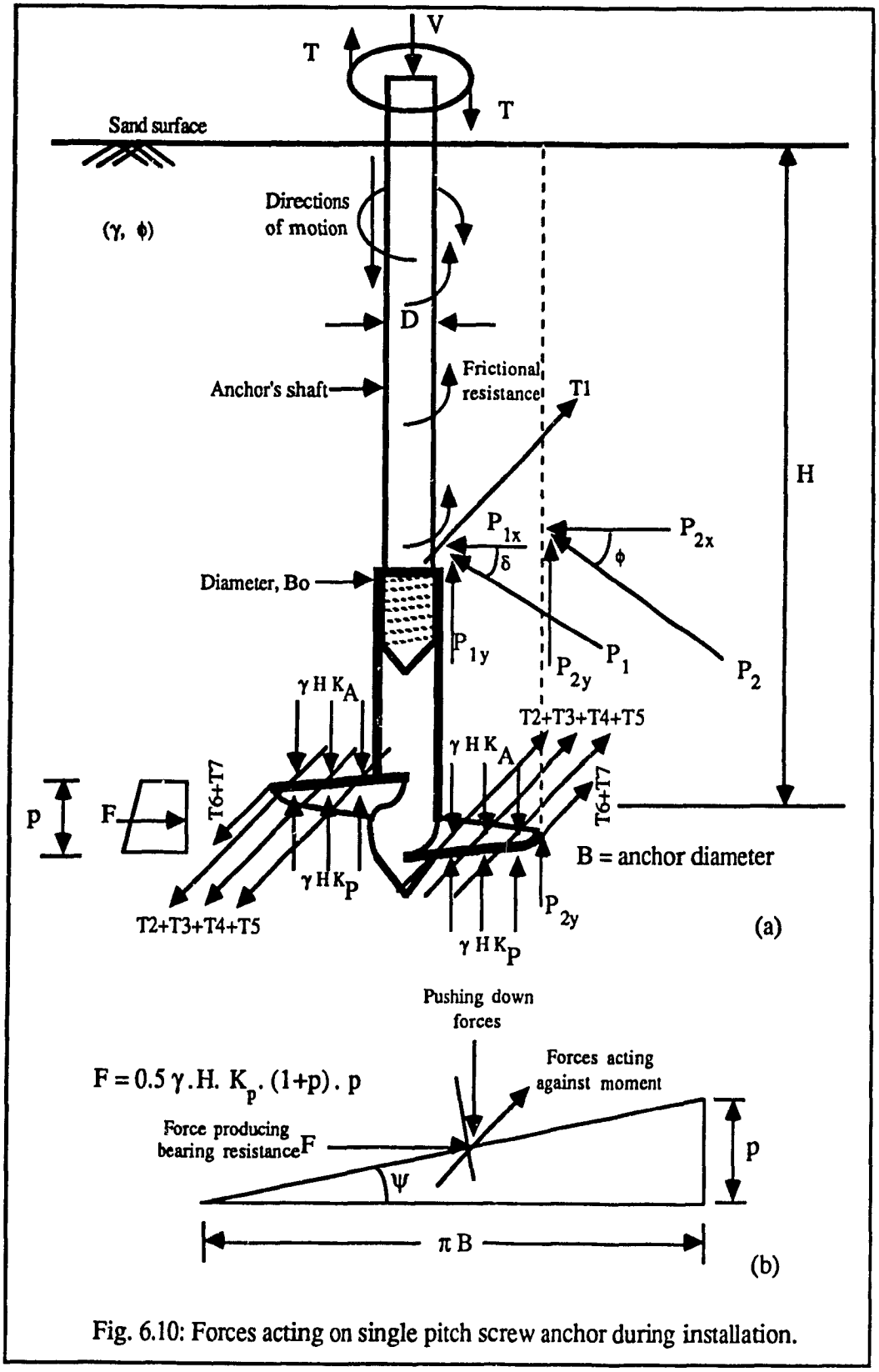

Fig. 6.10: Forces acting on single pitch screw anchor during installation.

moment acting on the anchor's blade (T_3).

3. Active and passive earth pressures exerted on the upper and the lower surface, respectively, of the screw blade due to the downward advancement of the anchor. These two forces produce frictional resistances (T_4 and T_5) on the upper and the lower blade's surfaces, respectively, resulting in a moment acting against the applied installation torque.
4. Force (F) due to the passive lateral earth pressure exerted on the upper surface area of the screw pitch due to its inclination in the third dimension. This force produces bearing resistance against rotation and its influence translates as torsional resistance (T_6) against the applied torque.
5. Force exerted on the outer perimeter of the screw blade due to the frictional resistance between its thickness and the surrounding sand. The existence of this force produces frictional resisting moment (T_7).

Consider A_t and A_b are the net surface areas of the upper and lower surfaces, respectively, of the screw blade. These areas are calculated on the actual inclined surface of the blade. Considering and elemental area of diameter b and thickness db, the actual surface area along the screw's pitch (p) can be found from the following integration:

$$A_t = \int_{B_o/2}^{B/2} \sqrt{(\pi b)^2 + p^2}\, db \qquad \ldots (6.1)$$

$$A_b = \int_{B_i/2}^{B/2} \sqrt{(\pi b)^2 + p^2}\, db \qquad \ldots (6.2)$$

Where A_t and A_b = actual surface area of the top and bottom surfaces of the screw blade, calculated on the inclined surface.

B_0 = inner diameter of the upper surface of the screw blade.

B_1 = inner diameter of the lower surface of the screw blade.

B = outer diameter of the screw anchor's blade

p = pitch of the screw anchor's blade.

Performing the integrations given by eq. (6.1) and eq. (6.2), and doing adequate contractions, the top and bottom surface areas can be given by the following equations:

$$A_t = (2/\pi)\,[(\pi B/4)\cdot Z_1 + p^2 \cdot \ln(\pi B/2 + Z_1) - (\pi B_0/4)\cdot Z_2 - p^2 \cdot \ln(\pi B_0/2 + Z_2)] \quad \ldots (6.3)$$

$$A_b = (2/\pi)\,[(\pi B/4)\cdot Z_1 + p^2 \cdot \ln(\pi B/2 + Z_1) - (\pi B_1/4)\cdot Z_2 - p^2 \cdot \ln(\pi B_1/2 + Z_2)] \quad \ldots (6.4)$$

Where Z_1 and Z_2 are constants given by the following expressions:

$$Z_1 = \sqrt{(\pi B)^2/4 + p^2} \quad \ldots (6.5)$$

$$Z_2 = \sqrt{(\pi B_1)^2/4 + p^2} \quad \ldots (6.6)$$

An average helix angle (ψ) of the screw anchor is given by the angle calculated on an average blade diameter (B_{av}), where:

$$B_{av} = (B + B_0)/2 \quad \ldots (6.7)$$

$$\psi = \tan^{-1}(p/\pi B_{av}) \quad \ldots (6.8)$$

The required installation torque value (T) can be given by the following equation (Fig. 6.10):

$$T = \Sigma_{i=1}^{n} T_i \qquad \text{... (6.9)}$$

$$T = T_1 + T_2 + T_3 + T_4 + T_5 + T_6 + T_7 \qquad \text{... (6.10)}$$

Where T_1 = resisting moment due to the force P_{1x} acting on the anchor's shaft.

T_2 = resisting moment due to the force P_{1y} acting on the anchor's blade.

T_3 = resisting moment due to the force P_{2y} acting on the anchor's blade.

T_4 = resisting moment acting on the upper surface of the anchor's blade due to the acting active earth pressure.

T_5 = resisting moment acting on the lower surface of the anchor's blade due to the acting passive earth pressure.

T_6 = resisting moment due to the bearing force F acting on the entire height of the screw pitch.

T_7 = resisting moment acting on the outer perimeter of the thickness of the screw blade.

The values of the terms that constitute eq. (6.10) can be given by the following expressions:

$$T_1 = 0.5 \cdot \gamma \cdot H^2 \cdot \cos\delta \cdot K_p' \cdot K_f \cdot (\pi \cdot D) \cdot (D/2) \qquad \text{... (6.10a)}$$

$$T_2 = 0.5 \cdot \gamma \cdot H^2 \cdot \sin\delta \cdot K_p' \cdot \tan(\delta + \psi) \cdot (\pi \cdot D) \cdot (D/2) \qquad \text{... (6.10b)}$$

$$T_3 = 0.5 \cdot \gamma \cdot H^2 \cdot \sin\phi \cdot K_p' \cdot \tan(\delta + \psi) \cdot (\pi \cdot B) \cdot (B/2) \qquad \text{... (6.10c)}$$

$$T_4 = \gamma \cdot H \cdot K_A \cdot A_t \cdot \tan(\delta + \psi) \cdot [(B + B_0)/4] \qquad \text{... (6.10d)}$$

$$T_5 = \gamma \cdot H \cdot K_P \cdot A_b \cdot \tan(\delta + \psi) \cdot [(B + B_0)/4] \qquad \text{... (6.10e)}$$

$$T_6 = F \cdot [(B - B_0)^2/8] \quad \text{... (6.10f)}$$

$$T_7 = \gamma \cdot H \cdot K_p \cdot K_f \cdot (\pi.B) \cdot (B/2) \cdot t \quad \text{... (6.10g)}$$

Where K_A = coefficient of active earth pressure.

= $(1 - \sin \phi) / (1 + \sin \phi)$

K_p = coefficient of passive earth pressure.

= $(1 + \sin \phi) / (1 - \sin \phi)$

K_p' = modified coefficient of passive earth pressure

D = the diameter of the anchor's shaft.

δ = angle of friction between the anchor's material and the soil.

K_f = coefficient of friction between the anchor's material and the surrounding soil,

($K_f = \tan \delta$).

H = installation depth of the screw anchor.

t = thickness of the screw blade.

The force F can be given by the following equation:

$$F = 0.5 \cdot \gamma \cdot H \cdot K_p \cdot (1 + p) \cdot p \quad \text{... (6.11)}$$

The angle of friction between the anchor's material and the surrounding sand (δ) was considered equal to (3/4 ϕ) for the machined stainless steel screw models. Based on the present experimental test results, the value of the modified coefficient of passive earth pressure K'_P, as given by the measurements of the stress transducers located around the installation path, can be given by [$K'_P = 0.3\ (K_P)$]. Clemence and Pepe (1984) [11], reported experimentally measured values of the coefficient of lateral earth pressure after installing multi helix screw anchors. For anchors installed in very dense sand, the developed lateral stress after installation was in the order of 0.4 - 0.5 from the full passive resistance, whereas it was about 0.2 - 0.3 in the case of loose sand. From this it follows that a ratio of $K'_P = 0.3\ K_P$, as deduced from the present investigation, can be adopted for the purpose of installation torque calculations.

The magnitude of the downward vertical force (V) required to overcome the forces acting against the downward motion can be given by the following equation (Fig. 6.10):

$$V = \Sigma_{i=1}^{n} V_i \qquad \ldots (6.12)$$

$$V = V_1 + V_2 + V_3 + V_4 \qquad \ldots (6.13)$$

Where V_1 = vertical component (P_{1y}) of the force P_1 acting on the anchor's shaft.

V_2 = vertical component (P_{2y}) of the force P_2 acting on the sand column overlying the anchor's blade.

V_3 = force resulting from the passive bearing resistance acting on the lower surface of the screw blade.

V_4 = drag force acting on the upper surface of the screw blade due to the acting active earth pressure.

The values of the terms that constitute eq. (6.13) can be given by the following expressions:

$$V_1 = 0.5 \cdot \gamma \cdot H^2 \cdot \sin \delta \cdot K'_P \cdot (\pi \cdot D) \quad \text{... (6.13a)}$$

$$V_2 = 0.5 \cdot \gamma \cdot H^2 \cdot \sin \phi \cdot K'_P \cdot (\pi \cdot B) \quad \text{... (6.13b)}$$

$$V_3 = \gamma \cdot H \cdot K_P \cdot A_b \cdot \cos \psi \quad \text{... (6.13c)}$$

$$V_4 = \gamma \cdot H \cdot K_A \cdot A_t \cdot \cos \psi \quad \text{... (6.13d)}$$

Substituting the values of V_1, V_2, V_3, and V_4 in eq. (6.13), the magnitude of the downward vertical force (V) can be determined.

6.3.2 Mutli equal pitch screw anchor

The equations given for single pitch screw anchor (eqs. 6.1 through 6.13) are also applicable to the case of multi pitch screw anchor, where they provide the solution for the problem of torque (T) and vertical force (V) determination. The main difference between the case of single pitch screw anchor and that of multi pitch one, lies in the system of the distribution of the forces acting on the blades of the screw unit. For multi equal pitch screw anchor with uniform diameter, the forces distribution is similar to that in the case of single pitch screw anchor, i.e., all the forces that acting on the upper surface of the blade of the single pitch screw anchor, are similarly acting on the upper surface of the top blade of the multi pitch screw anchor; whereas all the forces that acting on the lower surface of the blade of the single pitch screw anchor are also acting on the lower surface of the lowest blade of the multi pitch screw anchor.

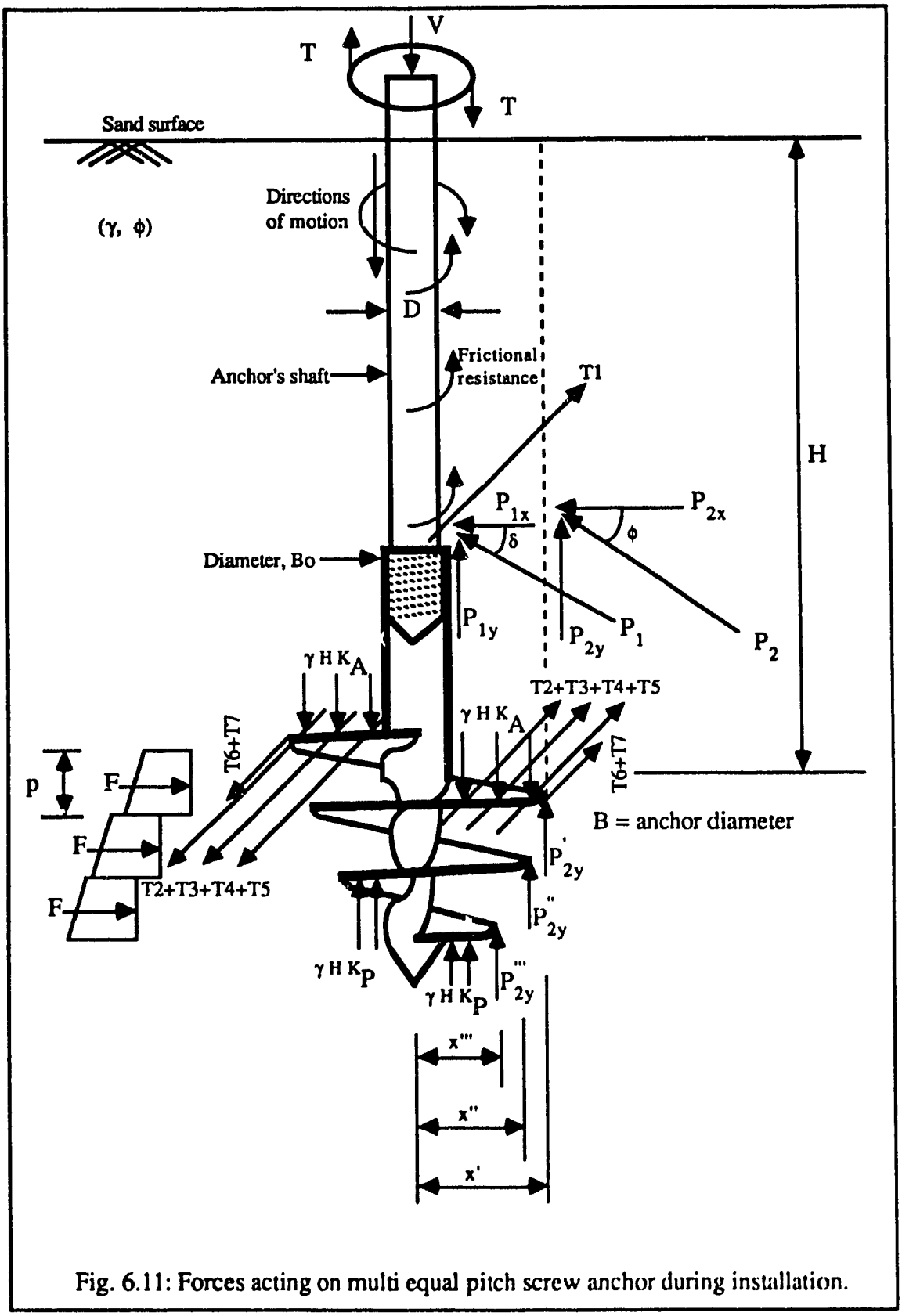

Fig. 6.11: Forces acting on multi equal pitch screw anchor during installation.

The case of multi equal pitch screw anchor with tapered configuration, i.e., diameters are not equal (case of unsymmetrical screw anchor, Type 4), is a quite complicated one. Figure 6.11 shows the forces distribution on the blades of this type of screw. A comparison between Fig. 6.11 and Fig. 6.12 indicates that the main difference between these two types of anchor is the surface of action of the force P_{2y}. As given by eq. (6.10c), for single pitch screw anchor, the force P_{2y} transmitts its influence directly to the screw blade, as a uniformly distributed circular line load acting on a circle its diameter is πB. In the case of multi equal pitch screw anchor with tapered configuration, the force P_{2y} will be partially distributed on every individual blade of the screw, see forces P'_{2y}, P''_{2y}, and P'''_{2y} in Fig. 6.11. This occurs due to the introductory effect of the conical end of the screw. The values of the forces P'_{2y}, P''_{2y}, and P'''_{2y} are directly proportional to the distance between the acting force and the anchor's axis, i.e., if the distances between the forces P'_{2y}, P''_{2y}, and P'''_{2y}, and the anchor's axis are x', x'', and x''', then [$P'_{2y} = (P_{2y} \cdot x') / (x'+x''+x''')$]. Taking into account, also, that there is a different helix angle for every pitch, the calculation of torque value encounters great difficulty. The results of the experimental investigation together with a theoretical analysis following the above mentioned method of analysis, suggest that an acceptable approximation is that the torque value required to install multi equal pitch screw anchor with tapered configuration is 10 - 15% more than that calculated for a single pitch screw anchor with a diameter and helix angle qual to those of the first blade of the multi pitch one. This percentage of torque increase almost vanishes in the case of multi equal pitch screw anchor with uniform diameter.

6.3.3 Multi variable pitch screw anchor

The main reason for using a variable pitch screw anchor, although it is very difficult to manufacture, is to have a constant helix angle (ψ), i.e., the blades are parallel (similar to Type 5). Figure 6.12 shows forces distribution of the anchor's blades. The method of torque calculation is

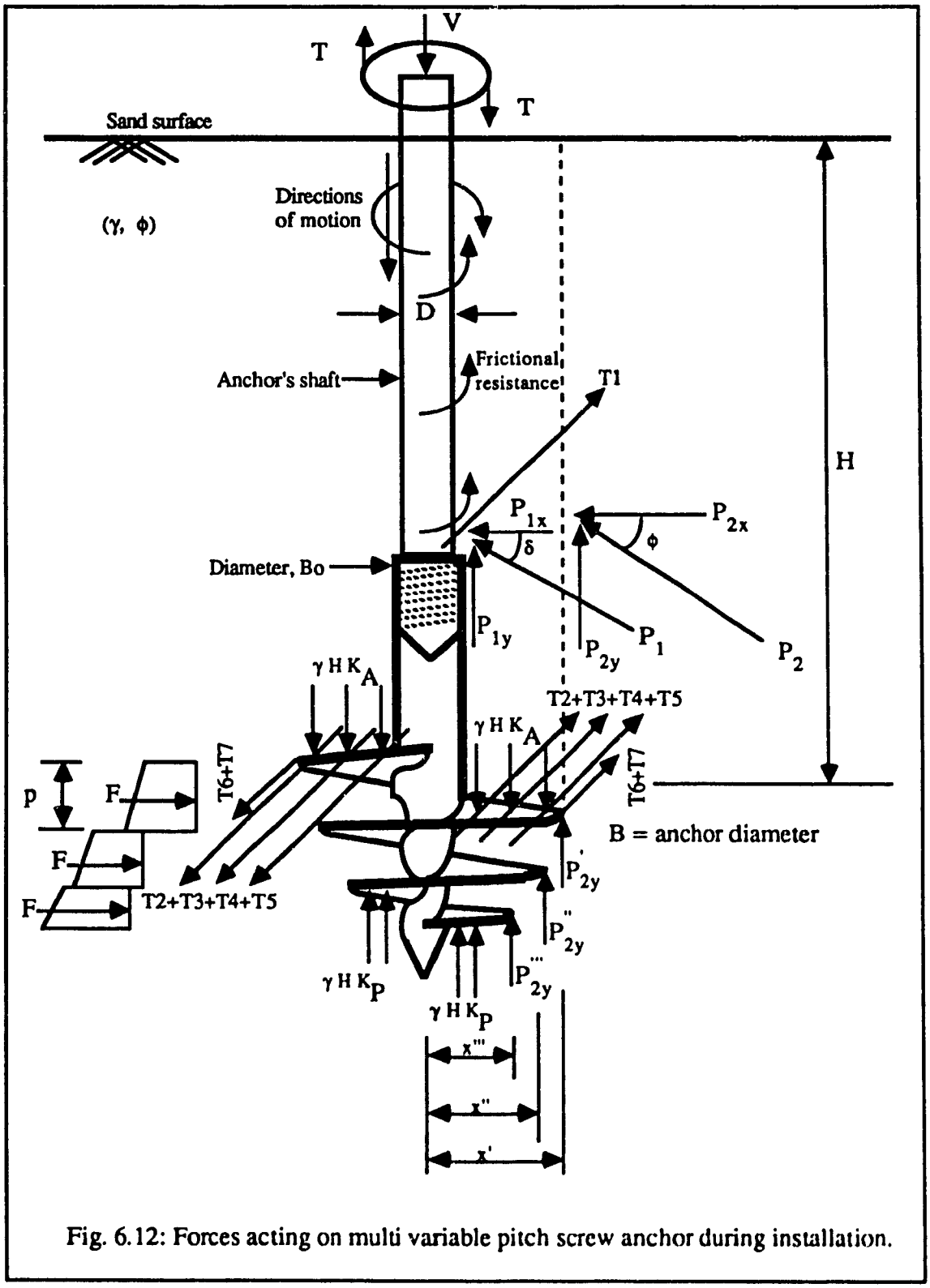

Fig. 6.12: Forces acting on multi variable pitch screw anchor during installation.

similar to that followed in the case of single pitch screw anchor (eqs. 6.1 through 6.13). The forces acting on every individual blade (P'_{2y}, P''_{2y}, and P'''_{2y}) can be determined according to the method described in the case of multi equal pitch screw anchor. The helix angle (ψ) is constant in this case, hence, eq. (6.10c) should be applied a number of times equal to the number of the blades to consider all the acting forces (P'_{2y}, P''_{2y}, and P'''_{2y}). To avoid this complexity in performing the required calculations, the results of the present experimental investigation, together with a theoretical analysis following the above mentioned method of forces distribution and analysis, suggest that the torque value calculated for a single pitch screw anchor with a diameter and helix angle equal to those of the first blade of the multi variable pitch one, can be accepted in the case of a mulki variable pitch screw anchor with a reduction ratio in the order of 10 - 15%. This reduction factor applies to the multi variable pitch screw anchor with tapered configuration and it vanishes in the case of a multi variable pitch screw anchor with uniform diameter.

6.4 Comparison of Theoretical and Experimental Results

A comparison of the theoretical and experimental torque results for single pitch screw anchors installed in dense, medium, and loose sand is shown in Fig. 6.13. From this figure, it can be indicated that there is a good agreement between the theoretical and the experimental results. Also, it shows that, for a given pitch, the theory is sensitive to the variation of the angle of shearing resistance of the sand. Similar comparison is given in Fig. 6.14 to show the sensitivity of the theory to the variation of the anchor's pitch (i.e., its helix angle). From this figure, it appears that, for a given type of sand, the torque required to install a single pitch screw anchor increases with the anchor's pitch.

A comparison of the theoretical and experimental torque results is shown in Fig. 6.15 for the mutli equal pitch (Type 4) and multi variable pitch (Type 5) screw anchors. From this figure, it can be observed that a good agreement exists between the theoretical and the experimental results.

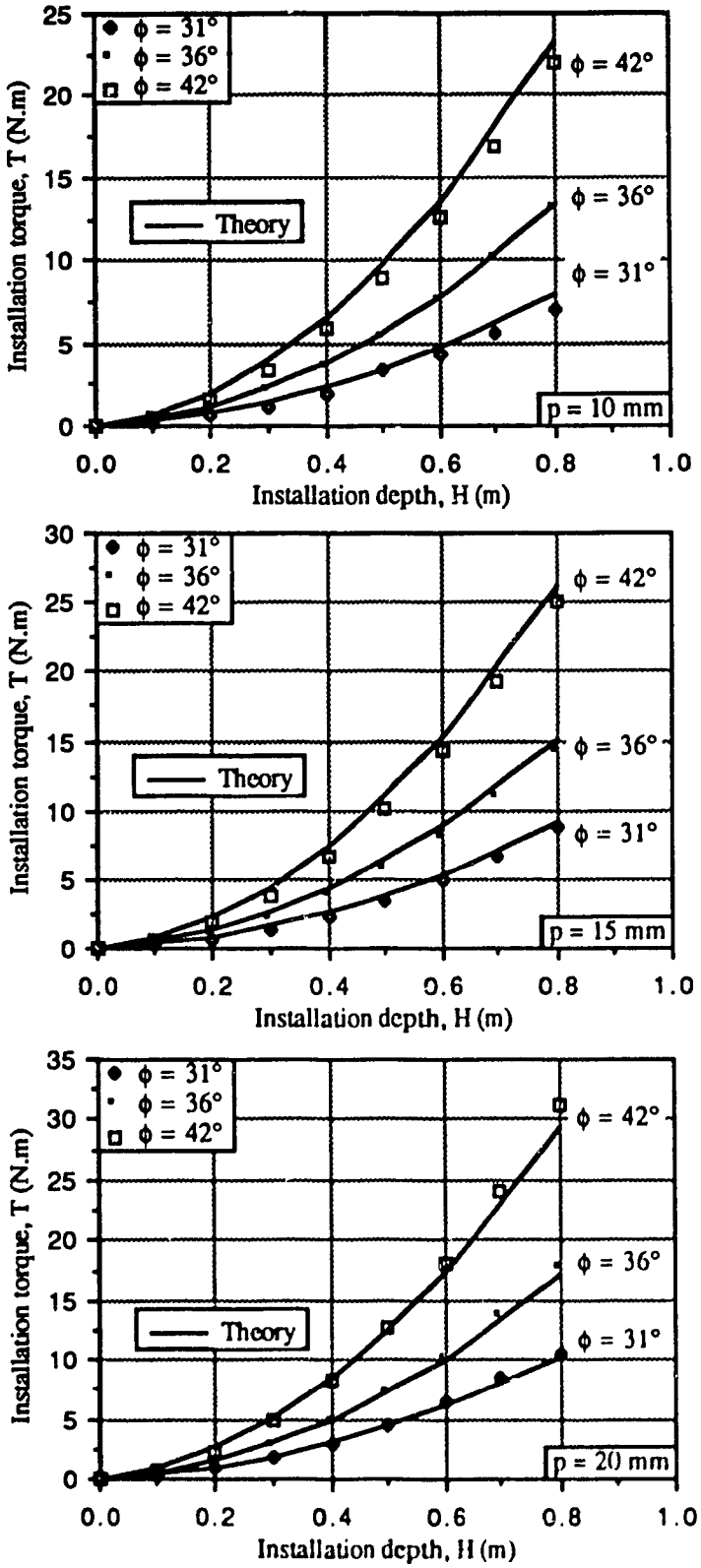

Fig. 6.13: Comparison of theoretical and experimental torque results for anchors with different pitches.

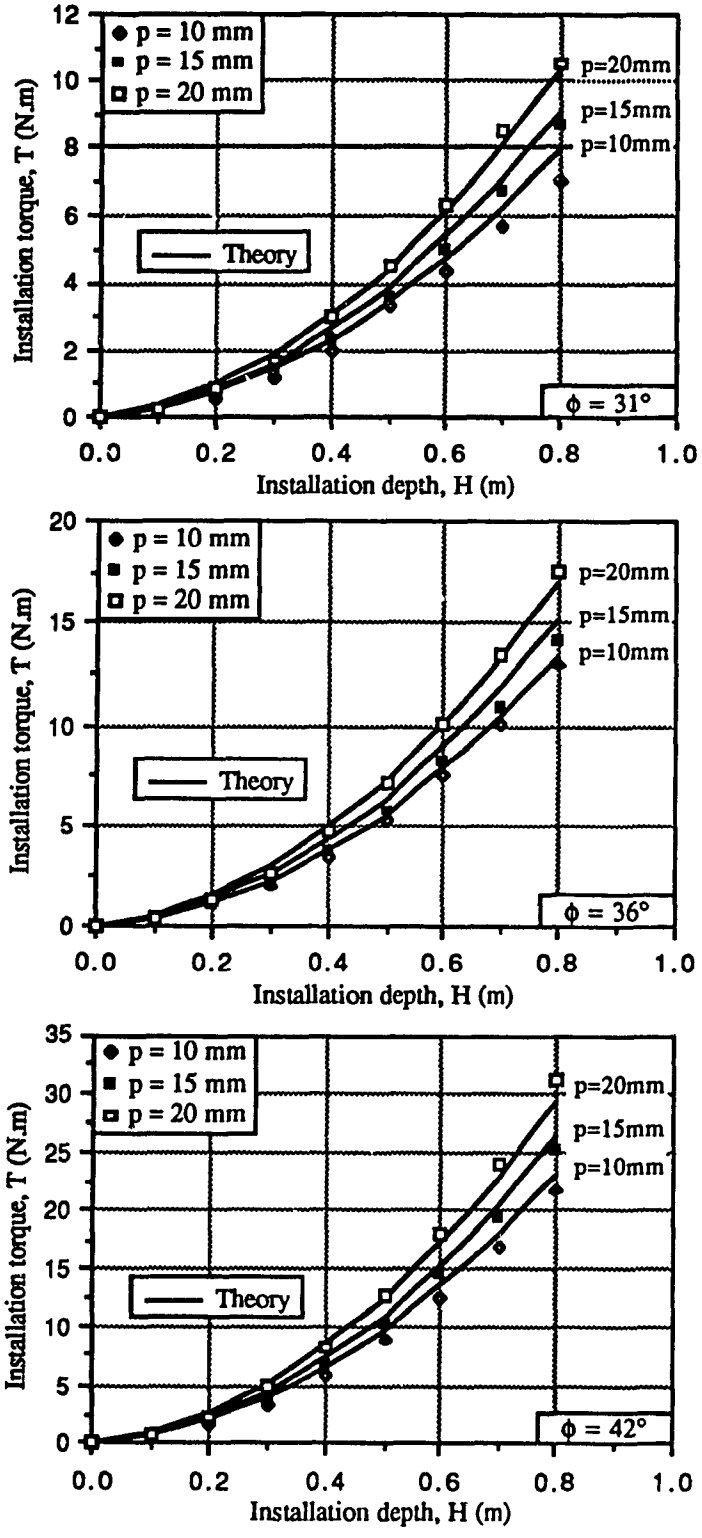

Fig. 6.14: Comparison of theoretical and experimental torque results for anchors installed in loose, medium, and dense sand.

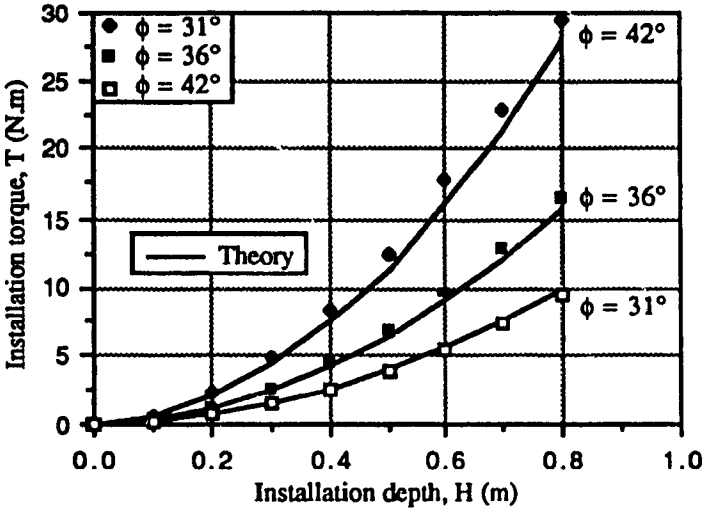

(a) Unsymmetrical screw anchor, Type 4.

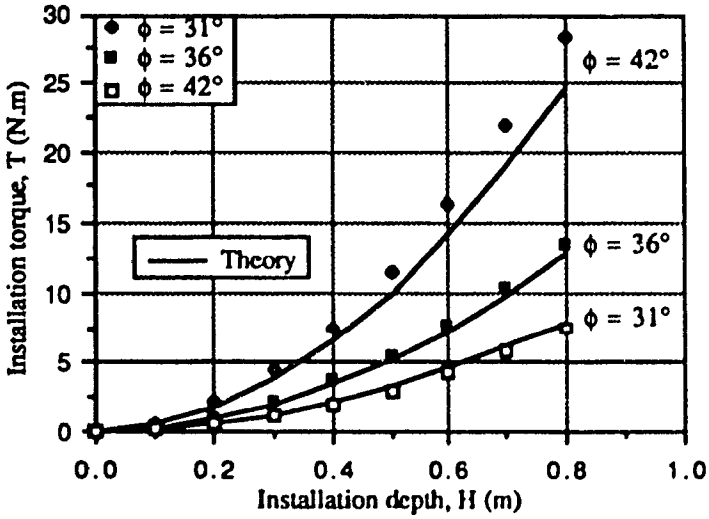

(b) Parallel blades screw anchor, Type 5.

Fig. 6.15: Comparison of theoretical and experimental torque results for unsymmetrical and parallel blades screw anchors.

Also, good agreement will be observed if the theoretical values of torque required to install Type 4 and Type 5 screw anchors were determined by using the theoretical torque values for a comparable single pitch screw anchor, and applying the appropriate factor (±10 - 15%) to the theoretically calculated values of the single pitch screw anchor.

The observed agreement between the theory proposed for torque determination and the experimental torque results, together with the agreement between the theory proposed for uplift capacity determination (Chapter 5) and the experimental uplift capacity results, were employed to develop a correlation from which the uplift capacity of a screw anchor can be predicted from the measured installation torque value. A torque factor (F_t) similar to the uplift capacity factor (Nq_u) was established to express the installation torque value in a nondimensional form. This torque factor includes all the terms that affect the installation torque magnitude. The torque factor is given by this expression: $F_t = T / \gamma AHp$ where T = the installation torque value, γ = unit weight of the sand, A = anchor's surface area, H = installation depth, and p = anchor's pitch (the variable that controls the value of the helix angle). The value of F_t was calculated for all tested single pitch screw anchors installed into dense, medium, and loose sand. The calculated F_t values were plotted against the corresponding Nq_u values ($Nq_u = Q / \gamma AH$) on a semi-logarithmic scale. For all tested types of single screw anchors installed to a wide range of depths into sand deposits with varying characteristics, a unique relationship exists between the Nq_u and F_t (Fig. 6.16). This suggests that the uplift capacity factor and the torque factor are equivalently subjected to variation when their terms change. A logarithmic curve was fitted well with the plotted data. The equation of this curve is:

$$Q / \gamma AH = 2 (T / \gamma AHp)^{(1.1)} \quad \ldots (6.14)$$

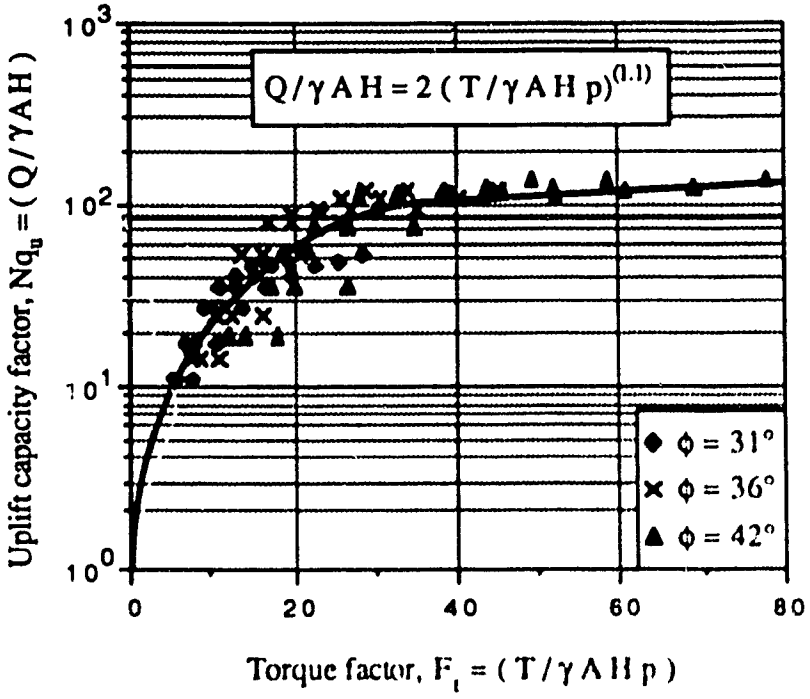

Fig. 6.16: Relationship between uplift capacity factor and torque factor

The correlation given by eq. (6.14) can be used as a guide for preliminary determination of the uplift capacity from the measured installation torque value. Although the data plotted in Fig. 6.16 was limited to the single pitch screw anchor (anchors that are used in practical applications), the correlation given by eq. (6.14) can be extended to other types of anchors after introducing the appropriate correction to the torque factor. Similarly, the uplift capacity of a group of anchors can be determined from the measured torque values for every individual anchor. Substituting, in eq. (6.14), by the average torque value measured for all the anchors of the group, and knowing the efficiency (E) of the group under consideration (from the theory given in Chapter 5), the uplift capacity of the group can be given by the following equation:

$$QU_g = N \cdot E \cdot QU_s \qquad \ldots (6.15)$$

Where QU_g = uplift capacity of anchors group.

QU_s = uplift capacity of single anchor as calculated from eq. (6.14).

N = number of anchors in the group.

E = group efficiency.

6.5 Comparison of Theoretical and Field Torque Results

A set of field torque results are reported in the literature for single and multi helix screw anchors installed in sand deposit. This field data is shown in Fig. 6.17 as a relationship of the uplift capacity factor versus torque factor, together with the curve resulted from the present investigation on single pitch screw anchors. From this figure, a good agreement can be observed between the present theory and the data reported by Radhakrishna (1976) [48] on single pitch screw anchors, and the data reported by Mitsch and Clemence (1985) [43] on triple helix screw anchors. From this agreement, it can be indicated that the Nq_u - F_t relationship is an effective tool for uplift capacity determination based on the measured torque value, for both single pitch and multi helix screw anchors.

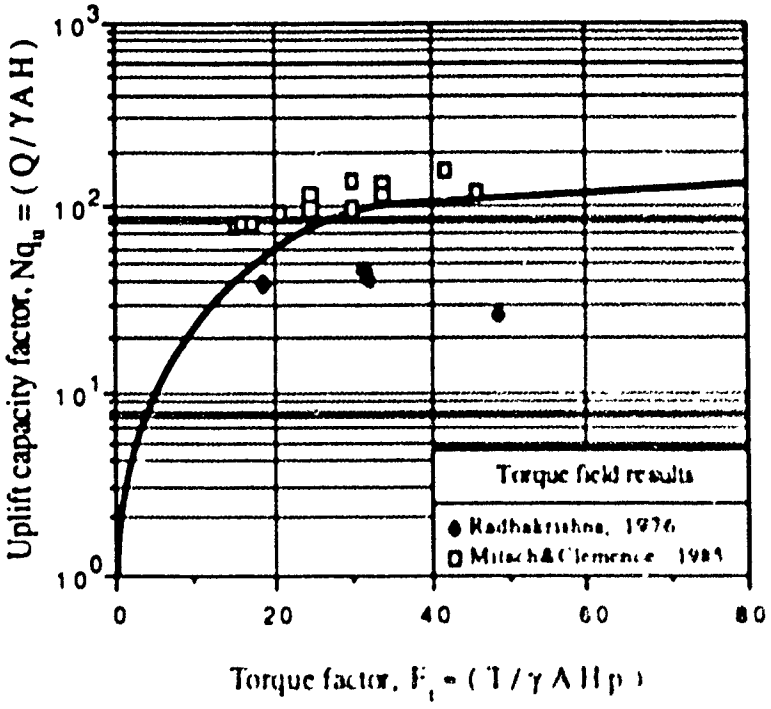

Fig. 6.17: Comparison of theoretical torque results and field results reported in the literature

CHAPTER 7

Conclusions and Scope of Future Research

7.1 Conclusions

Experimental and theoretical studies were conducted in order to identify the factors affecting the behaviour of single screw anchors and groups of anchors installed into sand deposit. Factors affecting the anchor's behaviour were evaluated, and their influence on anchor installation and during the application of the pullout load, were examined. Based on the results of the present investigation, the following conclusions can be drawn:

1. The performance of a single screw anchor during installation and pullout procedures depends on the anchor's diameter, installation depth, sand characteristics (unit weight and angle of shearing resistance), and geometrical properties of the screw unit.

2. The installation of a screw anchor into sand layer results in an increase in vertical and lateral stresses around and in the near vicinity of the installation path. The magnitude of stress increase is dependent on the initial relative density of the sand, and the geometrical properties of the screw unit.

3. The increase of the lateral and vertical stresses that takes place during the installation procedure is greater for a screw unit with large pitch/diamter ratio, i.e., it increases with the increase of the helix angle.

4. The behaviour of the multi pitch screw anchors during the installation process is quite complicated. A multi equal pitch screw anchor induces a stress increase in the sand layer larger than that induced by a single pitch screw anchor with helix angle equal to that of the first blade of the multi variable pitch screw anchor. This is attributed to a greater densification effect that is caused by the multi variable pitch screw anchor during installation due to the increase of the helix angle of the leading blades as a result to its tapered configuration.

5. The tapered configuration of a multi variable pitch screw results in a magnitude of stress increase in the sand layer lower than that induced by a single pitch screw anchor with helix angle equal to that of the mutli equal pitch screw anchor. This is due to the constant helix angle of the multi equal pitch screw anchor, and the introductory effect of the conical tapered configuration.

6. The sand placing technique affects the stress system within the sand layer. The application of a vibratory compaction to obtain high density induces high horizontal stresses which reflect their influence on the calculated lateral earth pressure coefficient at rest, this results in K_O value higher than that determined theoretically for a normally consolidated sand.

7. For overconsolidated sand, the overconsolidation ratio can be calculated from the relationship proposed by Wroth (1972), utilizing the experimentally measured coefficient of lateral earth pressure at rest for overconsolidated sand.

8. The application of pullout load to a screw anchor induces significant increase in lateral and vertical stresses around and in the near vicinity of the screw unit. This stress increase vanishes at distances extending several anchor diameters in the vertical and horizontal direction. The distance of extension depends on the relative density of the sand and the relative depth ratio of the screw anchor. The screw configuration does not affect the performance of the anchor in uplift.

9. Based on the results of the present investigation, the surface of rupture of a screw anchor can be represented by a segment of a logarithmic spiral. This surface of rupture is primarily dependent on the angle of shearing resistance of the sand and the relative depth ratio of the anchor. The shear resistance developed along the surface of rupture constitutes the major force contributing to the total capacity of the anchor against uplift.

10. The surface of rupture, in case of shallow anchors, extends from the anchor to the sand surface. For deeply installed anchors, the surface of rupture is of a local nature and its influence does not reach the sand surface.

11. There is no sudden conversion from the shallow behaviour to the deep one, rather, a transition zone exists in between these two modes of behaviour. The transition zone is a phase at which the anchor behaves initially as deep anchor then due to the lack of a sufficient surcharge it turns to a shallow one.

12. The results of the present study suggest that the deep mode of anchor behaviour takes place in dense sand at much greater depth than it does in loose sand. Based on the results of this investigation, the shallow mode of behaviour terminates at relative depth ratio (H/B) of 7, 9, and 11 for loose, medium, and dense sand respectively. The deep mode of behaviour takes place at H/B of 8, 10, 14 for loose, medium, and dense sand respectively. In between, the transition mode of behaviour takes place.

13. The installation process of a group of anchors results in significant changes in the original properties of the sand layer. These changes appear as an increase in the magnitude of the initial unit weight and angle of shearing resistance. This fact is more obvious for a large number of closely spaced anchors installed in dense sand. An empirical formula is proposed from which the amount of increase in the value of the angle of shearing resistance of the sand.

14. The uplift performance of a group of screw anchors depends on the group size, group configuration, anchor diameter, depth of installation, center-to-center spacing, installation technique, and sand characteristics (unit weight and angle of shearing resistance).

15. The load distribution amongst the individual anchors within a group depends on the cap rigidity, order of anchor installation, and the distance between the anchor and the point of load application. For a rigid cap, the central anchor or the central core of anchors resist a portion of the uplift load larger than the perimeter anchors. This fact is true at low load level whereas the amount of contribution of each anchor to the total value of the uplift capacity is almost the same for all anchors at failure.

16. The upward displacement measured at the location of every single anchor in a group is a function of the load portion resisted by this anchor; the greater the load, the larger is the displacement.

17. The upward displacement of an imaginary anchor representing the average of a group of anchors is generally higher than that of a single anchor tested under the same circumstances.

18. Efficiency of a group of screw anchors installed in medium or loose sand, increases with the spacing and decreases with the group size. This fact is true for shallow, transit, and deep anchors. Groups installed in dense sand to relatively shallow depths are not much affected by the spacing or the group size. For groups installed in dense sand to deep depths, efficiency is more than 100% for closely spaced anchors and it decreases with the increase of the spacing and with the size of the group. This behaviour is attributed to the fact that at closely spaced anchors installed in dense sand, higher stresses are induced in the sand layer due to the installation process.

19. For a rigid cap of anchors' group, the differential upward displacement of a single anchor as compared to the total upward displacement, can be minimized by following a cobweb installation procedure. This procedure provides consistency to the structure of the sand mass as it prevents the creation of highly stressed or densified zones.

20. Utilizing the observed rupture surface together with the data provided by the experimental program, a theory is developed from which the ultimate pullout load of isolated single pitch anchors as well as groups of anchors, can be predicted. The limit equilibrium method of analysis was used together with Kotter's differential equation to calculate the shear stresses acting on the observed "actual" surface of rupture.

21. A semi empirical relation based on data reported in the literature and verified by the information obtained from the present investigation, is proposed. This relation estimates the ultimate pullout load of an anchor installed in overconsolidated sand as a function of the overconsolidation ratio and the theoretically calculated value of ultimate pullout load of an anchor installed in normally consolidated sand.

22. A theoretical model is developed from which the required installation torque value for a given type of anchor can be calculated. The main forces affecting the torque magnitude are frictional resistance exerted on the anchor's shaft and the locally compacted column of sand overlying the screw blade, and the bearing resistance exerted on the screw blades.

23. Torque calculations for multi equal pitch screw anchor or multi variable pitch one are complicated. A factor is proposed to be in the order of 10 - 15%, as a percentage of increase of the torque value calculated for a single pitch screw anchor with pitch/diameter ratio equivalent to that of the multi equal pitch screw anchor. This percentage is a reduction factor in the case of multi variable pitch screw anchor.

24. A torque factor is established incorporating all the parameters affecting the torque

magnitude. A correlation is proposed between the uplift capacity factor and the torque factor. From this correlation, the uplift capacity can be determined from the measured value of installation torque. This correlation provides an effective tool for estimating a preliminary uplift capacity value for isolated screw anchors and groups of anchors as well.

25. A comparison of theoretical and experimental results of uplift capacity and installation torque value obtained from the present investigation showed good agreement. Also, good agreement was observed when the present theoretical values of the uplift capacity and installation torque were compared with the available field data reported in the literature.

7.2 Scope of Future Research

Results of laboratory tests are always subjected to scale effects and boundary conditions. However, if these tests are conducted with great care, they can provide an economical alternative for field tests and a good source of information. In order to enhance the knowledge on the performance of screw anchors in sand, future research in the subject should be directed in the following topics:

1. Conducting and collecting field data to complement the theories developed in this thesis

2. The effect of the rate of installation on the pullout capacity of the screw anchor. The rate of installation can be examined as a number of revolutions per unit time (RPM), or as a distance per unit time (m/min).

3. Simulating the field conditions concerning the decrease of the overconsolidation ratio (OCR) with the increase of the depth

4. The state of stresses acting on the anchor's shaft and blades. This can be conducted by means of instrumented models of screw anchors with built in measuring devices

5. The effect of group installation on the initial properties of the sand surrounding the group as well as that confined within individual anchors of the group.

6. Stress development in the sand layer due to group installation and the effect of order of installation on the developed stresses.

7. Load distribution amongst the individual anchors of a group of anchors with a flexible cap and the effect of using flexible cap on the total uplift capacity, differential upward displacement, and group efficiency.

REFERENCES

1. Abdel-Mallek, M. N., (1973). "The Effect of Uplift Pressure on Anchor Piles Under Water Structures," M. Sc. Thesis presented to the Faculty of Eng., Alexandria University, Egypt.

2. Adams, J. I., and Hayes, D.C., (1967). "The Uplift Capacity of Shallow Foundations," Ontario Hydro Research Quarterly, Vol. 19, No. 1, pp. 1 - 13.

3. Adams, J. I., and Klym, T. W., (1972). "A Study of Anchorages for Transmissionn Tower Foundations," Canadian Geotechnical Journal, Vol. 9, No. 1, pp. 89-104.

4. Andreadis, A., Harvey, R. C., and Burley, E., (1981). "Embedded Anchor Response to Uplift Loading," Proceedings, ASCE, Journal of the Geotechnical Engineering Division, Vol. 107, No. GT1, pp. 59-78.

5. Baker, W. H., and Kondner, R. L., (1966). "Pullout Load Capacity of a Circular Earth Anchor Buried in Sand," National Academy of Sciences, Highway Research Board, No. 108, pp. 1-10.

6. Balla, A., (1961). "The Resistance to Breaking-out of Mushroom Foundations for Pylons, "Proceedings, Fifth International Conferrence on Soil Mechanics and Foundation Engineering, Paris, France, Vol. 1, pp. 569-576.

7. Carr, R. W., and Hanna, T. H., (1971) "Sand Movement Measurement Near Anchor Plates," Proceedings, ASCE, Journal of the Soil Mechanics and Foundations Division, Vol. 97, No. SM5, pp. 833-840.

8. Chance, A. B. Company, (1977) "Encyclopedia of Anchoring," Bulletin 4 700, pp A-8-B-6.

9. Chaudhuri, K. P. R., and Symons, M. V., (1983). " Uplift Resistance of Model Single Piles," Proceedings, ASCE, Geotechnical Practice in Offshore Engineering, Edited by Stephen G. Wright, Austin, Texas, pp. 335-355.

10. Chen, W., (1975). "Limit Analysis and Soil Plasticity," Elsevier Scientific Publishing Company. Amesterdam.

11. Clemence, S. P., and Pepe, F. D., Jr., (1984). "Measurement of Lateral Stress Around Multihelix Anchors in Sand," Geotechnical Testing Journal, GTJODJ, Vol. 7, No. 3, pp. 145-152.

12. Daramola, O., (1980). "On Estimating K_O for Overconsolidated Granular Soils," Geotechnique, Vol.30, No. 3, pp. 310-313.

13. Das, B. M., and Jin, Y., (1987). "Uplift Capacity of Model Group Anchors in Sand," Foundations for Transmission Line Towers, Proceedings of a session sponsored by the Geotechnical Engineering Division of the ASCE, NJ, pp. 57-71.

14. Davis, A. G., Contribution to discussion session 9, (1979). "The Use of Physical Models in Design," Seventh European Conference on Soil Mechanics and Foundation Engineering, Brighton, England, Vol. 4, pp. 358.

15. Davis, A. G., and Plumelle, C. (1982). " Full Scale Tests on Ground Anchors in Fine Sand," Journal of the Soil Mechanics and Foundations Division, ASCE, Vol. 108, No. GT 3, pp. 335-353.

16. Dickin, E. A., (1988). " Uplift Behavior of Horizontal Anchor Plates in Sand," Journal of Geotechnical Engineering Division, ASCE,Vol. 114, No. GT 11, pp. 1300-1317.

17. Esquivel-Diaz, R. F., (1967)."Pullout Resistance of Deeply Buried Anchors in Sand," (Unpublished M.S. Thesis, Duke University).

18. Ghaly, Ashraf M., (1986). "Screw Pile, Its Uses to Resist Uplift Pressures in Seepage Conditions," M. Sc. Thesis, Faculty of Engineering, Alexandria University, Egypt.

19. Hanna, A. M., Das, B., and Foriero, A., (1988). " Behaviour of Shallow Inclined Plate Anchors in Sand," Special Topics in Foundations, Proceedings of a session sponsored by the Geotechnical Engineering Division of the ASCE, Nashville, pp. 54-72.

20. Hanna, T. H., and Carr, R. W., (1971). "The Loading Behaviour of Plate Anchors in Normally and Overconsolidated Sands", Proceedings, Fourth Budapest Conference on Soil Mechanics and Foundation Engineering, Budapest, pp. 589-600.

21. Hanna, T. H., and Sparks, R. W., (1973). "The Behaviour of Preloaded Anchors in Normally Consolidated Sands,", Proceedings, 8th International Conference on Soil Mechanics and Foundation Engineering, Vol. 2, pp. 137-142.

22. Hanna, T. H., Sparks, R., and Yilmaz, M., (1972). "Anchor Behaviour in Sand," Proceedings, ASCE, Journal of the Soil Mechanics and Foundations Division, Vol. 98, No. SM11, pp. 1187-1208.

23. Harr, M. E., (1966). "Foundations of Theoretical Soil Mechanics," McGraw-Hill Book Company, New York, pp. 27-34 and 151-156.

24. Healy, K.A., (1971). "Pullout Resistance of Anchors Buried in Sands, Journal of the Soil Mechanics and Foundations Division, ASCE, Vol. 97, No. SM 11, pp. 1615 - 1622.

25. Healy, K. A., and Welti, C. W., (1972). " Expansion of Cavities in Infinite Soil Mass," Discussion, Journal of the Soil Mechanics and Foundations Division, ASCE, Vol. 98, No. SM 11, pp. 1275-1276.

26. Hoyt, R. M., and Clemence, S. P., (1989). "Uplift Capacity of Helical Anchors in Soil," Proceedings, Regional South America Conference on Soil Mechanics and Foundation Engineering, Rio de Janeiro, Brasil, pp. 1019-1022.

27. Jaky, J., (1944). "The Coefficient of Earth Pressure at Rest," Journal of the Society of Hangarian Architects and Engineers, pp. 355-358.

28. Jumikis, A. R., (1969). "Theoretical Soil Mechanics," Van Nostrand Reinhold Company, New York, pp. 258-264.

29. Jumikis, A. R., (1987). "Foundation Engineering," Florida, Robert E Krieger Publishing Company, Inc., pp 436 441

30 Kanayan, A. S., (1966) "Experimental Investigation of the Stability of Bases of Anchor Foundations," Soil Mechanics and Foundation Engineering, Vol 4, No 6, pp 387 392.

31. Kezdi, A., (1964). "Design of Structures to Resist Earth Pressures," Proceedings of Lecture Series, sponsord by Soil Mechanics and Foundations Division, Illinois Section, ASCE, Chicago, Illinois, pp. 187-234.

32. Khadilkar, B. S., Paradkar, A. K., and Golait, Y. S., (1971). " Study of Rupture Surface and Ultimate Resistance of Anchor Foundations," Proceedings, 4 th Asian Regional Conference on Soil Mechanics and Foundation Engineering, Vol. 1, pp.121-127.

33. Krizek, R. J., Farzin, M. H., Wissa, A. E. Z., and Martin, R. T., (1974)."Evaluation of Stress Cell Performance," Proceedings, ASCE, Journal of the Geotechnical Engineering Division, Vol. 100, NO. GT12, pp. 1275-1295.

34. Kulhawy, F. H., (1985). " Draind Uplift Capacity of Drilled Shafts," Proceedings of the 11 th International Conference on Soil Mechanics and Foundation Engineering, San Fransisco, Calif., vol. 3, pp. 1549-1552.

35. Kulhawy, F. H., (1985). "Uplift Behavior of Shallow Soil Anchors - An Overview," Uplift Behavior of Anchor Foundations in Soil," Proceedings of a session sponsored by the Geotechnical Engineering Division of the ASCE, Michigan, pp. 1-25.

36. Lambe, W., and Whitman, R., (1969). "Soil Mechanics," John Wiley & Sons, Inc., New York.

37. Larnach, W. J., and Mc Mullan, D. J., (1974). " Behaviour of Inclined Groups of Plate Anchors in Dry Sand," Proceedings of the Conference organized by the Institution of Civil Engineers, London, England, pp. 153-156.

38. Lutenegger, A. J., Smith, B. L., and Kabir, M. G., (1988). " Use of In-Situ Tests to Predict Uplift Performance of Multihelix Anchors," Special Topics in Foundations, Proceedings of a session sponsored by the Geotechnical Engineering Division of the ASCE, Nashville, pp. 93-109.

39. Mariupol'skii, L. G., (1965)."The Bearing Capacity of Anchor Foundations, (English translation) Russian Soil Mechanics and Foundation Engineering, pp. 26-37.

40. Mayne, P. W., and Kulhawy, F. H., (1982). " K_0 - OCR Relationship in Soil," Journal of Geotechnical Engineering Division, ASCE,Vol. 108, No. GT 6, pp. 851-872.

41. Meyerhof, G. G., (1973). " Uplift Resistance of Inclined Anchors and Piles," Proceedings, 8th International Conference on Soil Mechanics and Foundation Engineering, Moscow, Vol. 2.1, pp. 167-172.

42. Meyerhof, G. G., and Adams, J. I., (1968). "The Ultimate Uplift Capacity of Foundations," Canadian Geotechnical Journal, Vol. 5, No. 4, pp. 224-244.

43. Mitsch, M. P., and Clemence, S. P., (1985). "The Uplift Capacity of Helix Anchors in Sand," Uplift Behavior of Anchor Foundations in Soil, Proceedings of a session sponsored by the Geotechnical Engineering Division of the ASCE, Michigan, pp. 26-47.

44. Mohamed, M. K., and Hanna, T. H., (1985). " Pressure Injected Anchors in Sand: Load and Creep Behaviour," Canadian Geotechnical Journal, Vol. 22, No. 4, pp. 456-465.

45. Murray, E. J., and Geddes, J. D., (1987). "Uplift of Anchor Plates in Sand," Journal of the Soil Mechanics and Foundations Division, ASCE, Vol. 113, No. GT 3, pp. 201-215.

46. Murray, E. J., and Geddes, J. D., (1988). "Uplift of Anchor Plates in Sand," Closure, Journal of Geotechnical Engineering Division, ASCE,Vol. 114, No. GT 12, pp. 1461-1462.

47. Nasr, A. N., (1980). "Anchored Construction Under Seepage Conditions," M. Sc. Thesis presented to the Faculty of Eng., Alexandria University, Egypt.

48. Radhakrishna, H. S., (1976)."Helix Anchor Tests in Sand - Essa T. S.," Ontario Hydro Research Division, Research Report.

49. Robison, K. E., and Taylor, H , (1969). " Selection and Performance of Anchors for Guyed Transmission Towers," Canadian Geotechnical Journal, Vol 6, No. 2, pp 119-137.

50. Rodgers, T. E., Jr., (1987). " High Capacity Multi Helix Screw Anchors for Transmission Line Foundations," Proceedings of a session sponsord by the Geotechnical Engineering Division, ASCE, NJ, pp 81-95

51. Rowe, R. K., and Davis, E H , (1982) "The Behaviour of Anchor Plats in Sand," Geotechnique, Vol 32, No 1, pp 25 41

52. Saeedy, H. S., (1971). "Analytical Experimental Stability of Earth Anchors," (Unpublished Doctoral Thesis, Oklahoma State University).

53. Schmidt, B., (1966). "Earth Pressure at Rest Related to Stress History," Discussion, Canadian Geotechnical Journal, Vol.3, No. 4, pp. 148-161.

54. Selig, E. T., (1980). "Soil Stress Gage Calibration," Geotechnical Testing Journal, Vol. 3, No. 4, pp. 153-158.

55. Sowa, V. A., (1970). " Pulling Capacity of Concrete Cast in Situ Bored Piles," Canadian Geotechnical Journal, Vol. 7, No. 3, pp. 482-493.

56. Su, Weizhi, and Fragaszy, R. J., (1988). " Uplift Testing of Model Anchors," Journal of Geotechnical Engineering Division, ASCE, Vol. 114, No. GT 9, pp. 961-983.

57. Sutherland, H. B., (1965). "Model Studies for Shaft Raising through Cohesionless Soils," Proceedings, Sixth International Conference on Soil Mechanics and Foundation Engineering, Montreal, Canada, pp. 410 - 413.

58. Sutherland, H. B., Finlay, T. W., and Fadl, M. O., (1983). "Uplift Capacity of Embedded Anchors in Sand," Proceedings of The International Conference on the Behaviour of Off-Shore Structures, Vol. 3, pp. 451 - 463.

59. Terzaghi, K.. (1959). "Theoretical Soil Mechannics," John Wiley and Sons, Inc., New York, pp. 66-76.

60. Terzaghi, Karl, and Peck, R. B., (1967). "Soil Mechanics in Engineering Practice," New York, John Wiley & Sons Inc., pp. 51 - 86.

61. Trofimenkov, J. G., and Mariupolskii, L. G., (1965). "Screw Piles Used for Mast and Tower Foundations, " Proceedings, Sixth International Conference on Soil Mechanics and Foundation Engineering, Montreal, Canada, Vol. 2, pp. 328-332.

62. Tucker, Keith D., (1986). " Uplift Capacity of Pile Foundations Using CPT Data," Proceedings, ASCE, Use of In Situ Tests in Geotechnical Engineering, Edited by Samuel P. Clemence, Virginia Tech., Blacksburg, Virginia, pp. 1077-1093.

63. Turner, E. A., (1962)."Uplift Resistance of Transmission Tower Footings," Proceedings, ASCE, Journal of the Power Division, Vol. 88, No. PO2, pp. 17-33.

64. Udwari, J. J., Rodgers, T. E., Jr., and Singh, H., (1979). "A Rational Approach to the Design of High Capacity Multi-Helix Screw Anchors," Proceedings, Seventh IEEE/PES, Transmission and Distribution Conference and Exposition, New York, pp. 606-610.

65. Vermeer, P. A., and Sutjiadi, W., (1985). " The Uplift Resistance of Shallow Embedded Anchors," Proceedings, 11th International Conference on Soil Mechanics and Foundation Engineering, San Fransisco, Calif., vol. 3, pp. 1635-1638.

66. Vesic, A. S., (1971). " Breakout Resistance of Objects Embedded in Ocean Bottom," Journal of the Soil Mechanics and Foundations Division, ASCE, Vol. 97, No. SM 9, pp. 1183-1205.

67. Vesic, A. S., (1972). " Expansion of Cavities in Infinite Soil Mass," Journal of the Soil Mechanics and Foundations Division, ASCE, Vol. 98, No. SM 3, pp. 265-290.

68. Vesic, A. S., (1972). " Expansion of Cavities in Infinite Soil Mass," Closure, Journal of the Soil Mechanics and Foundations Division, ASCE, Vol. 99, No. SM 5, pp. 409.

69. Wahba, M. A., (1966). "The Performance of Navigation Locks and Dry Docks Against Uplift Pressure," M. Sc Thesis presented to the Faculty of Eng., Alexandria University, Egypt.

70. Wang, M. C., (1988). "Uplift of Anchor Plates in Sand," Discussion, Journal of Geotechnical Engineering Division, ASCE,Vol. 114, No. GT 12, pp 1460

71. Wang, M. C., and Wu, A. H., (1980). " Yielding Load of Anchor in Sand," Proceedings, ASCE, Application of Plasticity and Generalized Stress - Strain in Geotechnical Engineering, R. N. Yong and E. T. Selig, Editors, Hollywood, Florida, pp 291 307

72. Weikart, A. M , and Clemence, S P , (1987) "Helix Anchor Foundations Two Case Histories," Proceedings of a session sponsored by the Geotechnical Engineering Division of the ASCE, New Jersey, pp 72 80

73. Wernick, E , (1977) "Stresses and Strains on the Surface of Anchors," Proceedings, 9th International Conference for Soil Mechanics and Foundation Engineering, Speciality Session 4 on Ground anchors, Tokyo, Japan, pp 113 119

74. Wroth, C. P., (1972). "General Theories of Earth Pressure and Deformation," Proceedings, 5th European Coference on Soil Mechanics, Madrid, Vol.2, pp. 33-52.

75. Wroth, C. P., (1972). "In Situ Measurements on Initial Stress and Deformation Characteristics," Proceedings, In Situ Measurement of Soil Properties, Noth Carolina State University, Geotechnical Engineering Division, pp. 181-230